

Seismic vulnerability of existing buildings

Report

Author(s):

Lang, Kerstin

Publication date:

2002

Permanent link:

<https://doi.org/10.3929/ethz-a-004333389>

Rights / license:

In Copyright - Non-Commercial Use Permitted

Originally published in:

IBK Bericht 273

Seismic vulnerability of existing buildings

Kerstin Lang

Institute of Structural Engineering
Swiss Federal Institute of Technology

Zurich
February 2002

Preface

Major earthquakes are rare in Switzerland; but when they occur the consequences can be disastrous. Comparative studies have shown that over a longer period of time the seismic risk is the most important natural risk in Switzerland. So far only rough estimates could be made, more precise statements on the actual seismic risk in a certain city or city quarter with a certain building population are not available. For this reason the Swiss Seismological Service (SED) and the Institute of Structural Engineering (IBK) launched a joint project “Earthquake Scenarios for Switzerland” with the goal to elaborate risk scenarios. For that purpose the effect of an earthquake on actual existing buildings has to be known.

In the present doctoral thesis a method is developed which allows the assessment of the seismic vulnerability of a larger number of existing buildings using an engineering approach, but which at the same time requires only a limited time expenditure. Unreinforced masonry buildings and reinforced concrete buildings as well as combinations of those two building types are dealt with and five different damage grades according to the European Macroseismic Scale are defined. One focal point is the evaluation of unreinforced masonry buildings. The application of this new method to 87 two- to six-storey buildings in a small target area in Basel shows, that for a seismic input according to the Swiss Standard SIA 160 (return period of 400 years) more than half of the buildings are expected to be very heavily damaged or destroyed.

With this thesis the development of a very efficient method has been achieved which is orientated towards the practising engineer. In addition this new method suggests to think about the improvement of the existing procedures for the seismic design of new unreinforced masonry buildings.

Zurich, February 2002

Prof. Dr. Hugo Bachmann

Acknowledgements

This work is part of the research project “Earthquake Scenarios for Switzerland”. It was a challenge but also a very interesting task to work on this project and to contribute one part. However, without the support from different sides it would not have been possible to accomplish this work and I would like to use this occasion to express my gratitude.

First of all I would like to thank my referee, Prof. Dr. Hugo Bachmann. His support and his interest in my work as well as his critical comments were essential for the completion of this work. I also would like to thank Prof. Dr. Marc Badoux for the valuable comments and for accepting to be co-examiner. My further thanks go to my co-examiners Prof. Dr. Gian Michele Calvi and Prof. Dr. Domenico Giardini.

The necessary building data were provided by the archives of the city of Basel. Their co-operation is gratefully acknowledged.

I thank Miss Rishmila Mendis and Mr. Joost Meyboom for the corrections of the English language. Further I want to thank Dr. Donat Fäh who coordinated the project for his help concerning the seismological aspects.

My special thanks go to my colleagues at the Institute of Structural Engineering and the Institute of Geophysics. I will always remember with pleasure the inspiring discussions and activities we had.

My deepest gratitude goes to my family, my parents and brothers, and Thomas Pfyl for their constant support and encouragement. This work is dedicated to them.

Zurich, February 2002

Kerstin Lang

Abstract

In order to assess the seismic risk for Switzerland, and particularly for the city of Basel, a joint project on the subject of “Earthquake Scenarios for Switzerland” was launched by the Swiss Seismological Service (SED) and the Institute of Structural Engineering (IBK) at the ETH Zurich. The goals of the study are to improve the assessment of seismic hazard, to investigate the vulnerability of the built environment and finally, to combine the results to elaborate risk scenarios as the first fundamental step in the mitigation process. The objective of this work is the evaluation of the seismic vulnerability of existing buildings with a focus on the residential building stock in the city of Basel. Since no major damaging earthquake has occurred in Switzerland in recent times, vulnerability functions from observed damage patterns are not available. A simple evaluation method based on engineering models of the building structures suitable for the evaluation of a larger number of buildings is therefore proposed.

First, the general idea of the evaluation method based on nonlinear static procedures is introduced in Chapter 3 which briefly discusses the two key elements of a vulnerability analysis, the capacity (strength and deformation capacity) of a building and the seismic demand. The results are vulnerability functions expressing the expected damage of a building as a function of the seismic input.

The application of the evaluation method to unreinforced masonry buildings and to reinforced concrete buildings is discussed in more detail in Chapters 4 and 5 respectively. Special attention is paid to the frame action due to the coupling of the walls by floors and spandrels. Comparisons with test results from model buildings in the case of masonry buildings and with a recently proposed and thoroughly checked deformation orientated method in the case of reinforced concrete buildings show that the proposed method suitably forecasts the capacity of a building.

Finally, a comprehensive inventory of the buildings in a small target area in Basel was established based on plans and a street survey. The inventory comprised a total number of 87 buildings which were then assessed using the evaluation method. Based on the results of the assessment, building classes were defined depending on the type of structure and the number of storeys. Corresponding fragility curves were determined, expressing the probability of a building belonging to a certain building class of reaching or exceeding a particular damage grade given a deterministic estimate of the spectral displacement. The classification of the buildings allows an extrapolation of the results to a larger area or to the whole city. A statement on the actual seismic risk, however, is not possible without the knowledge of the local seismic hazard which is not yet available.

Zusammenfassung

Zur Abschätzung des Erdbebenrisikos der Schweiz, und insbesondere der Stadt Basel, wurde vom Schweizerischen Erdbebendienst (SED) und dem Institut für Baustatik und Konstruktion (IBK) der ETH Zürich ein gemeinsames Forschungsprojekt mit dem Thema "Erdbebenszenarien der Schweiz" ins Leben gerufen. Das Ziel ist eine verbesserte Abschätzung der Erdbebengefährdung sowie der Verletzbarkeit der bestehenden Bausubstanz und, durch eine Zusammenführung der Ergebnisse, die Berechnung des Risikos möglicher Erdbebenszenarien als erster Schritt zur Risikoabminderung.

Die Zielsetzung der vorliegenden Arbeit ist die Bewertung der Erdbebenverletzbarkeit bestehender Gebäude, wobei der Schwerpunkt auf der Bewertung der Bausubstanz von Basler Wohngebieten liegt. Aus Mangel an stärkeren Erdbeben in der Schweiz in der letzten Zeit sind Verletzbarkeitsfunktionen aufbauend auf beobachteten Schadensbildern jedoch nicht verfügbar. Es wird daher eine einfache Evaluationsmethode vorgeschlagen, die sich auf Ingenieurmodelle der Tragwerke stützt und zur Bewertung einer größeren Anzahl von Gebäuden geeignet ist.

Zunächst wird die Grundidee der Evaluationsmethode, die auf nichtlinearen statischen Berechnungsverfahren beruht, in Kapitel 3 eingeführt. Die beiden Hauptaspekte einer Verletzbarkeitsstudie, die Kapazität (Tragwiderstand und Verformungsvermögen) eines Gebäudes und der Kapazitätsbedarf werden kurz diskutiert. Das Ergebnis sind Verletzbarkeitsfunktionen, die den zu erwartenden Schaden eines Gebäudes als Funktion der Bodenbewegung beschreiben.

Die Anwendung der Evaluationsmethode auf Gebäude aus unbewehrtem Mauerwerk und aus Stahlbeton wird in Kapitel 4 und 5 näher betrachtet. Besondere Aufmerksamkeit gilt der Rahmenwirkung, die durch die Koppelung der Wände durch Riegel und Decken entsteht. Vergleiche mit Versuchsergebnissen im Falle von Gebäuden aus unbewehrtem Mauerwerk und mit einem kürzlich vorgeschlagenen und gründlich geprüften verformungsorientierten Berechnungsverfahren im Falle von Stahlbetongebäuden zeigen, daß die vorgeschlagene Methode die Kapazität eines Gebäudes gut erfaßt.

Schließlich wurde anhand von Plänen und einer Besichtigung von außen ein umfassendes Inventar der Gebäude in einem kleinen Zielgebiet in Basel erstellt. Das Inventar umfaßt insgesamt 87 Gebäude, die anschließend mit der Evaluationsmethode bewertet wurden. Basierend auf den Ergebnissen dieser Bewertung wurden Gebäudeklassen definiert, die durch ihren Tragwerkstyp und die Anzahl Stockwerke zu unterscheiden sind. Für jede Gebäudeklasse wurde eine "fragility" Kurve definiert, die die Wahrscheinlichkeit ausdrückt, daß ein Gebäude einer bestimmten Gebäudeklasse für eine gegebene spektrale Verschiebung einen bestimmten Schadensgrad erreicht oder übersteigt. Die Bildung von Gebäudeklassen erlaubt eine Extrapolation der Ergebnisse auf ein größeres Zielgebiet. Eine Angabe zum Erdbebenrisiko ist jedoch ohne die noch nicht vorliegende Kenntnis der lokalen Erdbebengefährdung nicht möglich.

Table of contents

1 Introduction

1.1 Defining the problem	1
1.2 Objective	2
1.3 Limitations	3
1.4 Overview	3

2 State of the art

2.1 Introduction	5
2.2 Observed vulnerability	5
2.3 Vulnerability functions based on expert opinions	7
2.4 Analytical approach based on simple models	9
2.5 Score assignment	11
2.6 Detailed analysis procedures	14

3 A method to evaluate the vulnerability of existing buildings

3.1 Introduction	17
3.2 Positioning of the method	17
3.3 Difference between design and evaluation	18
3.4 Definition of a vulnerability function	19
3.5 Capacity curve of a building	20
3.5.1 General considerations	20
3.5.2 Identification of structural and non-structural elements	21
3.5.3 Terminology and structural models	23
3.5.4 Construction of the capacity curve	26
3.6 Seismic demand	29
3.7 Vulnerability function	34

4 Vulnerability of masonry buildings

4.1 Introduction	37
4.2 In-plane behaviour	37
4.2.1 Shear behaviour of unreinforced masonry	37
4.2.2 Structural model	42
4.2.3 Capacity curve of a masonry wall	44
4.2.4 Ductility of masonry structures	48
4.2.5 Cyclic loading	51
4.2.6 Capacity curve of a masonry building	52
4.2.7 Identification of damage grades according to the EMS	52

4.2.8 Vulnerability function of a masonry building	55
4.3 Out-of-plane behaviour	55
4.3.1 Structural modelling	56
4.3.2 Out-of-plane cracking	58
4.3.3 Out-of-plane failure	60
4.3.4 Influence on the vulnerability function	61
4.3.5 Some further remarks on the out-of-plane behaviour	61
4.4 Comparison with test results	62
4.4.1 Pavia University tests	62
4.4.2 ISMES tests	65
4.4.3 Conclusions	68
4.5 Evaluation method step by step	68
4.6 Conclusion	70

5 Vulnerability of RC buildings

5.1 Introduction	71
5.2 Moment-curvature relationship of reinforced concrete wall sections	71
5.3 Different types of reinforced concrete buildings	75
5.4 Capacity curve of a reinforced concrete building	77
5.4.1 Structural wall systems with negligible frame action	77
5.4.2 Structural wall systems with “separate” frame action	81
5.4.3 Structural wall systems with frame action due to coupling of the walls ..	83
5.4.4 Shear strength	85
5.4.5 Cyclic loading	87
5.5 Identification of damage grades according to the EMS	88
5.6 Vulnerability function of a reinforced concrete building	90
5.7 Comparison	90
5.8 Evaluation method step by step	92
5.9 Conclusion	93

6 Application to buildings in Basel

6.1 Introduction	95
6.2 Characteristics of the building stock in Basel	95
6.2.1 General	95
6.2.2 Corner buildings	97
6.2.3 Floors	98
6.3 Material Properties	100
6.3.1 Properties of masonry	100
6.3.2 Properties of reinforced concrete	106
6.4 Example masonry building	112

7 Earthquake scenarios

7.1 Results	129
7.2 Classification	132
7.3 Comparison with other vulnerability investigations	135
7.4 Conclusions	141

8 Summary and conclusions

8.1 Summary	143
8.2 Conclusions	144
8.3 Outlook	146

Appendix

A1 Classification of damage according to EMS 98	151
A1.1 Classification of damage to masonry buildings.....	151
A1.2 Classification of damage to reinforced concrete buildings.....	152
A2 Example RC building - Detailed calculations	153
A3 Example building with a mixed structure	165
A4 Example database record	167

Symbols	169
----------------	-----

Glossary	175
-----------------	-----

Bibliography	179
---------------------	-----

1 Introduction

1.1 Defining the problem

Switzerland has experienced destructive earthquakes throughout its history. Most notable were the events of 1356 in Basel and 1855 in the Valais. Although such events are very rare, their intensity is comparable to the major earthquakes of Northridge, California 1994 and Kobe, Japan 1995. Figure 1.1 shows an engraving from the chronicle of Christian Wurstisen which illustrates the city of Basel after the major earthquake of 1356 [Wu 78]. Contemporary descriptions also reported enormous damage [We 87]. The assigned intensity of the 1356 event according to the European Macroseismic Scale [EMS 98] is $_{EMS} = IX$.



Figure 1.1: Engraving from the chronicle of Christian Wurstisen illustrating the city of Basel after the major earthquake of 1356 [Wu 78]

Although these events are very rare, they are characterized by high exposure and their economic and social effects cannot be neglected. To reduce the potential damage, a comprehensive assessment of the seismic risk followed by a package of relevant remedial measures is needed. In order to assess the seismic risk for Switzerland, and particularly for the city of Basel, a joint project on the subject of “Earthquake Scenarios for Switzerland” was launched by the Swiss Seismological Service (SED) and the Institute of Structural Engineering (IBK) at the Swiss Federal Institute of Technology Zürich (ETH). The goals of this study are to improve the assessment of seismic hazard, to investigate the vulnerability of the built environment and, finally, to combine the results to elaborate risk scenarios as the first fundamental step in the mitigation process:

$$\text{Risk} = \text{Hazard} \times \text{Vulnerability} \times \text{Exposure}.$$

The project is divided into four research lines (Figure 1.2). The first research line is a paleoseismic study based on the analysis of coring samples of lakebed sediments to iden-

tify and date disturbances related to prehistoric earthquakes with the goal of constraining the return period of large events and extending the record used for probabilistic hazard assessment [BDG 01].

The second research line focuses on the simulation of strong ground motions for regional hazard assessment in Switzerland. Ground motion attenuation models are calibrated based on observed strong motion recordings and on theoretical computations taking into account realistic models for wave propagation as well as possible seismic source zones [Bay 02].

The third research line takes into account local site effects and will result in a microzonation for the city of Basel. Based on a detailed model of the local soil conditions and in-situ measurements of the soil properties, numerical one- and two dimensional wave propagation modelling is used to estimate the amplification effects with respect to the expected ground motion predicted by the regional hazard zonation from the second research line [Ki 02].

The fourth research line comprises a vulnerability analysis of the buildings in a small target area in the city of Basel. It requires a comprehensive inventory of the buildings. Vulnerability functions are established for the buildings describing the expected damage as a function of the seismic input.

The results of these four research lines shall be incorporated into a geographical information system (GIS) which allows the calculation of the expected damages for different earthquake scenarios.

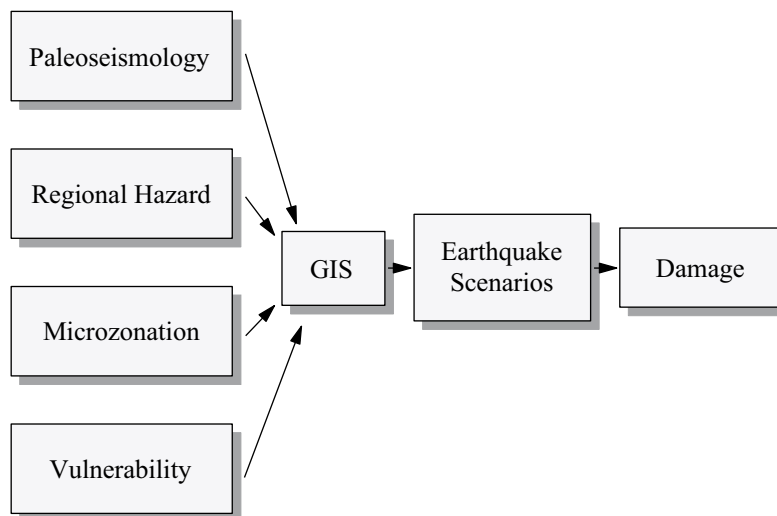


Figure 1.2: Earthquake scenarios for Switzerland - project organisation

1.2 Objective

This work focuses on the fourth research line, the vulnerability of existing buildings. The vulnerability is commonly expressed by functions or matrices which can be obtained either by statistical studies of damaged buildings in earthquake-struck areas or by simulations using numerical or analytical models of the buildings. Statistical studies are only valid in a probabilistic sense, while simulations have a very narrow validity and are only

available for a small fraction of the complete building stock. Since no major damaging earthquake has occurred in Switzerland in the last century, vulnerability functions or matrices from observed damage patterns are not available. As a consequence, a method is required that allows evaluation of the vulnerability of existing buildings with regard to the earthquake scenario project; this means that the evaluation of a larger building population is of interest rather than the evaluation of an individual building. Here the main objective is the development of the method which can also be applied to other cities rather than quantitative results.

The majority of the building population in the city of Basel consists of unreinforced masonry buildings. This is also the case for other cities in Switzerland. This work concentrates therefore especially on the behaviour of unreinforced masonry buildings, however, reinforced concrete buildings are considered as well.

1.3 Limitations

Considering the objective of this work, the assessment of a larger building population, the evaluation method needs to be quite simple. This precludes the consideration of the following effects:

- torsion
- pounding
- interaction of adjacent buildings.

Further simplifications are introduced when necessary in order to facilitate the procedure. Hence, even though in principle the method applies to all kinds of buildings, for buildings with a very irregular geometry in plan and elevation the simplifying assumptions need to be checked and more detailed calculations are necessary in order to grasp their complex dynamic behaviour. However, the principle of the evaluation method still holds.

The work focuses on residential buildings for several reasons. Firstly, residential buildings constitute the majority of the building population in Basel, nevertheless they often tend to be neglected. Other studies exist concentrating on the evaluation of life lines [BH 92] and industrial facilities [Si 98] in the city of Basel. For a more complete evaluation of the vulnerability of the building stock in Basel, the results of these studies could be incorporated into the earthquake scenario project. Secondly, residential buildings are usually quite regular in plan and elevation; thus the simplifying assumptions of the evaluation method apply. Lifelines often consist of very irregular structures requiring a more detailed evaluation. The vulnerability of industrial facilities is usually determined not only by the building structure but also by the equipment.

1.4 Overview

The second chapter gives an overview of existing earthquake scenario projects and their respective evaluation of the vulnerability of existing buildings ranging from statistical studies of damaged buildings following major earthquakes and expert opinions to simple simulation models.

Introduction

The third chapter presents the principle of the evaluation method in a general way, starting with the definition of the vulnerability function, introducing then the idea of the capacity curve of a building, illustrating the seismic demand and finishing by the description of the construction of the vulnerability function.

In the fourth chapter, the application of the evaluation method to unreinforced masonry buildings is discussed in more detail. A distinguishment is made between in-plane and out-of-plane behaviour. It is explained how the capacity curve of an unreinforced masonry building is obtained and how the identification of damage leads to the vulnerability function of an unreinforced masonry building. In a further step, the effect of out-of-plane behaviour on the vulnerability function is considered. Finally, the evaluation method is validated by its application to unreinforced masonry model buildings which were tested under cyclic static and under dynamic action.

In the fifth chapter, the application of the evaluation method to reinforced concrete buildings is discussed. Different approaches are considered depending on the type of reinforced concrete building.

The sixth chapter considers the application of the evaluation method to buildings in Basel. Local construction conditions are investigated and consequences for the evaluation method derived. A brief review of the development of the material properties follows and finally an example of an evaluation of a building in Basel is given.

The seventh chapter summarizes the results of the evaluation of the buildings in a small target area in Basel. A possible classification of the buildings with respect to the earthquake scenario project is introduced and a comparison with other vulnerability investigations discussed.

Finally, conclusions are given in the eighth chapter.

2 State of the art

2.1 Introduction

Earthquake loss estimation is a rapidly developing field. The need for an efficient and reliable estimation of the socio-economic impact of large earthquakes was again emphasized after major earthquakes in the 1990's in the United States and Japan. Advances in GIS (Geographical Information System) technology provide powerful new tools for loss estimation. In addition, experience from recent earthquakes have provided more data that have been useful in developing models to better assess the performance of structures in order to estimate the economic losses to buildings and lifelines and the social consequences such as casualties and needs for provisional accommodation.

In this chapter hitherto existing vulnerability assessment methods for loss estimation are described in order to provide the reader with an overview of the state of the art. This overview cannot be a complete listing, however it is tried to present the different possible approaches accompanied with a few examples of application.

The various methods for the assessment of the vulnerability of buildings differ in expenditure and precision. The type of method chosen depends on the objective of the assessment but also on the availability of data and technology. In the following the different approaches are outlined in the order of increasing computational effort starting from observed vulnerability and expert opinions (Sections 2.2 and 2.3) via simple analytical models and score assignments (Sections 2.4 and 2.5) to detailed analysis procedures in Section 2.6 (Table 2.1).

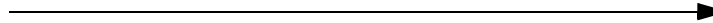
expenditure	increasing computation effort 				
application	building stock			individual building	
methods	observed vulnerability	expert opinions	simple analytical models	score assignment	detailed analysis procedures

Table 2.1: Methods for the assessment of the vulnerability of buildings

2.2 Observed vulnerability

Observed vulnerability refers to assessments based on statistics of past earthquake damage. It is especially suitable for non-engineered structures made of low-strength materials such as timber and unreinforced masonry whose earthquake resistance is rather difficult to calculate.

One of the first to have systematically compiled statistics on damage to buildings from experiences during actual earthquakes was Whitman et al. [WRH 74]. From a survey of damage caused by the San Fernando earthquake of 9 February 1971 covering approxi-

mately 1600 buildings having five or more storeys, damage probability matrices (DPM) were generated for different building types. The general form of such a damage probability matrix is shown in Table 2.2. Each number in the matrix (indicated by ...) expresses the probability that a building of a certain building class will experience a particular level of damage as a result of a particular earthquake intensity. The damage ratio is defined as the repair cost as a ratio of the replacement cost at the time of the earthquake.

Damage state	Structural Damage	Non-structural damage	Damage ratio (%)	Intensity of Earthquake				
				V	VI	VII	VIII	IX
0	None	None	0-0.05
1	None	Minor	0.05-0.3
2	None	Localized	0.3-1.25
3	Not noticeable	Widespread	1.25-3.5
4	Minor	Substantial	3.5-4.5
5	Substantial	Extensive	7.5-20
6	Major	Nearly total	20-65
7	Building Condemned		100
8	Collapse		100

Table 2.2: Format for Damage Probability Matrix, after [WRH 74]

This format of a damage probability matrix has become the most widely used form to define the probable distribution of damage which was also adapted by several other methods (see Section 2.3). The number of damage states considered are often reduced, ranging between four and six, as too many damage states are rather difficult to distinguish.

A set of vulnerability functions for different building types most commonly observed in earthquake prone areas are given by Coburn & Spence [CS 92]. They are based on data collected during different case studies of damage caused by a number of earthquakes from a range of different countries. Five different damage grades are considered. For each building type the scatter of the intensity at which each individual structure passes a given damage threshold is assumed to be normally distributed. The damage distribution is expressed graphically by the probability of exceedance of a certain damage grade given the seismic input defined by a parameterless scale of intensity. An example of these vulnerability functions is given in Figure 7.7 for low rise brick masonry buildings.

The Swiss Reinsurance Company has investigated the effects of two earthquakes on the insured portfolio: Albstadt, Germany on 3 September 1978 and central Chile on 3 March 1985 [PS 89]. The extent of the damage is expressed by the mean damage ratio of the affected buildings which is defined as the amount of loss of all affected buildings as a ratio of their value. With the aid of the data on the damage caused by the Chilean earthquake the relationship between type of construction, building height, the mean damage ratio of the affected buildings and the earthquake intensity were investigated. The effect of subsoil on the mean damage ratio was studied using the Albstadt earthquake data. The results were used to estimate the total amount of losses with the current building density for the Basle earthquake of 1356. Because any estimate of the intensity of historic events

is prone to uncertainties, two sets of intensity distribution were considered: scenario A is based on a more pessimistic assessment and scenario B on a more optimistic one. The total estimated damage caused by the Basle event for scenario A is 47'130 millions CHF and for scenario B 13'390 millions CHF.

Clearly, the definition of these relationships between damage and earthquake intensity on the basis of observed vulnerability requires a substantial quantity of data and is, strictly speaking, only valid for the region or town used for the definition or in areas of similar building population. Where data are missing or inadequate, other methods are required to enable reasonable assessments to be made. One of the major drawbacks of these methods is that modifications of the building structure such as upgrading or repair are not taken into account and hence improved seismic resistance of the buildings cannot be covered.

2.3 Vulnerability functions based on expert opinions

One of the first systematic attempts to codify the seismic vulnerability of buildings came from the Applied Technology Council (a non profit corporation established in 1971 for the assistance of the practising structural engineer to keep abreast of technological developments) summarized in a report [ATC 13] which was funded by the Federal Emergency Management Agency (FEMA). ATC-13 essentially derived damage probability matrices for 78 different earthquake engineering facility classes, 40 of which refer to buildings, by asking 58 experts (noted structural engineers, builders, etc.) to estimate the expected percentage of damage that would result to a specific structural type subjected to a given intensity. Based on their personal knowledge and experience, the experts had to fill in a formal questionnaire with their best estimates of damage ratios defined as dollar loss as a ratio of replacement value. In some cases, however, only a few felt themselves sufficiently expert with respect to a particular structural type to venture an opinion.

Clearly, the primary drawback of the ATC-13 approach is its subjectivity as the damage probability matrices are based exclusively on the subjective opinion of the experts. Hence, in addition to the uncertainties inherent to any estimation of damage due to the variability in actual building performance, there are the uncertainties related to the opinion of the experts. The damage probability matrices based on expert opinions are also difficult to calibrate or modify in order to incorporate new data or technologies. Also it is difficult to extend ATC-13 to other building types and other regions, as well as to individual building characteristics. Nevertheless, it was the first relatively thorough study on earthquake damage and loss estimation and became the standard reference for many earthquake vulnerability assessments until the mid 1990's.

Examples of the application of the ATC-13 damage probability matrices for risk assessment are the case studies of Palo Alto, California [KK 97] and Bogotá, Colombia [CY 97].

A second major attempt to develop a methodology for vulnerability assessment was undertaken by the National Institute of Building Science (NIBS), funded again by FEMA.

The result was an interactive software for risk assessment, HAZUS[®], released for the first time in 1997 and updated in 1999 [HAZUS 99][KNKH 97]. In HAZUS[®] intensities were replaced by spectral displacements and spectral accelerations as a measure of the seismic input. However, the HAZUS[®] study continues to rely on expert opinion to estimate the state of damage that would result from a given spectral displacement and acceleration.

36 model building types are considered by the methodology based on the classification system of FEMA 178 [FEMA 178] (cf. Section 2.5). For each building type descriptions for slight, moderate, extensive and complete structural damage are provided. Non structural damage is considered separately. Four possible seismic design levels are considered: high-code, moderate-code, low-code and pre-code, the latter referring to buildings without any seismic design. For each building type and design level, the parameters defining the building capacity, typical drift ratios and finally the spectral displacements at the threshold of the different structural damage states are given.

Another kind of vulnerability function based on observed vulnerability as well as expert opinions is the use of the vulnerability of the buildings implied in the macroseismic scales. Macroseismic intensities use building damage in conjunction with other phenomena in order to measure the strength of the ground motion in a certain region. From the description of building damage at different intensities vulnerability functions can be deduced.

This was done for a small earthquake scenario project for the city of Basel [FKLG 01] which served as a preliminary study for the earthquake scenario project for Switzerland (Section 1.1). Adopting the classification of the European Macroseismic Scale from 1998 [EMS 98] the different building structures were identified and the corresponding vulnerability class assigned. 15 types of structures and six vulnerability classes are distinguished, the assignment expressed by a most likely vulnerability class and a probable range. For each town quarter the percentage of buildings of one vulnerability class was estimated by a street survey.

For each damage grade DG_i , $i = 1 \dots 5$, a central damage factor (CDF) expressing the percentile damage was defined. The damage probability matrices (DPM) for the various vulnerability classes expressing the probability of occurrence of each damage grade DG_i given the earthquake intensity I , $P\langle DG_i|I \rangle$, were derived using the definition of the intensity degrees and quantifying the qualitative terms ‘few’, ‘many’ and ‘most’. In the EMS 98 only the quantity of the buildings suffering the highest damage grades at a given intensity are specified. The percentages of the buildings suffering lower damage grades are estimated following the frequency distribution of damage grades outlined in Section 4.6 of the EMS 98. For each vulnerability class a mean damage factor (MDF) for a given intensity was then defined as follows:

$$MDF_I = \sum_{i=1}^5 P\langle DG_i|I \rangle \cdot \frac{CDF_{DG_i}}{100} [\%] \quad (2.1)$$

The results are shown in Figure 2.1.

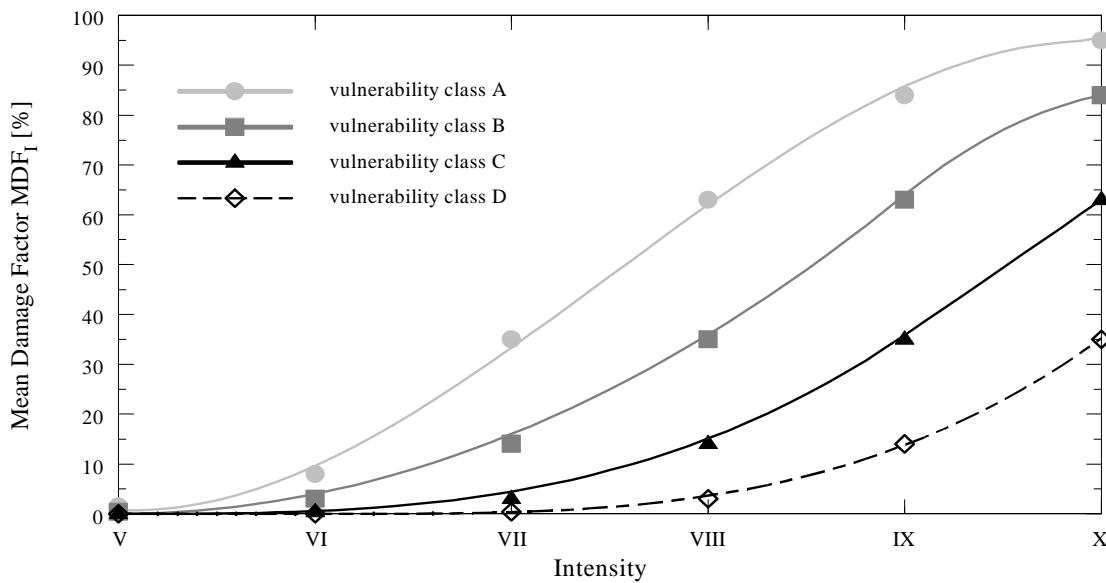


Figure 2.1: Mean damage factors (MDF_I) and vulnerability functions for the vulnerability classes of EMS 98 as a function of intensity

The vulnerability function implied in a macroseismic intensity scale was also used for the seismic risk evaluation for the city of Barcelona, Spain, referring however to the predecessor of the EMS, the MSK scale [PCM 00]. Only three classes of buildings are distinguished, class A (rubble stone, field stone, adobe masonry), class B (massive stone, non reinforced brick or concrete block masonry) and class C (reinforced concrete and steel structures).

2.4 Analytical approach based on simple models

In the absence of observed data vulnerability functions based on observations or expert opinions are not available. Other methods are therefore required to assess the vulnerability of the buildings. These methods should have the capacity to analyse a large number of buildings in a rather short period of time. This leads to analytical methods involving simple models of the buildings requiring only a few input parameters. The simpler the method, the less time consuming and the better for an efficient elaboration of earthquake scenarios. However, the results should be still reliable, hence the few input parameters must be able to capture the seismic behaviour of the buildings.

For earthquake loss estimation for historic town centres in Europe a vulnerability assessment method for masonry buildings was developed and applied to a case study in the Alfama district in Lisbon [DSOP 97] and to villages hit by the Umbria-Marche earthquakes in 1997 [SD 99]. The approach is based on the identification of potential collapse mechanisms yielding the equivalent shear capacity, expressed as the critical acceleration a/g , causing the mechanism to take place. In order to calculate the critical acceleration only geometry and boundary condition data based on visual estimates are necessary, the masonry is taken as a perfect rigid-plastic material. It is assumed that the most vulnerable

wall plane corresponds to a façade wall plane. This obliterates time consuming data acquisition such as the study of plans and elevations. Two classes of collapse mechanisms are studied: out-of-plane and in-plane. Four out-of-plane mechanisms are considered depending on the boundary conditions: simple overturning of a free-standing wall plane, overturning of a wall plane with ties at the top, overturning of a wall plane connected to transverse walls and overturning of a wall plane with ringbeam (Table 2.3).

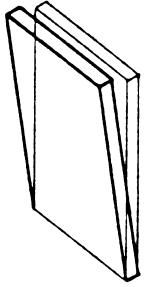
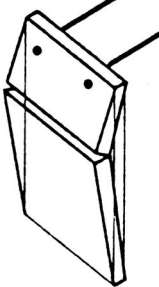
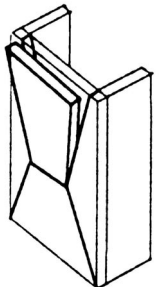

OP1 free-standing wall plane	OP2 with ties at the top	OP3 connected to transverse walls	OP4 with ringbeam
			

Table 2.3: Out-of-plane mechanisms after [DSOP 97]

The in-plane mechanisms considered are: sliding at joints, global overturning of a wall plane and crushing of the compressed edge of the piers (Table 2.4). However, if not prevented by special means such as ties or quoins out-of-plane behaviour is almost always critical.


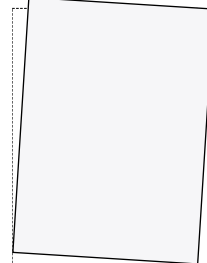
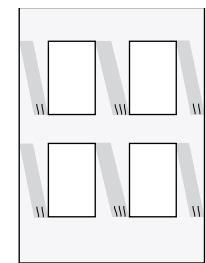
IP1 sliding at joints	IP2 global overturning	IP3 crushing of compressed edge of piers
		

Table 2.4: In-plane mechanisms after [DSOP 97]

Each collapse mechanism considered is then associated with a damage grade according to the European Macroseismic Scale 98 [EMS 98] (cf. appendix A1.1). Hence, calculating the equivalent shear of a building, i.e. the critical acceleration that triggers a collapse mechanism, results immediately in the expected damage grade.

Another analytical method grounded on very simple models was developed by Calvi and applied to the city of Catania [Ca 99][FPCB 99]. The approach is guided by the concepts for detailed analysis of existing buildings based on the assessment of the displacement

capacity of a building corresponding to several limit states and of the displacement demand resulting from a displacement spectrum. Possible out-of-plane mechanisms of masonry walls are not considered. The model is based on very few parameters only, i.e. the period of construction, the number of stories and the construction material (reinforced concrete or masonry). Four limit states are considered taking into account structural and non structural damage: LS1 below which there is no damage, LS2 below which there is only minor structural damage and moderate non structural damage, LS3 below which there is significant structural damage and extensive non structural damage and LS4 beyond which the building collapses. For each type of building structure and for each limit state a structural model is defined in terms of a secant stiffness to the corresponding maximum displacement of the limit state considered, from which the equivalent period of vibration is obtained, and a displacement demand reduction factor which depends on the energy dissipated by the structure. The reliability of those two parameters derived from very reduced data is rather small, and hence, intervals rather than deterministic values are given. The two intervals define a rectangle in the plane of the displacement spectrum; any additional data will result in a correction of the rectangles. The probability of occurrence of a certain limit state is then obtained by integrating a probability density function (in the most simple case assumed to be constant) in the area below the line of the displacement response spectrum.

Clearly, the simpler the model, the more rapid the evaluation, however, the less accurate the results. The results should be therefore considered with care when regarding individual buildings, having rather statistical meaning.

2.5 Score assignment

Score assignment procedures aim to identify seismically hazardous buildings by exposing structural deficiencies. They often form the first phase of a multi-phase procedure for identifying hazardous buildings which then must be analysed in more detail in order to decide on upgrading strategies. Potential structural deficiencies are identified from observed correlations between damage and structural characteristics. The scores for different deficiencies are usually calibrated by experts.

Again, it was the Applied Technology Council that developed a first comprehensive methodology for the evaluation of existing buildings in order to identify those buildings which present a risk to human lives [ATC 14]. The life-safety hazard in a building consists of the failure of any structural element of the building. The methodology therefore aims at identifying flaws and weaknesses which could cause structural failure. Potential weaknesses were determined from a detailed review of building performance observed in past earthquakes. 15 model building types are distinguished comprising all major types of construction materials. The procedure for the evaluation of the buildings consists of a collection of statements related to specific vulnerable areas in the structural system which require particular consideration. For each statement a commentary is given which explains the reason of the statement. Each evaluation statement is written such that a “true” response implies that the building structure is adequate in that area. For “false”

statements additional evaluation is required and adequate procedures are outlined comprising a quick check of strength and interstorey drift, equivalent lateral force procedure and a dynamic analysis procedure.

A few years later FEMA released a handbook for the seismic evaluation of existing buildings [FEMA 178] which utilizes the information and procedures developed for and documented in the ATC-14 report.

Only recently the American Society of Civil Engineers (ASCE) contracted with the FEMA to convert FEMA 178 into a prestandard as the first step in turning it into an approved national consensus standard. The resulting document was completed in 1998 and published as FEMA 310 [FEMA 310]. The new handbook reflects recent advancements in technology and incorporated lessons learned during recent earthquakes. Unlike in FEMA 178 not only life-safety is considered but also immediate occupancy performance level. The handbook provides a three-phase procedure: Screening phase, evaluation phase and detailed evaluation phase. The purpose of the screening phase is the identification of buildings with potential deficiencies using checklists of evaluation statements similar to those of ATC-14 and FEMA 178. For the evaluation of those buildings which do not pass the screening phase, however, instead of using force based procedures as proposed in ATC-14 and FEMA 178, now a displacement-based procedure is used consistent with the procedures used in FEMA 273 [FEMA 273] (cf. Section 2.6).

The procedures of ATC-14, FEMA 178 and FEMA 310, even in the screening phase, are already very detailed requiring plans and elevations of the building as well as some destructive examinations. They are therefore tailored to the evaluation of individual buildings rather than groups of structures and hence are not very suitable for earthquake scenarios. Also, the link between compliance or non-compliance with the evaluation statements to the expected damage as a function of the seismic input does not exist.

A more rapid screening procedure was proposed by the Applied Technology Council and sponsored by FEMA in 1988 [FEMA 154] [FEMA 155]. The screening is done from the sidewalk without building entry or structural drawings or calculations, taking an average of 15 to 30 minutes per building. Based on the visual inspection a data collection form is completed for each building. The screening begins with the identification of the primary structural lateral force resisting system and materials of the building. *Basic structural hazard scores* (BSH) for 12 different building types are provided which are then modified by adding or subtracting *performance modification factors* related to significant seismic-related deficiencies in order to arrive at the final *structural score*. The final structural scores typically range between 0 and 6, with higher scores corresponding to a better seismic performance. For buildings with a structural score of 2 or less, a more detailed evaluation is required.

The basic structural hazard for a building type is defined as the negative of the logarithm (base 10) of the probability of the damage D exceeding 60% of the building value for a specified effective peak acceleration a_g :

$$\text{BSH} = -\log[P(D \geq 0.6|a_g)]. \quad (2.2)$$

The estimate of the probability of the damage D exceeding 60% (threshold of major damage) was derived from ATC-13 damage probability matrices which apply to average

buildings in each class. As ATC-13 damage probability matrices are defined in terms of intensity, intensities had to be converted into effective peak acceleration first. The values of the performance modification factors, ranging between -2.0 and +2.0, are based on expert opinions such that the resulting structural score would approximate the probability of major damage given the presence of that deficiency.

In order to use the rapid screening procedure for loss estimation a continuous relationship between the mean damage factor ($MDF = P(D \geq 0.5)$) and the structural score was derived by McCormack and Rad under the assumption that the damage factor is log normally distributed [MCR 97].

The rapid screening procedure proposed in FEMA 154 served as prototype for two assessment studies in Switzerland: one concerning the lifeline buildings in the Valais [Cap 00] and the other one concerning lifeline buildings in the city of Basel [BH 92].

Unlike proposed by the original procedure plans and elevations of the buildings were studied and each building was entered. Some modifications were necessary in order to apply the procedure to buildings in Switzerland. Those modifications concerned primarily the type of buildings considered and the corresponding basic structural hazard scores. The latter were determined based on the values of the deformation coefficient of the SIA 160 [SIA160 89] and the behaviour factor of Eurocode 8 [EC 8] for the Basel study and the Valais study respectively.

For the assessment of public buildings in the canton Aargau in Switzerland a three-phase procedure was developed [BKNS 97][KB 01]. The first phase consists of a rapid screening of the buildings resulting in a risk score. The higher the risk score the higher the risk of collapse resulting in casualties. Only the buildings with a risk score above a certain threshold are considered in phase 2. The risk score is a product of the casualty score and collapse probability score. The building characteristics and corresponding scores were determined by experts.

A method for vulnerability assessment and damage estimation for earthquake scenarios based on score assignments was also developed and applied successfully in Italy (so called GNDT method), most recently to the city of Catania [BBP 88][FPCB 99]. Based on visual observations to identify the primary structural system of the buildings and significant seismic related deficiencies collected through field surveys, a vulnerability index is assigned to each building. The vulnerability index is obtained as a weighted sum of the scores of those structural elements which are supposed to play an important role in the seismic response of a building. The higher the vulnerability index the higher the vulnerability of the building. The application of the approach to a few thousands of mainly public buildings in Italy has led to a database of seismic vulnerability data. From this database statistical distributions of the vulnerability index as a function of a few basic parameters such as building type and period of construction have been derived suitable for scenario projects with a poor building inventory. The relation between damage, vulnerability index and the seismic input was calibrated on damage observations from different earthquakes in Italy.

Clearly, the advantage of a vulnerability assessment using score assignments with respect to damage probability functions based solely on observations or on expert opinions is that it allows to update the vulnerability function following a modification in the building structure. This becomes more and more important in regions such as Italy or California where the need for upgrading of older buildings has long been acknowledged. Score assignment can help to decide on the most appropriate methods for upgrading and the effect of these on the vulnerability of the building can be evaluated immediately.

2.6 Detailed analysis procedures

Already the methods for the assessment of the vulnerability of buildings based on score assignments are rather detailed and therefore time-consuming. More sophisticated methods, implying a more detailed analysis and more refined models, take even more time and serve therefore for the evaluation of individual buildings only, possibly as a further step after the rapid screening of potential hazardous buildings in a multi-phase procedure. They are not suitable for earthquake scenario projects where a large number of buildings have to be evaluated. Nevertheless, the concepts behind those methods can be valuable for the development of new simple methods and hence, the main analysis procedures shall be briefly outlined.

The analysis procedures can be divided into linear procedures (linear static and linear dynamic) and nonlinear procedures (nonlinear static and nonlinear dynamic).

1) Linear static procedures

In a linear static procedure the building is modelled as an equivalent single-degree-of-freedom (SDOF) system with a linear elastic stiffness and an equivalent viscous damping. The seismic input is modelled by an equivalent lateral force with the objective to produce the same stresses and strains as the earthquake it represents. Based on an estimation of the first fundamental frequency of the building using empirical relationships or Rayleigh's method, the spectral acceleration S_a is determined from the appropriate response spectrum which, multiplied by the mass of the building m , results in the equivalent lateral force V :

$$V = S_a \cdot m \cdot \sum_i C_i \quad (2.3)$$

The coefficients C_i take into account issues like second order effects, stiffness degradation, but also force reduction due to anticipated inelastic behaviour. The lateral force is then distributed over the height of the building and the corresponding internal forces and displacements are determined using linear elastic analysis.

These linear static procedures are used primarily for design purposes and are incorporated in most codes. Their expenditure is rather small. However, their applicability is restricted to regular buildings for which the first mode of vibration is predominant.

2) Linear dynamic procedures

In a linear dynamic procedure the building is modelled as a multi-degree-of-freedom (MDOF) system with a linear elastic stiffness matrix and an equivalent viscous damp-

ing matrix. The seismic input is modelled using either modal spectral analysis or time-history analysis. Modal spectral analysis assumes that the dynamic response of a building can be found by considering the independent response of each natural mode of vibration using linear elastic response spectra. Only the modes contributing considerably to the response need to be considered. The modal responses are combined using schemes such as the square-root-sum-of-squares. Time-history analysis involves a time-step-by-time-step evaluation of building response, using recorded or synthetic earthquake records as base motion input. In both cases the corresponding internal forces and displacements are determined using again linear elastic analysis. The advantage of these linear dynamic procedures with respect to linear static procedures is that higher modes can be considered which makes them suitable for irregular buildings. However, again they are based on linear elastic response and hence their applicability decreases with increasing nonlinear behaviour which is approximated by global force reduction factors.

3) Nonlinear static procedures

In a nonlinear static procedure the building model incorporates directly the nonlinear force-deformation characteristics of individual components and elements due to inelastic material response. Several methods exist (e.g. [ATC 40][FEMA 273]). They all have in common that the nonlinear force-deformation characteristic of the building is represented by a pushover curve, i.e. a curve of base shear vs. top displacement, obtained by subjecting the building model to monotonically increasing lateral forces or increasing displacements, distributed over the height of the building in correspondence to the first mode of vibration, until the building collapses (cf. Section 3.4). The maximum displacements likely to be experienced during a given earthquake are determined using either highly damped or inelastic response spectra.

Clearly, the advantage of these procedures with respect to the linear procedures is that they take into account directly the effects of nonlinear material response and hence, the calculated internal forces and deformations will be more reasonable approximations of those expected during an earthquake. However, only the first mode of vibration is considered and hence these methods are not suitable for irregular buildings for which higher modes become important.

4) Nonlinear dynamic procedures

In a nonlinear dynamic procedure the building model is similar to the one used in nonlinear static procedures incorporating directly the inelastic material response using in general finite elements. The main difference is that the seismic input is modelled using a time-history analysis which involves time-step-by-time-step evaluation of the building response.

This is the most sophisticated analysis procedure for predicting forces and displacements under seismic input. However, the calculated response can be very sensitive to the characteristics of the individual ground motion used as seismic input; therefore several time-history analysis are required using different ground motion records. The main value of nonlinear dynamic procedures is as a research tool with the objective to simulate the behaviour of a building structure in detail, i.e. to describe the exact dis-

State of the art

placement profiles, the propagation of cracks, the distribution of vertical and shear stresses, the shape of the hysteretic curves, etc.

3 A method to evaluate the vulnerability of existing buildings

3.1 Introduction

For the purpose of seismic risk assessment, an evaluation method was developed within the scope of the earthquake scenario project for the city of Basel, Switzerland, in order to determine the seismic vulnerability of existing buildings. In this chapter, the principle of the evaluation method is introduced in a general way, valid for masonry as well as for reinforced concrete buildings. The specific application to masonry buildings and reinforced concrete buildings follows in Chapters 4 and 5 respectively.

After some general remarks on the positioning of the method within currently available methods in Section 3.2 and on the difference between design and evaluation in Section 3.3, the definition of a vulnerability function is given in Section 3.4. In Section 3.5 the idea of the capacity curve of a building is introduced and how it can be constructed in a very simplified way. Section 3.6 focus on the description of the seismic demand. Finally the construction of the vulnerability function is described in Section 3.7.

3.2 Positioning of the method

In Chapter 2 currently available methods for the evaluation of existing buildings were introduced ranging from very simplified and rather global loss estimation methods based on observations and expert opinions, via simple analytical models and score assignments, to rather detailed analysis procedures (Table 2.1).

Global loss estimation methods based on observations and expert opinions have been used successfully in earthquake prone areas where they have a lot of experience with earthquakes and a statistical evaluation of observations is possible; however, the validity for cities in Switzerland and their building techniques is questionable. Score assignments are already rather time consuming and also require some experience from earthquakes in order to rate the structural deficiencies. The linear analysis procedures, although rather simple, are not considered suitable acknowledging the importance of the nonlinear displacement capacity for the seismic behaviour of a building. The nonlinear dynamic analysis procedures, however, imply very high computational effort with a rather limited validity (a unique building subjected to a specific earthquake) and are therefore not very practical for earthquake scenarios where a large number of buildings have to be evaluated. Also, the link from the results of a nonlinear dynamic analysis to some statement on the loss is usually not made.

For the earthquake scenario project for the city of Basel, Switzerland, it was therefore decided to use an analytical approach with simple models of the buildings based on the nonlinear static procedures. The method, which is presented in the following, is simple enough to allow the evaluation of a large number of buildings; still, the use of engineer-

ing models of the structure allow an understanding of the important parameters. In comparison with the two existing analytical approaches (cf. Section 2.4) the method is more detailed reflecting the lack of experience from past earthquakes in Switzerland.

3.3 Difference between design and evaluation

The essential difference between the design of new buildings and the evaluation of existing buildings is the point of view. In design the objective is to create a new building which can resist the expected forces (horizontal and vertical) with an appropriate safety margin. Starting from a structural model of the building and the expected applied forces the required sections of the structural elements have to be determined for a chosen material. It is common practice to choose a slightly conservative model, i.e. to neglect the positive influence of some elements, firstly to simplify the model and secondly to be on the safe side. Also, the material strength is usually multiplied by a certain strength reduction factor, whereas the expected applied forces are enhanced to take into account uncertainties. The choice of the strength reduction factors and the design forces are governed by the aim for economic optimization, however they are usually chosen to keep the risk of damage extremely low i.e in building design this compares with an accepted annual probability for achieving the ultimate capacity of about 0.01% [PP 92]. In earthquake engineering a rational design becomes more important accepting a higher risk of damage. Here the annual probability for achieving the ultimate capacity can be as high as 1 to 3%. In evaluation the objective is to determine how an existing building will respond to given forces. This corresponds to an analysis of a building structure where the structural elements, the materials and the dead loads are given. It is not desired to calculate a worst case scenario by choosing a conservative model and making conservative assumptions on the material properties but to assess the most probable behaviour of the building subjected to the applied action. Thus, the real material properties and the real loading have to be taken without any safety factors as these would falsify the results. Also the model should be as close as possible to reality taking into account all structural elements that help to support the applied forces.

It follows that the use of codes of practice for the evaluation of existing buildings is not always appropriate as these are usually too stringent in order to assure a safe design of a new building. This is especially true for unreinforced masonry buildings for which the code procedures tend to be very conservative (usually based on elastic mechanics of materials) due to a lack of understanding. In fact, non-compliance to most codes for unreinforced masonry buildings does not necessarily imply an inadequate seismic behaviour; some unreinforced masonry buildings have performed excellently during major earthquakes [Br 94a].

The evaluation of existing buildings plays an important role in earthquake scenario projects where the risk of damage in a certain area is estimated in order to decide on appropriate risk reduction strategies.

3.4 Definition of a vulnerability function

In general, a vulnerability function is a relationship which defines the expected damage for a building or a class of buildings as a function of the ground motion (Figure 3.1). The two key elements of a vulnerability analysis are the capacity of the building and the seismic demand. In order to estimate the damage D , the ability of the building to resist constraints (capacity of the building) must be compared with the constraints on the structure due to the earthquake ground motion (seismic demand).

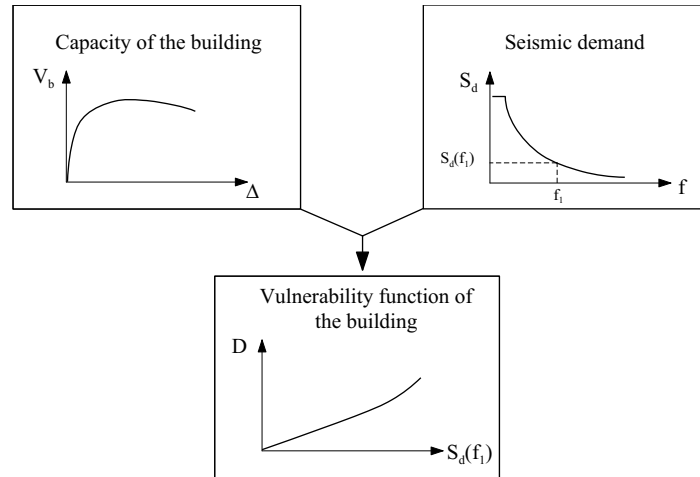


Figure 3.1: Principle of a vulnerability function

In earthquake engineering the capacity of a building to resist seismic action is presented by a capacity curve which is defined as the base shear V_b acting on the building as a function of the horizontal displacement at the top of the building Δ , also often referred to as a pushover curve. The shear capacity of the building refers to the maximum base shear the building can sustain $V_{b,m}$ and the displacement capacity refers to the ultimate displacement at the top of the building $\Delta_{b,u}$.

In a more general way, it is possible to express the capacity of any structure (building) or structural element (wall, wall element) to resist seismic action by the shear force acting on it as a function of the horizontal displacement at the top (capacity curve). Likewise, the shear capacity of any structure or structural element refers to the maximum shear force it can sustain, and the displacement capacity refers to its ultimate horizontal displacement.

To express the seismic demand, until very recently, the “intensity” was used nearly exclusively. This is a descriptive parameter of an earthquake based on observations of the effects of the earthquake on the environment. It has the advantage that historical data on earthquakes are available. However, information on the real ground movement is lost and empirical relationships between intensity and peak ground acceleration vary a lot (cf. Section 7.3). Some methods use the peak ground acceleration as the parameter defining the earthquake. However, in that case, not only the information on the duration of the earthquake is lost, but also the information on the frequency content. Thus, a better parameter is the spectral acceleration S_a , or, as we will see, the spectral displacement S_d .

For the purpose of comparison with other methods and/or test results the peak ground acceleration a_g is also used.

The ground movement due to an earthquake does not happen in a fixed direction, on the contrary, in a horizontal plane the direction of the ground movement varies, including all angles from 0 to 360°. However, the biggest amplitudes of the ground movement usually occur in one direction, the amplitudes in the other directions, especially orthogonal to the direction of the biggest amplitudes, are much smaller [Mo 93]. Thus the constraints on the building are predominant in the direction of the biggest amplitudes which is referred to in the following as the ‘direction’ of the earthquake.

For regular buildings, it is common practice in earthquake engineering to consider the earthquake action (i.e. the direction of the biggest amplitudes of the ground movement) separately in two orthogonal directions, usually corresponding to the principal axes of the building, using plane analysis. Thus for one building two vulnerability functions are calculated. For earthquake scenarios, the direction of an earthquake is usually not taken into account and, based on the two vulnerability functions in the two principal directions, a single representative vulnerability function of the building has to be calculated. This representative vulnerability function should describe the overall behaviour of the building and hence should be some sort of ‘mean’ of the two vulnerability functions in the two principal directions. Choosing the more unfavourable vulnerability function of the two would lead to a “worst case scenario” which is not desired in the case of earthquake scenarios, as it can be assumed that on average the building behaves better. For very irregular buildings the two vulnerability functions in the two principal directions might be very different and thus the direction of the earthquake action plays an important role. Since this is not taken into account, the inaccuracy resulting from the introduction of a single representative function increases. This has to be kept in mind when considering the evaluation method proposed here.

3.5 Capacity curve of a building

3.5.1 General considerations

The capacity curve is generally constructed to represent the first mode response of the building based on the assumption that the structure responds to a seismic input predominantly in its fundamental mode of vibration (Figure 3.2). Thus the distribution of the horizontal force over the height of the building should comply with the first mode shape, the lateral storey forces being proportional to the product of the mass and the fundamental mode shape:

$$F_i = \frac{m_i \phi_i}{\sum m_i \phi_i} \cdot V_b. \quad (3.1)$$

m_i is the concentrated mass and ϕ_i the first mode displacement at the i -th floor level. V_b is the base shear and corresponds to the sum of the lateral storey forces. However, the fundamental mode shape is usually not known at the beginning. To determine a first approximation, either the shape can be estimated, considering that depending on the

structural system, walls or frames, the first mode shape corresponds to a parabola (flexural displacement) or a nearly straight line (shear displacement), or lateral forces in accordance with the code can be applied at each storey and the resulting displacements used as approximation of the first fundamental mode shape:

$$F_i = \frac{m_i h_i}{\sum m_i h_i} \cdot V_b. \quad (3.2)$$

h_i is the height of the i -th storey. However, the results are not very sensitive to the force distribution, any reasonable distribution will do.

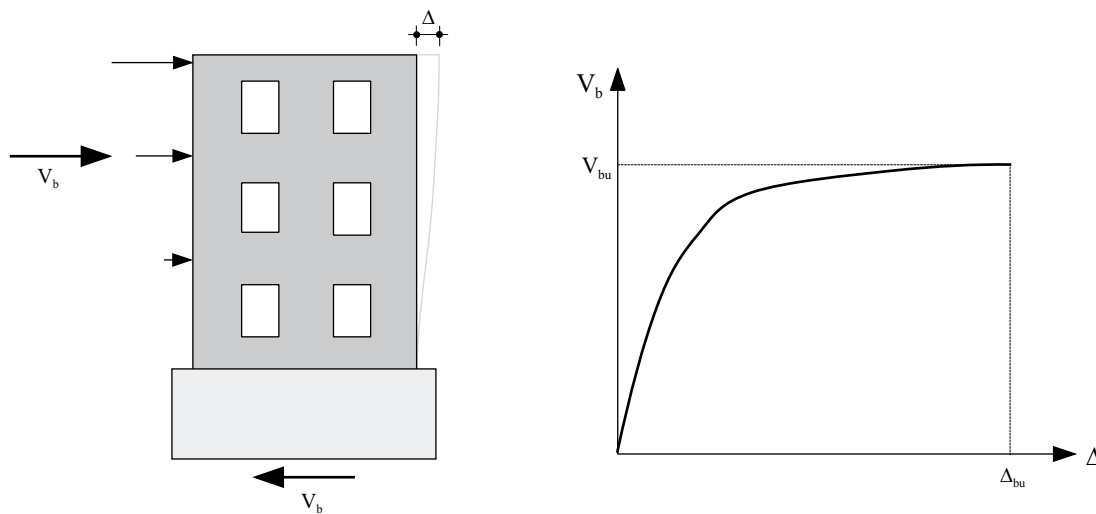


Figure 3.2: Capacity curve

Increasing the total horizontal force acting on the building or the displacements respectively, the capacity curve of the building is obtained by plotting the base shear V_b as a function of the top displacement Δ (Figure 3.2). As the application of the horizontal forces is first considered under monotonic action, the effects of cyclic loading have to be included in a further step (cf. Section 4.2.5 for masonry buildings and Section 5.4.5 for reinforced concrete buildings).

3.5.2 Identification of structural and non-structural elements

In every building it must be distinguished between structural and non-structural elements. Structural elements are those elements of the building that help to support the horizontal and vertical forces acting on a building. The sum of all structural elements constitutes the structural system. The most common structural systems found in buildings are:

- Structural frame systems: The structural elements are beams and columns, either made of steel or reinforced concrete, meeting at nodes.
- Structural wall systems: The structural elements are (structural) walls, either made of reinforced concrete or masonry.

A method to evaluate the vulnerability of existing buildings

- Dual systems: In these, reinforced concrete frames are combined with reinforced concrete or masonry walls to carry the vertical and horizontal forces.

Non-structural elements are those elements of the building that are connected to the structural system, but without a force bearing function. Examples of non structural elements are:

- Non-structural walls (partitions), used for separation purposes, however they do not carry any vertical or horizontal forces.
- Gable walls
- Façade elements, including windows and balustrades
- Staircases
- Ceilings
- Installations (mains, air-conditioning).

In contrast to the design of a building, where the structural system is chosen and therefore known, the evaluation of the building requires first the identification of the structural system with all its structural elements, since only these contributes to the capacity of the building. The non-structural elements add to the weight only. In the case of reinforced concrete buildings the identification of the structural elements is usually done without difficulty, as the structural walls and/or the frames can be easily identified. In the case of masonry buildings, this is usually less obvious since all the walls (façade walls and inner walls) consist of masonry and often no clear distinction exists. However, it is common practice to consider all walls with a thickness $t \geq 12$ cm to be structural walls, i.e. acting to support the vertical and horizontal forces [Ba 94]. Not all the walls with a thickness $t \geq 12$ cm need to be structural, especially in modern buildings more and more non-structural walls exists with a thickness $t \geq 12$ cm, nevertheless, in the absence of more detailed information the above assumption seems reasonable.

Considering the plan of the building in Figure 3.3, the walls shaded in black are considered as structural walls, having a thickness $t \geq 12$ cm whereas the walls shaded in grey with a thickness $t < 12$ cm are considered as non-structural walls.

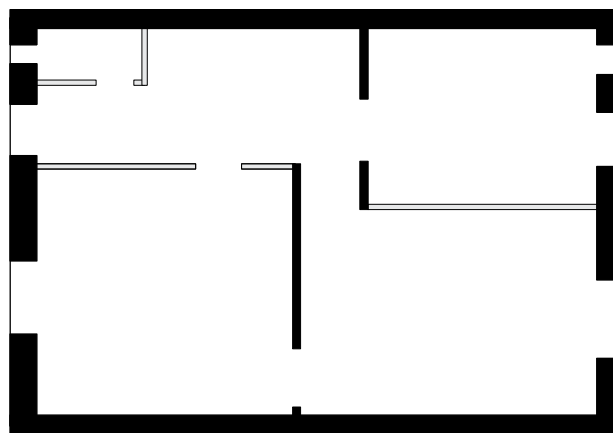


Figure 3.3: Identification of structural and non-structural walls

3.5.3 Terminology and structural models

Considering the building in Figure 3.4, the following terminology used in the context of the construction of the capacity curve of a building, irrespective of the material (masonry or reinforced concrete), is introduced:

- A wall is defined as a structural element of the building of length l_w and a height equal to the total height of the building, H_{tot} (indicated by the hatched area in Figure 3.4).
- A wall element can be any part of a wall of length l_w and any height h (not shown in Figure 3.4).
- A pier is a wall element of length l_w and of a height h_p equal to the height of the adjacent opening, which can be a window or a door (indicated by the lightly shaded areas).
- The spandrels are those parts of the building which lie between two openings in the vertical direction, thus joining the walls in one plane (indicated by the darkly shaded areas).
- All the walls in one plane joined by floors and spandrels constitute a wall plane. Thus a façade of a building constitutes a wall plane but likewise all the walls in one plane in the interior of the building.
- A wall panel is defined as part of a wall plane of any length l and a height equal to the storey height h_{st} (not shown in Figure 3.4).

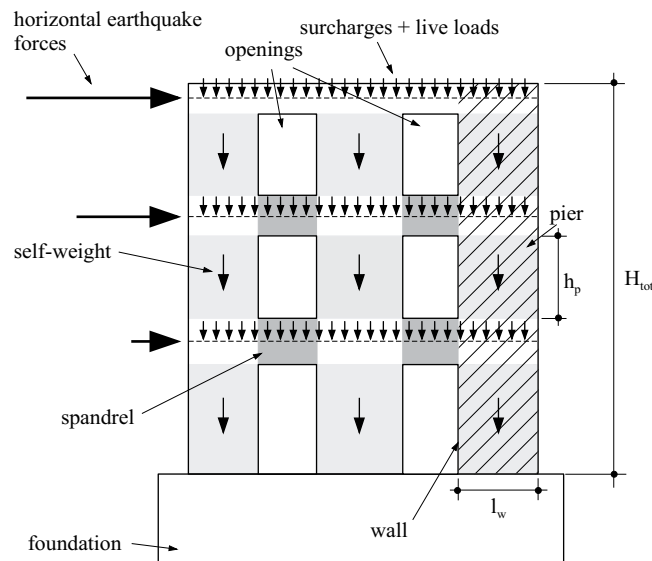


Figure 3.4: Terminology

Also shown in Figure 3.4 are the applied forces:

- The equivalent horizontal earthquake forces are assumed to be induced at the floor levels where the mass is the highest.
- The vertical loads include the self weight of the structure as a volume force, and the surcharges (non structural elements) and the live loads applied at the floor levels.

A method to evaluate the vulnerability of existing buildings

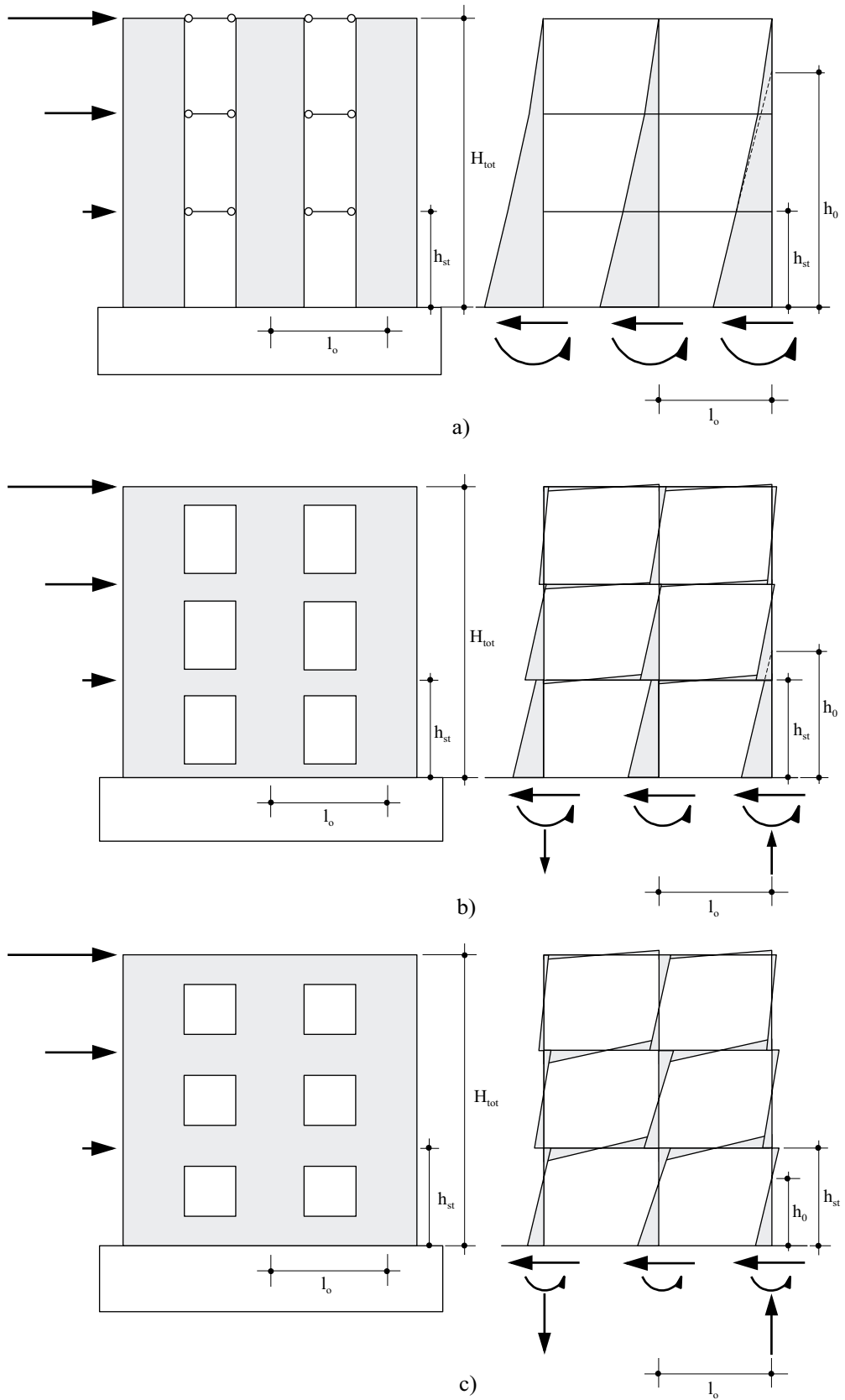


Figure 3.5: Bending moment distribution for three cases of coupled walls a) negligible coupling effect (interacting cantilever walls), b) intermediate coupling effect and c) strong coupling effect due to horizontally acting earthquake forces and corresponding reactions

Due to the fact that the walls are joined by floors and spandrels, a coupling effect is produced. Depending on the extent of the spandrels, this coupling effect will be bigger or smaller. In the absence of spandrels where the walls are joined only by the floors (usually the case for reinforced concrete buildings) the coupling effect is negligible and the walls can be regarded as interacting cantilever walls. For deep spandrels (often found in masonry buildings) the coupling effect is considerable and has to be taken into account. A system of coupled walls can be analysed using a frame model.

In a general way, every wall plane can be regarded as a system of coupled walls, the case of interacting cantilever walls being a “limit case” where the stiffness of the spandrels becomes negligible with respect to the stiffness of the walls and hence the coupling effect reduces to zero.

Figure 3.5 shows the bending moment distribution for three cases of coupled walls submitted to horizontal forces. Figure 3.5 a) shows the case where the walls are only joined by the floors and hence the coupling effect is negligible, the whole system can be regarded as interacting cantilever walls. Figure 3.5 c) shows the case of very deep spandrels producing a considerable coupling effect and Figure 3.5 b) shows an intermediate case, with some coupling effect.

In the case of interacting cantilever walls (Figure 3.5 a), the total overturning moment due to the applied horizontal forces is carried by the walls alone, proportional to their stiffness, resulting in very high bending moments at the base of the walls. In the case of strongly coupled walls (Figure 3.5 c), the total overturning moment due to the applied horizontal forces is mainly carried by high normal forces in the outer walls resulting from the vertical shear forces transmitted by the spandrels. The bending moments at the base of the walls are therefore rather small compared to those of a cantilever wall. In the intermediate case (Figure 3.5 b) the frame action is less and hence that part of the total overturning moment carried by the walls is increased whereas the normal forces are reduced.

For regular frames the extent of the coupling effect can be expressed by a single parameter, the height of zero moment h_0 (Figure 3.5). The smaller the value of h_0 , the bigger the coupling effect. For infinitely stiff spandrels the limit value of $h_0 = 0.5 \cdot h_{st}$. As the coupling effect reduces, the height of the zero moment h_0 increases, eventually becoming greater than h_{st} .

Note that for $h_0 > h_{st}$, h_0 does not indicate the height of a true point of zero moment but corresponds to the height of the extrapolated zero moment of the pier.

The value of h_0 depends on the ratio of the flexural stiffness of the spandrel to the flexural stiffness of the pier $(EI_{sp}/l_o)/(EI_p/h_{st})$. Figure 3.6 a) gives the ratio of h_0/h_{st} as a function of $(EI_{sp}/l_o)/(EI_p/h_{st})$ for a 3x3 frame (where the first number indicates the number of walls and the second number the number of storeys) as shown in Figure 3.5 with a uniform storey height h_{st} , a uniform distance between the centre lines of the walls l_o and a triangular horizontal force distribution. For very deep spandrels, $(EI_{sp}/l_o)/((EI_p)/h_{st}) \geq 1$, the ratio of h_0/h_{st} tends to 0.6 for the outer piers and to 0.5 for the inner pier. For very flexible spandrels, h_0 might reach h_{st} , and in the limit state when the stiffness of the spandrels reduces to zero, the ratio of h_0/h_{st} will be greater than one, the bending moment distribution of the structure approaching the bending moment distribution of interacting cantilever walls.

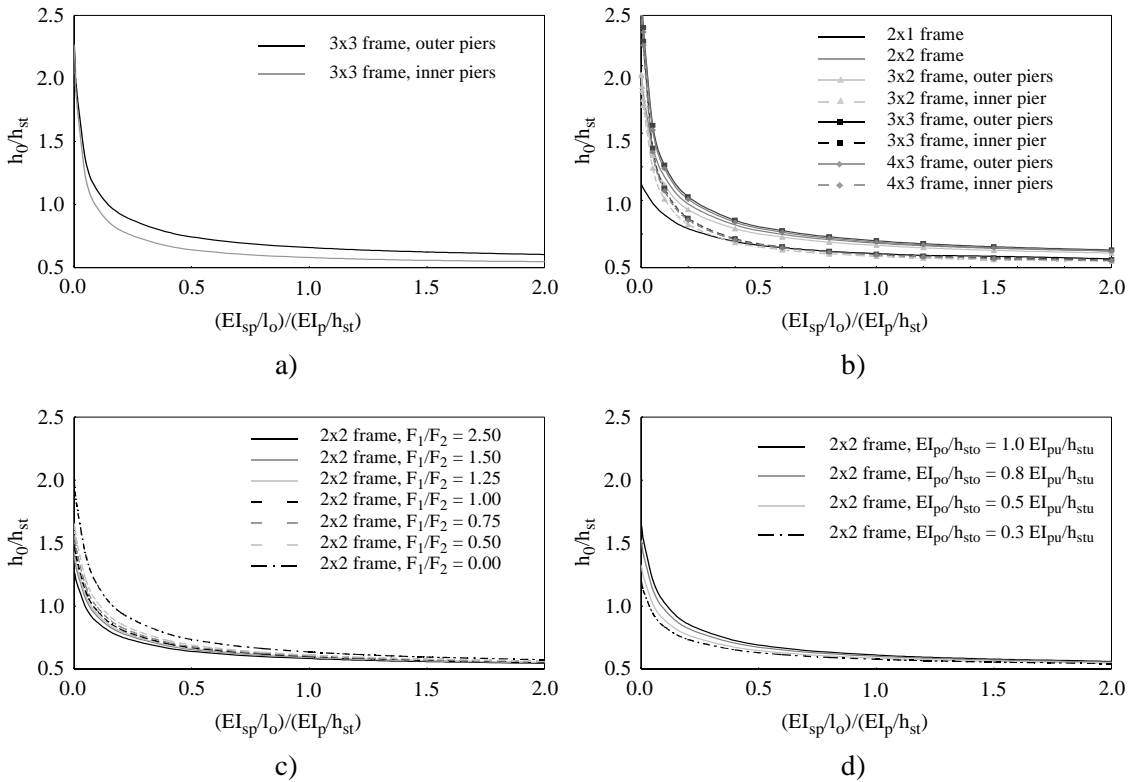


Figure 3.6: Ratio of h_0/h_{st} as a function of the ratio of the flexural stiffness of the spandrels to the flexural stiffness of the piers

Strictly speaking, the relationship of h_0/h_{st} vs. $(EI_{sp}/l_o)/(EI_p/h_{st})$ depends on various parameters. Figure 3.6 b) shows the variation of h_0/h_{st} vs. $(EI_{sp}/l_o)/(EI_p/h_{st})$ for different frames, Figure 3.6 c) shows the variation of h_0/h_{st} vs. $(EI_{sp}/l_o)/(EI_p/h_{st})$ under different horizontal force distributions (ratio F_1/F_2) and Figure 3.6 d) shows the variation of h_0/h_{st} vs. $(EI_{sp}/l_o)/(EI_p/h_{st})$ for various ratios of the stiffness of the upper piers to the stiffness of the lower piers (ratio $(EI_{po}/h_{sto})/(EI_{pu}/h_{stu})$) for a 2x2 frame. The figures show clearly that the variation in the relationship of h_0/h_{st} vs. $(EI_{sp}/l_o)/(EI_p/h_{st})$ for different input parameters is rather limited, the use of a single representative relationship therefore seems appropriate.

The transfer of the horizontal inertia forces of the floors onto the walls has to be provided by the floor-wall connection. In the case of concrete floors, the connection between floors and walls is usually good, and thus the transfer of the horizontal forces onto the walls can be guaranteed. In the case of timber floors, the connection between floors and walls can be very poor if not improved by special means such as steel bar anchorages, and the transfer of forces onto the walls may not be guaranteed leading to an uneven distribution of the forces, overstressing some walls, while others remain almost unstressed (cf. Section 6.2.3). This, however, is neglected in the following.

3.5.4 Construction of the capacity curve

It is assumed that a wall only carries shear forces about its strong axes; the shear carrying capacity about the weaker axes is neglected. Assuming the floors to be totally rigid in

their plane, thus assuring equal displacements of the walls at the floor levels, the capacity curve of the building in one direction can be obtained by superimposing the capacity curves of all the walls acting in this direction:

$$V_b(\Delta) = \sum_j V_j(\Delta). \quad (3.3)$$

j is the wall index, $j = 1 \dots n$, n being the total number of walls acting in one direction. This is allowed as long as the geometry of the building is relatively regular and torsional effects can be neglected.

Figure 3.7 shows plan and three elevations of a fictitious example building. Considering the x -direction, four walls acting in this direction can be identified, denoted by wall 1, wall 2, wall 3 and wall 4. The contribution of the two walls in y -direction is neglected. Wall 3 and wall 2 lie in one plane constituting one wall plane of the building (a façade wall plane). Wall 1 constitutes the second wall plane of the building (also a façade wall plane). Wall 4 constitutes a third wall plane in the interior of the building. Also given are three elevations of the buildings along the axes A-A, B-B and C-C. In the two outer wall planes which constitute the two façades (A-A and C-C) the spandrels are rather deep, producing a considerable coupling effect, whereas in the inner wall plane (B-B) the wall is only 'linked' by the floors leading to a very reduced coupling effect.

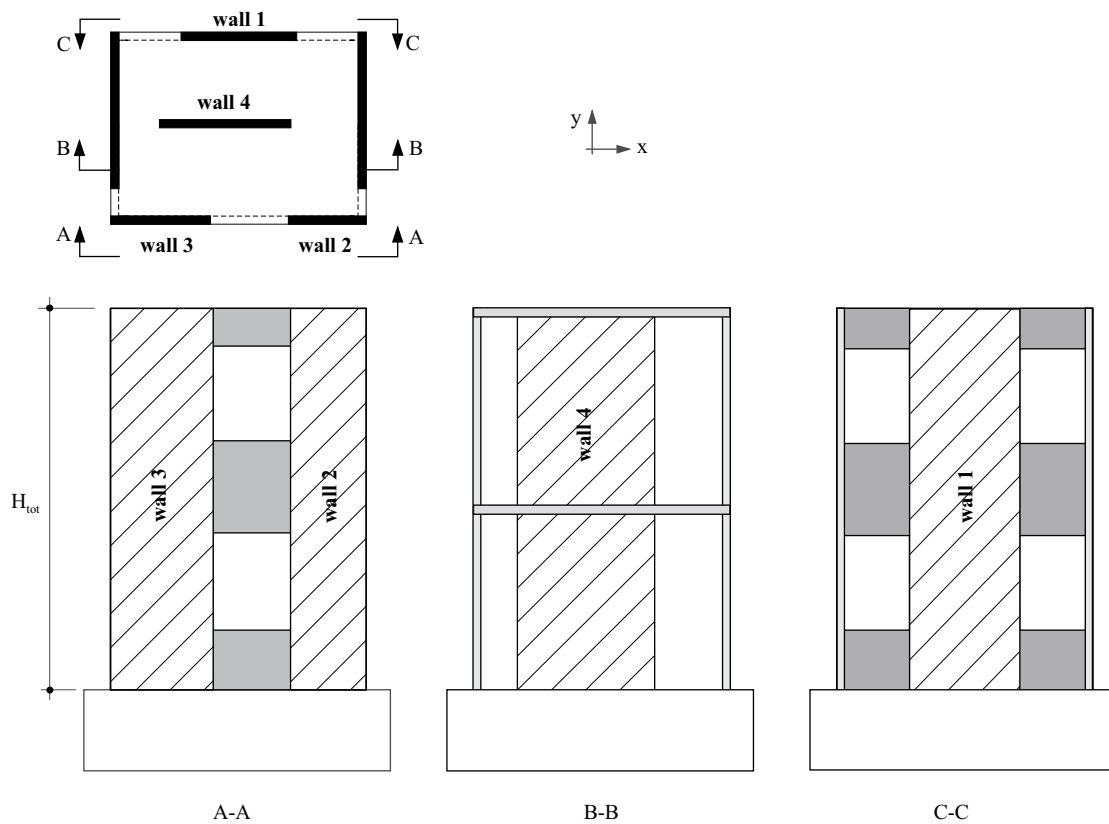


Figure 3.7: A fictitious example building

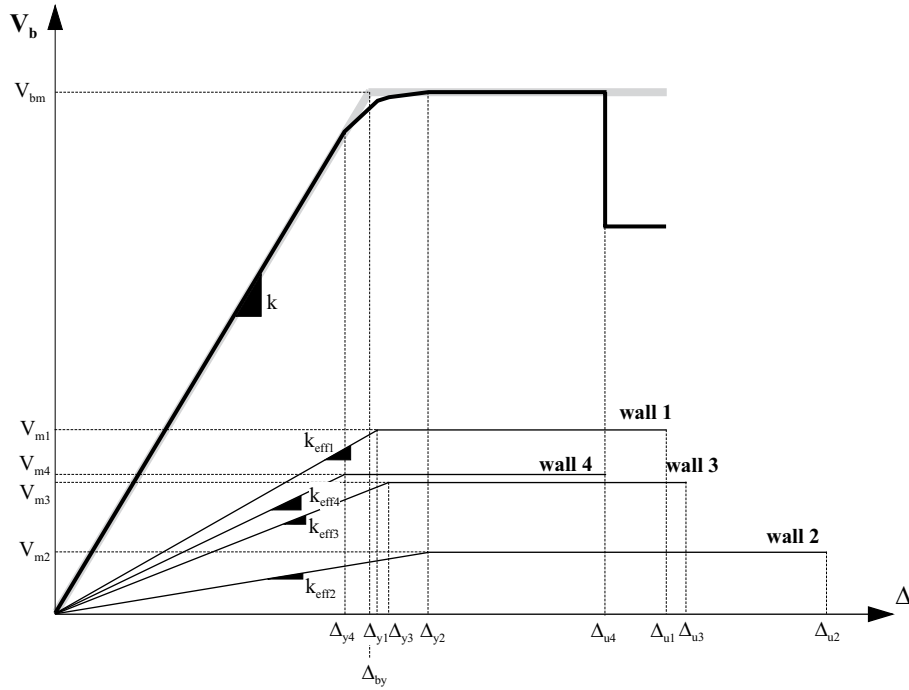


Figure 3.8: Capacity curve of the fictitious example building of Fig. 3.7

The corresponding capacity curve as shown in Figure 3.8 is given by:

$$V_b(\Delta) = V_1(\Delta) + V_2(\Delta) + V_3(\Delta) + V_4(\Delta). \quad (3.4)$$

Using a bilinear approximation of the capacity curve of the fictitious example building, the stiffness of the linear elastic part k corresponds to the sum of the effective stiffnesses of the walls:

$$k = \frac{V_{bm}}{\Delta_{by}} = \sum_j k_{effj}. \quad (3.5)$$

V_{bm} is the shear capacity and Δ_{by} the nominal top yield displacement of the building (Figure 3.8).

In the case shown in Figure 3.8 this leads to a stiffness of the building k :

$$k = k_{eff1} + k_{eff2} + k_{eff3} + k_{eff4}. \quad (3.6)$$

Hence, in order to determine the capacity curve of the building, the capacity curves of the walls have to be determined first.

For the capacity curve of a wall, a bilinear approximation is used with a linear elastic part up to the point where the shear capacity of the wall V_m is reached and a perfectly plastic part with zero stiffness (Figure 3.9).

Thus, the bilinear capacity curve of a wall is defined by three parameters, the shear capacity of the wall V_m , the nominal yield displacement at the top of the wall Δ_y and the nominal ultimate displacement at the top of the wall Δ_u . They are determined depending on the material of the wall, masonry or reinforced concrete, and will be discussed in detail in Section 4.2.3 for masonry walls and Section 5.4 for reinforced concrete walls.

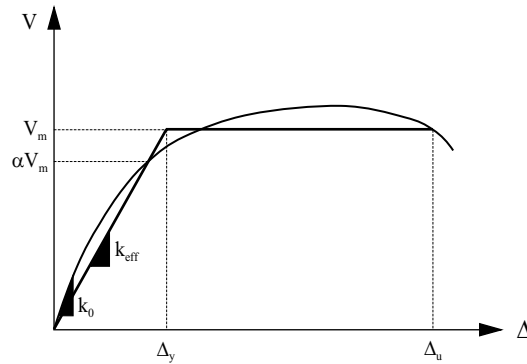


Figure 3.9: Capacity curve of a wall

3.6 Seismic demand

The seismic demand is determined using a response spectrum. A response spectrum presents the maximum response of single-degree-of-freedom systems (SDOF) as a function of their frequencies. Traditionally in earthquake engineering an acceleration response spectrum is used with regard to force based design and assessment procedures. Recently, design and assessment procedures focus more on displacements and deformations which are considered to be the more relevant parameters. The use of a displacement response spectrum seems therefore more appropriate. However, except for very small frequencies ($f < 0.2\text{Hz}$) the following simple relationship holds:

$$S_a \approx \omega^2 \cdot S_d. \quad (3.7)$$

S_a and S_d are the spectral acceleration and the spectral displacement respectively, and ω is the corresponding circular frequency, $\omega = 2\pi \cdot f$ (f is the frequency in Hz).

As an example, the elastic design acceleration response spectrum for medium stiff soils and 5% damping according to the Swiss Standard for zone 3a [SIA160 89] is shown in Figure 3.10 a). Figure 3.10 b) shows the corresponding displacement response spectrum using Equation (3.7).

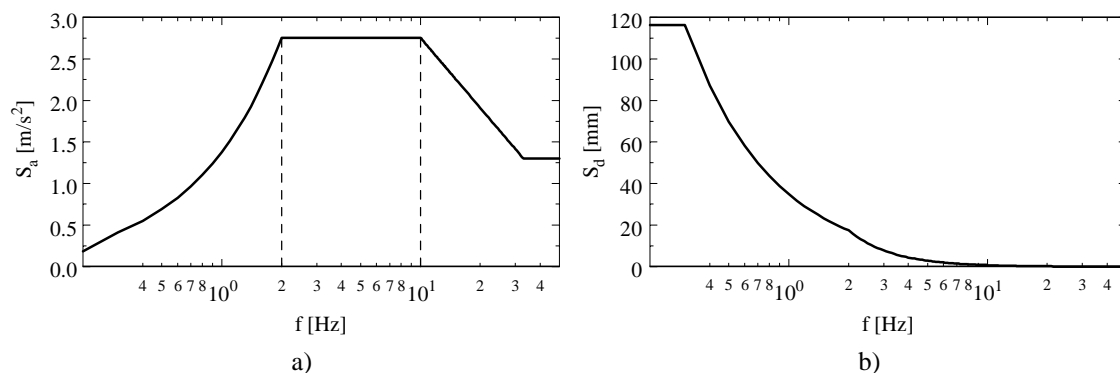


Figure 3.10: a) Elastic design acceleration response spectrum for medium stiff soils and 5% damping according to the Swiss Standard for zone 3a [SIA160 89] and b) the corresponding displacement response spectrum

It should be noted that even though the response spectrum of Figure 3.10 is considered to be valid for a whole region, response spectra depend on the local site conditions and may vary significantly in a region such as the city of Basel. This effect is taken into account in the earthquake scenario project for the city of Basel by a microzonation [Ki 02]. Recently the use of response spectra in the ADRS format has become increasingly popular [ATC 40][Fa 98]. ADRS stands for Acceleration-Displacement Response Spectrum. As the name indicates, this is a diagram where the spectral acceleration is plotted vs. the spectral displacement. Lines radiating from the origin of this diagram have constant periods $T = 2\pi/f$. The advantage of this format is that capacity and demand can be plotted in the same diagram allowing a graphical solution. However, it should be noted that it is only a different representation of the same data, it does not give further information. The use of either formats is therefore the choice of the engineer. In the following, the displacement response spectrum will be used to represent the seismic input throughout this work.

The use of a response spectrum assumes that the building, which can be seen as a multi-degree-of-freedom system (MDOF) where the masses are concentrated at the floor levels and the mass of the walls is divided between the two levels above and below (Figure 3.11), can be described by an equivalent SDOF system characterised with an equivalent mass m_E and an equivalent stiffness k_E , having the same fundamental frequency as the MDOF system:

$$f_1 = \frac{1}{2\pi} \cdot \sqrt{\frac{k_E}{m_E}} \quad (3.8)$$

If the stiffness k of the real structure obtained from the bilinear approximation of the capacity curve of the building (cf. Figure 3.8 and Equation (3.5)) is used as the equivalent stiffness k_E of the SDOF system

$$k_E = k = \frac{V_{bm}}{\Delta_{by}} \quad (3.9)$$

the equivalent mass is given as

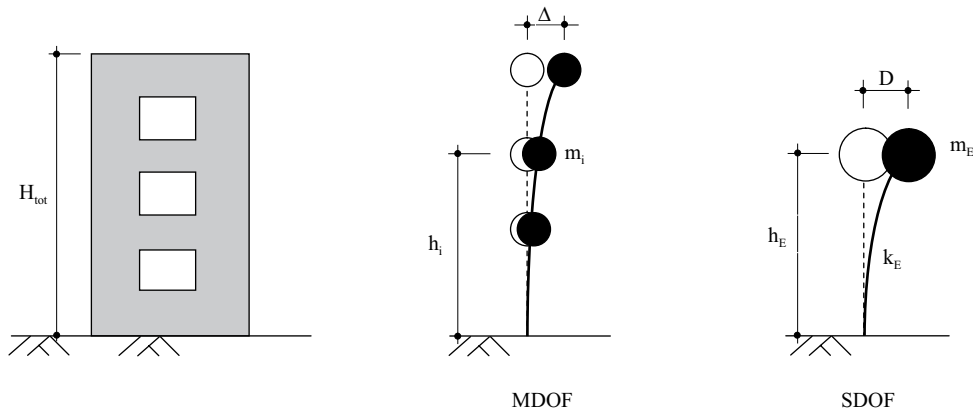


Figure 3.11: Equivalent SDOF system

$$m_E = \sum m_i \phi_i \quad (3.10)$$

in which m_i is the concentrated mass and ϕ_i is the first mode displacement at the i -th floor level normalized such that the first mode displacement at the top storey $\phi_n = 1$. The equivalent height is

$$h_E = \frac{\sum h_i m_i \phi_i}{\sum m_i \phi_i} \quad (3.11)$$

in which h_i is the height of the i -th floor level.

Each quantity of the MDOF system can be transformed into the equivalent SDOF system using the following equation:

$$Q = \Gamma \cdot Q_E. \quad (3.12)$$

Q represents the quantities in the MDOF system (base shear V_b , top displacement Δ) and Q_E represents the quantities in the equivalent SDOF system (force F_E , displacement D , with the maximum displacement denoted as S_d). Γ is the modal participation factor defined as

$$\Gamma = \frac{\sum m_i \phi_i}{\sum m_i \phi_i^2}. \quad (3.13)$$

Two different approaches exist to obtain the displacement demand Δ_D at the top of the building taking into account the nonlinear behaviour of the building. One is the use of inelastic demand spectra, the other is the use of highly damped elastic spectra.

Using inelastic demand spectra, the displacement demand Δ_D at the top of the building (= n -th storey) is related to the equivalent elastic displacement Δ_{be} :

$$\Delta_D = c_n \cdot \Delta_{be}. \quad (3.14)$$

This is illustrated in Figure 3.12 showing the base shear - top displacement relationship for a linear elastic behaviour and a nonlinear behaviour.

The constant c_n can be determined as a function of the strength reduction factor R and the ductility demand μ_D :

$$c_n = \frac{\mu_D}{R}. \quad (3.15)$$

μ_D is defined as:

$$\mu_D = \frac{\Delta_D}{\Delta_{by}} \quad (3.16)$$

and the strength reduction factor R is defined as:

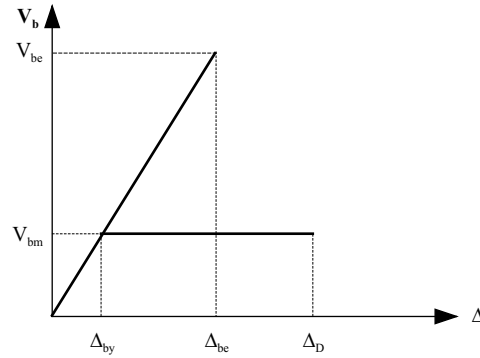


Figure 3.12: Base shear - top displacement relationship for a linear elastic behaviour and a non-linear behaviour

$$R = \frac{V_{be}}{V_{bm}} \quad (3.17)$$

with

$$V_{be} = k \cdot \Delta_{be} = k \cdot \Gamma \cdot S_d(f_1). \quad (3.18)$$

The first to have studied this kind of relationship were Newmark et al. [VN 60] [VNC 65]. Based on elastic and inelastic response spectra of the El Centro, California, earthquake of May 18, 1940, they observed that:

- i) in the low frequency range, an elastic and an inelastic system have approximately the same maximum displacement;
- ii) in the intermediate frequency range, the principle of conservation of energies gives a good enough approximation, i.e. the area under the base shear - top displacement diagram of the linear elastic system is equal to the area under the base shear - top displacement diagram of the nonlinear system.
- iii) in the high frequency range, an elastic and an inelastic system have the same force.

In a simplified way, these results can be represented as a function of the frequency:

- i) Principle of equal maximum displacement, valid for $f_1 < f_{c1}$

$$R = \mu_D \quad (3.19)$$

- ii) Principle of equal energy, valid for $f_1 > f_{c2}$

$$R = \sqrt{2\mu_D - 1} \quad (3.20)$$

- iii) $f_1 > 33$ Hz

$$R = 1 \quad (3.21)$$

The third case does usually not apply to buildings. The two limiting frequencies f_{c1} and f_{c2} depend on the ductility of the system and the characteristic values of the elastic spectrum. Typical values are $f_{c1} \approx 1.4$ Hz and $f_{c2} \approx 2$ Hz. For frequencies between f_{c1} and f_{c2} , R is obtained by interpolation between the two principles. These results should not

be considered as being ‘exact’ but rather as presenting an average tendency. However, discrepancies are not unusual.

Having found the constant c_n the displacement demand Δ_D at the top of the building (= n-th storey) can be obtained from the following equation:

$$\Delta_D = c_n \cdot \Gamma \cdot \phi_n \cdot S_d(f_1). \quad (3.22)$$

ϕ_n corresponds to the first mode displacement at the top storey (= n-th storey) of the MDOF system.

Other $R - \mu_D - f_1$ relationships have been developed, based on the same principle. Vidic et al. [VFF 94] proposed the following $R - \mu_D - f_1$ relationship:

$$R = \begin{cases} 1.35(\mu_D - 1)^{0.95} \cdot \frac{T_1}{T_0} + 1, & T_1 \leq T_0 \\ 1.35(\mu_D - 1)^{0.95} + 1, & T_1 > T_0 \end{cases} \quad (3.23)$$

with

$$T_0 = 0.75\mu_D^{0.2} \cdot T_c \leq T_c \quad (3.24)$$

T_c is the characteristic period of ground motion and usually defined as the transition period from the constant acceleration segment of the response spectrum to the constant velocity segment of the spectrum. T_1 is the fundamental period of the building $T_1 = 2\pi/f_1$.

Many other $R - \mu_D - f_1$ relationships exist, a good overview is given by Miranda and Bertero [MB 94] and Chopra and Goel [CG 99].

It is often considered as the major drawback of all these methods that they do not regard the change in the fundamental frequency with increasing nonlinear behaviour nor the hysteretic energy dissipation characteristics. As the damage increases, the stiffness reduces which will affect directly the fundamental frequency (and thus the spectral response $S_d(f_1)$) and the damping increases. Also looking at displacements as the most relevant parameter it is felt that the inelastic spectrum approach focuses too much on strength.

In the second approach, based on the substitute-structure approach of Shibata and Sozen [SS 76], the displacement demand Δ_D at the top of the building is found from a highly damped elastic spectrum and an equivalent stiffness corresponding to the secant stiffness:

$$k_{equ} = \frac{V_m}{\Delta_D}. \quad (3.25)$$

The equivalent stiffness depends on the required top displacement Δ_D and illustrates the fact that the capacity of a building and the seismic demand are not independent.

It should be noted that the equivalent stiffness only corresponds to the final point of the response independent of the initial stiffness and the change in the stiffness along the load path.

The critical point of the procedure is the use of highly damped elastic spectra. Eurocode 8 [EC 8] proposes the following correction factor for response spectra for damping values different from 5% which is frequently adopted in studies on displacement based design [Ca 99][BCE 01]:

$$\eta = \sqrt{\frac{7}{2 + \beta_{\text{equ}}}}. \quad (3.26)$$

β_{equ} is the equivalent viscous damping which corresponds to a combination of viscous damping that is inherent in the structure (usually taken as 5%) and hysteretic damping that is related to the area inside the hysteresis loop and therefore depends on the ductility demand. The most common way to define equivalent viscous damping is to equate the energy dissipated in a hysteresis loop of the structure to the energy of an equivalent viscous system [Ch 95] resulting in:

$$\beta_{\text{equ}} = \frac{1}{4\pi} \cdot \frac{E_D}{E_{s0}} + \beta_v. \quad (3.27)$$

E_D is the energy dissipated by damping which corresponds to the area enclosed by the hysteresis loop, E_{s0} is the maximum strain energy and β_v is the viscous damping related to the elastic response.

Shibata and Sozen [SS 76] proposed the following relationship to calculate the equivalent viscous damping based on dynamic tests of reinforced concrete elements and one-storey frames:

$$\beta_{\text{equ}} = 20 \cdot \left(1 - \frac{1}{\sqrt{\mu_D}}\right) + \beta_v. \quad (3.28)$$

Figure 3.13 shows a comparison of the different approaches where the displacement demand Δ_D at the top of a building with $f_1 > 2$ Hz is given as a function of the peak ground acceleration a_g . The effects of non-linearity are taken into account using the principle of equal energy, the $R - \mu_D - f_1$ relationships proposed by Vidic et al. [VFF 94] and the substitute structure approach.

The discussion of these approaches goes beyond the scope of this work. The engineer should be aware that different approaches exist, however, for the purpose of the earthquake scenario project the variation of the results is of little consequence and since the first approach using the principle of equal energy and the principal of equal displacement gives a straight forward formulation of the required top displacement Δ_D , it will be used in the following.

3.7 Vulnerability function

Varying the “intensity” of the seismic demand by increasing the spectral displacement $S_d(f_1)$ continually from zero onwards, the displacement demand of a building Δ_D increases continually following Equation (3.22) and a $S_d(f_1) - \Delta$ curve is obtained (Figure 3.15). However, this is not yet a vulnerability function. Only when the damage

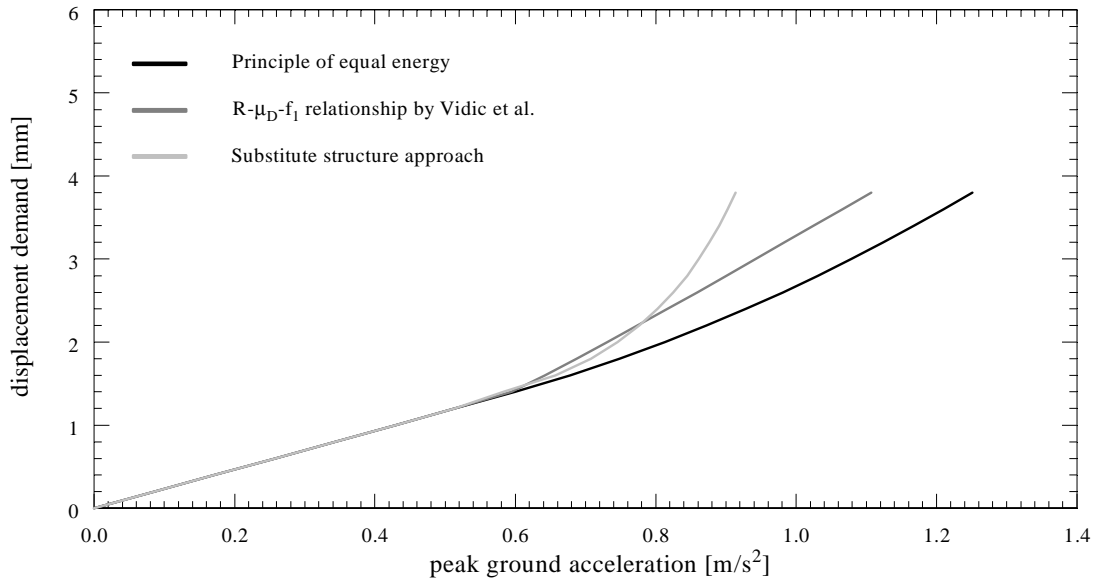


Figure 3.13: Comparison of the different approaches to take into account the effects of non-linearity

is taken into account, the vulnerability function is obtained (Figure 3.1). The top displacement Δ must therefore be associated with a measure of damage.

Various approaches exist, often using a quantitative measurement where the damage is expressed as a proportion of the total destruction [ATC 13] or as a proportion of the ultimate deformation capacity [FG 96]. It is felt by the author that these quantitative measurements are not very suitable for earthquake scenario projects where the interest lies rather in monetary loss and casualties. A qualitative description of damage is therefore suggested based on the classification of damage proposed by the European Macroseismic Scale [EMS 98] that divides the damage into 5 grades ranging from negligible damage to destruction. A copy of this classification of damage is given in the Appendix A1. In order to use these damage grades, “indicators” must be defined that determine the point on the capacity curve of the building at which the building enters the next damage grade. This is shown in Figure 3.14 with reference to the capacity curve of the fictitious example building in Figure 3.8.

The main parameter used as indicator is structural damage, looking at individual walls as well as the whole building. The definition of the indicators is done separately for masonry structures (Section 4.2.7) and for reinforced concrete structures (Section 5.5).

Introducing the indicators of the damage grades from Figure 3.14 into the $S_d(f_1) - \Delta$ relationship, the vulnerability function is obtained (Figure 3.15).

The vulnerability function is linear for $\Delta < \Delta_{by}$ since the capacity curve of the building for $\Delta < \Delta_{by}$ is in the linear elastic region (Figure 3.14) and hence $c_n = 1$ in Equation (3.22). For $\Delta > \Delta_{by}$ the capacity curve of the building is in the plastic region and hence $c_n = \mu_D/R$ in Equation (3.22). For buildings with $f_1 \geq f_{c1}$ the vulnerability function is therefore nonlinear for $\Delta > \Delta_{by}$.

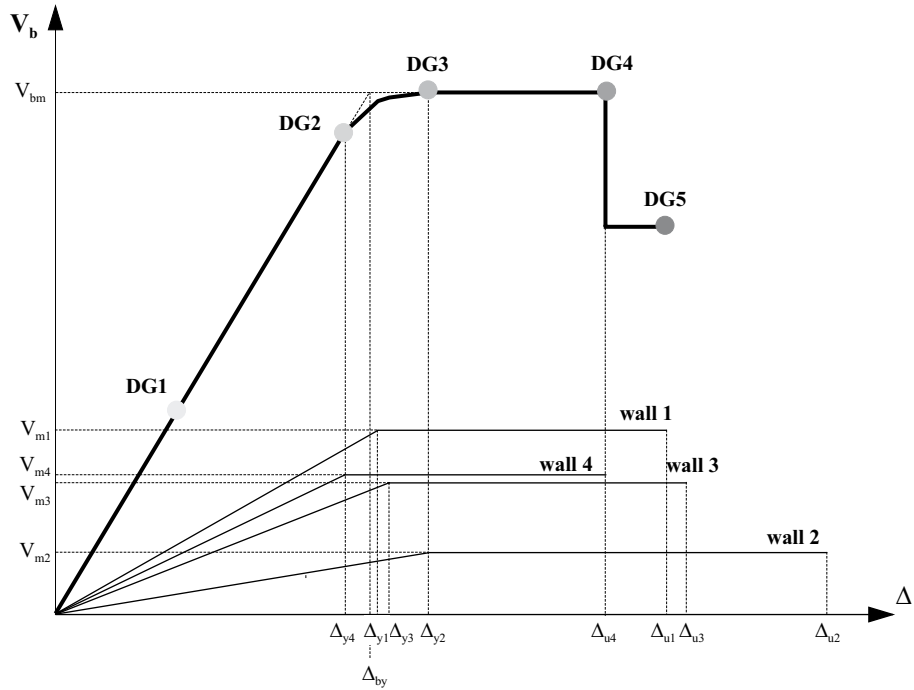


Figure 3.14: Capacity curve of the fictitious example building of Fig. 3.7 including the damage grades.

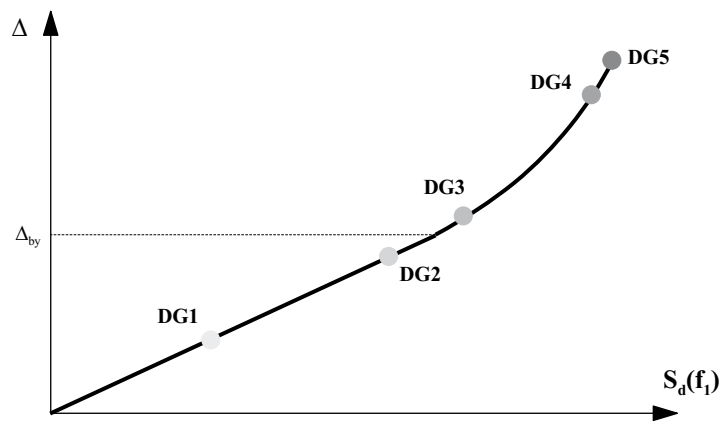


Figure 3.15: Vulnerability function of the fictitious example building of Fig. 3.7

The use of these damage grades allows a “visual” interpretation of the damage. Depending on the facility and the local practice, the financial loss (structural as well as non structural) and the casualties can be derived from the physical condition of the building.

4 Vulnerability of masonry buildings

4.1 Introduction

For a long time research in earthquake engineering has focused on reinforced concrete structures. This is due to the fact that reinforced concrete is the material of our time and also due to the understanding of research to improve the design of new structures rather than to analyse existing structures. However, in many seismically active areas of the world this type of structure only constitutes a small part of the building stock whereas a major part of the buildings are older structures made of unreinforced masonry representing a significant risk during an earthquake. Thus the demand for upgrading strategies of these buildings has become increasingly stronger in the last few years, implying the assessment of existing unreinforced masonry buildings.

In this chapter the application of the evaluation method, introduced in a general way in Chapter 3, is discussed with reference to unreinforced masonry buildings (short: masonry buildings). For masonry buildings it is customary to distinguish between the in-plane behaviour and the out-of-plane behaviour. Under in-plane behaviour, the construction of a capacity curve as described in Chapter 3 is considered. This is described in Section 4.2 with a detailed derivation of the capacity curve of a masonry wall and the identification of the damage grades. The out-of plane behaviour is considered in a further step in Section 4.3 and may lead to a correction of the vulnerability function. In order to validate the evaluation method, it is applied to two unreinforced masonry model buildings that have been tested in Section 4.4. Section 4.5 summarizes the method into 11 steps and in Section 4.6 some conclusive remarks are given.

4.2 In-plane behaviour

4.2.1 Shear behaviour of unreinforced masonry

The behaviour of in-plane loaded masonry walls subjected to horizontal and vertical forces has been investigated in various test programs. Figure 4.1 shows the three possible modes of local failure that can occur depending on the condition of biaxial stress [Pa 96].

- Tensile failure at the heel (region A) is characterised by the development of tensile stresses normal to the bed joints with a consequent horizontal crack resulting in horizontal sliding along the bed joints. It usually occurs for low vertical loads in relation to the horizontal force (large angle of inclination of resultant).
- Flexural failure at the toe (region B) ensues from the development of tensile cracks at the base of the wall, the increasing shear is carried by the compressed masonry. Final failure occurs by overturning of the wall and/or crushing of the compressed corner. This type of failure usually occurs for walls with a large aspect ratio, i.e. a large ratio

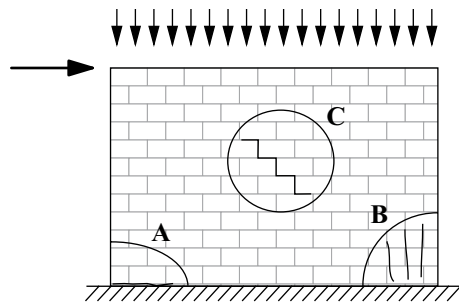


Figure 4.1: Different types of failure that can occur in masonry walls

of height to length (small angle of inclination of resultant). It can display large displacements (rigid body rocking motion) which reduce for increasing vertical loads.

- Shear failure (region C) is characterised by the formation of diagonal cracks. This type of failure usually occurs for a relatively small aspect ratio. For small vertical loads and especially when the mortar is rather weak, the diagonal cracks usually occur in the mortar bed and butt joints (typical stepped cracks). In this case the separated parts of the masonry wall can slide onto each other resulting in large deformations. For large vertical loads and especially when the strength of the bricks is rather low the diagonal cracks can also go through the bricks. In this case the separated parts of the wall tend to slide with little ductility downwards along the more regular diagonal crack.

The stress distribution within a masonry wall is rather complex and, depending on the type of masonry, the geometry of the wall, the applied forces and the support conditions, local failure can occur at the base or at the centre of the wall. However, unless major discontinuities are present none of these local failures will lead to a complete collapse of the wall. After local failure the wall will progressively degrade, final failure is usually a combination of two or three different modes of failure.

Different failure criteria can be found in the literature using half empirical formulations of the failure mechanisms. Flexural failure is usually defined by an ultimate stress distribution in the wall section or by simple stability considerations. Shear failure is often related to the diagonal tension capacity by principal stresses relationship using Mohr's Circle. A detailed discussion of those, however, is beyond the scope of this chapter and the reader is referred to the work by Bruneau [Br 94a] which gives an overview of different approaches that exist, Magenes and Calvi [MC 97] and Abrams [Ab 00a] [Ab 00b], the latter being also incorporated into the "NEHRP (Natural Earthquake Hazard Reduction Program) guidelines for the seismic rehabilitation of buildings" [FEMA 273].

The failure criteria used in the following were derived by Ganz [Ga 85] based on tests carried out at the ETH Zurich [GT 84] and were the basis for the new version of the Swiss Standard for Masonry [SIA177 95].

According to Ganz, the failure conditions for unreinforced masonry can be described by five mechanisms, neglecting the tensile strength of masonry:

I) Tensile failure of the stones

$$\tau_{xy}^2 - \sigma_x \sigma_y \leq 0 \quad (4.1)$$

II) Compression failure of the stones

$$\tau_{xy}^2 - (\sigma_x + f_{mx})(\sigma_y + f_{my}) \leq 0 \quad (4.2)$$

III) Shear failure of the stones

$$\tau_{xy}^2 + \sigma_y(\sigma_y + f_{my}) \leq 0 \quad (4.3)$$

IV) Sliding along the mortar beds

$$\tau_{xy}^2 - (c - \sigma_x \tan \phi)^2 \leq 0 \quad (4.4)$$

V) Tensile failure in the mortar beds

$$\tau_{xy}^2 + \sigma_x \left(\sigma_x + 2c \tan \left(\frac{\pi}{4} + \frac{\phi}{2} \right) \right) \leq 0. \quad (4.5)$$

The four independent material parameters are: Strength of the material in the x- and y-direction, f_{mx} and f_{my} (x being the direction orthogonal to the mortar bed and y the direction parallel to the mortar bed), the angle of internal friction ϕ and cohesion in the mortar beds c .

In the three-dimensional stress field (σ_x , σ_y and τ_{xy}) the failure conditions are represented by two elliptical cones, two circular cylinders and a flat plane (Figure 4.2).

For application purposes it is convenient to transform the failure conditions into the directions of principal stresses:

$$\sigma_x = \sigma_2 \cdot (\cos \alpha)^2 + \sigma_1 \cdot (\sin \alpha)^2 \quad (4.6)$$

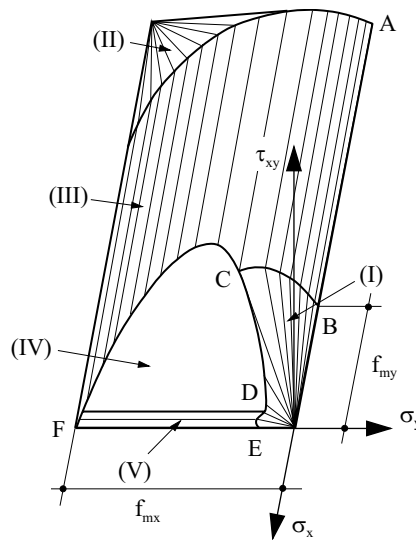


Figure 4.2: Failure conditions for unreinforced masonry according to [Ga 85]

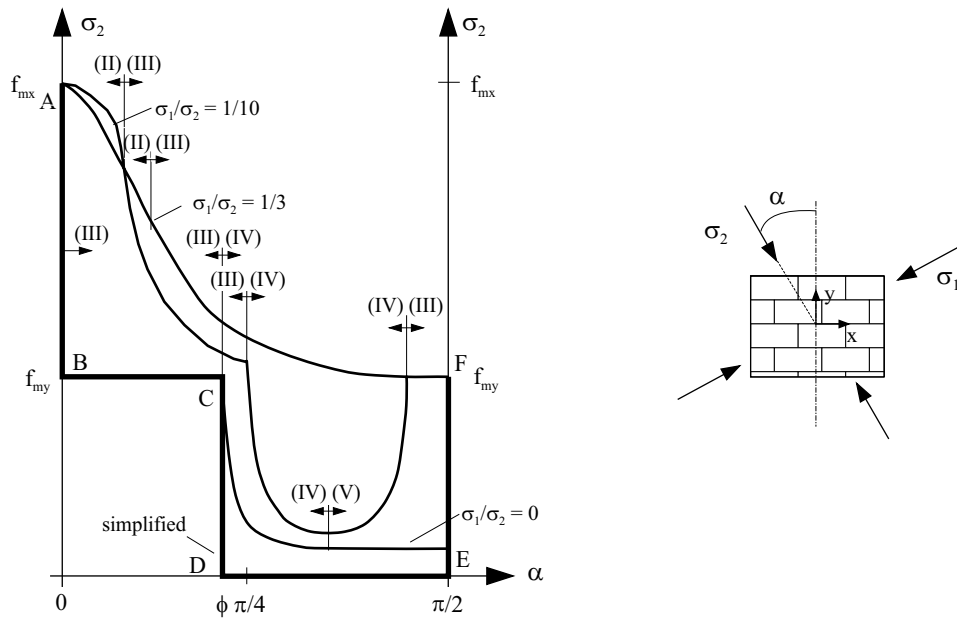


Figure 4.3: Compression strength as a function of the angle α after [Ga 85]

$$\sigma_y = \sigma_2 \cdot (\sin \alpha)^2 + \sigma_1 \cdot (\cos \alpha)^2 \quad (4.7)$$

$$\tau_{xy} = \sigma_2 \cdot \left(\frac{\sigma_1}{\sigma_2} - 1 \right) \cdot \sin \alpha \cdot \cos \alpha. \quad (4.8)$$

Using as parameter the ratio of the two principal stresses σ_1/σ_2 the compression strength can be presented as a function of the angle of inclination α of σ_2 to the orthogonal to the mortar bed (Figure 4.3). Also indicated are the regions for which the different failure mechanisms are valid. Following points are worth noting:

- For uniaxial compression, $\sigma_1/\sigma_2 = 0$, the compression strength parallel to the mortar bed f_{my} cannot be exceeded except for an angle of inclination $\alpha = 0$.
- For an angle of inclination greater than the angle of internal friction, $\alpha > \phi$, the uniaxial compression strength reduces dramatically and stays at a minimum up to $\alpha = \pi/2$.
- Even a small increase in biaxial compression, $\sigma_1/\sigma_2 > 0$, increases the compression strength considerably.

Also shown in Figure 4.3 is a simple approximation of the uniaxial compression strength neglecting the cohesion in the mortar beds c . Thus for an angle of inclination α bigger than the angle of internal friction ϕ the compression strength reduces to zero.

The value of ϕ , the angle of internal friction, varies little for different types of masonry and can be assumed to lie between $0.7 < \tan \phi < 0.8$ [Ga 85].

The ratio of f_{my}/f_{mx} depends on the type of the stone units, on the workmanship of the butt joints and on the type of assemblage, ranging typically from 0.3 to 0.5 for brick and limestone masonry.

Figure 4.4 shows the internal forces acting on a wall element of height h and length l_w . N , V , M_1 and M_2 are the normal force, the shear force, both considered constant over

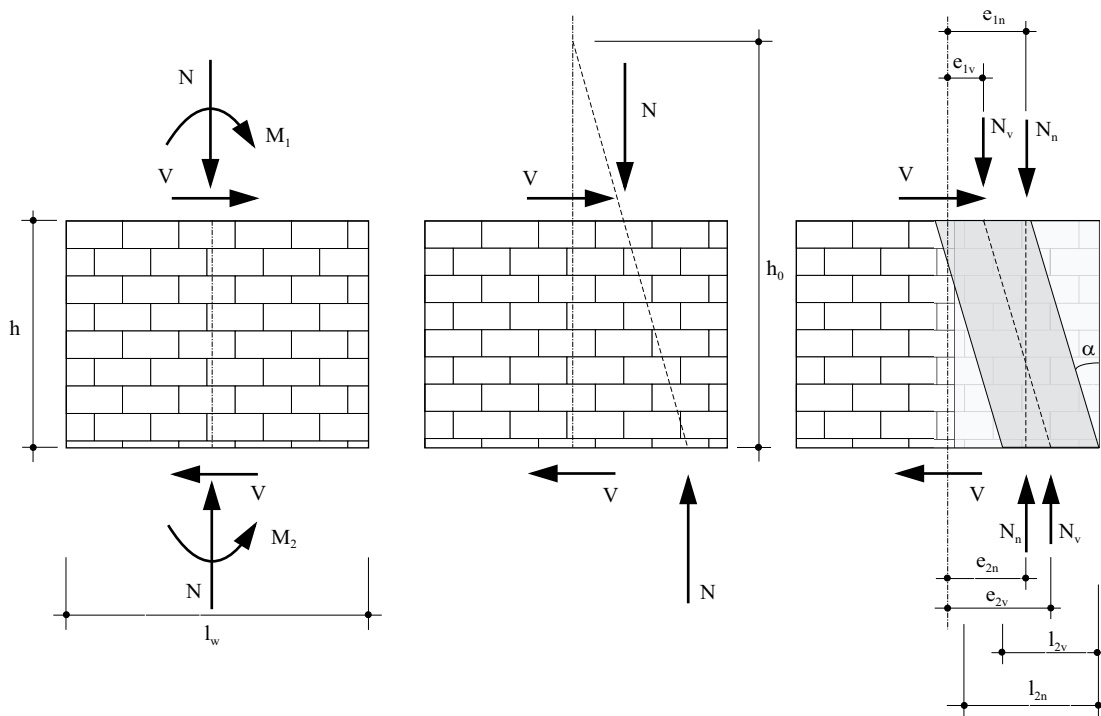


Figure 4.4: Internal forces and corresponding stress field of a wall element

the element height, and the bending moments at the top and bottom of the wall element respectively. The thickness of the wall is denoted by t . It is assumed that the normal force N is given by the vertical loads and therefore approximately known. Note that strictly speaking, in the case of coupled walls, part of the total overturning moment is carried by normal forces in the outer piers (Section 3.5.3) and hence the normal force N does not only depend on the vertical loads but also on the total overturning moment and the coupling effect. In fact, due to the cyclic nature of the earthquake, the normal force will vary from one cycle to the other about its mean value given by the vertical loads. For reason of simplicity, this variation due to the overturning moment is not considered in the following and the normal force is simply calculated as a function of the vertical loads.

The moments M_1 and M_2 depend on the earthquake action represented by the shear force V , the unknown in this problem. h_0 is the height of zero moment measured from the bottom of the wall element as introduced in Section 3.5.3 and depends on the structural model. In the case shown in Figure 4.4 $h_0 > h$, indicating a rather weak coupling effect, however, the equations developed in the following hold also for $h_0 < h$ (cf. Section 4.2.3).

In order to calculate the shear capacity of a wall element, i.e. the maximum shear force the wall element can sustain, the lower bound theorem of plasticity is used. For this a statically admissible stress field has to be found which satisfies equilibrium and the material conditions. A simple stress field is shown in the right picture of Figure 4.4 with two stress struts, one vertical and one inclined at an angle α to the vertical. Assuming that the reinforced concrete floors and/or the stiff joint regions can accommodate the stresses at the nodes the normal force N can be divided into two components N_v and N_n which satisfy the equilibrium conditions:

$$N_v + N_n = N \quad (4.9)$$

$$N_n \cdot e_{1n} + N_v \cdot e_{1v} = M_1 \quad (4.10)$$

$$N_n \cdot e_{2n} + N_v \cdot e_{2v} = M_2 = M_1 + V \cdot h. \quad (4.11)$$

The shear force V is transmitted through the inclined stress strut:

$$V = N_v \cdot \tan \alpha. \quad (4.12)$$

The internal forces have to satisfy the material conditions in the stress field, given by Equations (4.1) - (4.5). For the simple stress field chosen, using the simplified description of the compression strength in Figure 4.3, this reduces to the following three conditions:

$$f_{\text{inclined}} = \frac{N_v}{l_{2v} \cdot t \cdot (\cos \alpha)^2} \leq f_{\text{my}} \quad (4.13)$$

$$f_{\text{vertical}} = \frac{N_n}{l_{2n} \cdot t} \leq (f_{\text{mx}} - f_{\text{my}}) \quad (4.14)$$

$$\tan \alpha \leq \tan \phi \quad (4.15)$$

with

$$l_{2v} = l_w - 2e_{2v} \quad (4.16)$$

$$l_{2n} = l_w - 2e_{2n}. \quad (4.17)$$

The shear capacity of the wall element is obtained by gradually increasing the shear force V until one of the three conditions (4.13) - (4.15) is violated.

Equations (4.9) - (4.15) represent a system of seven equations with 8 unknowns: N_v , N_n , e_{1n} , e_{2n} , e_{1v} , e_{2v} , V and α . Thus the system is statically indeterminate and one parameter can be chosen freely. However, using the lower bound theorem of plasticity, the shear capacity calculated will always be a lower bound to the real shear capacity. As we are not interested in a conservative value but in a description as close as possible to reality, the one parameter should be chosen so as to maximise the admissible shear force V in the wall section. This is a trial and error process. However good results can be obtained by choosing $e_{2v} = e_{2n}$.

Note that here the term admissible is used to stress the fact that the lower bound theorem of plasticity only gives a lower bound approximation of the shear capacity. The true shear capacity is independent of the stress struts chosen, only the approximation of the shear capacity using the lower bound theorem of plasticity depends on the choice of the stress struts and hence, can be maximised.

4.2.2 Structural model

Observations have shown, that the damage in masonry buildings due to seismic action is usually localised in some regions (piers and spandrels, shaded in Figure 3.4) while some

other regions remain almost undamaged. Considering the flow of the forces through the structure it seems obvious that although the spandrels transfer the horizontal forces horizontally, all forces, vertical and horizontal, have to be transmitted to the ground through the piers. Thus they will be the most critical part of the building determining the capacity.

Site investigations of damaged buildings after an earthquake have also shown that a considerable part of the structural damage can lie inside the building. Thus it is important for the evaluation of masonry buildings to consider not only the external but also the internal walls. As already mentioned in Section 3.5.2, in order to identify the structural walls in masonry buildings, a very common practice is to consider all walls with a thickness $t \geq 12\text{cm}$ to be structural walls.

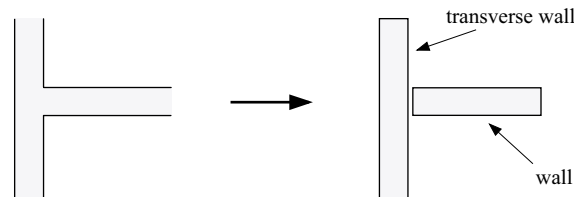


Figure 4.5: Transverse walls

It is also common to consider transverse walls as individual walls with no flange action (Figure 4.5). This can be justified by the following considerations:

- The interlocking of a wall with the transverse wall is usually very weak, especially inside the buildings, usually only three to four stones form the connection. Thus the transfer of shear is not guaranteed.
- To create a flange action, the shear force induced must be distributed over the whole transverse wall. This is not possible for longer walls. The introduction of an effective width taking into account part of the transverse wall would be possible, however, because the increase in resistance is very small, the influence of the transverse wall is usually neglected.

As presented in Section 3.5.3, the structural model depends on the depth of the spandrels. Very simple design models such as recommended by codes of practice neglect this coupling effect and the walls are regarded as interacting cantilever walls. However, in the case of masonry buildings the openings are rather small, especially in the façade, and hence the extent of the spandrels is such that their influence on the stiffness and the displacement behaviour of the structure is not negligible. Comparisons with experimental results of unreinforced masonry model buildings show that this simplified model can lead to an underestimation of the capacity (cf. Section 4.4). A more appropriate model can be found considering the coupling effect and regarding the walls as coupled walls which can be analysed using a frame model.

In fact, in most cases the coupling effect varies throughout the building. The coupling effect in the wall plane constituting a façade will be different from the coupling effect in a wall plane in the interior of the building. Figure 4.6 shows three cases of coupled masonry walls. In Figure 4.6 a) the opening is relatively small and the spandrels rather deep

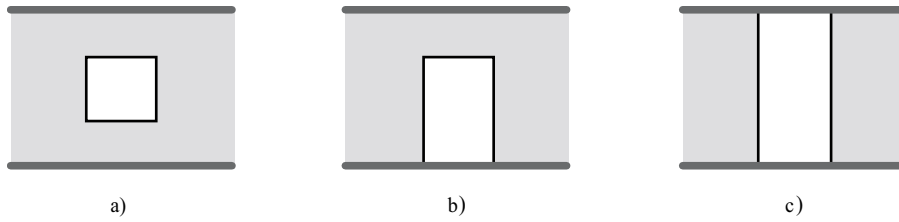


Figure 4.6: Three cases of coupled masonry walls

producing a considerable coupling effect. This is a typical case of a façade wall plane. In Figure 4.6 b) the opening is larger and hence the coupling effect will be reduced. This is usually the case for door openings. In Figure 4.6 c) the opening extends over the whole storey height. This is a typical example of modern interior wall planes.

The analysis of a masonry building as a system of coupled walls using a frame model assumes that the spandrels are able to carry the bending moments that balance the bending moments in the piers. As the normal forces in the spandrels are relatively low, the bending moment capacity of the spandrels is rather low. Thus the spandrels are usually the first to crack reducing the coupling effect.

4.2.3 Capacity curve of a masonry wall

According to Section 3.5.4, the bilinear capacity curve of a wall is determined by three parameters, the maximum shear strength of the wall V_m , the nominal yield displacement at the top of the wall Δ_y and the nominal ultimate displacement at the top of the wall Δ_u . In the next three sections it is demonstrated how these three parameters can be determined for a masonry wall. In the following, even though masonry structures do not yield, the point of transition between the linear elastic and perfectly plastic region of the bilinear capacity curve will be referred to as the “yield point” in analogy to reinforced concrete structures.

According to definition (Figure 3.4), a wall consists of several piers, one per storey, separated by relatively stiff joint regions. It follows that the capacity of a wall is determined by the capacity of the pier that fails first. The joint regions as well as the spandrels are not considered, assuming that they can accommodate the internal forces that are required for equilibrium conditions. As already mentioned, this is not really the case for the spandrels which usually won't be able to accommodate the forces required for equilibrium at the yield point of the first pier without damage, but will have cracked. This can be considered in a very simplified way by introducing a reduced stiffness of the spandrels, thus taking into account a reduced coupling effect due to the formation of early cracks in the spandrels. A more complex model could also consider the capacity of the spandrels.

Therefore, in order to calculate the capacity curve of a wall, the capacity of a pier of height h_p and length l_w is considered first. Figure 4.7 is in essence a repetition of Figure 4.4, the wall element being now a pier.

Due to the coupling effect of the spandrels, at a height h_0 there will be a zero moment (cf. bending moment distribution of a frame in Figure 3.5). The dependence of h_0 from the stiffness of the spandrels was discussed in Section 3.5.3. In the following it is assumed that h_0/h_p behaves like h_0/h_{st} and hence the values from Figure 3.6 can be used. h_0 is always measured from the bottom of the respective element. In the case of finite

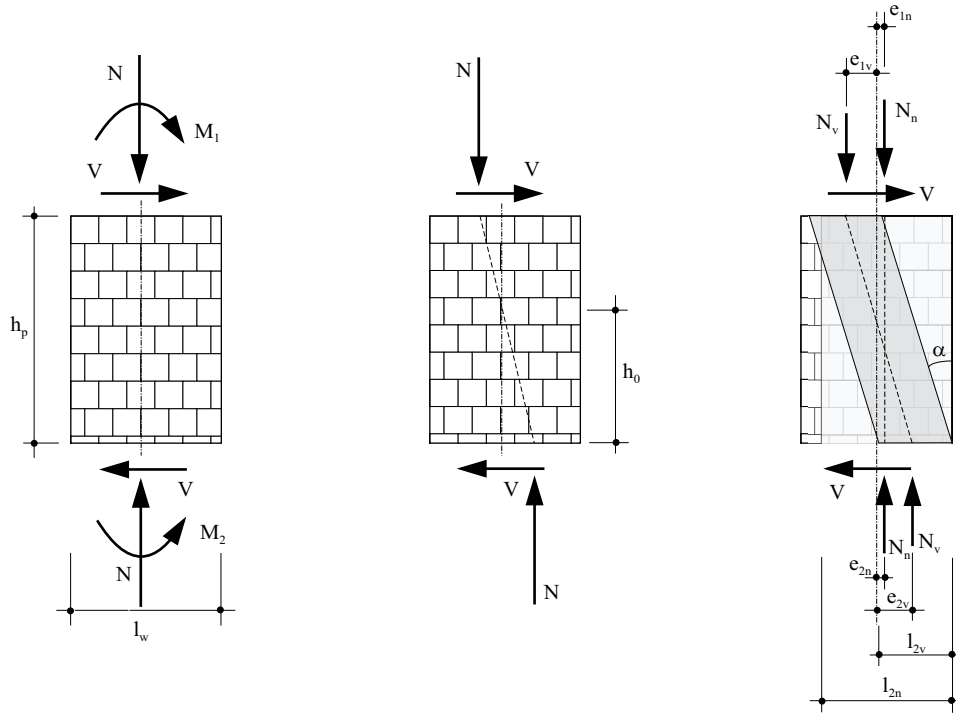


Figure 4.7: Geometry of a pier + applied forces

joint regions this leads to an error which increases with increasing dimension of the joint regions and with decreasing coupling effect. Since, however, deeper spandrels and hence an increased dimension of the joint regions imply an increased coupling effect and vice versa, the error will be small and is therefore neglected in the following.

In the case shown in Figure 4.7 $h_0 < h_p$ indicating a rather strong coupling effect. To take into account the reduction of the coupling effect due to the formation of early cracks in the spandrels a reduction of the stiffness of the spandrels by 50% is proposed.

For a given value of h_0 , M_1 and M_2 can be expressed in terms of V :

$$M_1 = V \cdot (h_0 - h_p) \quad (4.18)$$

$$M_2 = V \cdot h_0 \quad (4.19)$$

For $h_0 < h_p$, the bending moment in the pier changes its sign as in the case of Figure 4.7. For $h_0 > h_p$, the bending moment does not change its sign. This is the case in Figure 4.4. Having obtained M_1 and M_2 from Equations (4.18) and (4.19), the lower bound theorem of plasticity, as explained in Section 4.2.1, can be used to calculate the shear capacity of the pier, with $h = h_p$. That pier of a wall that yields first under the given force distribution determines the shear capacity of the whole wall. In most cases it is the pier at ground level, but in cases where there is a high variation of stiffness and mass over the height of the building, a pier at mid height can yield first.

As explained in Section 3.5.4, a bilinear approximation is used for the capacity curve of a wall (Figure 3.9) with a linear elastic part up to the point where the shear capacity of the wall V_m is reached and a perfectly plastic part with zero stiffness. In reality the re-

response of masonry is strongly nonlinear; as the damage due to cracking increases, masonry experiences both strength and stiffness degradation. Nevertheless, for practical purposes a bilinear approximation is often used to idealize the shear behaviour of a masonry wall.

The effective stiffness of the linear elastic part can be determined using a secant stiffness at αV_m , with $0.6 < \alpha < 0.75$, and choosing V_m such that the bilinear curve is equivalent to the experimental curve in an energetic sense [CM 97]. Comparisons with experimental results [GT 84] show that in this case a stiffness reduction factor of 0.5 to 0.7 is appropriate:

$$k_{\text{eff}} = (0.5 \div 0.7) \cdot k_0. \quad (4.20)$$

k_0 is the uncracked stiffness of the wall (Figure 3.9).

Figure 4.8 shows the elastic displacement shape of a six-storey masonry building due to a triangular distributed horizontal force using frame analysis. It can be seen that the displacement at the bottom is less than one would expect for a frame structure. This is due to the fact that the walls in a masonry structure are rather massive and hence the built in condition at the base of the building becomes more significant than in the case of reinforced concrete frame structures where the columns are rather slender. Also given is the displacement using a constant drift over the building height equal to the drift of the first storey and it can be seen that this simple approximation gives good results for the top displacement.

Using the assumption of constant drift δ over the building height H_{tot} the elastic top displacement Δ of a wall can be written as follows:

$$\Delta = \delta \cdot H_{\text{tot}}. \quad (4.21)$$

The drift δ can be calculated using the principle of virtual work. Considering a pier of height h_p , with the point of zero moment at a height h_0 , the bending moment and shear force distributions due to a) the real forces and b) a virtual unit force are shown in

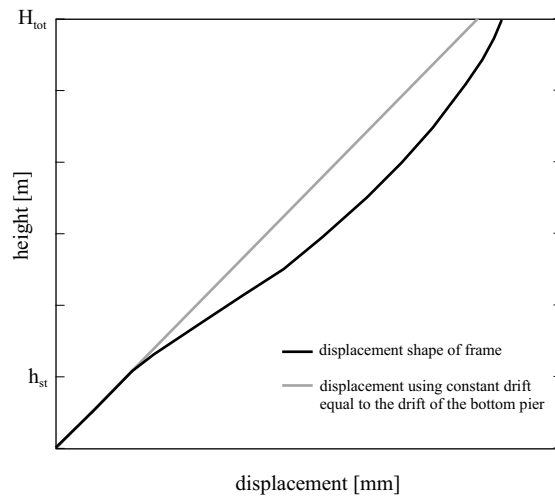


Figure 4.8: Displacement shape of a six-storey masonry building due to a triangular distributed horizontal force

Figure 4.9. This assumes that the drift of the first storey is in fact equal to the drift of the pier. In reality the displacement over one storey is not uniform. The piers as the most slender part of a wall will deform the most whereas the joint regions are rather stiff and will deform less. Hence, the assumption of a constant drift equal to the drift of the pier overestimates the linear elastic deflection. Nevertheless, for the purpose of this evaluation method, the results are good enough (see comparison with experimental results in Section 4.4).

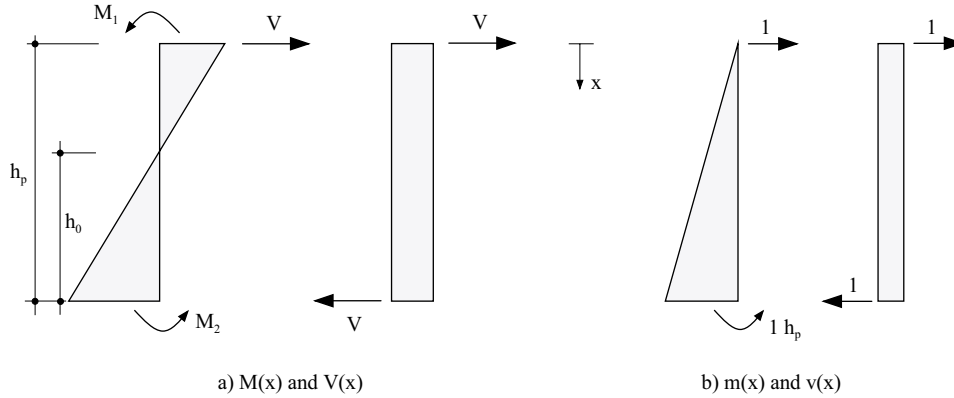


Figure 4.9: Bending moment and shear force distribution of the bottom pier of a wall due to a) the real forces and b) a virtual unit force

The horizontal deformation at the top of the pier d in the direction of the unit force can then be calculated:

$$d = \int_0^{h_p} \frac{M(x) \cdot m(x)}{EI_{\text{eff}}} dx + \int_0^{h_p} \frac{\kappa \cdot V(x) \cdot v(x)}{GA_{\text{eff}}} dx. \quad (4.22)$$

with

$$M(x) = M_1 + V \cdot x, \quad V(x) = V, \quad m(x) = x \quad \text{and} \quad v(x) = 1.$$

EI_{eff} and GA_{eff} are the effective flexural stiffness and the effective shearing stiffness of the pier, respectively.

Substituting the expressions for $M(x)$, $V(x)$, $m(x)$ and $v(x)$ in Equation (4.22) and integrating from zero to h_p the displacement at the top of the pier d is obtained:

$$d = \frac{V \cdot h_p^3}{3 \cdot EI_{\text{eff}}} + \frac{M_1 \cdot h_p^2}{2 \cdot EI_{\text{eff}}} + \kappa \cdot \frac{V \cdot h_p}{GA_{\text{eff}}}. \quad (4.23)$$

κ is a form factor depending on the particular shape of the cross section. For a rectangular cross section $\kappa = 6/5$.

Substituting Equation (4.18) for M_1 and dividing by the height of the pier h_p an expression for the drift δ is obtained:

$$\delta = V \cdot \left(\frac{h_p \cdot (3h_0 - h_p)}{6 \cdot EI_{\text{eff}}} + \frac{\kappa}{GA_{\text{eff}}} \right) \quad (4.24)$$

The yield displacement at the top of the wall Δ_y can then be determined as the displacement for $V = V_m$ using Equations (4.24) and (4.21):

$$\Delta_y = V_m \cdot H_{tot} \cdot \left(\frac{h_p \cdot (3h_0 - h_p)}{6 \cdot EI_{eff}} + \frac{\kappa}{GA_{eff}} \right). \quad (4.25)$$

Even though Figure 4.9 shows the bending moment and shear force distribution for $h_0 < h_p$, Equation (4.24) is also true for the case $h_0 > h_p$, since the boundary conditions are fully determined by h_0 .

The point at which the shear strength of the masonry wall is reached does not necessarily imply failure of the wall. Unreinforced masonry walls need not to be considered brittle; in fact, measured behaviour of wall elements showed that unreinforced masonry can possess considerable capacity for plastic deformations [GT 84]. Plastic deformations as large as eight times the yield deformations were observed! Based on a linear elastic-perfectly plastic behaviour, the ultimate displacement Δ_u can therefore be expressed:

$$\Delta_u = \mu_w \cdot \Delta_y \quad (4.26)$$

μ_w is the ductility of the wall. In the next section, the ductility of masonry is discussed.

4.2.4 Ductility of masonry structures

The definition of ductility is based on a linear elastic-perfectly plastic behaviour and is defined as the ratio of the total elasto-plastic deformation to the elastic deformation at yield:

$$\mu = \frac{\dots u}{\dots y} \quad (4.27)$$

In the case of reinforced concrete structures it is common to distinguish between local ductility (curvature ductility, rotational ductility) and system ductility (displacement ductility). For unreinforced masonry it is convenient to distinguish between the following the types of ductility:

- i) Displacement ductility of a wall element μ_{WE}
- ii) Displacement ductility of a wall μ_w
- iii) Displacement ductility of the building μ_Δ .

The ductility decreases from i) to iii): $\mu_{WE} > \mu_w > \mu_\Delta$.

The ductility of unreinforced masonry is not a ductility in a conventional sense such as the ductility of reinforced concrete which is derived from the plastic deformation of the reinforcing steel. Here, the ductility according to definition (4.27) is obtained by the relative sliding of parts of the wall elements along crack surfaces without significant loss in strength. It is a function of the acting normal stress σ_n , the geometry expressed by the aspect ratio h/l_w , the material properties expressed by the compression strength f_{mx} and the boundary conditions bc :

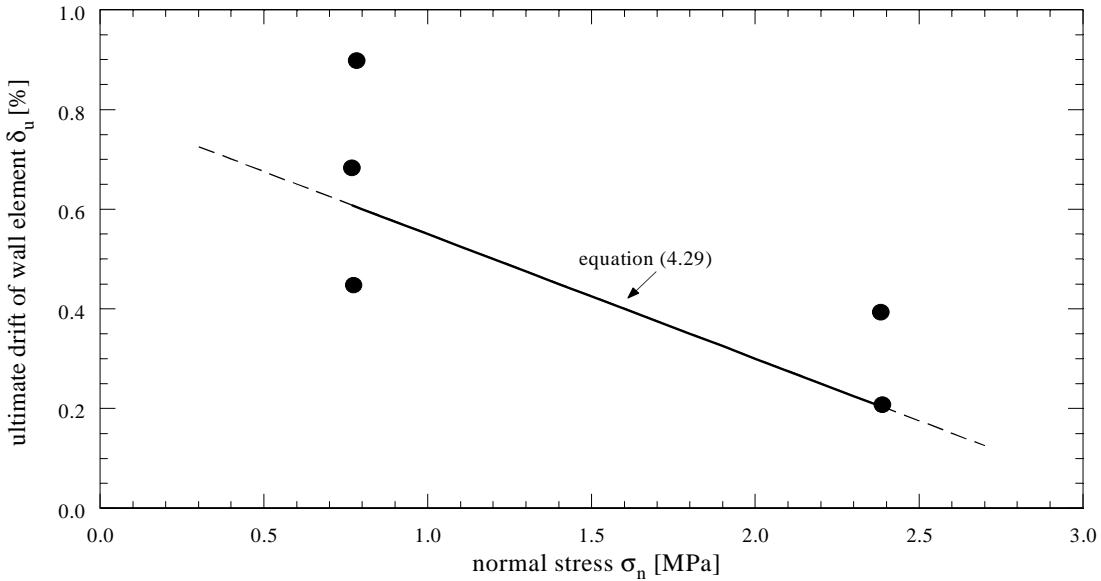


Figure 4.10: Relationship between ultimate drift and normal stress of the wall elements tested at the ETH Zürich [GT 94]

$$\mu = \mu\left(\sigma_n, \frac{h}{l_w}, f_{m,x}, bc\right). \quad (4.28)$$

The dependence of the ductility on the normal stress is quantified using the results of the masonry wall elements tested at the ETH Zürich by Ganz [GT 84]. Using a linear interpolation of the test results (Figure 4.10), the ultimate drift of a wall element δ_u (in [%]) is determined as a function of the normal stress σ_n (in [MPa]) acting on the wall element:

$$\delta_u = 0.8 - 0.25 \cdot \sigma_n. \quad (4.29)$$

The ductility of the wall element is then obtained:

$$\mu_{WE} = \frac{\delta_u}{\delta_y}. \quad (4.30)$$

Determining first the ultimate drift is more reliable since the value of μ_{WE} depends on the yield point which, however, involves high uncertainties.

Equation (4.29) illustrates the fact that for low axial forces the cracks usually pass by the bed joints in a diagonal pattern; the separated parts of the wall can slide onto each other resulting in large relative deformations without significant loss of strength. For high axial loads, however, the cracks pass through the brick units and as a result the separated parts of the wall tend to slide with little deformation downwards along the more regular crack surfaces.

As the tests were all carried out on test specimens with the same geometry (walls of the same height, length and thickness) and with the same compression strength orthogonal to the mortar bed $f_{m,x} = 8.25$ MPa, neither the influence of the geometry nor the influence of the compression strength on the ductility could be studied. The influence of the geometry was revealed by cyclic static tests on masonry test specimens of different as-

pect ratios carried out at the Joint Research Centre of the European Commission, Ispra, Italy [AMM 94]. The results show that in wall elements with high aspect ratios a rocking mode develops leading to high drift capacities without apparent strength degradation. Wall elements with low aspect ratios, however, tend to fail in shear leading to reduced drift capacities. To take into account the different behaviour of masonry wall elements with different aspect ratios it is suggested to enhance or reduce the ultimate drift capacity of a pier in the following simplified manner:

$$\delta_u = \begin{cases} 0.8 \cdot (0.8 - 0.25\sigma_n) & \frac{h_p}{l_w} < 0.5 \\ 0.8 - 0.25\sigma_n & 0.5 < \frac{h_p}{l_w} < 1.5 \\ 1.2 \cdot (0.8 - 0.25\sigma_n) & \frac{h_p}{l_w} > 1.5 \end{cases} \quad (4.31)$$

This, however, needs further investigations, especially considering the energy dissipation of a rocking mode and its implication on the strength reduction factor R.

An upper limit of the ductility of a wall element is set to $\mu_{WE_{max}} = 12$.

In most cases, where the walls are quite slender, it is usually the bottom pier that first reaches the limiting conditions and enters the plastic state. Assuming the upper part of the walls as well as the spandrels to remain elastic, a pier sway mechanism is formed (cf. Section 5.4.3). This is illustrated in Figure 4.11.

From Figure 4.11:

$$\Delta_u = \Delta_y + (d_u - d_y) \quad (4.32)$$

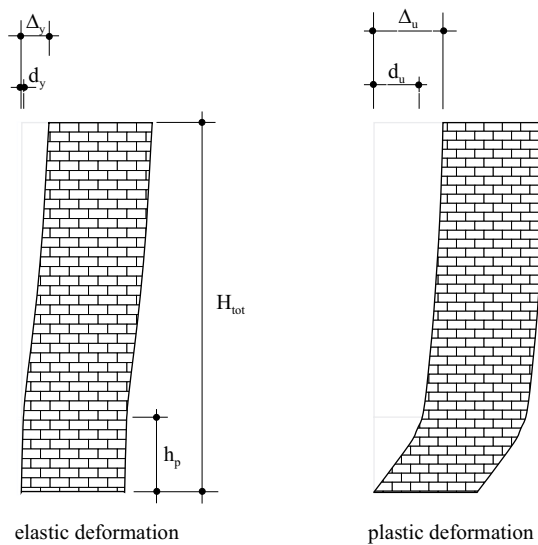


Figure 4.11: Deformation of a masonry wall

d_y is the deformation of the bottom pier at yield, Δ_y is the top displacement of the wall at the point of yield of the bottom pier (corresponding to the point of yield of the whole wall) and d_u the ultimate deformation of the bottom pier:

$$d_u = \mu_{WE} \cdot d_y. \quad (4.33)$$

Thus the displacement ductility of the wall can be deduced assuming a linear elastic displacement shape:

$$\mu_w = 1 + \frac{h_p}{H_{tot}} \cdot (\mu_{WE} - 1). \quad (4.34)$$

As comparison with test results on unreinforced model buildings will show (cf. Section 4.4), the assumption of a pier sway mechanism may lead to rather conservative estimates of the ultimate displacements. A mechanism with partial plastification of the spandrels seems therefore worth considering. However, this needs considering the capacity of the spandrels which is not taken into consideration in this work.

In the case of squat walls combined with low normal forces it is the upper part that first reaches the limiting condition determined by sliding along the mortar beds (Equation (4.15)). Some thoughts to this case can be found in [Li 00].

4.2.5 Cyclic loading

So far, the loading considered has been applied monotonically. The effect of the cyclic nature of the earthquake action has now to be taken into account. In reality the cyclic behaviour of masonry structures is very complex and not very easily quantified. However, for the purpose of this evaluation a very simple approach is used by introducing two reduction factors, a force reduction factor RF_F and a deformation reduction factor RF_D . A similar approach has already been used for reinforced concrete structures in the form of an equivalent ductility factor [Fa 98]. The idea is to reduce the monotonic force and deformation capacity of the structure to take into account the increased deterioration due to cyclic loading. The study of the experimental results of Ganz [GT 84] and Schwegler [Sc 93] suggests the following reduction factors:

$$RF_F = \frac{(V_m)_{cyclic}}{(V_m)_{monoton}} = 0.85 \quad RF_D = \frac{(\mu_w)_{cyclic}}{(\mu_w)_{monoton}} = 0.75. \quad (4.35)$$

$(V_m)_{cyclic}$ and $(V_m)_{monoton}$ are the shear capacity, and $(\mu_w)_{cyclic}$ and $(\mu_w)_{monoton}$ are the ductility of the wall element under cyclic loading and under monotonic loading respectively.

Cyclic static tests on two masonry wall elements at the University of Illinois, however, revealed virtually no deterioration due to cyclic loading [AB 92]. Reversing the lateral force closed the previous opened cracks and resulted in an identical crack pattern. No reduction of stiffness was observed. This would rather suggest reduction factors close to one.

4.2.6 Capacity curve of a masonry building

Sections 4.2.3 to 4.2.5 determine fully the capacity curve of a masonry wall. The capacity curve of a masonry building in one direction can then be obtained by superposition of the capacity curves of all the walls acting in this direction as explained in Section 3.5.4 using Equation (3.3). An example of such a capacity curve is shown in Figure 3.8 for the fictitious example building.

4.2.7 Identification of damage grades according to the EMS

In order to obtain the vulnerability function of a masonry building, i.e. the damage as a function of the spectral displacement, the displacement at the top of the building Δ is associated with the damage grades according to the European Macroseismic Scale [EMS 98]. A copy of this classification of damage to masonry buildings is given in the appendix A1.1. For each damage grade, indicators are defined that allow the identification of the points at which the building enters the next damage grade on the capacity curve of the building.

Grade 1) Negligible to slight damage (no structural damage, slight non-structural damage)

The description of this damage grade for masonry buildings states *hair-line cracks in very few walls*. This is considered to coincide with the point of onset of cracking, i.e. the point at which the stress distribution becomes zero at one point neglecting the tensile strength of masonry. Considering a wall element of length l_w the stress distribution at the onset of cracking is shown in Figure 4.12, assuming that prior to cracking the stress distribution in the wall element is linear elastic.

The moment at cracking is given by

$$M_{cr} = \frac{Nl_w}{6}. \quad (4.36)$$

Hence, as soon as the moment in a wall element reaches the value of M_{cr} the wall element is supposed to be cracked. Considering a pier of height h_p with the applied forces V , M_1 and M_2 as shown in Figure 4.7 for $h_0 < h_p$ or in Figure 4.4 for $h_0 > h_p$, substituting Equation (4.19) into Equation (4.36) and solving for V , the shear force at the onset of cracking is determined by:

$$V_{cr} = \frac{M_{cr}}{h_0} = \frac{N \cdot l_w}{6 \cdot h_0}. \quad (4.37)$$

The corresponding displacement at the top of the wall Δ_{cr} is determined using Equation (4.25). Substituting Δ_{cr} into Equation (3.3) the corresponding base shear of the building can be determined:

$$V_{bcr} = V_b(\Delta_{cr}) = \sum_i V_i(\Delta_{cr}). \quad (4.38)$$

In the case of the fictitious example building in Figure 3.7 it is wall 4 which cracks first.

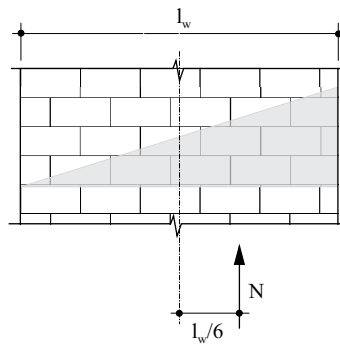


Figure 4.12: Stress distribution in a wall element at the onset of cracking

The couple (Δ_{cr}, V_{bcr}) determines the point on the capacity curve of the building at which the building enters damage grade 1. Before this point the building is considered to be undamaged.

Grade 2) Moderate damage (slight structural damage, moderate non-structural damage)

Cracks now appear in many walls of the building. This indicates that the behaviour of the building starts to become more nonlinear. Thus it is considered to coincide with the point at which the first wall enters the plastic part of its capacity curve and the stiffness of the building starts to reduce. Returning to the capacity curve of the fictitious example building in Figure 3.8, this corresponds to a displacement equal to Δ_{y4} , the wall 4 being the first wall to enter the plastic state. Substituting Δ_{y4} into Equation 3.4 the corresponding base shear of the building can be determined:

$$V_b(\Delta_{y4}) = V_1(\Delta_{y4}) + V_2(\Delta_{y4}) + V_3(\Delta_{y4}) + V_4(\Delta_{y4}). \quad (4.39)$$

The couple $(\Delta_{y4}, V_b(\Delta_{y4}))$ determines the point on the capacity curve of the fictitious example building at which the building enters damage grade 2. Before this point, all walls behave linear elastically and the stiffness of the building is equal to k .

Grade 3) Substantial to heavy damage (moderate structural damage, heavy non-structural damage)

Most walls of the building have now large and extensive cracks; failure of individual non-structural elements (partitions and gable walls) can occur. Gable walls usually fail in an out-of-plane mechanism, thus their point of failure can be easily defined (cf. Section 4.3 on the out-of-plane behaviour). The extent of the cracks indicate an increased nonlinear behaviour of the building with a very reduced stiffness. Thus, the indicator of this damage grade is the point at which the stiffness of the building tends to zero. This often corresponds to the point at which the last wall enters the plastic state, the stiffness of the building becoming zero at that point. Returning to the capacity curve of the fictitious example building in Figure 3.8, this corresponds to a displacement equal to Δ_{y2} , wall 2 being the last wall to enter the plastic state, and hence the stiffness of the building becomes zero. Substituting Δ_{y2} into Equation (3.4) the corresponding base shear of the building can be determined:

$$V_b(\Delta_{y2}) = V_1(\Delta_{y2}) + V_2(\Delta_{y2}) + V_3(\Delta_{y2}) + V_4(\Delta_{y2}). \quad (4.40)$$

The couple $(\Delta_{y2}, V_b(\Delta_{y2}))$ determines the point on the capacity curve of the fictitious example building at which the building enters damage grade 3.

Grade 4) Very heavy damage (heavy structural damage, very heavy non-structural damage)

This damage grade corresponds to the onset of *serious failure of walls*. Thus as soon as the first wall reaches its ultimate displacement Δ_u it is considered to have failed and the building to be very heavily damaged, the base shear of the building dropping significantly. Returning to the capacity curve of the fictitious example building in Figure 3.8, this corresponds to a displacement equal to Δ_{u4} , wall 4 being the first wall to reach its ultimate state. Substituting Δ_{u4} into Equation (3.4) the corresponding base shear of the building can be determined:

$$V_b(\Delta_{u4}) = V_1(\Delta_{u4}) + V_2(\Delta_{u4}) + V_3(\Delta_{u4}) + V_4(\Delta_{u4}). \quad (4.41)$$

The couple $(\Delta_{u4}, V_b(\Delta_{u4}))$ determines the point on the capacity curve of the fictitious example building at which the building enters damage grade 4. Beyond this point the base shear of the building starts to reduce.

Grade 5) Destruction (very heavy structural damage)

This corresponds to *total or near total collapse*. After the failure of the first wall, the remaining walls have to carry more gravity loads and horizontal forces, thus they will sooner reach their ultimate displacement. After the failure of a certain number of walls the remaining walls are not able to carry the load and the building will collapse. On the capacity curve of the building this is considered to coincide with the point at which the base shear has reduced to about 2/3 of its maximum value.

The identification of the damage grades on the capacity curve of the fictitious example building is shown in Figure 3.14. A summary of the indicators of the damage grades for masonry buildings according to the European Macroseismic Scale [EMS 98] is given in Table 4.1.

Even though in terms of financial loss damage grade 4 and damage grade 5, both indicate 100% loss (or even more, considering that the building first has to be pulled down completely before a new building can be constructed, thus increasing the cost) it is important to distinguish between these two, as in terms of casualties, the chance of survival in a house which is very heavily damaged but has not collapsed yet is much higher. However, in some cases the failure of the first wall will lead immediately to the collapse of the building and hence $DG4 = DG5$.

It is not always possible to identify clearly all damage grades. A very common case is that the first wall reaches its ultimate condition and fails, indicating damage grade 4, before the last wall has yielded, indicating damage grade 3.

Damage grade	EMS 98	Identification
DG1	Negligible to slight damage (no structural damage, slight non-structural damage) Hairline cracks in very few walls. Fall of small pieces of plaster only. Fall of loose stones from upper parts of buildings in very few cases.	point of onset of cracking, => stress distribution becomes zero at the extreme fibre of the wall section
DG2	Moderate damage (slight structural damage, moderate non-structural damage) Cracks in many walls. Fall of fairly large pieces of plaster. Partial collapse of chimneys.	behaviour of the building becomes nonlinear, the stiffness of the building starts to reduce, => yield of the first wall
DG3	Substantial to heavy damage (moderate structural damage, heavy non-structural damage) Large and extensive cracks in most walls. Roof tiles detach. Chimneys fracture at the roof line; failure of individual non-structural elements (partitions, gable walls).	increased nonlinear behaviour of the building, the stiffness of the building tends to zero, => yield of the last wall
DG4	Very heavy damage (heavy structural damage, very heavy non-structural damage) Serious failure of walls; partial structural failure of roofs and floors.	=> failure of first wall
DG5	Destruction (very heavy structural damage) Total or near total collapse.	=> drop of the base shear of the building V_b below $2/3 \cdot V_{bm}$

Table 4.1: Damage grades of masonry buildings

4.2.8 Vulnerability function of a masonry building

Using Equation (3.22), the top displacement Δ can be plotted as a function of the spectral displacement $S_d(f_1)$. Having identified the points on the capacity curve of the building at which the building enters the next damage grades, these can be presented on the plot of top displacement Δ versus spectral displacement $S_d(f_1)$ resulting in the vulnerability function of the building (Figure 3.15).

4.3 Out-of-plane behaviour

So far the in-plane behaviour of masonry walls aligned in the direction of the earthquake was considered. However, masonry walls aligned orthogonal to the earthquake direction can also fail in an out-of-plane mode and this may endanger the gravity load carrying capability of a building (Figure 4.13).

The out-of-plane behaviour of masonry walls depends very much on the floor-wall connections (cf. Section 6.2.3). For masonry walls which are properly anchored to the floors, the out-of-plane behaviour is usually not critical and the vulnerability function of the building is determined by its in-plane behaviour. In the case where the connection between orthogonal walls and between walls and floors is rather poor, the walls might fail in an out-of-plane mechanism before an in-plane mechanism can be triggered leading to a correction of the vulnerability function established for in-plane behaviour. In the absence of any floor-wall connections, the masonry walls behave like tall unrestrained cantilevers which are most vulnerable to flexural out-of-plane failure determining the vulnerability function of the building.

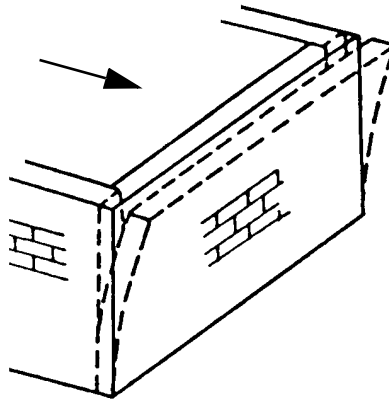


Figure 4.13: Out-of-plane behaviour

Furthermore, in reality the earthquake action does not correspond to one of the principal directions of the building. Thus the walls are subjected to both, in-plane and out-of-plane actions. However, this is not considered in the following.

Two different stages in the out-of-plane behaviour are distinguished, the occurrence of cracking and failure.

4.3.1 Structural modelling

As for in-plane behaviour, the floors are assumed to be completely rigid (no amplification of the out-of-plane loaded wall accelerations by floor response) and hence the accelerations at all points along a floor will be equal to the acceleration of the in-plane loaded walls at the floor height. An estimate of the storey accelerations from the spectral acceleration of the equivalent SDOF $S_a(f_1)$ is shown in Figure 4.14 [PP 92].

At heights above the height h_E of the equivalent SDOF system the storey acceleration at the i -th storey a_i is given by the mode shape (assumed to be linear) from the spectral acceleration $S_a(f_1)$:

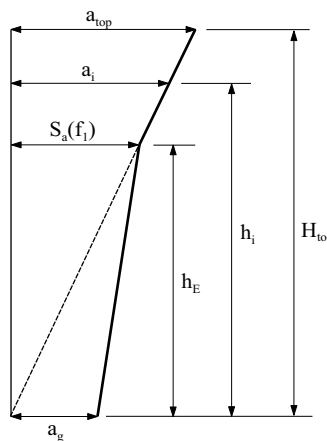


Figure 4.14: Variation of response acceleration with height

$$a_i = \frac{S_a(f_1)}{h_E} \cdot h_i. \quad (4.42)$$

At heights below h_E the influence of the ground acceleration is taken into account by a linear interpolation between a_g and $S_a(f_1)$:

$$a_i = h_i \cdot \left(a_g + \frac{S_a(f_1) - a_g}{h_E} \right). \quad (4.43)$$

The capacity of unreinforced masonry subjected to out-of-plane action depends upon the dimensions of the wall, the boundary conditions, the compressive stress and the tensile strength of the masonry (neglected in the following). Let's consider a wall panel between two floor levels of height h_{st} and length l , the applied normal forces due to the gravitational loads indicated by N . Assuming the acceleration at the i -th storey a_i to be constant over the storey height, the out-of-plane loading of a wall due to inertia is:

$$q = m \cdot a_i \quad (4.44)$$

where m is the mass per unit height.

The maximum moment in the wall panel due to the out-of-plane loading will be determined by the boundary conditions. Each wall panel has four boundaries. For a wall panel of height h_{st} the top and bottom boundary conditions are given by the floor-wall connection. In the case of free boundary conditions at both sides, the wall panel can be regarded as a one-way slab and the problem is reduced to a 2-D problem. This is shown in Figure 4.15. In the case where the sides are somehow supported, the wall panel has to be regarded as a two-way slab. The effect is to reduce the maximum moment due to the out-of-plane loading. However, the influence of the supported sides on the maximum moment reduces very rapidly with increasing length to height ratio and hence most out-of-plane problems can be reduced to a 2-D problem.

Note, for design purpose, considering a 2-D problem always gives a conservative result. Depending on the floor-wall connection, the maximum moment in the wall element can be expressed as a function of the vertical force distribution q .

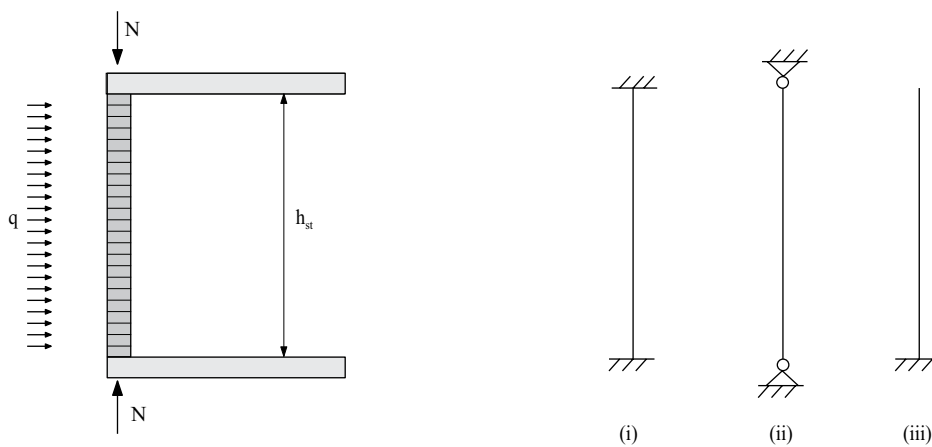


Figure 4.15: Out-of-plane loaded wall with different boundary conditions

Vulnerability of masonry buildings

For a built in beam (Figure 4.15 i) the maximum moment is:

$$M_{\max} = \frac{q \cdot h_{\text{st}}^2}{12}. \quad (4.45)$$

An example of this case would be a concrete floor system, where the normal forces are usually high, preventing the top and the bottom of the wall element to rotate, or a timber floor systems with ties connecting the wall element to the floors.

For a simply supported beam (Figure 4.15 ii) the maximum moment is:

$$M_{\max} = \frac{q \cdot h_{\text{st}}^2}{8}. \quad (4.46)$$

An example of this case is a floor system with joints at the top and bottom of the wall element.

In the case of a cantilever (Figure 4.15 iii) the maximum moment is:

$$M_{\max} = \frac{q \cdot h_{\text{st}}^2}{2}. \quad (4.47)$$

A typical example of this case is a gable wall or a balustrade.

4.3.2 Out-of-plane cracking

On the analogy of in-plane behaviour the onset of cracking is determined by the stress distribution becoming zero at the extreme fibre neglecting the tensile strength of masonry (Figure 4.16) [PP 92].

The moment at cracking is:

$$M_{\text{qcr}} = \frac{Nt}{6}. \quad (4.48)$$

Knowing the normal force acting on a wall panel, the out-of-plane moment that causes cracking can be determined using Equation (4.48). From this, using Equations (4.45) to (4.47), depending on the floor-wall connection, the vertical force distribution that causes

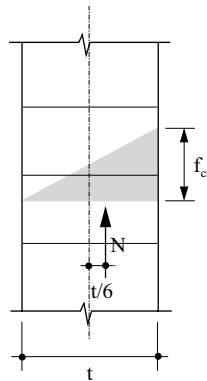


Figure 4.16: Stress distribution at cracking

cracking q_{cr} and thus the acceleration at the i -th storey that causes cracking a_{cri} can be calculated using Equation (4.44).

Hence, knowing a_{cri} , the spectral acceleration at which cracking occurs in an out-of-plane mode $S_a(f_1)_{OPcr}$ can be determined using Equations (4.42) and (4.43).

As can be seen from Figure 4.14, the storey acceleration increases with height, the maximum storey acceleration being at the roof level. Since this is combined with the lowest normal force N , and hence the lowest admissible M_{qcr} , cracking in an out-of-plane mode occurs first in a wall panel at the upper floor level.

So far it was assumed that the floors are horizontal and the normal force is applied centrally on the wall panel (cf. point of application of N in Figure 4.15). However, the surcharge being applied on the floors, the floors will bend creating an additional out-of-plane moment dm which can be additive or subtractive to the moment due to the storey accelerations M_q .

Assuming the floors to be “built in” into the walls, the bending moment distribution is given in Figure 4.17.

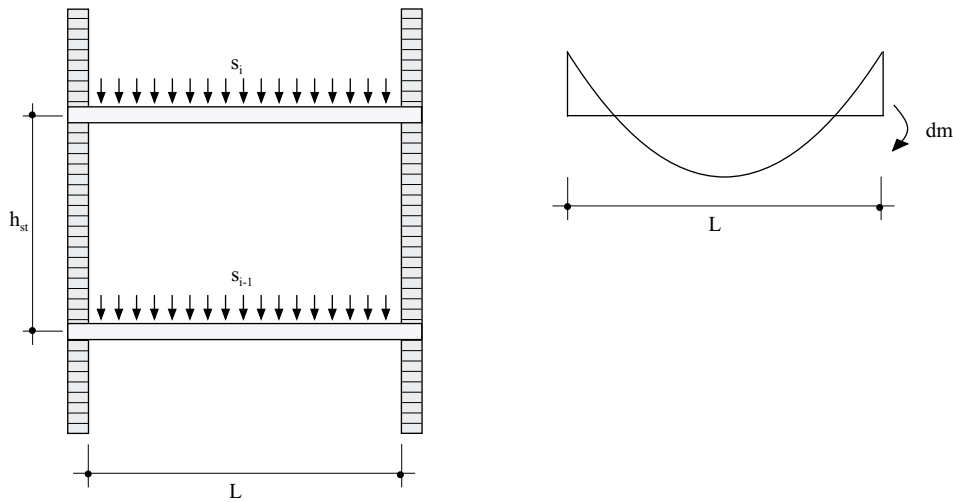


Figure 4.17: Out-of-plane moment due to the deflection of the floors

The moment at the fixed ends dm due to the horizontally distributed load s_i at the i -th storey is:

$$dm = \frac{s_i \cdot L^2}{12}. \quad (4.49)$$

L is the span between two walls (Figure 4.17).

The moment dm has to be accommodated by the walls creating an additional out-of-plane moment. In the worst case dm acts in the same direction as the moment due to the storey acceleration M_q . In this case, the “net” moment due to the storey acceleration that causes out-of-plane cracking will be less than determined before:

$$(M_{qcr})_{net} = M_{qcr} - dm \quad (4.50)$$

On the other hand, if dm acts into the opposite direction it will counteract M_q , increasing the “net” moment due to the storey acceleration that causes out-of-plane cracking. In reality, the direction of the floor acceleration will change during the earthquake and hence there will always be a point at which dm will be additive. It seems therefore appropriate to take this effect into account using Equation (4.50).

4.3.3 Out-of-plane failure

The formation of cracks does not imply out-of-plane failure of the masonry wall panel. After the onset of cracking, the crack will propagate through the thickness of the wall, the maximum compressive stress will increase and the compression zone decrease until at ultimate condition the compressive strength of masonry orthogonal to the mortar bed f_{mx} is reached. The stress distribution at ultimate can be approximated by a rectangular distribution as shown in Figure 4.18 a) and hence the moment at ultimate is:

$$M_{qu} = N \cdot \frac{t-a}{2}. \quad (4.51)$$

Substituting for a , the extension of the compression zone:

$$a = \frac{N}{f_{xm} \cdot l}, \quad (4.52)$$

Equation (4.51) can be rewritten as:

$$m = \frac{1}{2} \cdot n \cdot (1 - n) \quad (4.53)$$

with

$$m = \frac{M_{qu}}{l \cdot t^2 \cdot f_{mx}} \quad \text{and} \quad n = \frac{N}{l \cdot t \cdot f_{mx}}. \quad (4.54)$$

This is a normalised parabola as shown in Figure 4.18 b) [ZSS 99].

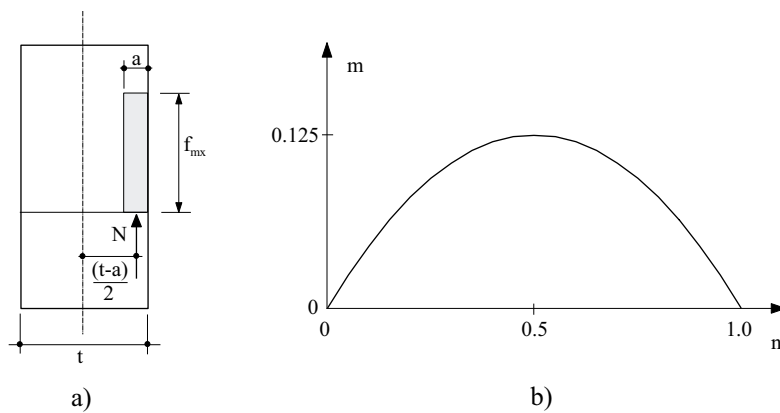


Figure 4.18: a) Stress distribution at ultimate and b) moment-normal force interaction

Thus, from the applied normal force N , the moment M_{qu} that causes out-of-plane failure can be determined and hence the vertically distributed load q_u that causes out-of-plane failure using Equations (4.46) to (4.48) depending on the floor-wall connection. Using Equation (4.44) the acceleration at the i -th storey a_{ui} that causes out-of-plane failure of the wall panel can be calculated from which the spectral acceleration $S_a(f_1)_{OPu}$ at which the wall panel fails in an out-of-plane mode can be determined using Equations (4.42) and (4.43).

Again, the influence of the additional out-of-plane moment dm due to bending of the floors has to be taken into account, the “net” moment due to floor acceleration that causes out-of-plane failure being:

$$(M_{qu})_{net} = M_{qu} - dm. \quad (4.55)$$

4.3.4 Influence on the vulnerability function

So far out-of-plane cracking and out-of-plane failure have been considered and the corresponding spectral accelerations at the fundamental frequency of the building, $S_a(f_1)_{OPcr}$ and $S_a(f_1)_{OPu}$, determined. To compare these values with the vulnerability function, established in Section 4.2.7 for in-plane behaviour, the spectral accelerations have to be converted into spectral displacements using Equation (3.7). The spectral displacement at which out-of-plane cracking occurs $S_d(f_1)_{OPcr}$ can then be compared with the spectral displacement at which cracking occurs in-plane, corresponding to damage grade 1, $S_d(f_1)_{DG1}$. If $S_d(f_1)_{OPcr} < S_d(f_1)_{DG1}$, cracking in an out-of-plane mode occurs first and thus the building enters earlier damage grade 1. Hence the vulnerability function must be corrected by displacing the point at which the buildings enters damage grade 1 down to $S_d(f_1)_{OPcr}$. If $S_d(f_1)_{OPcr} > S_d(f_1)_{DG1}$, cracking in an out-of-plane mode occurs after cracking in an in-plane mode has occurred and thus no correction of the vulnerability function is needed.

Considering out-of-plane failure, two different cases have to be distinguished. In the case of a structural wall panel, the out-of-plane failure corresponds to damage grade 4 (serious failure of walls) and the resulting spectral displacement $S_d(f_1)_{OPu}$ has to be compared with the spectral displacement corresponding to damage grade 4, $S_d(f_1)_{DG4}$. If $S_d(f_1)_{OPu} < S_d(f_1)_{DG4}$, out-of-plane failure occurs before the in-plane failure. Hence the vulnerability function must be corrected by displacing the point at which the building enters damage grade 4 down to $S_d(f_1)_{OPu}$. If $S_d(f_1)_{OPu} > S_d(f_1)_{DG4}$, in-plane failure occurs before out-of-plane failure and thus no correction of the vulnerability function is needed. In the case of a gable wall, the resulting spectral displacement $S_d(f_1)_{OPu}$ has to be compared with the spectral displacement corresponding to damage grade 3, $S_d(f_1)_{DG3}$, as the failure of a gable wall corresponds only to a moderate structural damage.

4.3.5 Some further remarks on the out-of-plane behaviour

The calculation of the out-of-plane loading, expressed as the vertical force distribution q , using Equations (4.45) to (4.47) depends strongly on h , the height of the wall panel. So far it was assumed that the wall panel considered extends over a storey height i.e. $h = h_{st}$. In the absence of any floor-wall connection the overall out-of-plane behaviour

of a wall plane has to be assessed. In that case the wall plane will behave as a tall unrestrained cantilever with a high vulnerability to out-of-plane loading. The same principles as outlined above can be applied.

Even for good floor-wall connections the predicted out-of-plane resistance is rather low. Although for masonry buildings with poor floor-wall connections the out-of-plane behaviour is predominant, the results tend to be rather too conservative. One reason is the neglect of the tensile strength of masonry which becomes particularly important in the case of low compressive stresses such as gable walls. Furthermore, although the moment that causes out-of-plane failure M_{qu} is calculated considering ultimate conditions, the corresponding spectral acceleration $S_a(f_1)_{OPu}$ is still assumed to be an elastic spectral value without considering the inelastic behaviour.

Priestley proposed an alternative approach including the inelastic displacement capacity based on energy equivalence to predict out-of-plane failure [PP 92] [Pr 00]. It is based on the assumption that failure only occurs when instability results i.e. when the point of application of the normal force N is displaced sufficiently so that it lies outside the centre of compression of the ultimate stress block. The relationship between the acceleration of the wall panel and its displacement is described as nonlinear elastic with a linear part up to the onset of cracking (Figure 4.19). Priestley then suggested an equivalent linear elastic model which yields the same energy at failure as the nonlinear elastic model.

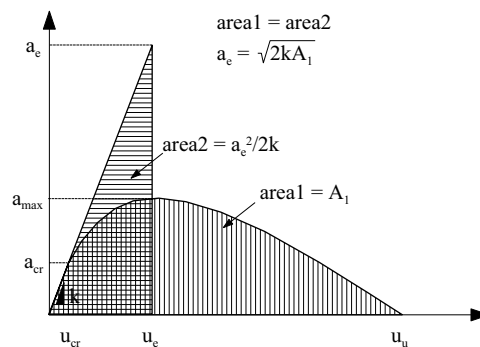


Figure 4.19: Nonlinear acceleration-displacement relationship for out-of-plane loaded wall panels and principal of equal energy after [PP 92]

4.4 Comparison with test results

In order to validate the method presented before it has been applied to two unreinforced masonry model buildings that have been tested, one under cyclic static action, the other dynamically on a shaking table.

4.4.1 Pavia University tests

At the University of Pavia a full-scale two-storey masonry model building has been tested under cyclic static action. The full description of the test procedure and the measured experimental response can be found in [MKC 95].

The materials of the building were chosen to represent a typical old urban construction in Italy. Thus solid fired-clay bricks with a mean compressive cube strength of 16 MPa

were used. The mortar was a mix of hydraulic lime and sand in a proportion of 1:3. The measured compressive strength of a masonry prism orthogonal to the mortar bed was $f_{mx} = 6.2 \text{ MPa}$.

The geometry of the building is shown in Figure 4.20. It consisted of four solid brick wall planes with a total wall thickness $t = 0.25 \text{ m}$. The wall plane D was disconnected from the adjacent transverse wall planes A and C, while the wall plane B was connected to the adjacent wall planes A and C with an interlocking brick pattern around the corner.

The floors consisted of a series of isolated steel beams (I-section, depth = 140 mm) designed to simulate a flexible floor diaphragm. Both vertical and horizontal forces were applied through these floor beams. To simulate gravity loads, concrete blocks were used

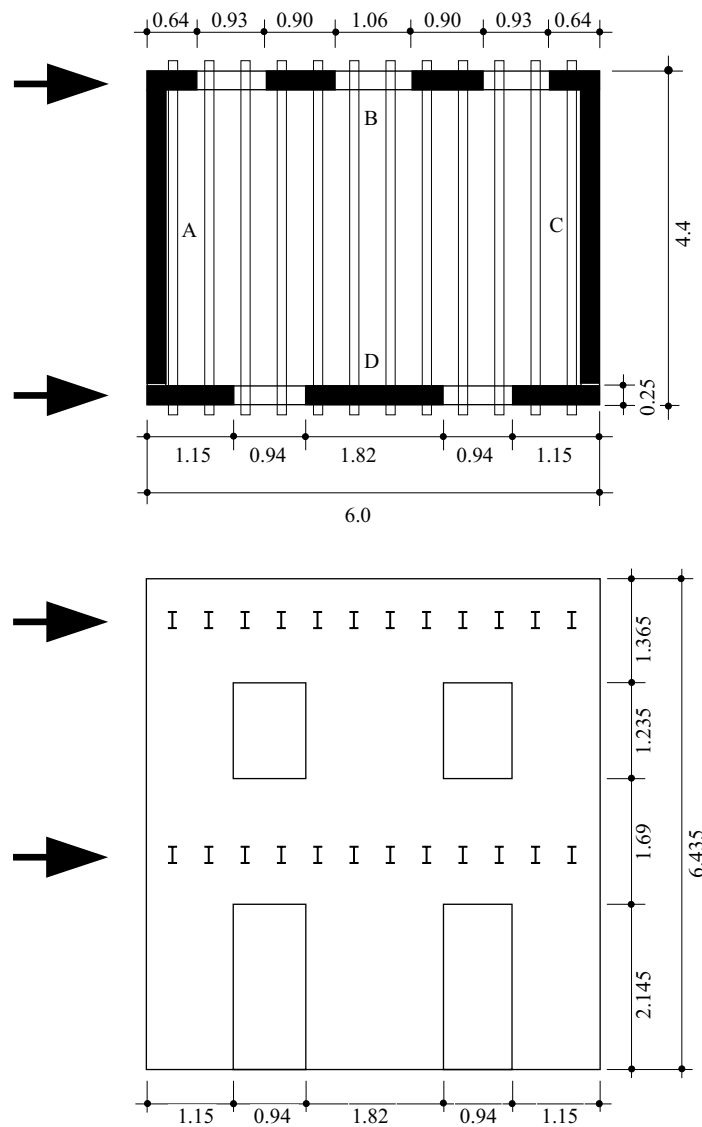


Figure 4.20: Plan and elevation of the model building tested under cyclic static action at the University of Pavia + points of application and direction of seismic forces [MKC 95], dimensions in m

for a total added vertical load of 248.4 kN at the first floor and 236.8 kN at the second floor ($\sim 10\text{kN/m}^2$ per floor).

The seismic forces were simulated by the application of four equal concentrated horizontal forces applied at wall plane B and wall plane D as shown in Figure 4.20.

The building was tested under cyclic static action. The applied displacements were programmed to simulate dynamic load-displacement patterns with reference to a 3/8 scale exact copy of a building tested dynamically on the shaking table at the University of Illinois. Figure 4.21 gives the displacement history imposed.

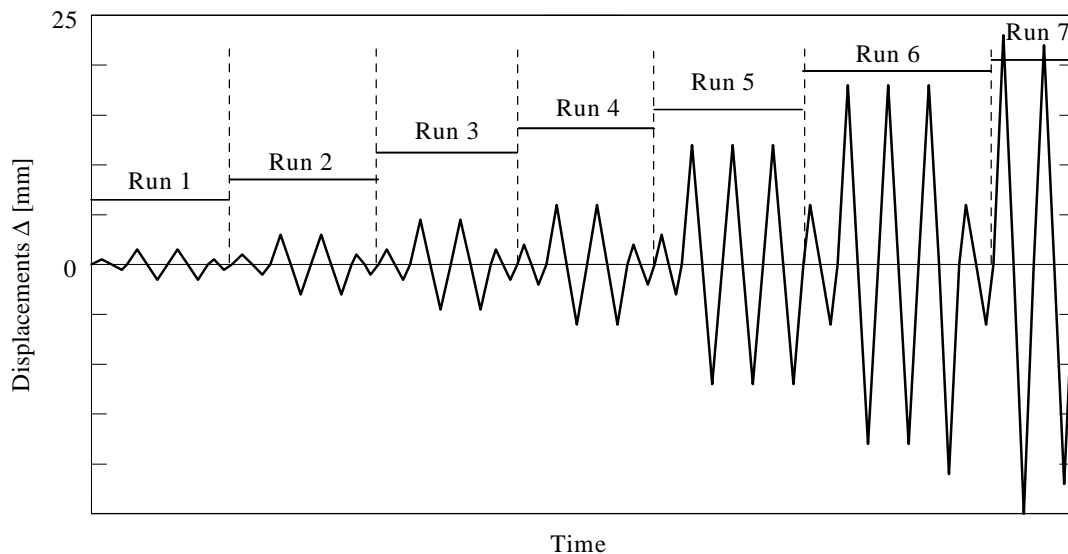


Figure 4.21: Displacement history applied to the second floor of the building model tested under cyclic static action at the University of Pavia [MKC 95]

Due to the flexible floor beams, wall plane D and wall planes A+B+C constitute in practice two independent structural systems. The grey curve in Figure 4.22 shows the overall response of wall plane D as an envelope of the hysteresis curves of the total base shear V_b versus the horizontal displacement of the second floor Δ .

The solid black curve shows the theoretical capacity curve using the evaluation method taking into account the coupling effect due to the spandrels. Also given are the points at which the building enters the next damage grade. Here, the failure of the first wall, indicating damage grade 4, leads to the collapse of the whole building: $DG4 = DG5$.

The comparison between the experimental result and the theoretical result for the overall response shows that the evaluation method gives a rather conservative estimate of the capacity curve of the building, especially concerning the displacement capacity which is underestimated by 50%, whereas the shear capacity lies within 15% of the measured shear capacity and, hence, can be considered as sufficiently accurate.

Also given in Figure 4.22 is the theoretical capacity curve of the wall plane D modelled as interacting cantilever walls (no coupling effects). It shows clearly the invalidity of this approach with respect to the experimental result.

As the building was tested under cyclic static action no vulnerability function of the type defined in Chapter 3 could be recorded as this needs some information on the ground

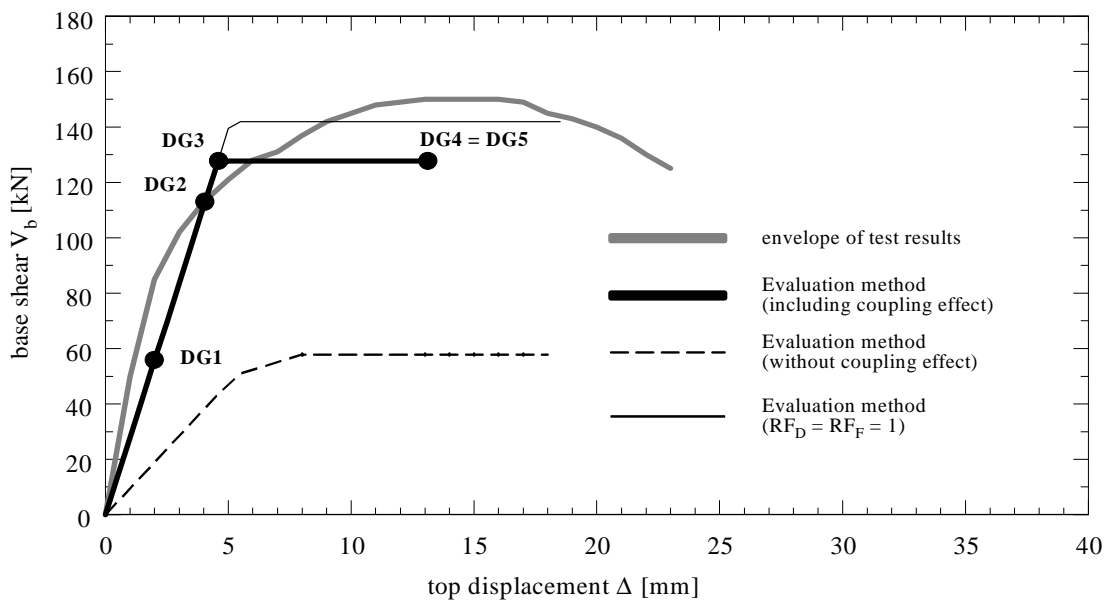


Figure 4.22: Total base shear vs. second floor displacement of wall plane D of the model building tested under cyclic static action at the University of Pavia

movement and hence the validation of the theoretical vulnerability function from the evaluation method is not possible.

4.4.2 ISMES tests

Within the scope of the environment program funded by the Commission of the European Community for the “Experimental evaluation of technical interventions to reduce the seismic vulnerability of old existing buildings” a series of tests on two storey masonry model buildings, scaled at 1:2, were carried out by the use of the shaking table of the testing centre ISMES (Bergamo, Italy). The full description of the test procedure and the measured experimental response can be found in [BP 96].

A total number of 8 models were tested: four limestone masonry models and four brick masonry models. The main features of the four brick masonry models are:

- model A1 and D1: regular brick masonry model buildings with timber floors. Their connection to the walls were improved by steel bars anchored to them.
- model B1 and C1: regular brick masonry model buildings with timber floors with no additional device to improve the floor-wall connection.

The models were intended to represent elementary buildings in the Mediterranean area. The materials of the models were chosen to reproduce the bad conditions of real existing buildings, solid bricks with a mortar of poor quality. The compressive strength of the masonry was $f_{mx} = 2.2$ MPa.

The floor slabs were composed of 6 x 9 cm fir beams which were regularly spaced at 20.4 cm intervals and supported a layer of 2 cm thick timber planks, nailed against the beams below.

The geometry of the model buildings is shown in Figure 4.23. The thickness of all walls was 0.45 m.

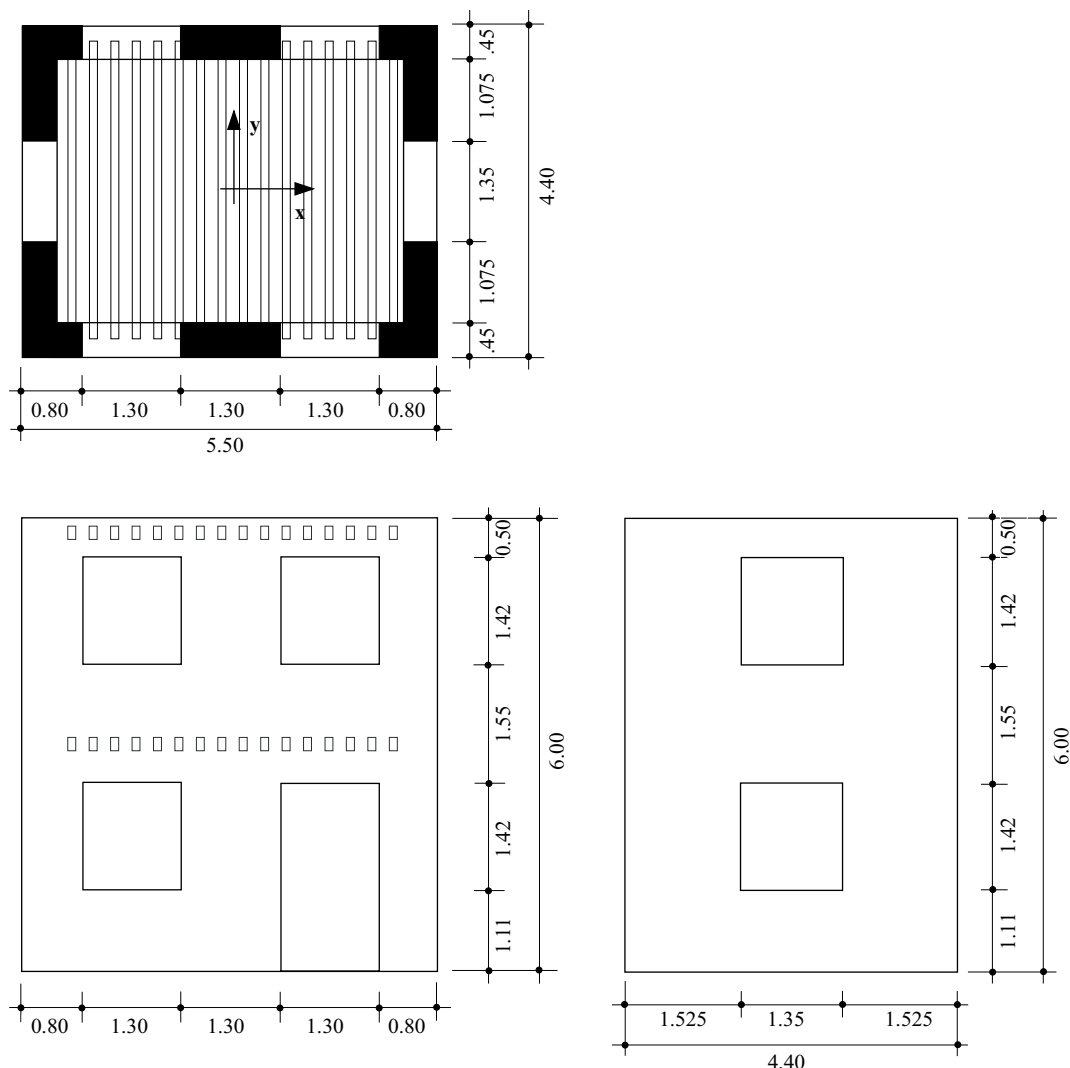


Figure 4.23: Plan and elevation of the model buildings tested dynamically at the testing centre ISMES [BP 96], dimensions in m

Two different base inputs were used, both derived from the signals recorded at Calitri during the 1980 Irpinia earthquake; a long duration record with a duration $T = 90$ s for models B1 and C1, and a short duration record with a duration $T = 40$ s for models A1 and D1.

Each model was subjected to a series of tests with increasing peak values of ground acceleration. In the following it is concentrated on the x-direction as it is better recorded than the y-direction. For each test the peak response acceleration at the two floor levels were recorded, as well as the frequencies, the damping coefficients β_{eqj} and the modal participation factors Γ_j for the first five eigenmodes, $j = 1 \dots 5$.

Figure 4.24 shows the overall response of the four models as the envelope of the hysteresis curves of the total base shear V_b versus the top displacement Δ . It is evident that the behaviour of the two identical model buildings A1 and D1 with improved connections differ even though submitted to the same seismic input (short duration input), the same for the two identical model buildings B1 and C1 (without improved connections, long duration input).

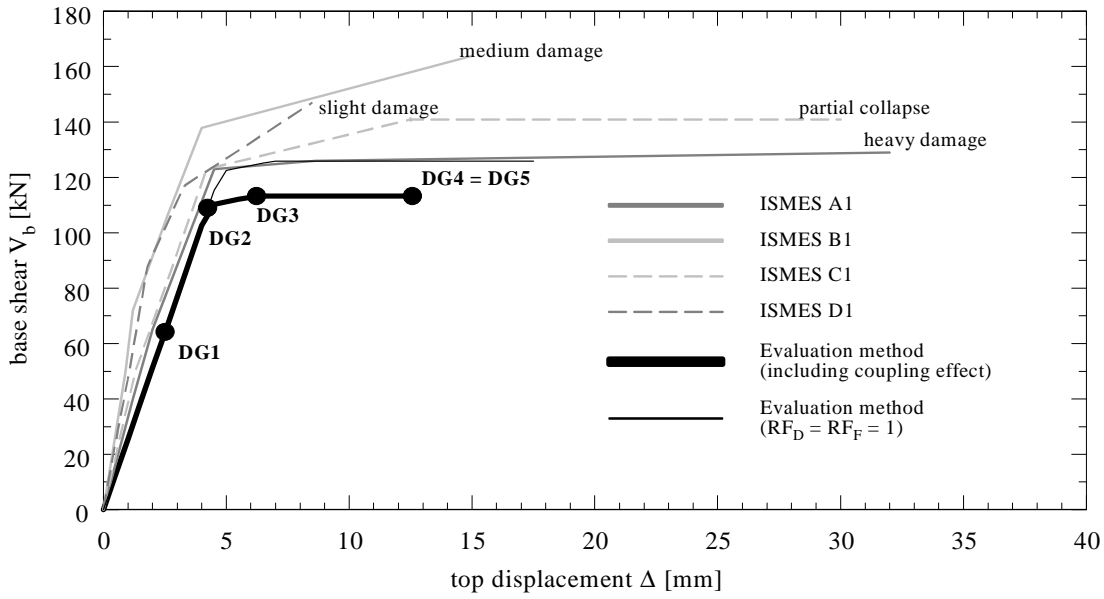


Figure 4.24: Total base shear vs. second floor displacement in x -direction of the model buildings tested dynamically at the testing centre ISMES

The theoretical capacity curve using the evaluation method is given in the same figure. Again, it is a conservative estimate of the capacity, the shear capacity being underestimated by about 15%, the displacement capacity by nearly 60%! Also given are the damage grades according to the European Macroseismic Scale. Since the failure of the first wall leads to a reduction in the capacity of the building to less than $2/3 \cdot V_{bm}$, it indicates also the collapse of the whole building i.e. DG4 = DG5.

As the model buildings were tested dynamically, it is also possible to compare the measured and calculated displacement demand as a function of the seismic input (Figure 4.25). Here, the seismic input is expressed using the peak ground acceleration of the base input instead of the spectral displacement, as this parameter was given in the report. For the theoretical curve the peak ground acceleration was derived from the spectral displacement as follows:

$$a_g = \frac{S_d(f_1)}{(2\pi f_1)^2 \cdot A(f_1)} \quad (4.56)$$

$A(f_1)$ is the amplification factor at the fundamental frequency of the building.

Figure 4.25 shows the theoretical displacement demand as a function of the seismic input for the model buildings using first the classical equal energy approach and secondly taking into account an equivalent stiffness and thus the change in the fundamental frequency (Section 3.6). During the elastic phase, both approaches are identical, the difference occurs when the structure becomes inelastic, the equal energy approach leading to a smaller displacement demand for a given peak ground acceleration.

The underestimation of the displacement capacity by the evaluation method seems to become less important with regard to the seismic input since the increase in displacement with nearly zero stiffness happens for a very small increase in peak ground acceleration and hence the estimated peak ground acceleration for damage grade 5 is very close to the

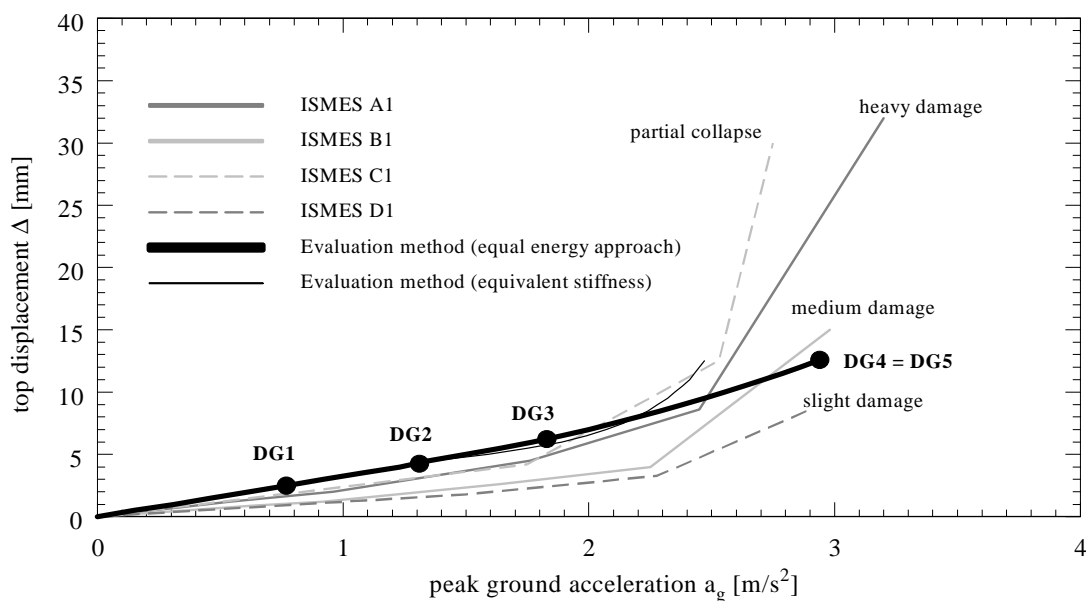


Figure 4.25: Top displacement as a function of peak ground acceleration of the model buildings tested dynamically at the testing centre ISMES

measured peak ground accelerations of the model buildings A1 and C1 at heavy damage and partial collapse.

4.4.3 Conclusions

The theoretical estimate of the capacity of the building using the evaluation method is rather conservative, even when considering the coupling effect. However, it is reminded that the calculation of the theoretical capacity curve includes two arbitrary reduction factors, $RF_F = 0.85$ and $RF_D = 0.75$ (Section 4.2.5), introduced to take into account the cyclic nature of the earthquake action. Setting both reduction factors equal to 1 would definitely improve the results with respect to the shear capacity (cf. thin black curves in Figures 4.22 and 4.24). This could be justified since the calculation of the shear capacity is based on the lower bound theorem of plasticity, and thus the results are always a lower bound to the true shear capacity. The displacement capacity, however, will still be underestimated, but, as we have seen, this becomes less important with regard to the peak ground acceleration (Figure 4.25).

It is also reminded that the evaluation method was developed to evaluate existing buildings within the earthquake scenario project for which the required accuracy lies well within these results, especially when considering the scatter of the test results of the identical model buildings A1 and D1, and B1 and C1 submitted to the same seismic input.

4.5 Evaluation method step by step

So far the principle of the evaluation method and its application to masonry buildings was discussed. In the following, the method is summarised into a step by step procedure to facilitate its application to real buildings.

Step 1) Input Data

First of all the input data to the evaluation method has to be gathered such as the overall geometry of the building (total floor area A_{tot} , building height H_{tot} and storey height h_{st}), the material properties (compressive strength orthogonal to the mortar bed f_{mx} , compressive strength parallel to the mortar bed f_{my} , angle of internal friction ϕ , Youngs modulus and shear modulus of the masonry E_m and G_m , stiffness reduction factor k_{eff}/k_0 and specific weight of the masonry γ_m) and the vertical loads (self weight of the floors and the walls g_{fl} and g_w , surcharge q_d , live load q_N and weight of the roof q_{roof}).

Step 2) Identification of structural walls

All the structural walls acting in the direction considered have to be identified with their main characteristics: length l_w , thickness t and height of the pier h_p .

Step 3) Calculation of normal forces

For each wall the normal forces due to the vertical loads have to be calculated at each storey.

Step 4) Capacity curves of the walls

For each wall the three parameters that determine the bilinear capacity curve of the wall, V_m , Δ_y and Δ_u , are calculated as explained in Sections 4.2.3 to 4.2.5.

Step 5) Capacity curve of the building

The capacity curve of the building in one direction is obtained by superposition of the capacity curves of all the walls acting in this direction.

Step 6) Identification of damage grades

The damage grades are identified on the capacity curve of the building as a function of the top displacement Δ .

Step 7) Bilinear approximation of the capacity curve of the building

In order to define an equivalent SDOF system, a bilinear approximation of the capacity curve of the building has to be defined by means of the stiffness of the linear elastic part k and the shear capacity V_{bm} determining the yield displacement of the building Δ_{by} .

Step 8) Equivalent SDOF system

Using modal analysis, the equivalent SDOF system is defined by the equivalent stiffness k_E , the equivalent mass m_E , the equivalent height h_E and the modal participation factor Γ . The frequency of the SDOF system corresponds to the fundamental frequency of the building.

Step 9) Vulnerability

For a given elastic response spectrum, knowing the fundamental frequency of the building and hence the spectral displacement, the corresponding top displacement of the

Vulnerability of masonry buildings

building Δ is calculated taking into account the effects of non linearity. Thus the damage as a function of the spectral displacement can be determined.

Step 10) Out-of-plane cracking

The spectral displacement that triggers out-of-plane cracking is determined and compared to the spectral displacement that triggers in-plane cracking.

Step 11) Out-of-plane failure

The spectral displacement that triggers out-of-plane failure of a wall is determined and compared to the spectral displacement that triggers in-plane failure of a wall.

The application to a real building is illustrated in Section 6.4.

4.6 Conclusion

A relatively simple evaluation method based on engineering knowledge has been developed with the goal to assess the vulnerability of existing masonry buildings within the scope of the earthquake scenario project for Switzerland. Comparisons with experimental results have shown that the results from the evaluation method lie within the accuracy required for earthquake scenarios.

However, many assumptions had to be made in order to use this method in practice as the behaviour of unreinforced masonry buildings under earthquake action is not yet very well understood. Further research could help to reduce the lack of knowledge and to improve the reliability of the evaluation method.

5 Vulnerability of RC buildings

5.1 Introduction

Even though the majority of new buildings consist of reinforced concrete, they only constitute a small part of the building stock in Switzerland. Previous work [Pe 00] has shown that they are usually not critical in regions of low and medium seismicity, even though older structures tend to lack ductility due to poor detailing and lack of capacity design principle. However, for the complete evaluation of a town or a town quarter, their seismic vulnerability has to be evaluated as well.

Extensive research on the seismic behaviour of reinforced concrete buildings exists and it is not the aim of this work to go deeper into this topic but to use already existing models and methods and to fit these into the evaluation method presented in Chapter 3.

After a very brief review of the moment curvature relationship of reinforced concrete wall sections in Section 5.2, the different types of reinforced concrete buildings that can be encountered in Switzerland are presented in Section 5.3. The derivation of the capacity curve of a reinforced concrete building is described in Section 5.4. Different methods are introduced depending on the type of reinforced concrete building. The identification of the damage grades according to the European Macroseismic Scale and the derivation of the vulnerability function follow in Sections 5.5 and 5.6. Section 5.7 compares the results of two methods presented in Section 5.4 and finally the evaluation method is summarized in a step-by-step procedure in Section 5.8.

5.2 Moment-curvature relationship of reinforced concrete wall sections

Given the section of a wall with the distribution of reinforcement and the acting normal force, a bilinear approximation of the moment-curvature relationship can be established (Figure 5.1). This bilinear approximation is determined by two points, (ϕ'_y, M_y) and (ϕ_u, M_u) (Figure 5.1 a). In most cases (ϕ'_y, M_y) coincides with the first yield of the tensile reinforcement. The first-yield curvature ϕ'_y is then given from Figure 5.1 c) as

$$\phi'_y = \frac{\varepsilon_y}{(d - x_y)}. \quad (5.1)$$

ε_y is the yield strain of the reinforcement, $\varepsilon_y = f_y/E_s$, with f_y the yield strength and E_s the modulus of elasticity of the reinforcement, d is the depth of the extreme tensile reinforcement and x_y is the corresponding depth of the neutral axes.

For very high reinforcement ratios or high axial loads, high compressive strains may develop before the first yield of reinforcement occurs. In such cases, the first-yield curvature ϕ'_y is given as:

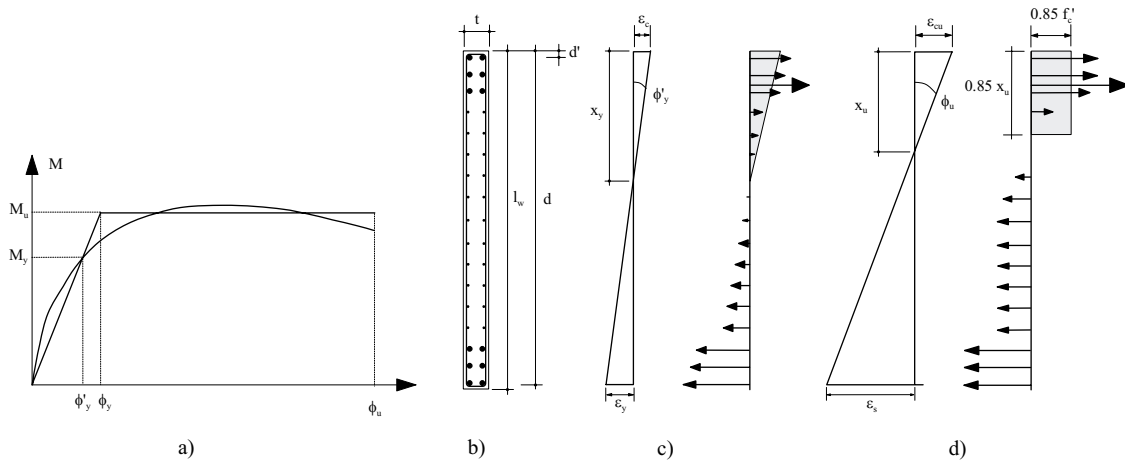


Figure 5.1: a) Bilinear moment curvature relationship, b) wall section, c) strain and corresponding stress resultants at first yield and d) at ultimate

$$\phi'_y = \frac{\epsilon_c}{x_y}. \quad (5.2)$$

ϵ_c is the strain in the concrete at the extreme compressive fibre and can be assumed to be 0.0015. The moment at first yield M_y is obtained by taking moments of the stress resultants about the centre of gravity of the section, assuming a linear stress distribution in the concrete under compression (Figure 5.1 c).

(ϕ_u, M_u) corresponds to the ultimate point, which is usually defined by the extreme compressive fibre reaching the ultimate compressive strain of concrete ϵ_{cu} . This assumes that the strain ductility capacity of the reinforcement is high and not critical. In this case the ultimate curvature ϕ_u is given as:

$$\phi_u = \frac{\epsilon_{cu}}{x_u} \quad (5.3)$$

x_u is the corresponding depth of the neutral axis. Note, x_u is always smaller than x_y and hence $\phi_u > \phi_y$.

However, latest research has revealed that nowadays the ductility capacity of reinforcing steel in Switzerland is often insufficient [BW 98]. This is mainly due to new production procedures leading to high strength steel with very small strain-hardening ratios and very small strain ductility capacities. As a consequence rupture of the reinforcement may occur before the concrete reaches its ultimate compressive strain [DWB 99] [LWB 99], and hence, the ultimate curvature is given as:

$$\phi_u = \frac{\epsilon_s}{d - x_u}. \quad (5.4)$$

M_u is the plateau value of the bilinear approximation. It is not necessarily the moment at ultimate condition nor the maximum. Normally M_u is taken to be the moment at $\phi = 5 \cdot \phi_y$. However, the difference being negligible, M_u can be taken as the moment at ultimate. The stress distribution in the compressed concrete can be approximated by

an equivalent stress block with an extension of $0.85 \cdot x_u$ and a mean compressive strength of $0.85 \cdot f'_c$, f'_c being the cylinder compressive strength of the concrete (Figure 5.1 d).

The nominal yield curvature ϕ_y of the bilinear approximation can then be extrapolated:

$$\phi_y = \phi'_y \cdot \frac{M_u}{M_y} \quad (5.5)$$

The rotational ductility of the wall section is defined as:

$$\mu_\phi = \frac{\phi_u}{\phi_y} \quad (5.6)$$

For wall sections with only minimum transverse reinforcement and/or bad detailing (inadequate spacing of transverse reinforcement, only corner bars are restrained against buckling by a bent of transverse reinforcement and hoops are not bent back into the core [PC 91]), f'_c is taken to be the cylinder compressive strength of unconfined concrete and ϵ_{cu} is usually taken between 0.0035 and 0.005. At this point spalling of concrete occurs and due to the lack of adequate transverse reinforcement, the longitudinal bars will start to buckle.

Note that the actual concrete strength in a structure usually exceeds the nominal 28-day strength. This must be taken into account when evaluating existing buildings (cf. Section 6.3).

For wall sections with increased transverse reinforcement ratio and/or special stabilising hoops around the end reinforcement bars such as required for capacity design [Ba 95] the confining effect of the transverse reinforcement can be taken into account using the model developed by Mander et al. [MPP 88]. Still more important than the increase in the compressive strength is the increase in the ultimate compressive strain. Even for very small transverse reinforcement ratios where the increase in the compressive strength is less than 1%, the increase in the ultimate strain can be in the range of 50 - 100%! Although spalling of the concrete cover will have occurred, buckling of the longitudinal bars is prevented by the hoops leading to an increased ductility.

This simple bilinear approximation of the moment-curvature relationship of a wall section gives very good results as comparisons with test results can show. Figure 5.2 shows the comparison of the bilinear approximation of the moment-curvature relationship with the envelopes of the hysteretic response of 5 walls, WSH2 - WSH6, that have been tested under cyclic static action at the Swiss Federal Institute of Technology [DWB 99].

The envelopes of the moment-curvature relationships of the walls tested were obtained by taking at each ductility step the maximum moment at the base of the wall from the hysteresis curves and the corresponding calculated curvature as found in [DWB 99]. At each ductility step the average values over the displacement to the north and the displacement to the south were taken. The point of failure corresponds to the last complete cycle.

Extensive studies on cantilever walls have shown that the yield curvature and the ultimate curvature are rather insensitive to variations of axial load ratio, longitudinal reinforcement ratio and distribution of longitudinal reinforcement, but depend almost exclu-

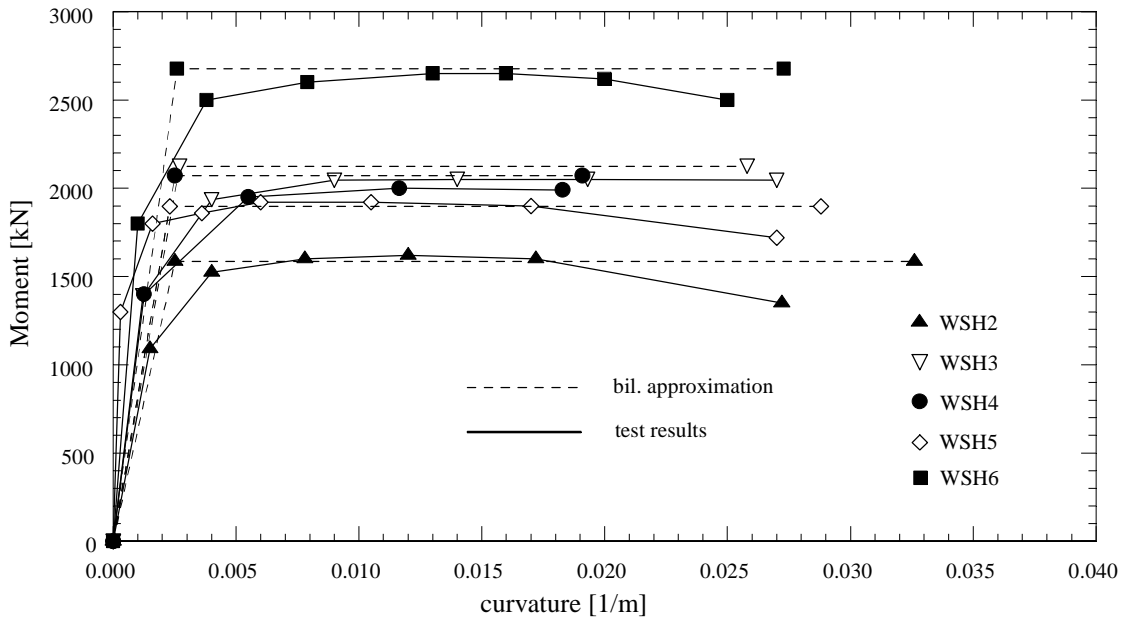


Figure 5.2: Comparison of the bilinear approximation of the moment-curvature relationship with the test results of the walls WSH2-WSH6 tested under cyclic static action at the ETH [DWB 99]

sively on the yield strain of the reinforcement ε_y and the length of the wall l_w [PK 98]. Priestley and Kowalsky proposed the following expression for the yield curvature ϕ_y :

$$\phi_y = K_1 \cdot \frac{\varepsilon_y}{l_w}. \quad (5.7)$$

The value suggested for $K_1 = 2.0$, the variation with axial load ratio and longitudinal reinforcement being very small, $\pm 5\%$.

The expression proposed for the ultimate curvature ϕ_u is:

$$\phi_u = \frac{K_2}{l_w}. \quad (5.8)$$

The value suggested for $K_2 = 0.072$, the variation with axial load ratio and longitudinal reinforcement being around $\pm 10\%$.

The expression for the ultimate curvature seems to be too simple. The influence of the transverse reinforcement on the ultimate curvature was not investigated and is completely neglected in Equation (5.8). However, the transverse reinforcement does have a significant influence on the ultimate compressive strain of the concrete ε_{cu} [MPP 88] and hence on the ultimate curvature of the wall section which should be taken into account. Also, to neglect the influence of the axial load does not seem justified as the axial load does critically affect the ultimate curvature. Earlier on Priestley even recommended the inclusion of the variation of the axial load due to seismic action when estimating plastic rotations for reinforced concrete columns [Pr 95].

It is also assumed that the ultimate condition is defined by the extreme compressive fibre reaching the ultimate compressive strain of concrete ε_{cu} . However, this is not always true for structural walls in Switzerland where rupture of the reinforcement bars may oc-

cur before concrete crushing due to the bad characteristics of the reinforcement steel [DWB 99] [LWB 99]. In that case Equation (5.8) overestimates the ultimate curvature ϕ_u .

In the following, therefore, these simple expressions are not used but the basic formulas presented earlier as they are considered to be equally simple and straight forward without neglecting important parameters. The variation of the normal force due to the cyclic nature of the earthquake (cf. Section 3.5.3), however, will be neglected as in the case of masonry walls (cf. Section 4.2.1).

5.3 Different types of reinforced concrete buildings

Most reinforced concrete buildings in Switzerland are structural wall systems, structural frame systems are hardly ever used. Looking at structural wall systems, three different types can be distinguished:

- a) structural wall systems with negligible frame action,
- b) structural wall systems with “separate” frame action,
- c) structural wall systems with frame action due to coupling of the walls.

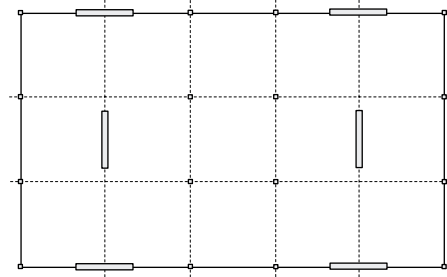
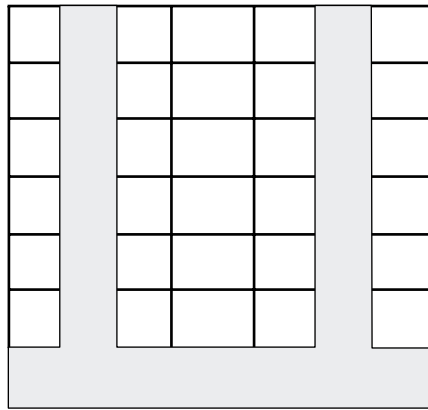
Figure 5.3 shows plan and elevation of the three types of structural wall systems. The structural wall system with negligible frame action (Figure 5.3 a) consists of rather slender reinforced concrete walls that act to transmit the horizontal forces to the ground, slender, possibly pin-connected, columns that carry only gravity loads and flat reinforced concrete floors. The frame action being negligible the building can be seen as a system of interacting cantilevers with a moment distribution over the height of the building due to horizontally acting equivalent earthquake forces corresponding to Figure 3.5 a).

If the columns are less slender and/or the floors have underbeams a moderate frame action develops which should be taken into account. However, the frame action derives largely from the gravity load columns and not only from the walls, hence “separate”. This is shown in Figure 5.3 b). The moment distribution over the height of the building due to horizontally acting equivalent earthquake forces corresponds to Figure 3.5 b).

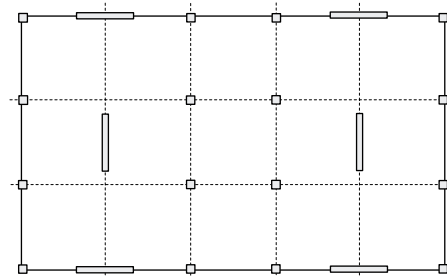
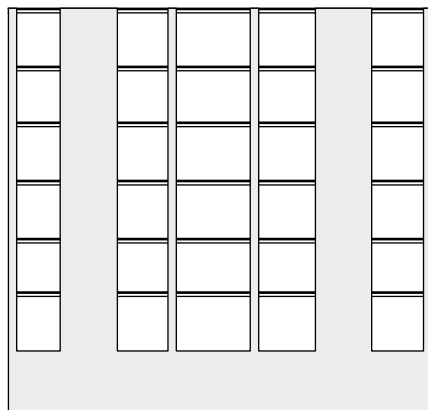
Both types of structural wall systems are usually used for office buildings. Figures 5.3 a) and b) show ideal versions of these structural wall systems. Their simple and regular layout allow a straight forward application of the principles of capacity design [PP 92] and hence a favourable seismic behaviour. In reality, in most existing buildings the structural walls are grouped around staircases and lift shafts. Their seismic behaviour is usually less favourable, however, the same classification applies.

The third type of structural wall systems with frame action due to coupling of the walls is shown in Figure 5.3 c). It consists only of walls which carry both, horizontal and vertical forces and no gravity load columns exist. The frame action derives entirely from the coupling of the walls by floors and spandrels. The moment distribution over the height of the building due to horizontally acting earthquake forces corresponds to Figure 3.5 b) or for very deep spandrels even to Figure 3.5 c). This type of structural wall system is usually found in residential housings. However, pure reinforced concrete systems are

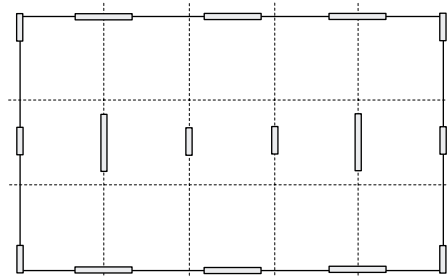
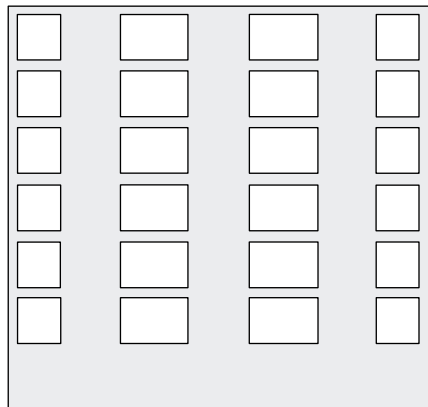
Vulnerability of RC buildings



a)



b)



c)

Figure 5.3: Three types of structural wall systems: a) with negligible frame action, b) with “separate” frame action and c) with frame action due to coupling of the walls

less often used. Much more frequently used are mixed systems of reinforced concrete walls combined with unreinforced masonry walls.

5.4 Capacity curve of a reinforced concrete building

As defined in Section 3.5.1 the capacity curve of a building is a plot of the base shear V_b as a function of the top displacement Δ and can be obtained by superposition of the capacity curves of the walls (Section 3.5.4). The bilinear capacity curves of the walls are defined by three parameters: The shear capacity of the wall V_m , the nominal yield displacement at the top of the wall Δ_y and the nominal ultimate displacement at the top of the wall Δ_u . The shear capacity of reinforced concrete walls derives primarily from its flexural strength. Hence, it can be deduced from the moment-curvature relationship as a function of the force distribution and the frame action. However, in some cases, the shear strength of a wall section can be critical and must be checked (Section 5.4.4).

In the following, the construction of the capacity curve of a reinforced concrete building is considered separately for the three types of structural wall systems: wall systems with negligible frame action, wall systems with separate frame action and wall systems with frame action due to coupling of the walls.

5.4.1 Structural wall systems with negligible frame action

In this case, there is virtually no coupling between the walls and the building can be seen as a system of interacting cantilever walls. The top displacement of a cantilever wall due to triangularly distributed forces is:

$$\Delta = \frac{11}{60} \cdot \frac{V \cdot H_{\text{tot}}^3}{EI} \quad (5.9)$$

For slender walls, the shear deformation is negligible.

The height of the resultant force is equal to $2/3 \cdot H_{\text{tot}}$. And hence the maximum shear force the wall can sustain is:

$$V_m = \frac{M_u}{(2/3 \cdot H_{\text{tot}})} \quad (5.10)$$

From Engineers bending theory comes:

$$\phi = \frac{M}{EI} \quad (5.11)$$

Substituting Equations (5.10) and (5.11) into Equation (5.9) yields:

$$\Delta_y = \frac{11}{40} \cdot \phi_y \cdot H_{\text{tot}}^2 \quad (5.12)$$

A more general formulation of the yield displacement of a cantilever wall for force distributions differing from the triangular one would be:

$$\Delta_y = \chi \cdot \phi_y \cdot H_{\text{tot}}^2 \quad (5.13)$$

As stated in Section 3.5.1 the force distribution should be such that the resulting displacement shape corresponds to the first mode shape. For force distributions that corre-

spond sufficiently close to the first mode, the coefficient χ varies between 0.17 for a single force applied at a height h_E and 0.275 for a triangular force distribution. Hence a value of $\chi = 0.2$ is suggested.

The ultimate displacement at the top of the wall Δ_u is calculated using the following relationship:

$$\Delta_u = \mu_w \cdot \Delta_y. \quad (5.14)$$

μ_w is the displacement ductility of the wall (cf. Section 4.2.4) and can be expressed in terms of the rotational ductility μ_ϕ :

$$\mu_w = 1 + \frac{1}{\chi \cdot H_{tot}^2} \cdot (\mu_\phi - 1) \cdot l_p \cdot \left(H_{tot} - \frac{l_p}{2} \right). \quad (5.15)$$

l_p is the length of the plastic hinge. The value of l_p has a crucial influence on the displacement ductility μ_w of the wall and it seems therefore appropriate to discuss this concept of the length of the plastic hinge, the notion itself being used ambiguously in the literature. Three different definitions of l_p can be found:

- 1) the length over which the detailing of the transverse reinforcement is applied according to capacity design principles,
- 2) the length over which the longitudinal reinforcement has yielded,
- 3) the length which multiplied by the plastic curvature $\phi_p = \phi_u - \phi_y$ results in the correct plastic rotation θ_p , i.e. the plastic rotation that is used to predict the top displacement of the wall in the simplified approach used above.

Strictly speaking definitions one and two refer to a region, only the third definition refers to the length of a hinge. In the following l_p is always used according to the third definition. Many empirical expressions for the estimation of the length of the plastic hinge exist, usually as a function of the wall height H_{tot} and the wall length l_w , or the diameter of the longitudinal reinforcement \emptyset and the corresponding yield strength f_y . Paulay and Priestley [PP 92] suggest the following expression to determine l_p :

$$l_p = 0.08 \cdot H_{tot} + 0.022 \cdot \emptyset \cdot f_y \quad [\text{m}] \quad (5.16)$$

H_{tot} and \emptyset are in [m] and f_y in [MPa]. This expression yields good results provided that the characteristics of the reinforcing steel correspond to those used in New Zealand with a high strain hardening ratio f_u/f_y . This is often not the case for the reinforcing steel used in Switzerland where the strain hardening ratio is usually much smaller (Section 6.3.2). However the strain hardening ratio does have an important influence on the length of the plastic hinge l_p which should be taken into account. In the following, a simple approach to estimate l_p is presented. Figure 5.4 shows the moment and curvature distribution for a cantilever wall with equivalent horizontal force.

l'_p indicates the height of the region over which the reinforcement has yielded (definition 2) i.e. where $M(x) > M_y$. Assuming first that the length of the plastic hinge extends over the whole plastified region, $l_p = l'_p$, l_p is determined by the point at which $M(x) = M_y$.

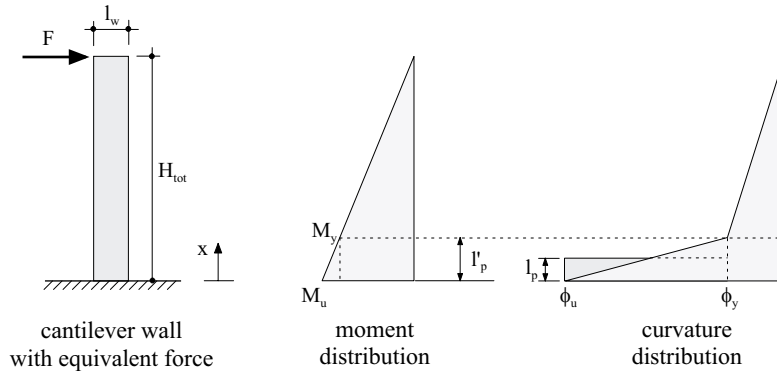


Figure 5.4: Cantilever wall with equivalent horizontal force and the corresponding moment and curvature distribution at ultimate

For a single equivalent force applied at the height H_{tot} as shown in Figure 5.4 this yields:

$$M(x = l_p) = M_y = M_u \cdot \left(1 - \frac{l_p}{H_{tot}}\right). \quad (5.17)$$

Solving for l_p :

$$l_p = H_{tot} \cdot \left(1 - \frac{M_y}{M_u}\right). \quad (5.18)$$

As the force distribution changes so too does the moment distribution and hence the length of the plastic hinge l_p . For triangularly distributed horizontal forces Equation (5.17) changes to:

$$M(x = l_p) = M_y = M_u \cdot \left[1 + \frac{1}{2} \cdot \left(\frac{l_p}{H_{tot}}\right)^3 - \frac{3}{2} \cdot \left(\frac{l_p}{H_{tot}}\right)\right]. \quad (5.19)$$

Solving for l_p :

$$l_p = 2 \cdot H_{tot} \cdot \cos\left(\frac{\varphi}{3} + \frac{4}{3} \cdot \pi\right), \text{ with } \cos \varphi = \frac{M_y}{M_u} - 1. \quad (5.20)$$

Equations (5.18) and (5.20) express l_p as a function of M_y/M_u which is very convenient because M_y and M_u are known from the bilinear moment-curvature relationship calculated in Section 5.2, and include implicitly important parameters such as the strain hardening ratio f_u/f_y , but also the diameter of the longitudinal reinforcement \varnothing and the length of the wall l_w .

Equations (5.18) and (5.20) give an upper limit of the length of the plastic hinge l_p assuming that beyond the yield point the curvature is equal to the ultimate curvature ϕ_u . However, in reality, the curvature increases from ϕ_y to ϕ_u within l'_p and hence $l_p < l'_p$. Assuming a linear increase of the curvature from ϕ_y to ϕ_u as shown in Figure 5.4, for a single equivalent horizontal force applied at the height H_{tot} , the length of the plastic hinge becomes:

$$l_p = \frac{H_{tot}}{2} \cdot \left(1 - \frac{M_y}{M_u}\right). \quad (5.21)$$

And for triangularly distributed horizontal forces:

$$l_p = 2 \cdot H_{tot} \cdot \cos\left(\frac{\varphi}{3} + \frac{4}{3} \cdot \pi\right), \text{ with } \cos\varphi = \frac{1}{2} \cdot \left(\frac{M_y}{M_u} - 1\right). \quad (5.22)$$

Figure 5.5 shows the relative length of the plastic hinge l_p/H_{tot} as a function of M_u/M_y resulting from Equations (5.18) and (5.21) for the walls WSH2 - WSH6 that have been tested under cyclic static action at the Swiss Federal Institute of Technology [DWB 99]. Also shown are the values for l_p/H_{tot} using Equation (5.16), the values for l'_p/H_{tot} , the height of the plastified region as obtained from the calculated curvatures in [DWB 99], and the values for l_p/H_{tot} required to obtain the observed displacement ductility using Equation (5.15). Solving Equation (5.15) for l_p gives:

$$l_p = H_{tot} \cdot \left[1 - \sqrt{1 - 2 \cdot \alpha \cdot \frac{(\mu_w - 1)}{(\mu_\phi - 1)}}\right] \quad (5.23)$$

From the results of Equation (5.23) in Figure 5.5 it can be seen that in general l_p/H_{tot} increases with an increase in M_u/M_y . This is well reflected by the results obtained from Equations (5.18) and (5.21). Equation (5.16), however, is independent of M_u/M_y and therefore tends to overestimates l_p at lower values of M_u/M_y . Equation (5.18) overestimates the length of the plastic hinge l_p , as expected, whereas the results obtained from Equation (5.21) are very close to the required values of l_p/H_{tot} , in general rather underestimating l_p . This is mainly due to two reasons:

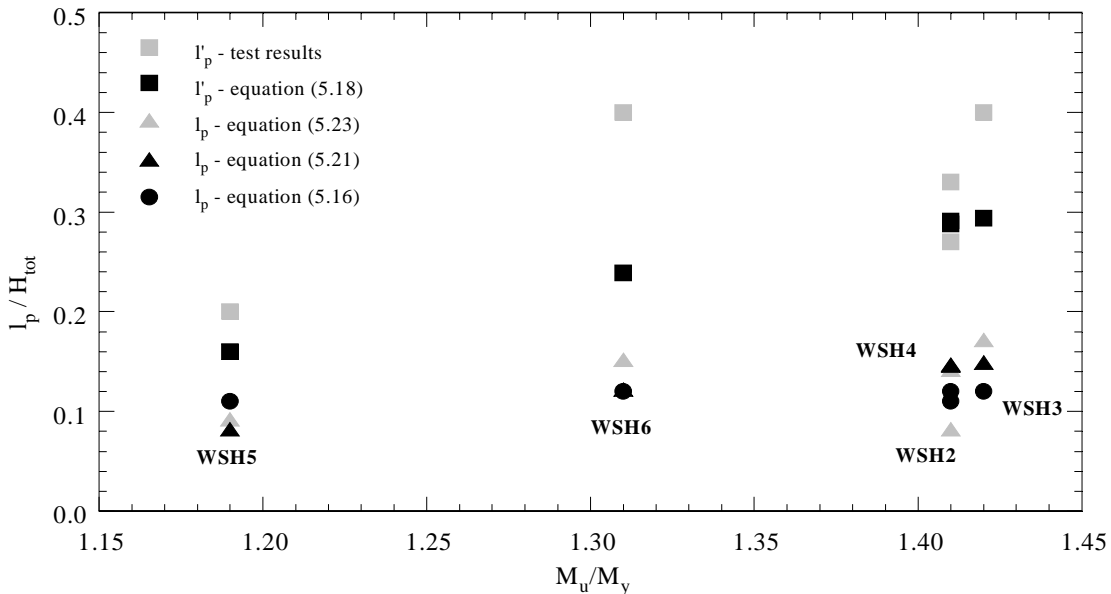


Figure 5.5: Relative length of the plastic hinge l_p/H_{tot} as a function of M_u/M_y for the walls WSH2-WSH6 tested under cyclic static action at the ETH [DWB 99]

- 1) The elongation of the longitudinal reinforcing bars beyond the theoretical base leads to additional rotations and deflections.
- 2) Due to the inclined flexure-shear cracks, the strain in the longitudinal reinforcing bars under tension at some distance above the base is higher than predicted by the bending moment at that level, resulting in a spread of plasticity.

The investigation of those two phenomena, however, goes beyond the scope of this work.

With the estimation of the length of the plastic hinge l_p the three parameters defining the bilinear capacity curve of a cantilever wall V_m , Δ_y and Δ_u are determined. The capacity curve of the building in one direction can then be obtained by superposition of the capacity curves of all the walls acting in this direction using Equation 3.3.

5.4.2 Structural wall systems with "separate" frame action

These are structural wall systems where the frame action is no longer negligible but derives largely from the gravity load columns and not only from the walls.

In this case the frame action can be considered in a further step after having constructed the capacity curve of the system of cantilever walls as explained in Section 5.4.1 following the method proposed by Dazio [Da 00] based on [BD 97]. The complete method can be looked up in [Da 00] or in [D0171 02]. In this section only a few directions are given.

The contribution of the frame action can be essentially described by a shear beam with a shear stiffness $k_{s, tot}$. In order to assess the shear stiffness of the shear beam the shear stiffnesses k_s of the assemblages consisting of horizontal elements such as floors and spandrels and vertical elements such as walls and columns have to be estimated. Figure 5.6 shows four cases of standardized assemblages for the estimation of the frame action according to [Da 00] based on [BD 97].

The height of the assemblages corresponds to the storey height h_{st} . The distance a is the distance between the node of the assemblage and the point of contraflexure in the floor

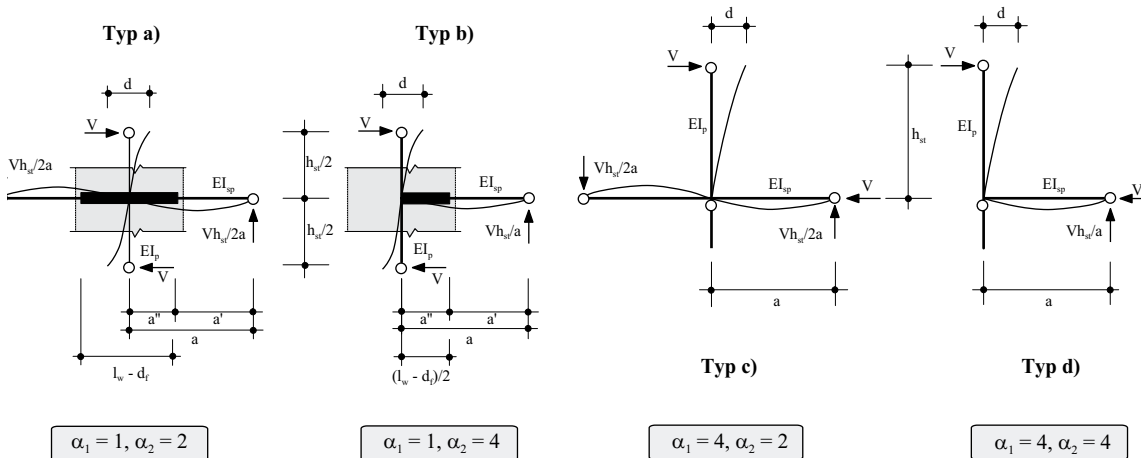


Figure 5.6: Standardized assemblages for the estimation of the frame action after [Da 00]

and has to be estimated. In the case of structural walls the floor is assumed to be rigid over the distance a'' and only flexible over the distance a' . Bachmann and Dazio [BD 97] proposed the following equation for the estimation of a' :

$$a' = a - \frac{l_w - d_f}{2}. \quad (5.24)$$

l_w is the length of the wall and d_f is the thickness of the floor. Using the principle of virtual work the shear stiffness of an assemblage corresponds to the force that results in a unit storey drift $\delta = d/h_{st} = 1$:

$$k_s = \frac{12 \cdot EI_p}{\alpha_1 \cdot h_{st}^2 + \alpha_2 \cdot h_{st} \cdot a' \cdot (a'/a)^2 \cdot (EI_p/EI_{sp})}. \quad (5.25)$$

EI_p is the section stiffness of the vertical element of the assemblage such as a wall or a column and EI_{sp} is the section stiffness of the horizontal element such as the floor or a spandrel. α_1 and α_2 are two coefficients that depend on the boundary conditions of the assemblage and can be taken from Figure 5.6.

The total shear stiffness of the shear beam is equal to the sum of the shear stiffnesses k_s of the assemblages:

$$k_{s, \text{tot}} = \sum k_s. \quad (5.26)$$

The behaviour of the whole structural system is determined by the contribution of walls and of frame action. Proceeding from the capacity curve of the system of cantilever walls as established in Section 5.4.1, taking into consideration the frame action, the capacity curve of the whole structural system consisting of cantilever walls and frame action is obtained.

The base shear of the whole structural system at which yielding occurs, $V_{by, \text{sys}}$, can be determined from the shear capacity of the system of cantilever walls $V_{bm, w}$ as follows:

$$V_{by, \text{sys}} = \frac{V_{bm, w}}{\omega_m}. \quad (5.27)$$

ω_m is a dimensionless parameter that can be approximated for a triangular force distribution to:

$$\omega_m = \frac{1}{\sqrt{\zeta + 1}} \quad (5.28)$$

with

$$\zeta = \frac{k_{s, \text{tot}} \cdot H_{\text{tot}}^2}{2 \cdot EI_{w, \text{tot}}}. \quad (5.29)$$

$EI_{w, \text{tot}}$ is the sum of the section stiffnesses of the walls.

The yield displacement of the whole system, $\Delta_{by, \text{sys}}$, can be determined from the yield displacement of the system of cantilever walls $\Delta_{by, w}$:

$$\Delta_{by, sys} = \frac{\omega_d}{\omega_m} \cdot \Delta_{by, w} \quad (5.30)$$

ω_d is a second dimensionless parameter that can be approximated for a triangular force distribution to:

$$\omega_d = \frac{1.32}{1.32 + \zeta} \quad (5.31)$$

Thus the modified fundamental frequency of the whole structural system can be determined:

$$f_{1, sys} = \frac{1}{2\pi} \cdot \sqrt{\frac{V_{by, sys}}{\Delta_{by, sys} \cdot m_E}} \quad (5.32)$$

Hereby it is assumed that the change in the modal mass m_E is negligible.

Finally, the displacement ductility of the whole structural system $\mu_{\Delta, sys}$ can be calculated from the displacement ductility of the system of cantilever walls $\mu_{\Delta, w}$:

$$\mu_{\Delta, sys} = \sqrt{\frac{\omega_m^2 \cdot \mu_{\Delta, w}^2}{\omega_d}} \quad (5.33)$$

5.4.3 Structural wall systems with frame action due to coupling of the walls

In this case, horizontal and vertical forces are carried entirely by the structural walls, no gravity load columns exist. Here, the frame action is due to the coupling of the walls by floors and spandrels alone. The approach used is the same as for masonry buildings.

The extent of the coupling effect can be expressed by a single parameter, the height of zero moment h_0 (Section 3.5.3). h_0 is determined as a function of the ratio of the flexural stiffness of the spandrel (i.e. of the floor in the absence of spandrels) to the flexural stiffness of the pier, $(EI_{sp}/I_o)/(EI_p/h_{st})$, using Figure 3.6.

Knowing the height of zero moment h_0 and the ultimate moment capacity of the wall section, the shear capacity of the wall can be determined solving Equation (4.19) for V :

$$V_m = \frac{M_2}{h_0} = \frac{M_u}{h_0} \quad (5.34)$$

As for masonry walls the yield displacement at the top of the wall Δ_y can be calculated using Equation (4.25):

$$\Delta_y = V_m \cdot H_{tot} \cdot \left(\frac{h_p \cdot (3h_0 - h_p)}{6 \cdot EI_{eff}} + \frac{\kappa}{GA_{eff}} \right) \quad (5.35)$$

The effective section stiffness of the cracked section can be obtained from the bilinear moment curvature relationship (Figure 5.1):

$$EI_{\text{eff}} = \frac{M_y}{\phi'_y}. \quad (5.36)$$

The shear deformation (second term of Equation (5.35)) is often very small and can be neglected. Otherwise, an effective shear stiffness of the section GA_{eff} has to be estimated.

The ultimate displacement at the top of the wall Δ_u is a function of the rotational ductility μ_ϕ and the appropriate mechanism (Figure 5.7). Depending on the flexural strength ratio, hinges may form first in the spandrels leading to a spandrel sidesway mechanism or in the piers, leading to a pier sidesway mechanism [Pa 97].

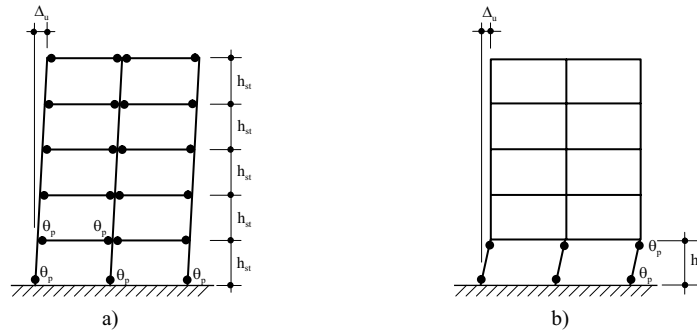


Figure 5.7: Calculation of ultimate lateral displacement for a) a spandrel sidesway mechanism and b) a pier sidesway mechanism

For a spandrel sidesway mechanism as shown in Figure 5.7 a) the ultimate displacement can be written as:

$$\Delta_u = \Delta_y + \left(H_{\text{tot}} - \frac{l_p}{2} \right) \cdot \theta_p = \Delta_y + \left(n \cdot h_{\text{st}} - \frac{l_p}{2} \right) \cdot (\phi_u - \phi_y) \cdot l_p. \quad (5.37)$$

Substituting Equation (5.35) for Δ_y , neglecting the shear deformation, the displacement ductility of the wall is obtained:

$$\mu_w = 1 + (\mu_\phi - 1) \cdot \frac{6 \cdot h_0 \cdot l_p}{H_{\text{tot}} \cdot h_p \cdot (3h_0 - h_p)} \cdot \left(n \cdot h_{\text{st}} - \frac{l_p}{2} \right). \quad (5.38)$$

For a pier sidesway mechanism as shown in Figure 5.7 b) the ultimate displacement can be written as:

$$\Delta_u = \Delta_y + \left(h_{\text{st}} - \frac{l_p}{2} \right) \cdot \theta_p = \Delta_y + \left(h_{\text{st}} - \frac{l_p}{2} \right) \cdot (\phi_u - \phi_y) \cdot l_p. \quad (5.39)$$

Substituting Equation (5.35) for Δ_y , neglecting the shear deformation, the displacement ductility of the wall is obtained:

$$\mu_w = 1 + (\mu_\phi - 1) \cdot \frac{6 \cdot h_0 \cdot l_p}{H_{\text{tot}} \cdot h_p \cdot (3h_0 - h_p)} \cdot \left(h_{\text{st}} - \frac{l_p}{2} \right) \quad (5.40)$$

In the intermediate case of a mixed sidesway mechanism i.e. plastic hinges form in the piers before all the plastic hinges in the spandrels have formed, the displacement ductility can be written:

$$\mu_w = 1 + (\mu_\phi - 1) \cdot \frac{6 \cdot h_0 \cdot l_p}{H_{tot} \cdot h_p \cdot (3h_0 - h_p)} \cdot \left(\beta \cdot h_{st} - \frac{l_p}{2} \right), \quad 1 \leq \beta \leq n. \quad (5.41)$$

As discussed in Section 5.4.1 the length of the plastic hinge depends on the force distribution. In the case of a structural wall systems with frame action due to coupling of the walls, the length of the plastic hinge becomes:

$$l_p = \frac{h_0}{2} \cdot \left(1 - \frac{M_y}{M_u} \right). \quad (5.42)$$

Thus the three parameters defining the bilinear capacity curve of a wall with coupling effects V_m , Δ_y and Δ_u are determined. The capacity curve of the building in one direction can then be obtained by superposition of the capacity curves of all the walls acting in this direction using Equation 3.3.

5.4.4 Shear strength

Reinforced concrete walls cannot only fail in a flexural mode but also in a shear mode. If the shear strength of a wall is reached before its flexural strength, failure occurs very suddenly with little warning. In that case the ductility of the wall μ_w is close to 1. Most code procedures consider the shear strength of a wall V_{shear} to be the sum of the shear carried by the concrete V_c and the shear carried by the transverse reinforcement V_s considering a 45° truss model:

$$V_{shear} = V_c + V_s. \quad (5.43)$$

The shear carried by the concrete is due to mechanisms such as aggregate interlock along crack interfaces, dowel action of longitudinal reinforcement and the shear transfer by concrete in the flexural compression region. Paulay and Priestley suggested the following expression to estimate the contribution of the concrete taking into account the cyclic nature of an earthquake [PP 92]:

$$V_c = 0.6 \cdot t \cdot z \cdot \sqrt{\frac{N}{l_w \cdot t}}. \quad (5.44)$$

z is the effective depth of the wall section, normally taken as $z = 0.8 \cdot l_w$.

In fact, this is a rather conservative estimate of the contribution of the concrete suitable for design purposes. Being concerned with the evaluation of existing buildings, a more realistic estimate of the contribution of the concrete is of interest (cf. Section 3.3).

The contribution of the transverse reinforcement to the total shear strength can be estimated based on the 45° truss model:

$$V_s = A_{sh} \cdot f_{yh} \cdot \frac{z}{s_h}. \quad (5.45)$$

A_{sh} is the area of a set of transverse reinforcement, f_{yh} is the yield strength and s_h the spacing of the transverse reinforcement.

For sections with a high ratio of transverse reinforcement, crushing of the web can occur before yielding of the transverse reinforcement. Hence, the upper limit of the shear strength can be estimated using [Ba 95]:

$$V_{shear} < 0.9 \cdot t \cdot z \cdot \sqrt{f'_c} \quad (5.46)$$

For design purposes a lower upper limit of the shear strength tends to be used nowadays, $V_{shear} \leq 0.16 \cdot f'_c \cdot t \cdot z \leq 6 \cdot t \cdot z$ MPa [PP 92], however, again in the case of the evaluation of existing buildings it is not the aim to be conservative but to assess the behaviour of the building as realistic as possible.

Recent studies have shown that these code procedures do not provide a good estimate of the shear strength. For low ductility levels the estimates tend to be very conservative with a high scatter and at high ductility levels the estimates tend to be non conservative [PVX 94] [Pr 95] [PSC 96]. An improved approach by Priestley et al. [PVX 94] considers the shear strength to consist of three components: The shear carried by the concrete V_c and whose magnitude depends on the level of ductility, the shear carried by the transverse reinforcement V_s and the shear strength enhancement resulting from the axial compression V_N :

$$V_{shear} = V_c + V_s + V_N \quad (5.47)$$

The contribution of the concrete is expressed as a function of the flexural ductility:

$$V_c = t \cdot z \cdot k \cdot \sqrt{f'_c} \quad (5.48)$$

The factor k decreases from 0.29 for curvature ductilities $\mu_\phi < 2$ to 0.1 for $\mu_\phi > 4$.

The contribution of the transverse reinforcement is based on a 30° truss mechanism:

$$V_s = A_{sh} \cdot f_{yh} \cdot \frac{z'}{s_h} \cdot \cot 30^\circ \quad (5.49)$$

z' is the distance between centres of the peripheral transverse reinforcement.

Finally, it is considered that the axial load acting on a wall enhances the shear strength by arch action forming an inclined strut as shown in Figure 5.8. Thus

$$V_N = N \cdot \tan \alpha = N \cdot \frac{l_w - a}{2h_0} = N \cdot \frac{l_w - N/(t \cdot f'_c)}{2h_0} \quad (5.50)$$

Note that this is in fact equivalent to the inclined compression strut through which the shear force is transmitted for masonry walls (cf. Equation (4.12)).

So far, it was considered that the buildings respond predominantly in their first mode and that the influence of the higher modes can be neglected. For cantilever walls, the maximum shear force is then given by equation (5.10), the height of the resultant force being equal to $2/3 \cdot H_{tot}$. However, if the behaviour is strongly influenced by the second or

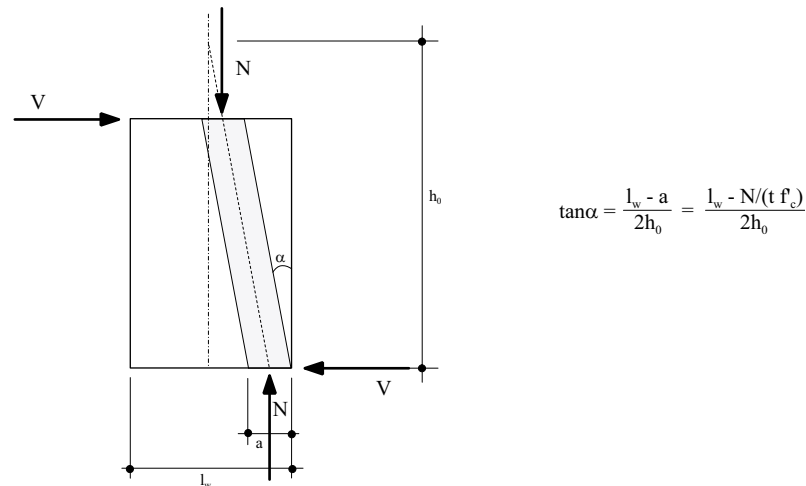


Figure 5.8: Contribution of the axial force to the shear strength after [PVX 94]

third mode the height of the resultant force is located lower, $h_R < 2/3 \cdot H_{\text{tot}}$, leading to an increased shear force:

$$V'_m = \frac{M_u}{h_R} > V_m. \quad (5.51)$$

This should be taken into account when checking structural walls for shear failure. The influence of higher modes increases with decreasing fundamental frequency. This is a result of the typical shape of a response spectrum where for decreasing fundamental frequencies in the region of the descending branch of the spectrum the spectral acceleration $S_a(f_1)$ decreases and hence, the contribution of higher modes to the base shear increases. Simple procedures therefore propose to estimate the dynamic magnification factor ω_n which is defined as the ratio V'_m/V_m as a function of the number of storeys. Typical values for ω_n range between 1 and 1.5. A more refined estimate is given by Keintzel taking into account the influence of the ductile behaviour on ω_n [Ke 90].

With increasing frame action the dynamic magnification of V_m becomes less important and is therefore neglected in the evaluation of the buildings in the target area in Basel.

5.4.5 Cyclic loading

So far the capacity curve of a reinforced concrete wall was obtained considering monotonic loading. However cumulative damage effects caused by several inelastic cycles during an earthquake can be important. Analogous to masonry buildings this effect of the cyclic nature of the earthquake action is taken into account by the use of a force reduction factor RF_F and a displacement reduction factor RF_D . Proposed values for the displacement reduction factor that can be found in the literature are as low as 0.625 [Fa 98]. But again, these are values used for design purpose, for evaluation purpose values close to 1.0 are suggested in order to prevent conservatism.

5.5 Identification of damage grades according to the EMS

In analogy to masonry buildings indicators for the different damage grades of reinforced concrete buildings according to the European Macroseismic Scale [EMS 98] are defined that allow to identify the points on the capacity curve at which the building enters the next damage grade. A copy of this classification of damage to reinforced concrete buildings is given in the Appendix A1.2. Again, Figure 3.14 can be used as illustration.

Grade 1) Negligible to slight damage (no structural damage, slight non-structural damage)

The description of this damage grade states *fine cracks in walls at the base*. This is considered to coincide with the point of onset of cracking, i.e. the point at which the tensile stress at the extreme tensile fibre of the wall section reaches the tensile strength of concrete. The curvature at the onset of cracking is then given:

$$\phi'_{cr} = \frac{\varepsilon_{ct}}{l_w - x_{cr}}. \quad (5.52)$$

ε_{ct} is the strain in the concrete at the extreme tensile fibre at the onset of cracking, $\varepsilon_{ct} = f_{ct}/E_c$, with f_{ct} the tensile strength of concrete, and x_{cr} is the corresponding depth of the neutral axis. The moment at the onset of cracking, M_{cr} , is obtained by taking moments of the stress resultants about the centre of gravity of the section.

Since the stiffness of the uncracked section is much higher than the stiffness of the cracked section, the point (ϕ'_{cr}, M_{cr}) does not lie on the bilinear approximation of the moment-curvature relationship (cf. Figure 5.1 a). The equivalent curvature on the bilinear approximation at the onset of cracking is defined as follows:

$$\phi_{cr} = \frac{M_{cr}}{M_u} \cdot \phi_y. \quad (5.53)$$

For cantilever walls the top displacement at cracking Δ_{cr} is determined using Equation (5.12) and substituting ϕ_{cr} for ϕ_y ; for coupled walls the top displacement at cracking Δ_{cr} is determined using Equation (5.35) calculating first the shear force at the onset of cracking V_{cr} using Equation (5.34) and substituting M_{cr} for M_2 .

Substituting Δ_{cr} into Equation (3.3) the corresponding base shear of the building V_{bcr} can be determined (cf. Equation (4.38)):

$$V_{bcr} = V_b(\Delta_{cr}) = \sum_j V_j(\Delta_{cr})$$

The couple (Δ_{cr}, V_{bcr}) determines the point on the capacity curve of the building at which the building enters damage grade 1. Before this point the building is considered to be undamaged.

Grade 2) Moderate damage (slight structural damage, moderate non-structural damage)

Cracks now appear in *structural walls* of the building. This indicates that the behaviour of the building starts to become more nonlinear. In analogy to masonry buildings it is thus considered to coincide with the point at which the first wall yields and the stiffness of the building starts to reduce. The corresponding displacement is the smallest yield displacement of all the walls of a building $\Delta_{y, \min}$.

The couple $(\Delta_{y, \min}, V_b(\Delta_{y, \min}))$ determines the point on the capacity curve of the building at which the building enters damage grade 2. Before this point all walls behave linear elastically and the stiffness of the building is equal to k .

Grade 3) Substantial to heavy damage (moderate structural damage, heavy non-structural damage)

Spalling of concrete cover and *buckling of reinforced rods* occur. Hence, one indicator of this damage grade is the point at which the strain of the extreme compressive fibre of one wall section reaches $\epsilon_{cu} = 0.0035$. However, for wall sections with minimum transverse reinforcement this corresponds also to the point of failure of the wall section (cf. Section 5.2). Hence, in analogy to masonry buildings, a second indicator of this damage grade, considering the increased non linearity of the building, is the point at which the stiffness of the building tends to zero, which usually corresponds to the point at which the last wall yields, the stiffness of the building becoming zero at that point. The corresponding displacement is the maximum yield displacement of all the walls of a building $\Delta_{y, \max}$.

The couple $(\Delta_{y, \max}, V_b(\Delta_{y, \max}))$ determines the point on the capacity curve of the building at which the building enters damage grade 3.

Grade 4) Very heavy damage (heavy structural damage, very heavy non-structural damage)

This damage grade corresponds to *compression failure of concrete* and *fracture of re-bars*. This is equivalent to the ultimate displacement of a wall (Section 5.4). At this point the reinforced concrete wall, unlike unreinforced masonry walls, does not collapse but enters a rocking mode. As a consequence the displacements become very large leading finally to the collapse of parts of the building. Hence, when the smallest ultimate displacement of all the walls of a building $\Delta_{u, \min}$ is reached, the building is considered to be very heavily damaged.

The couple $(\Delta_{u, \min}, V_b(\Delta_{u, \min}))$ determines the point on the capacity curve of the building at which the building enters damage grade 4. Beyond this point the base shear of the building starts to reduce.

Grade 5) Destruction (very heavy structural damage)

This corresponds to the *collapse of ground floor or parts of buildings*. After the first wall has reached its ultimate displacement the base shear of the buildings reduces. Analogous to masonry buildings reinforced concrete buildings are assumed to be destructed if the base shear reduces below a certain limit which is considered to be 2/3 of its maximum value.

Damage grade	EMS 98	Identification
DG1	Negligible to slight damage (no structural damage, slight non-structural damage) Fine cracks in plaster over frame members or in walls at the base. Fine cracks in partitions and infills	point of onset of cracking, => tensile stress at the extreme tensile fibre of the wall section reaches the tensile strength of concrete
DG2	Moderate damage (slight structural damage, moderate non-structural damage) Cracks in columns and beams of frames and in structural walls. Cracks in partition and infill walls; fall of brittle cladding and plaster. Falling mortar from the joints of wall panels.	behaviour of the building becomes nonlinear, the stiffness of the building starts to reduce, => yield of the first wall
DG3	Substantial to heavy damage (moderate structural damage, heavy non-structural damage) Cracks in columns and beam column joints of frames at the base and at joints of coupled walls. Spalling of concrete cover, buckling of reinforced rods. Large cracks in partition and infill walls, failure of individual infill panels.	increased nonlinear behaviour of the building, the stiffness of the building tends to zero, => yield of the last wall
DG4	Very heavy damage (heavy structural damage, very heavy non-structural damage) Large cracks in structural elements with compression failure of concrete and fracture of re-bars; bond failure of beam reinforced bars; tilting of columns. Collapse of a few columns or of a single upper floor.	=> ultimate displacement of the first wall, determined either by compression failure of concrete or fracture of the reinforcing bars
DG5	Destruction (very heavy structural damage) Collapse of ground floor or parts (e.g. wings) of buildings.	=> drop of the base shear of the building V_b below $2/3 \cdot V_{bm}$

Table 5.1: Damage grades of reinforced concrete buildings

The indicators of the damage grades of reinforced concrete buildings according to the European Macroseismic Scale [EMS 98] are summarized in Table 5.1.

5.6 Vulnerability function of a reinforced concrete building

Using Equation (3.22) the top displacement Δ can be plotted as a function of the spectral displacement $S_d(f_1)$. Including the points at which the buildings enters the different damage grades results in the vulnerability function of the building i.e. the damage as a function of the spectral displacement (Figure 3.15).

5.7 Comparison

In analogy to masonry buildings the evaluation method for reinforced concrete buildings as presented in Section 5.4.3 should be validated (cf. Section 4.4). In the absence of test results of reinforced concrete wall structures the method Dazio presented in Section 5.4.2. is used as reference method in the same way as the test results of Pavia and Ismes were used for the validation of the evaluation method for masonry buildings.

The example building used for the validation is a modification of the building shown in Figure 5.3 c) where the two long walls in the y-direction are removed and replaced by short walls for reason of simplicity. As far as the other characteristics of the building are concerned, geometry and materials, they were chosen following the example building of Dazio [Da 00]. It is a six-storey building with a storey height of $h_{st} = 3.4$ m, adding up to a total building height of $H_{tot} = 20.4$ m. The layout of the plan is shown in Figure 5.9 a) with a total area of $A_{tot} = 30 \cdot 18 = 540$ m². The surface load per storey excluding the self weight of the walls is assumed to be $q_{fl} = 12.5$ kN/m².

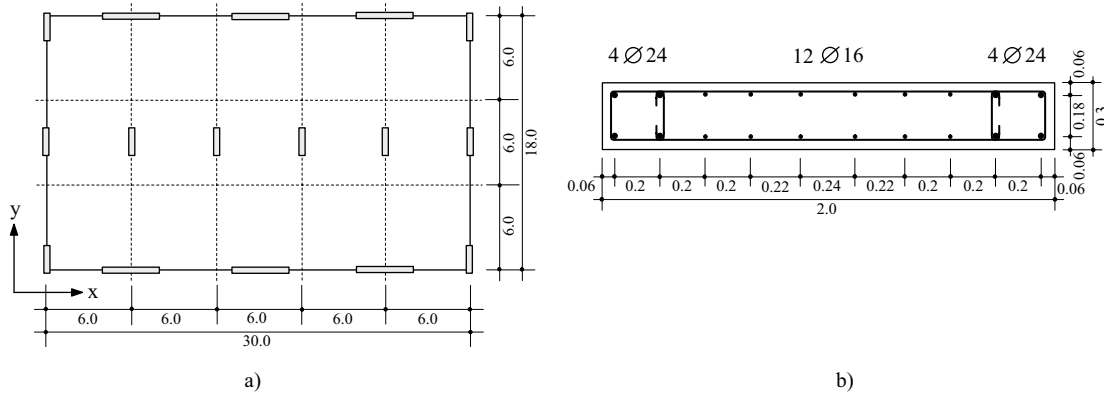


Figure 5.9: a) Layout of example building and b) wall section

For the comparison of the two methods only the y-direction is considered. In this direction all walls have the same length $l_w = 2.0$ m; their section is given in Figure 5.9 b). The floors have a thickness of $d_f = 0.24$ m and underbeams in y-direction in the axis of the walls with a depth of $d_u = 0.4$ m. The properties of the materials are summarized in Table 5.2.

structural element	f'_c [MPa]	E_c [GPa]	f_y [MPa]	E_s [GPa]
wall	45	37.5	500	210
floor	28	30	460	210

Table 5.2: Properties of the materials

The detailed calculations of the capacity curve using the evaluation method for reinforced concrete buildings as presented in Section 5.4.3 are given in the Appendix A2. In this section only the results are presented and discussed.

Figure 5.10 shows the comparison of the two capacity curves. Note that unlike proposed by Dazio, the plastic stiffness of the building is set to zero since all the vertical elements have yielded. Also given are the points on the capacity curve of method 5.4.3 at which the building enters the next damage grade. Here, the ultimate condition of the first wall, indicating damage grade 4, leads to the collapse of the whole building: $DG4 = DG5$. In the elastic range, the two capacity curves are very close. The stiffnesses of the linear elastic part are nearly identical and so are the fundamental frequencies: From the method Dazio, the reference method, $f_1 = 1.24$ Hz and from the evaluation method presented in 5.4.3 $f_1 = 1.27$ Hz. However, the shear capacity obtained from the evaluation meth-

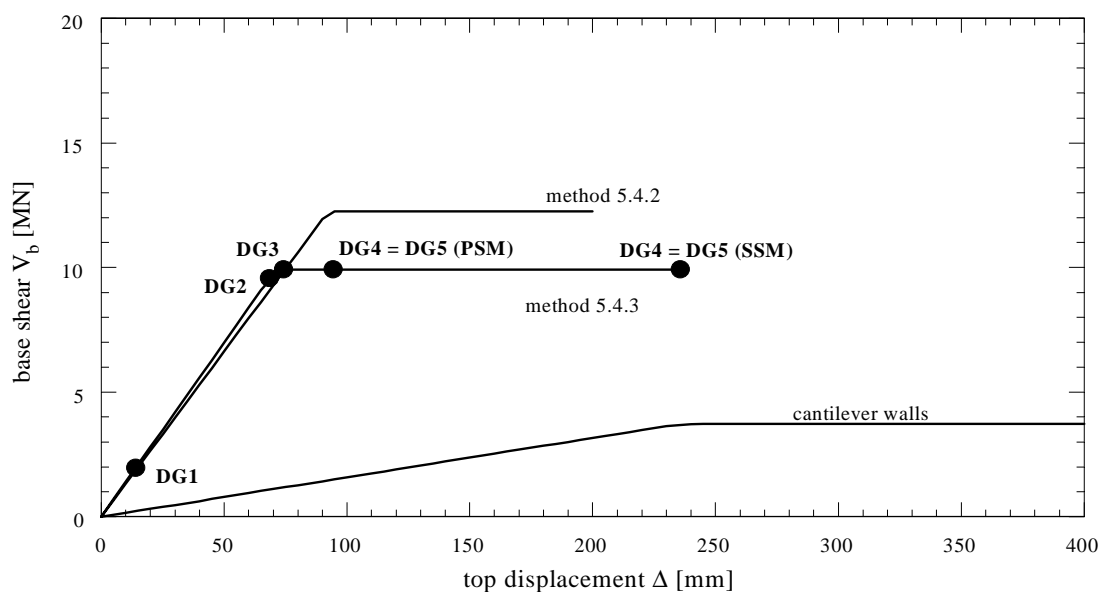


Figure 5.10: Capacity curve of the fictitious example building

od presented in Section 5.4.3 is lower than the one obtained from the method Dazio, 9.9 MN instead of 12.2 MN, as is the yield displacement, 71 mm instead of 92 mm.

In the plastic range the correspondence between the two capacity curves depends very much on the assumed mechanism. Assuming a pier sidesway mechanism (PSM), the plastic deformation capacity is considerably underestimated giving $\Delta_u = 95$ mm instead of 201 mm as predicted by the method Dazio, whereas assuming a spandrel sidesway mechanism (SSM) $\Delta_u = 235$ mm. It is therefore crucial to choose the right mechanism. In the case of reinforced concrete wall structures, the spandrels are usually much weaker than the walls leading rather to a spandrel sidesway mechanism.

It should be noted that in this example the frame action is rather high ($\zeta \approx 10$) and hence the assumed displacement shape of the building with a constant drift equal to the drift of the first storey (Section 4.2.3) approximates well the real displacement shape. For smaller frame actions, the real displacement shape diverges more and more from this linear displacement shape towards the displacement shape of interacting cantilever walls. Thus the drift of the first storey is not representative any more of the mean drift along the building height, leading to an underestimation of the top displacement.

5.8 Evaluation method step by step

In analogy to masonry buildings, the method for the evaluation of reinforced concrete buildings can be subdivided into the following steps (Section 4.5):

- Step 1) Input Data
- Step 2) Identification of structural walls
- Step 3) Calculation of normal forces
- Step 4) Capacity curves of the walls
- Step 5) Capacity curve of the building
- Step 6) Identification of damage grades

Step 7) Bilinear approximation of the capacity curve of the building

Step 8) Equivalent SDOF system

Step 9) Vulnerability

Note that step 10 and 11 of the step-by-step evaluation for masonry buildings concern the out-of-plane behaviour of unreinforced masonry walls and do not apply to reinforced concrete buildings.

5.9 Conclusion

A simple evaluation method for existing reinforced concrete buildings has been proposed in analogy to the evaluation method for unreinforced masonry buildings presented in Chapter 4. A comparison with a thoroughly checked deformation orientated method, recently proposed by Dazio [Da 00] based on [BD 97], has shown that the results lie within the accuracy required for earthquake scenarios.

The evaluation of reinforced concrete buildings and the evaluation of unreinforced masonry buildings are based on the same principle as presented in Chapter 3. They only differ in the capacity curves of the walls which are calculated depending on the material (Section 3.5). It is therefore possible to consider mixed structures, i.e. buildings with reinforced concrete walls and unreinforced masonry walls. Like for “pure” buildings (buildings consisting only of unreinforced masonry walls as presented in Chapter 4 or buildings consisting only of reinforced concrete walls as presented in Chapter 5) the capacity curve of the building is obtained by superposition of the capacity curves of all the walls, reinforced concrete walls and unreinforced masonry walls (cf. Appendix A3).

Vulnerability of RC buildings

6 Application to buildings in Basel

6.1 Introduction

The evaluation method, developed in Chapter 3 and elaborated for masonry and reinforced concrete buildings in Chapters 4 and 5 respectively, shall now be applied to buildings in the city of Basel which is the target area for the earthquake scenario project for Switzerland.

In principle, the evaluation method can be used for the assessment of any building stock. However, since it was developed for the assessment of the building stock in the city of Basel, the characteristics of the building stock in Basel and the consequences on the application of the evaluation method are outlined in Section 6.2. Hereby it is concentrated on residential buildings for several reasons: Even though they constitute the majority of the building population, residential buildings tend to be neglected in other studies which focus rather on industry, the historical centre and life lines. In this respect two studies have been carried out for the city of Basel, one focusing on life lines [BH 92], the other one on industrial facilities [Si 98] for which the critical component determining the vulnerability is often the equipment rather than the building structure. For the earthquake scenario project for the city of Basel these studies could be taken into account. Besides, residential buildings tend to be rather regular and hence the simplifications of the evaluation method apply. In Section 6.3 a short guideline for the derivation of the material properties is given. Finally, in Section 6.4 the evaluation method is applied to a two-storey masonry building which is considered typical for the building stock in Basel, following the 11 steps outlined in Section 4.5.

6.2 Characteristics of the building stock in Basel

6.2.1 General

Due to historical reasons which allowed the construction of houses outside the old town wall only in the second half of the 19th century, the larger part of Basel consists of a rather mixed building population dating from the last 120 years. After the law came out that allowed the construction of houses outside the old town wall, the town spread very rapidly and soon covered the area it covers today. Since then, new buildings were constructed between the older ones, some of which had to be demolished; a reconstruction of a whole town quarter, however, never took place. This applies to most parts of the town except for the old city centre and the industrial quarter in Kleinhüningen, where the building stock is rather special, and the two single dwelling quarters Bruderholz and Riehen. Most residential buildings have between 2 to 7 storeys. The residential buildings constructed until 1950 are usually made of unreinforced masonry, mostly with timber floors. Residential buildings form the second half of the 20th century are often mixed

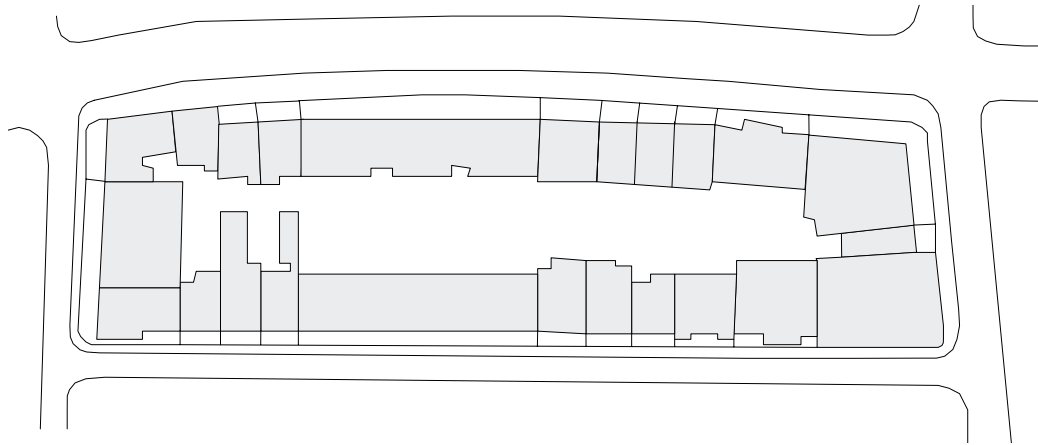


Figure 6.1: Building block in Basel

structures of reinforced concrete combined with unreinforced masonry, pure reinforced concrete systems as discussed in Chapter 5 are less often used.

Figure 6.1 shows a plan view of a typical residential building block in Basel. It can be seen that all buildings are connected to each other to form a single block and the first problem that arises is the identification of “the building”. This is not always straight forward as the buildings often share a common wall, the fire protection wall. A very frequent situation is that a new building is constructed in between two older buildings, using the already existing fire protection walls. In this case there is a coupling effect between the buildings and it is strictly speaking not allowed to consider each building individually. Alternatively, a joint separates the fire protection walls of two adjacent buildings. In this case the buildings behave independently, however, pounding effects could be a problem, particularly when the floors of adjacent buildings are at different elevations. They can then act like rams battering the walls of the other building. In the following, these two problems (coupling and pounding) are not considered.

Figure 6.2 gives a closer look to the typical building layout of two adjacent residential buildings. In the y-direction there are the fire protection walls extending over the whole depth of the building and some walls, usually less long and less thick, in the interior, whereas in the x-direction the wall planes are divided by windows and doors and hence the walls are much more slender.

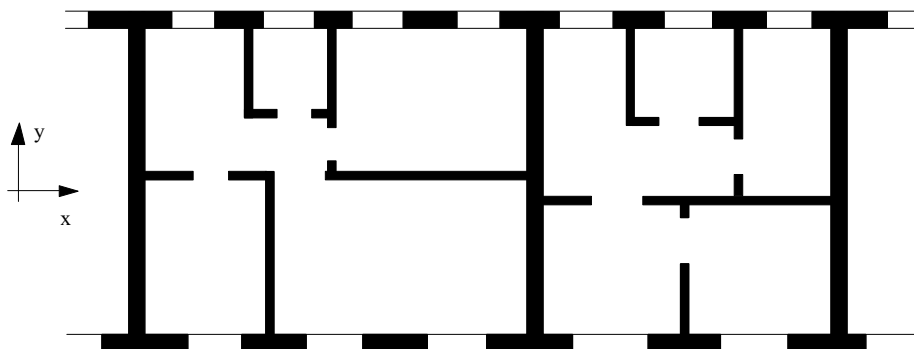


Figure 6.2: Typical building layout in Basel

walls such as the fire protection walls with hardly any normal forces acting on them, except their own weight, is not very well described by the simple assessment procedure based on the simplified failure criteria developed by Ganz [Ga 85] neglecting cohesion, their capacity being largely underestimated. In these cases the sliding criterion (Equation (4.15)) will be very soon activated at the upper floor corresponding to the maximum admissible shear force of the wall. This, however, leads to a very low capacity in the y-direction, sometimes less than the capacity in the x-direction, which is not reasonable. It is more probable that the fire protection walls are rather uncritical and the damage will be more concentrated in the x-direction. Hence, it does not seem appropriate to use the sliding criterion in the same way as the stress criteria (Equations (4.13) and (4.14)). Also, due to the high stiffness of the fire protection walls, the deformation in the y-direction will be such that the remaining interior walls in this direction will not be badly damaged.

Hence, the vulnerable direction that will determine the damage is the x-direction, and it is concentrated on this direction for the determination of the vulnerability functions of the buildings in Basel. This may lead to a rather conservative assessment as the direction of the earthquake does not always coincide with the x-direction (Section 3.4).

6.2.2 Corner buildings

Each building block contains four corner houses (cf. Figure 6.1). These are characterized by two orthogonal façade wall planes and two orthogonal fire protection walls. The effect is to increase the eccentricity of the centre of rigidity R to the centre of mass M leading to an increased torsional effect. In fact, observations have shown, that the degree of damage of corner houses is usually higher than of the adjacent buildings [RC 00]. This is partly due to the increased torsional effect and partly due to pounding. Figure 6.3 shows a simplified plan view of a corner house and its displacement under horizontal forces.

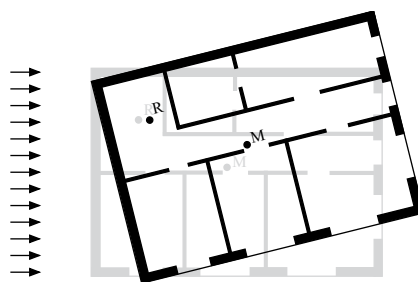


Figure 6.3: Plan view of corner house and its displacement under horizontal forces

Due to the twist deformation, the displacement of the façade walls increase whereas the fire protection walls are almost only twisted. It is therefore suggested for the purpose of a simplified evaluation within the scope of the earthquake scenario project to establish the vulnerability function of a corner house by taking the mean of the vulnerability functions in the two orthogonal directions, however, without taking into account the shear resistance of the fire protection walls.

6.2.3 Floors

So far, only failure related to the walls was discussed assuming the floors to be non critical, acting as rigid diaphragms and distributing the inertia forces derived from the floors onto the walls. This is a valid assumption for reinforced concrete floors which generally possess large in-plane stiffness and relatively good interconnection with the vertical walls. However, the diaphragm action may be jeopardized if the openings which are necessary for staircases and lift shafts are rather large. For timber floors the assumption of rigid floor diaphragms and good floor-wall connection is usually less valid. A full discussion of this problem is beyond the scope of this work, nevertheless, as it may have a significant influence on the behaviour of the building a few comments seem appropriate.

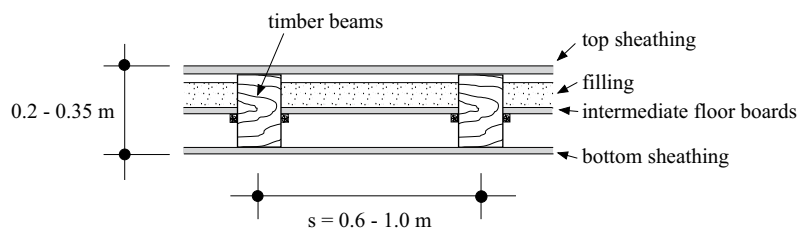


Figure 6.4: Typical timber floor construction

A typical timber floor construction is shown in Figure 6.4. The timber beams which run parallel at a distance of about 0.6 - 1.0 m are connected by the top sheathing nailed onto them. Typically the sheathing is orientated orthogonal to the timber beams. At mid-height of the beams intermediate floor boards are located supporting a filling which acts as thermal and sound insulation. The bottom sheathing usually acts to support the ceiling plaster.

Floor-wall connection

This is the most critical point in all buildings with timber floors since the floor-wall connection not only determines the transfer of the inertia forces derived from the floors onto the walls but also determine the out-of-plane behaviour of the walls. And even more important, in cases where the timber beams rest on the walls being simply supported, a global failure of the building can occur by the slippage of the beams from their supports. Any retrofit strategy should therefore assure proper floor-wall connections.

Floor-wall connections are not indicated in any plan available for the buildings in the small target area in Basel. However, the use of wall anchors was well established by the middle of the 19th century [AK 91][St 04]. Figure 6.5 shows a typical arrangement of wall anchors. The timber beams usually rest on the façade walls where every third or fourth beam is anchored to the wall. The fire protection walls (also often called gable walls) do not support any floor load. They are connected with the floors about every two meters with anchors fixed to at least three parallel beams.

Flexible diaphragm

Reinforced concrete floors are usually very stiff in their plane and hence the floor deformations are negligible and the accelerations equal to the wall acceleration at that storey.

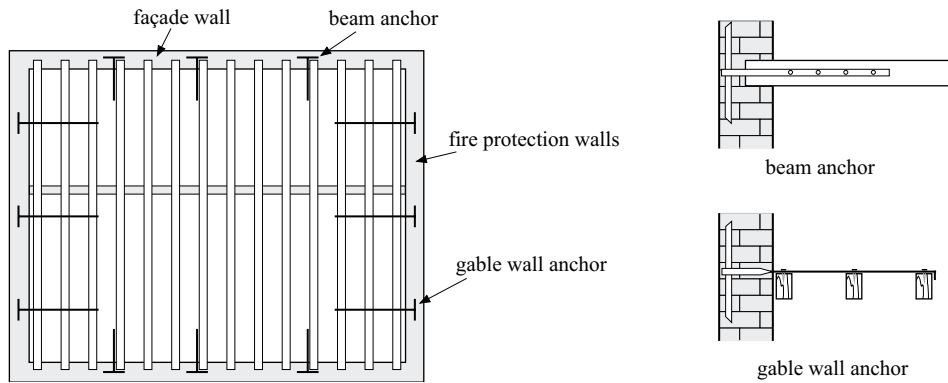


Figure 6.5: Typical floor-wall connections around 1900

Timber floors however are much more flexible and hence their deformation and increase in acceleration can be significant leading to differential displacements between in-plane loaded walls and enhancing the excitation of the out-of-plane loaded walls. Amplifications of up to 3 or 4 are possible. Static and dynamic tests of floor diaphragms (timber and steel constructions) have shown, however, that more flexible diaphragms have a “highly nonlinear hysteretic behaviour reducing the peak accelerations of the diaphragm and, in turn, the out-of-plane excitation of the unreinforced masonry wall” [Br 94a]. Still, amplifications of up to 2 have to be accounted for.

Modification of structural response

In the case of flexible floor diaphragms the response of the structure will be modified. Figure 6.6 shows two equivalent MDOF systems for a two storey building with a) rigid diaphragms and b) flexible diaphragms.

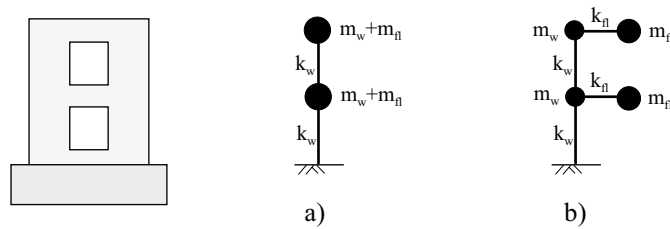


Figure 6.6: Equivalent MDOF system for a two storey building with a) rigid diaphragms and b) flexible diaphragms

The modification of the structural response due to flexible floor diaphragms is shown in Figure 6.7. Figure 6.7 right shows the frequencies of the four eigenmodes as a function of the ratio of the stiffness of the diaphragm to the stiffness of the wall system k_{fl}/k_w . The two lower frequencies correspond to modes which are dominated by diaphragm deformation whereas the two higher frequencies correspond to modes which are dominated by wall system deformation. Figure 6.7 left shows the effective modal mass of the first and third mode corresponding to the first mode of diaphragm deformation and to the first mode of wall structure deformation respectively. In the limit state where k_{fl}/k_w tends to

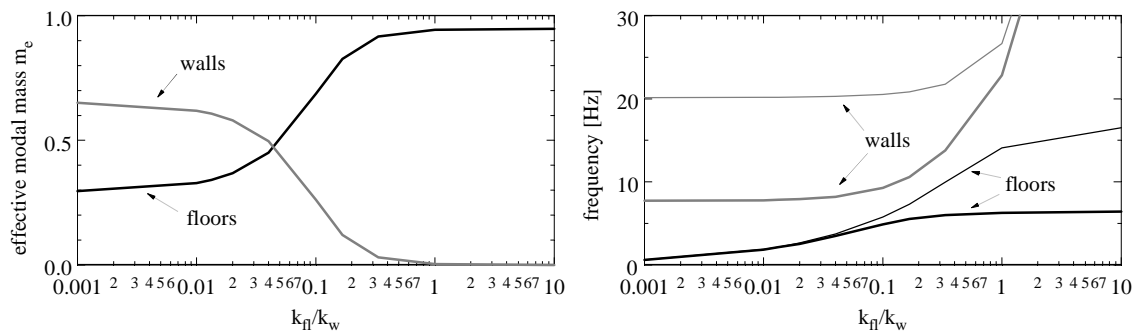


Figure 6.7: Modification of structural response due to flexible floor diaphragms

infinity, the structural response approaches the response of a structure with rigid diaphragms.

Diaphragm failure

Diaphragm failure is hardly ever observed following earthquakes [Br 94b], they usually remain in the elastic state. Yielding of the diaphragm limits the shear forces transmitted to the walls.

6.3 Material Properties

In order to evaluate the buildings in Basel, the materials of the buildings and their properties have to be known. Although for most buildings the plans and elevations are accessible, the material properties are usually not given. This is especially true for older buildings made of unreinforced masonry. For more recent buildings the building plans are usually more detailed including sometimes static calculations and indications of the material properties. However, for the assessment of existing buildings realistic values of the material properties are of interest in order to obtain the best estimate of the probable strength of an element. The use of design values is therefore inappropriate leading to a conservative estimate of the member strength.

In this section guidelines are given how to deduce the material properties, first for masonry buildings and then for reinforced concrete buildings.

6.3.1 Properties of masonry

In cases where a detailed assessment of an individual existing building is necessary, for example to decide on retrofit strategies, the exact properties of the masonry have to be known. A variety of non destructive and mildly destructive tests exists, which can be applied in situ to quantitatively assess the critical parameters of masonry behaviour [Ma 00] [CKM 96]. Non destructive tests include thermography and radar, used to find out defective joints and cavities, and sonic tomography that uses the velocity of the waves as an assessment of the strength of the material. Partially destructive methods include the flat-jack tests, the single flat jack test for the measurement of in-situ stresses and the modulus of elasticity and the double flat jack test for the measurement of the material strength, and the shove test to measure the in situ shear strength of the bed joints.

These in situ tests for the assessment of the critical parameters imply high expenditure, both financially and in time. The validity is limited to the particular building considered. It is therefore not very suitable for earthquake scenario projects.

In the following, a very simple way is outlined of how to deduce the properties of masonry given the construction year. It is a very rough estimation, based on old documents with the objective to include the general trend in the development of masonry. For an individual building, this estimation can lead to very wrong results; on average, however, the properties of the masonry should be assessed with an accuracy good enough for the purpose of the earthquake scenario project, where a large number of buildings have to be evaluated, and hence the average behaviour of a group of building is of interest rather than the behaviour of an individual building.

Unlike other materials, masonry is characterised by a large variety of its compound materials and the importance of their interaction on the properties of the assemblage. Even though much progress has been made in recent years in the field of constitutive models, no reliable analytical model exists that relates the properties of the compound materials (stone and mortar) to the properties of the masonry assemblage. However, experimental tests on masonry units in the laboratory have given valuable information on the influence of certain parameters and their priority.

In the following it is focused on regular clay brick masonry (short brick masonry), this being the principal material for the residential masonry buildings in the city of Basel.

Though one of the oldest and wide spread construction materials in the world, the use of brick masonry is poorly documented, the design being based on experience and very rough guidelines. The research is rather limited, the interest growing only in the last few decades, and uniform procedures to determine brick masonry properties did not exist for a long time.

It was not until 1924 that the first regulation for the design of masonry was published in Switzerland by the Swiss Federal Railways [SBB 24] and only in 1943 the first provisional standard for the “Design and calculation of natural stone and manufactured brick masonry structures” was published by the Swiss Society of Engineers and Architects [SIA113 43]. The material requirements concerning the compressive strength of the brick units, the mortar used and its mean compressive strength and hence the admissible stresses are shown in Table 6.1.

	compressive strength of brick units f_b [MPa]	admissible stresses [MPa]		
		cement mortar $f_m = 20$ [MPa]	lime-cement mortar $f_m = 3$ [MPa]	lime mortar $f_m = 1$ [MPa]
normal brick units (N)	22	1.4	0.9	0.6
high grade brick units (H)	35	2.2	1.3	0.8

Table 6.1: Material requirements for brick masonry according to SIA 113, 1943

The admissible stresses reduce considerably from 2.2 MPa for a masonry assemblage made of high grade brick units bound by cement mortar to 0.8 MPa for a masonry assemblage made of high grade brick units bound by lime mortar reflecting the significant influence of the mortar on the strength of the masonry. Figure 6.8 illustrates the relation-

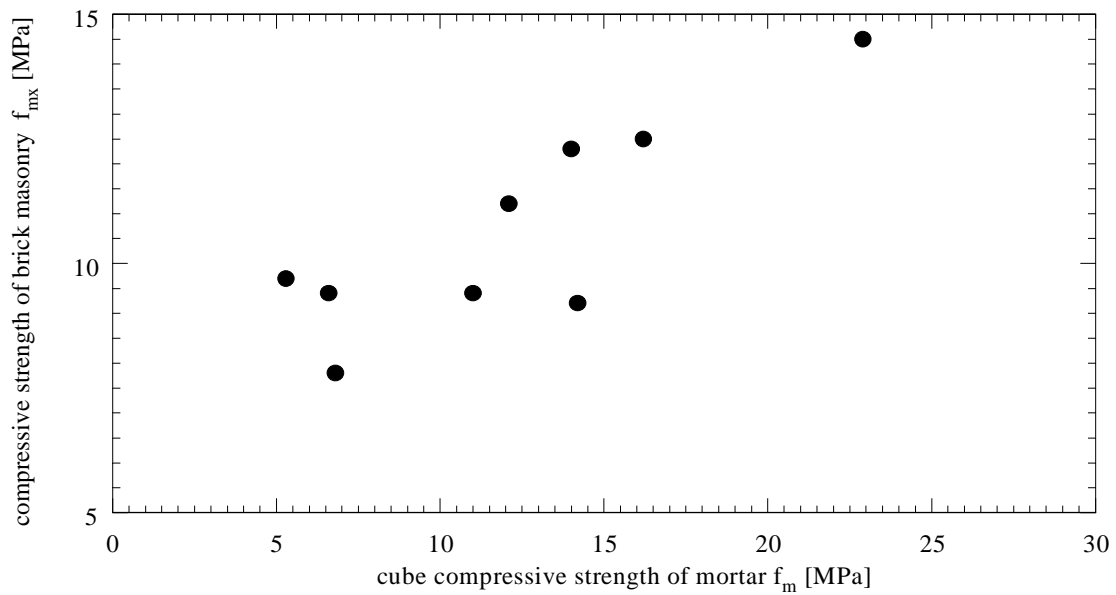


Figure 6.8: Compressive strength of a brick masonry assemblage as a function of the cube compressive strength of the mortar [Ma 94]

ship of the compressive strength of a brick masonry assemblage f_{mx} as a function of the cube compressive strength of the mortar f_m . It represents the results of several test series on masonry assemblages using the same brick units but different mortars [Ma 94]. It clearly shows the dependence of f_{mx} on f_m .

In 1965 a new edition of SIA 113 [SIA113 65] was published. The material requirements regarding the compressive strength of the brick units, the mortar and the minimum nominal strength of the masonry orthogonal to the mortar bed are shown in Table 6.2. At this time the use of pure lime mortar was not allowed any more.

	compressive strength of brick units f_b [MPa]	nominal strength of masonry [MPa]	
		cement mortar $f_m = 20$ [MPa]	lime-cement mortar $f_m = 3.5$ [MPa]
normal brick units (BN)	15	-	3.0-5.5
high grade brick units (BH)	25-35	8.5-15	5.0-9.5
special brick units (BS)	40	16-25	-

Table 6.2: Material requirements for brick masonry according to SIA 113, 1965

In 1980 the standard was revised and split into the standard for natural stone masonry (SIA 178) and the standard for manufactured brick masonry [SIA177 80] which was valid until 1995 with the exception of Chapter 3: “Design and Calculation” which was replaced in 1992 [SIA177/2 92]. The requirements on the materials have only slightly changed (Table 6.3), the use of lime-cement mortar being even more restricted.

The latest edition of SIA 177 was edited in 1995 [SIA177 95] and is valid until now. It reduced the multitude of different possible types of brick masonry obtained by different combinations of brick and mortar to two types, brick masonry (MB) and light brick masonry (MBL) with increased perforation of the bricks improving the thermal insulation.

	compressive strength of brick units f_b [MPa]	nominal strength of masonry [MPa]	
		cement mortar $f_m = 20$ [MPa]	lime-cement mortar $f_m = 3.5$ [MPa]
normal brick units (BN)	20	6.0-10	3.0-5.5
high grade brick units (BH)	25-35	10-15	-
special brick units (BS)	40	16-23	-

Table 6.3: Material requirements for brick masonry according to SIA 177, 1980

The minimum material requirements are listed in Table 6.4. For ordinary brick masonry the use of lime-cement mortar is now virtually excluded by the requirements on the compressive strength of the mortar.

	compressive strength of brick units f_b [MPa]	compressive strength of mortar f_m [MPa]	compressive strength of masonry f_{mx} [MPa]
brick masonry (MB)	28	15	8
light brick masonry (MBL)	14	5	4

Table 6.4: Material requirements for brick masonry according to SIA 177, 1995

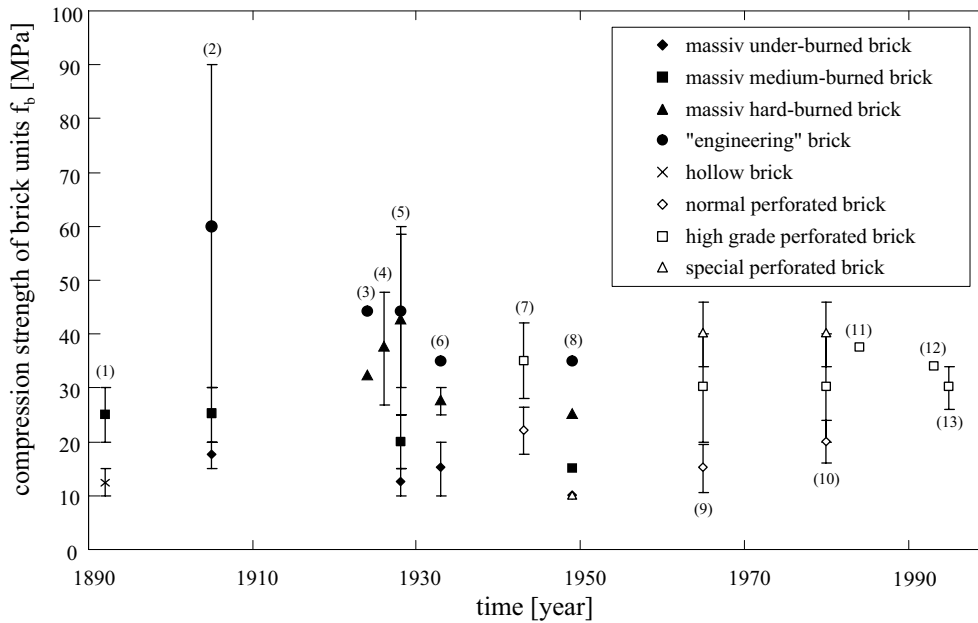
This short history of the development of the Swiss Standard for masonry structures indicates how recent the interest is in a better understanding and documentation of the properties and behaviour of masonry structures.

However, many unreinforced masonry buildings in the target area in Basel date from the first half of the 20th century i.e. before the first provisional standard in Switzerland. In order to trace the development of brick masonry before 1943 additional information was used from different sources such as lecture notes, engineering handbooks, articles and test reports from Switzerland and Germany throughout the last century.

Figure 6.9 shows a summary of the development of the compressive strength of brick units in the last 100 years. It can be seen that there is a high variation in the compressive strength of the brick units f_b . This is mainly due to the fact that no uniform terminology existed, the term brick being used for very different units so that a direct comparison is sometimes difficult to make. However, neglecting the very high compressive strength given to engineering brick in the engineering handbook from 1905, it seems that although the brick units have changed from massive bricks with different burning until the mid 20th century to perforated bricks with a rather uniform burning by the end of the 20th century, the compressive strength of “brick” units has not really increased in the last century.

However, the compressive strength of the masonry depends also on the quality of the mortar and not only on the compressive strength of the brick units. And here a profound change has taken place. Whereas around 1900 lime mortar was used nearly exclusively, nowadays only cement mortar is used. Experimental tests [Gr 24a][Gr 24b][Gr 26][GT 84][Sc 93] have shown that using cement mortar (cm) the compressive strength of

Application to buildings in Basel



- (1) lecture notes of the Eidgenössische Polytechnische Schule 1892 [Re 92]
- (2) engineering handbook 1905 [IT 05]
- (3) article 1924 [Gr 24a] [Gr 24b]
- (4) article 1926 [Gr 26]
- (5) engineering handbook 1928 [TBI 28]
- (6) engineering handbook 1933 [BK 33]
- (7) SIA 113 1943 [SIA113 43]
- (8) engineering handbook 1949 [TBI 49]
- (9) SIA 113 1965 [SIA113 65]
- (10) SIA 177 1980 [SIA177 80]
- (11) test report 1984 [GT 84]
- (12) test report 1993 [Sc 93]
- (13) SIA 177 1995 [SIA177 95]

Figure 6.9: Compressive strength of brick units with time

the masonry orthogonal to the mortar bed f_{mx} reaches about 20 to 40% of the compressive strength of the brick units f_b :

$$\left(\frac{f_{mx}}{f_b}\right)_{cm} \approx 0.2 - 0.4, \quad (6.1)$$

whereas using lime mortar (lm), the compressive strength of the masonry orthogonal to the mortar bed f_{mx} reaches only 7 to 10% of the compressive strength of the brick units f_b :

$$\left(\frac{f_{mx}}{f_b}\right)_{lm} \approx 0.07 - 0.1. \quad (6.2)$$

This means that, assuming a constant compressive strength of the brick units, on average the compressive strength of masonry has increased by more than 300% between 1900 and today. In between there is a transition period where the masonry is partly made with lime mortar, lime-cement mortar or cement mortar. A building permission around 1945

states that the load bearing walls at the ground level must be made with cement mortar, ten years later another building permission requires all load bearing walls to be made with cement mortar.

For the purpose of earthquake scenarios, a very simplified presentation of the development of the compressive strength of masonry orthogonal to the mortar bed f_{mx} with respect to the compressive strength of the brick units f_b is shown in Figure 6.10, assuming a linear transition with the corner points set to 1910 and 1960. Note that the corner points were set quite arbitrarily due to the lack of more detailed information. More information might narrow the transition period.

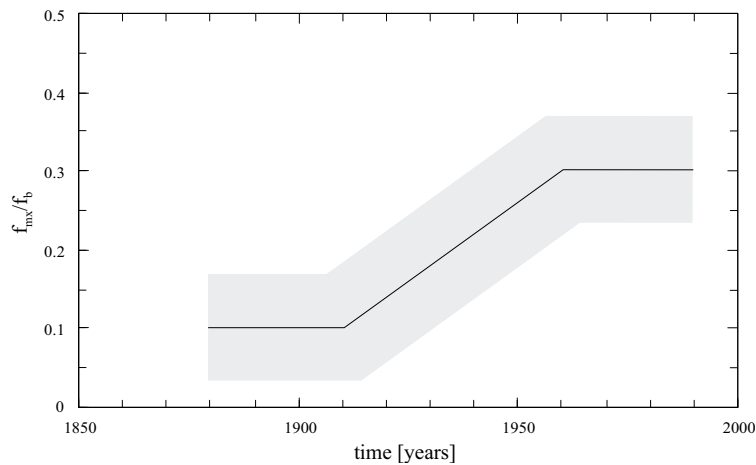


Figure 6.10: Development of the compressive strength of masonry with time

Assuming for instance a constant compressive strength of the brick units $f_b \approx 30$ MPa for the last 100 years, the compressive strength of masonry orthogonal to the mortar bed $f_{mx} \approx 0.3 \cdot f_b = 10$ MPa using cement mortar and $f_{mx} \approx 0.1 \cdot f_b = 3$ MPa using lime mortar.

Knowing the compressive strength of the masonry orthogonal to the mortar bed f_{mx} , the compressive strength parallel to the mortar bed can be deduced:

$$f_{my} \approx 0.3 \div 0.5 \cdot f_{mx} . \quad (6.3)$$

Again, this is a very crude estimation, since the compressive strength parallel to the mortar bed depends very much on the type of brick units, on the quality of the butt joints and on the type of the assemblage.

Finally, an estimate of the modulus of elasticity E_m and the shear modulus G_m of the masonry assemblage has to be made. They depend on the compressive strength of the masonry assemblage. Figure 6.11 shows the modulus of elasticity E_m for different types of masonry plotted over the compressive strength of the masonry orthogonal to the mortar bed f_{mx} . Also shown is the regression line which can be used to determine the modulus of elasticity for any masonry as a function of its compressive strength orthogonal to the mortar bed.

The shear modulus is always taken to be $G_m = 0.3 \cdot E_m$.

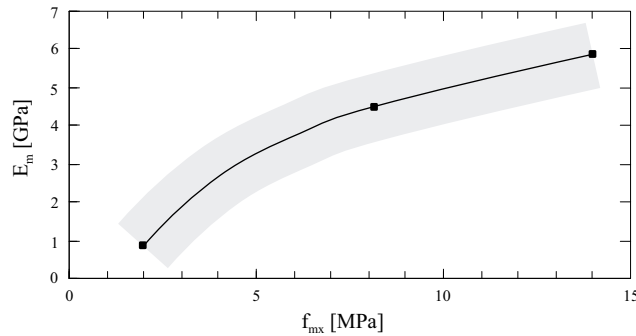


Figure 6.11: Relationship between the modulus of elasticity of masonry E_m and the compressive strength orthogonal to the mortar bed f_{mx}

6.3.2 Properties of reinforced concrete

Again, a number of quasi-non-destructive tests exists which allow the assessment of the exact properties of reinforced concrete required for a detailed assessment of an individual existing building. One of the best known is the rebound hammer test, devised by Ernst Schmidt in order to estimate the compressive strength of the concrete. Another, almost non-destructive test is the penetration resistance test which estimates the strength of concrete from the depth of penetration by a metal rod driven by a standard charge of power. Others include the use of ultrasonic waves and x-rays that allow the location of reinforcing steel bars and possible flaws. There exist many more, a detailed listing can be found in the handbook of the German Institute for the Research and Testing of Materials [SKW 90]. However, like for masonry buildings, these in situ tests are not very suitable for earthquake scenario projects since the expenditure is very high and the validity is limited to an individual building.

Contrary to masonry, the use and the material properties of reinforced concrete are well documented. Since the very beginning of the use of reinforced concrete for structural engineering existed regulations which were renewed regularly in order to present the state of the art. They are the key to the properties of the concrete used as well as of the reinforcing steel.

The first provisional standard for reinforced concrete structures in Switzerland was published in 1903 by the Swiss Society of Engineers and Architects (SIA) and the Federal Institute for the Testing of Buildings Material (EMPA) [SIA 03] and comprised 18 pages including explanations. The requirements on the materials were a minimum cube compressive strength of concrete of 16 MPa after 28 days, the reinforcement was to be a special homogenous iron with a minimum tensile strength of 360-420 MPa.

It followed a provisional regulation from the Swiss Railway Department in 1906, regulations from the Swiss Commission for Reinforced Concrete in 1909 and again regulations from the Swiss Railway Department in 1915.

In 1935 a joint standard for the calculation of steel, concrete and reinforced concrete structures [SIA112 35] was published which was partly revised in 1946. In the 1950's this standard was split into the standard for steel structures SIA 161, the standard for concrete and reinforced concrete structures SIA 162 and the standard for the action on structures SIA 160. The first edition of SIA 162 was published in 1956 [SIA162 56]. It was

renewed first in 1968 [SIA162 68] and then again in 1989 and partly revised in 1993 [SIA162 93].

Properties of reinforcing steel

The SIA 112 from 1935 distinguished between two types of reinforcing steel, “normal” steel and “high grade” steel. The minimum strength requirements are listed in Table 6.5.

group	reinforcing steel	yield limit f_y [MPa]	tensile strength f_u [MPa]
I	normal steel	240	360 - 450
II	high grade steel	350	520 - 620

Table 6.5: Minimum strength requirements on reinforcing steel according to SIA 112, 1935

In the first edition of SIA 162 from 1956 the high grade steel was distinguished between “naturally hard” (NH) and cold worked (K) steel. The minimum requirements had not really changed (Table 6.6).

group	reinforcing steel	yield limit f_y [MPa]	tensile strength f_u [MPa]
I	normal steel	240	360
II a	cold worked steel	350	420
II b	high grade, naturally hard steel	350	520

Table 6.6: Minimum strength requirements on reinforcing steel according to SIA 162, 1956

The next generation of SIA 162 was published in 1968 (Table 6.7).

group	reinforcing steel	\varnothing [mm]	minimum f_y [MPa]	nominal f_y [MPa]	minimum f_u [MPa]
I	reinforcing steel	6 - 30	240	-	370
II	not standardized any more				
III	reinforcing steel				
	III a naturally hard	6 - 30	430	460	560
	III b cold worked	6 - 30	430	460	480
IV	reinforcing meshes	4 - 12			
	without welded joints		500	540	570
	at the welded joint		-	-	540

Table 6.7: Strength requirements on reinforcing steel according to SIA 162, 1968

At that time, the most common naturally hard steels (NH) were Box, Box Ultra and Baro steel. The ductility properties of these reinforcing steels were excellent. The strain hardening ratio f_u/f_y was between 1.3 and 1.55; the percentage total elongation at maximum force A_{gt} was between 8 and 12%. The most common cold worked steels (K) were Caron and Tor steel. The strain hardening ratio f_u/f_y was between 1.2 and 1.3; the percentage total elongation at maximum force A_{gt} was between 5 and 8% (Figure 6.12 a) [BW 98].

These characteristics were typical for the reinforcing steel produced from the mid fifties to the beginning of the eighties. Then, the steel characteristics have changed due to new

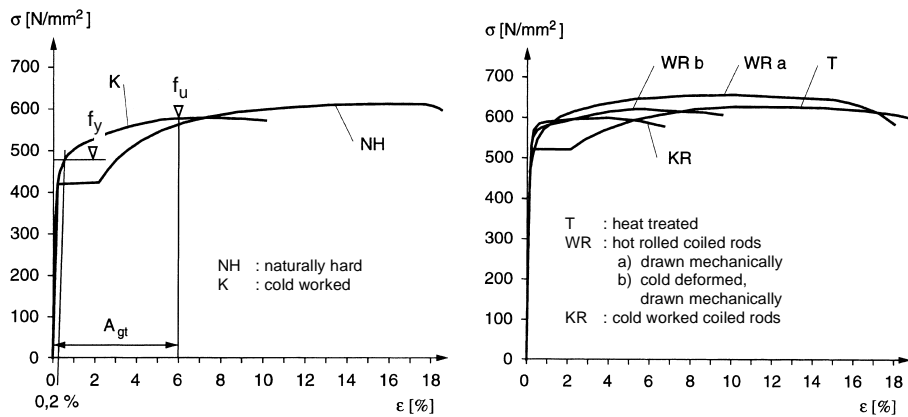


Figure 6.12: Stress-strain relationship for reinforcing steels a) NH and K b) T, WR and KR after [BW 98]

rationalised production procedures. The steel types that exist nowadays are heat treated steel bars (T), and hot rolled (WR), heat treated (TR) and cold worked (KR) coiled rods. The properties of the heat treated steel bars are still very good with a strain hardening ratio f_u/f_y between 1.1 and 1.25 and the percentage total elongation at maximum force A_{gt} between 10 and 14%. However, due to its economic process the production of coiled rods has become more and more important for reinforcing steel with a diameter $\varnothing < 14$ mm. For these reinforcing steels the ductility properties can be problematic, especially for the cold worked coiled rods which are also used for reinforcing meshes. Their strain hardening ratio f_u/f_y is very low, between 1.02 and 1.05 and the percentage total elongation at maximum force A_{gt} lies only between 2 and 5%. The strain hardening ratios f_u/f_y of hot rolled and heat treated coiled rods are 1.1 - 1.3 and 1.15 - 1.3 respectively and the percentages total elongation at maximum force A_{gt} are 6 - 12% and 8 - 10% respectively (Figure 6.12 b) [BW 98].

The classification of the reinforcing steel according to the latest edition of SIA 162 with its minimum strength requirement is shown in Table 6.8.

group	reinforcing steel	\varnothing [mm]	minimum f_y [MPa]	nominal f_y [MPa]	minimum f_u [MPa]
S 235	mild steel		235	-	360
S 500 a	nat. hard/micro alloyed	6 - 30	460	500	600
S 500 b	cold worked	6 - 30	460	500	550
S 500 c	heat treated	6 - 30	460	500	580
S 500 d	coiled rods	6 - 12	460	500	550
S 550	cold worked meshes	4 - 14	520	550	580

Table 6.8: Strength requirements on reinforcing steel according to SIA 162, 1993

These strength requirements give an important clue about the properties of the reinforcing steel throughout the twentieth century. However, being intended for design, they are usually on the conservative side, the actual strength of the reinforcing steel exceeding the requirements.

Between 1940 and 1950 a series of tests on different commercial types of reinforcing steel were carried out at the Federal Institute for Testing of Building Material (EMPA)

within the scope of a larger test program on the behaviour of reinforced concrete structures [Ro 42], [Ro 50]. Corresponding to the four classes of Portland cement concrete the reinforcing steel was classified into four groups with the average values of strength as stated in Table 6.9.

group	reinforcing steel	yield limit f_y [MPa]	tensile strength f_u [MPa]
I	normal steel	300	400
II	high grade steel: cold worked steel	400	500
	naturally hard steel	400	600
III	special steel: cold worked steel	550 - 600	700 - 800
	naturally hard steel	600 - 700	800 - 1000
IV	special steel according to a patent proceeding	1200 - 1800	1500 - 2200

Table 6.9: Average strengths of reinforcing steels tested at the Federal Institute for the Testing of Buildings Material [Ro 50]

As expected, the average strengths of the reinforcing steels tested exceed the minimum requirements according to SIA 162 / 1956 by up to 25%.

Tests on reinforcing steel of a 30 year old bridge in the canton Uri /Switzerland [ZV 00] have shown similar results, the actual yield strength and the actual tensile strength lie above the strength requirements by about 25%. The steel used was a reinforcing steel of group III according to SIA 162 / 1968. A total number of 24 reinforcing steel bars with a diameter $\varnothing = 8$ mm were tested. The average yield strength was 544 MPa with a standard deviation of ± 58 MPa, the average tensile strength was 600 MPa with a standard deviation of ± 39 MPa. Also the mechanical properties of reinforcing steel change with time, however much less significantly as the mechanical properties of concrete. The effect is a higher yield limit with time, the tensile strength remaining constant, and a reduction in the total elongation at maximum force [DWB 99].

Within the scope of cyclic-static tests on reinforced concrete walls [DWB 99] a series of reinforcing steel has been tested. For bar diameters of $\varnothing = 8, 10$ and 12 mm the steel used was a Topar-R 550s i.e. hot rolled coiled rods. This is a S500d reinforcing steel according to SIA 160 / 1993 with a minimum yield limit of 460 MPa and a minimum tensile strength of 550 MPa. The actual average yield limit was 566 MPa with a standard deviation of ± 24 MPa and the average tensile strength was 700 MPa with a standard deviation of ± 40 MPa. Hence, the actual strengths exceed the required strengths by 23% at yield and by 27% at ultimate.

It is therefore suggested, for the purpose of the evaluation of existing buildings in Basel, to increase the minimum required strengths from the respective standard at the time of construction by at least 20% in order to obtain a reasonable estimate of the actual strengths.

Another point of consideration is the use of deformed or plain round bars for the longitudinal reinforcement. For plain round bars, as were used formerly, the bond degradation during cyclic loading is much more significant than for deformed bars. As a consequence

older buildings reinforced with plain round bars will exhibit a greater stiffness reduction during cyclic loading [Pa 97].

Finally the modulus of elasticity of steel E_s can be assumed to lie between 190 and 210 GPa, the variation in the value being very limited.

Properties of concrete

The SIA 112 from 1935 distinguished between two types of concrete, “normal” concrete and “high grade” concrete. Depending on the amount of Portland cement, the required mean cube compressive strengths after 28 days are listed in Table 6.10.

amount of Portland cement /m ³ [kg]	compressive strength f_c [MPa]	
	normal concrete	high grade concrete
150	7	-
200	11	-
250	16	22
300	22	30
350	28	38

Table 6.10: Required mean cube compressive strength of concrete after 28 days according to SIA 112, 1935

Individual results were allowed to differ by a maximum of 25% for normal concrete and by a maximum of 20% for high grade concrete. For reinforced concrete the required amount of Portland cement was 300 kg/m³.

In the first edition of SIA 162 from 1956 the requirements on the mean cube compressive strength were adopted unchanged from SIA 112 with one exception, high grade concrete always required a minimum of Portland cement of 300 kg/m³.

The next generation of SIA 162, published in 1968, distinguished between three types of concrete: normal concrete (BN), high grade concrete (BH) and special concrete (BS).

amount of Portland cement /m ³ [kg]	nominal compressive strength f_c [MPa]		
	BN	BH	BS
300	20		
≥ 300		30	≥ 37,5

Table 6.11: Nominal cube compressive strength of concrete after 28 days according to SIA 162, 1968

The minimum required cube compressive strength of concrete after 28 days according to the latest edition of SIA 160 is shown in Table 6.12.

	(LB) 20/10	(L)B 25/15	(L)B 30/20	(L)B35/25	(L)B 40/30	(L)B 45/35
f_c [MPa]	10	15	20	25	30	35

Table 6.12: Minimum required cube compressive strength of concrete after 28 days according to SIA 162, 1993

All strength requirements are given in terms of cube compressive strength. However, due to the small height to width ratio, the restraining effect of the plates of the testing machine is considerable leading to an increased compressive strength. As the height to width ratio increases, the restraining effect reduces. Therefore, cylinders with a height to width ratio of 2 are very often used to measure the compressive strength of concrete. The compressive strength of concrete measured with these standard cylinders is about 15 - 25% smaller than the cube compressive strength of concrete: $f'_c \cong (0.75 \div 0.85) \cdot f_c$. The strength requirements in the different generation of codes illustrate the development of the concrete properties throughout the twentieth century, but again, being used for design they are on the conservative side, underestimating the real strength of the material. In fact, it is very likely that the actual compressive strength exceeds the nominal strength considerably as a result of conservative mix design and age. It is therefore rather difficult to estimate the concrete strength of a wall of an existing building without testing. Especially the effects of a conservative mix design are difficult to quantify. The increase of the compressive strength with age is due to the fact that the hydration process is not completed after 28 days. Even though the rate of gain of strength decreases considerably after 28 days, the increase in strength can be up to 100% after 5 to 10 years. Figure 6.13 shows the increase in strength measured on standard concrete cylinders between 1916 and 1970 [Ne 81].

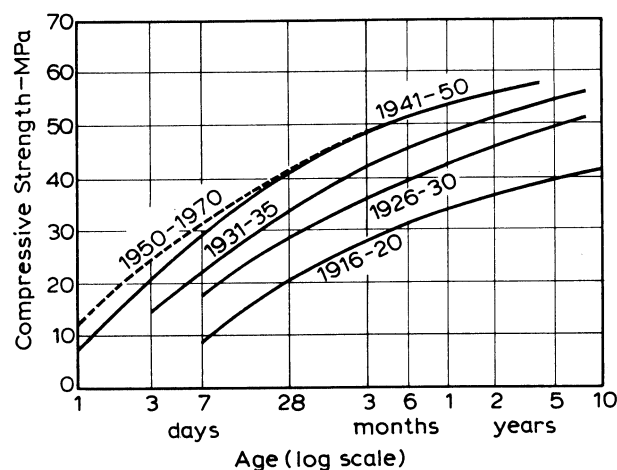


Figure 6.13: Rate of gain of strength measured on standard concrete cylinders between 1916 and 1970 after [Ne 81]

Recent tests on concrete cubes of a 30 year old bridge in the canton Uri / Switzerland showed a compressive strength approximately twice the design value [ZV 00]. For the insitu concrete a concrete BH 300 according to SIA 162 / 1968 was used with a nominal cube compressive strength after 28 days of 30 MPa. The mean strength of 16 cubes tested was 73.3 MPa with a standard deviation of 14 MPa. For the prefabricated parts a concrete BS 450 was used with a nominal cube compressive strength after 28 days of 45 MPa. The mean strength of 27 cubes tested was 79.5 MPa with a standard deviation of 6.9 MPa. Tests on the concrete of 30 year old bridges in California have shown similar results [Pr 95].

Application to buildings in Basel

It is therefore suggested, for the purpose of the evaluation of existing buildings in Basel, to increase the required mean compressive strength at the time of construction by at least 50%.

The modulus of elasticity of concrete E_c is related to the compressive strength and can be calculated for normal-weight concrete as follows [PP 92]:

$$E_c = 0.043 \cdot \rho_c^{1.5} \cdot \sqrt{f'_c} \quad [\text{MPa}] \quad (6.4)$$

ρ_c is the density of concrete (in kg/m^3) and lies usually around 2300 to 2500 kg/m^3 for normal-weight concrete. The unit of f'_c is MPa. Another possibility to estimate the modulus of elasticity is to use Figure 31 of SIA 162 / 1993.

The shear modulus of concrete is assumed to be

$$G_c = 0.4 \cdot E_c. \quad (6.5)$$

For the calculation of the moment capacity of a wall section the tensile strength of the concrete is ignored. However in order to estimate the moment at the onset of cracking, the tensile strength of concrete may be assumed as a function of the compressive strength [PP 92]:

$$f_{ct} = 0.75 \cdot \sqrt{f'_c} \quad [\text{MPa}] \quad (6.6)$$

where the unit of f'_c is again MPa.

6.4 Example masonry building

In this section the evaluation method developed in general in Chapter 3 and in more detail for masonry buildings in Chapter 4 is applied to a real example building (Figure 6.14). The 2-storey building considered is typical for the residential building stock in Basel. It is a terrace masonry building with timber floors. Figure 6.15 shows plan and elevation.



Figure 6.14: Real example building from the city of Basel

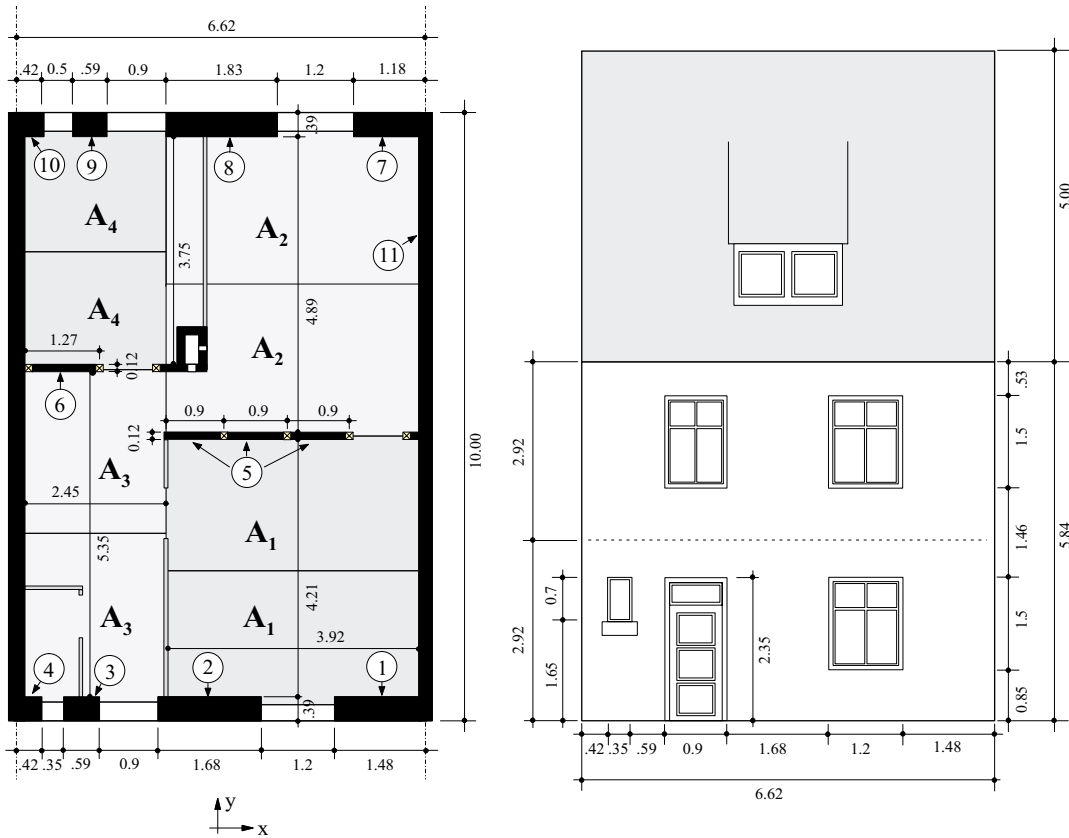


Figure 6.15: Plan and elevation of the 2-storey example building, all dimensions in m

The y-direction indicates the direction of the fire protection walls which extend over the whole depth of the buildings and are shared by two adjacent buildings. The x-direction indicates the direction of the façades. The timber floor beams run in the y-direction and hence are supported by the walls running in the x-direction. The fire protection walls do not act to support the floors. Hence, all the surcharges applied at the floor levels are carried by the walls in the x-direction only. This is also indicated by the shape of the tributary areas which are rectangular.

The following assumptions are made:

- The timber floors will act as a diaphragm even though the in-plane stiffness of timber floors is rather low and the floor-wall connections often very weak.
- The dynamic interaction of adjacent buildings is neglected.

The evaluation is done in 11 steps as stated in Section 4.5.

Step 1) Input Data

Overall Geometry

Total floor area	$A_{\text{tot}} = l_x \cdot l_y = 6.62 \cdot 10.00 = 66.2 \text{ m}^2$
Total building height	$H_{\text{tot}} = 5.84 \text{ m}$
Storey height	$h_{\text{st}} = 2.92 \text{ m}$

Materials

Since the material properties are not given, they are estimated as a function of the construction year of the building as illustrated in Section 6.3.

Compression strength orthogonal to the mortar bed	$f_{mx} = 5.1 \text{ MPa}$
Compression strength parallel to the mortar bed	$f_{my} = 0.3 \cdot f_{mx} = 1.5 \text{ MPa}$
Angle of internal friction	$\tan \phi = 0.8$
Modulus of elasticity of masonry	$E_m = 3000 \text{ MPa}$
Shear modulus of masonry	$G_m = 1000 \text{ MPa}$
Stiffness reduction factor	$k_{eff}/k_0 = 0.5$
Specific weight of massive brick masonry	$\gamma_m = 16 \text{ kN/m}^3$

Vertical loads

Self weight of the floors	$g_{fl} = 1.5 \text{ kN/m}^2$
Self weight of the façade walls	$g_w = \gamma_m \cdot t = 16 \cdot 0.39 = 6.24 \text{ kN/m}^2$
Self weight of the interior walls	$g_w = \gamma_m \cdot t = 16 \cdot 0.12 = 1.92 \text{ kN/m}^2$

In the absence of more precise information the values for the surcharges and the live loads are assumed as follows:

Surcharge floor	$q_d = 0.60 \text{ kN/m}^2$
Surcharge wall	$q_w = 0.03 \text{ kN/m}^2$
Live loads	$q_N = 0.60 \text{ kN/m}^2$

As we are interested in the “real” behaviour of the building no load factors are applied. The total floor load is equal to

$$q_{fl} = g_{fl} + q_d + q_N = 1.5 + 0.6 + 0.6 = 2.7 \text{ kN/m}^2.$$

The roof is considered only as an additional vertical load acting on the façade walls in the x-direction:

$$\text{Weight of the roof} \quad q_{roof} = 1.2 \text{ kN/m}^2.$$

Step 2) Identification of structural walls

The direction considered is the x-direction (cf. Section 6.2). In this direction 12 structural walls can be identified, wall number 5 occurs three times. Table 6.13 gives a summary of the main characteristics of the walls, the length l_w , the thickness t and the height of the pier i.e. the height of the adjacent opening at the ground floor h_p .

wall	1	2	3	4	5	6	7	8	9	10
length l_w [m]	1.48	1.68	0.59	0.42	0.9	1.27	1.05	1.83	0.59	0.42
thickness t [m]	0.39	0.39	0.39	0.39	0.12	0.12	0.39	0.39	0.39	0.39
pier height h_p [m]	1.5	1.5	0.7	0.7	2.92	2.92	1.5	1.5	1.5	1.5

Table 6.13: Main characteristics of the structural walls

Note that as the building is regular, it is assumed that the most critical section determining the capacity of the structural walls is at the ground floor where the stresses are the highest.

Step 3) Calculation of normal forces

In this step the normal forces acting on the walls at the ground level have to be calculated. It should be done with great care as the method is very sensitive to the variation of the normal forces.

In order to calculate the normal forces the floor loads have to be distributed among the walls. This can be done in a very simple way using the following procedure:

- 1) Division of the floor into reasonable tributary areas (Figure 6.15: A1 to A4) in accordance with the floor system.
- 2) Distribution of the floor load from each tributary area onto the walls in proportion to their length.

As an example this is done for wall 1:

$$\begin{aligned} \text{Tributary area } A_1 &= 0.5 \cdot 4.21 \cdot 3.92 = 8.25 \text{ m}^2 \\ \text{Proportion carried by wall 1} &= (1.48 + 0.5 \cdot 1.2) / 3.92 = 0.53 \\ \text{Floor load carried by wall 1} &= Q_1 = 0.53 \cdot 8.25 \cdot 2.7 = 11.8 \text{ kN} \end{aligned}$$

In this way the floor load carried by each wall can be calculated. The results are summarized in Table 6.14. The total floor load adds up to 151.8 kN.

wall	1	2	3	4	5	6	7	8	9	10	sum
floor load Q [kN]	11.8	16.2	8.8	4.3	16.1	21.1	10.9	20.6	6.5	3.4	151.8

Table 6.14: Floor loads acting on each wall

In the same way the roof load can be distributed among the façade walls. Including the self weight of the walls, dividing the mass of the walls at mid height between two floor levels, the following matrix can be established presenting the normal forces acting on each wall at each floor level (Table 6.15).

level\wall	N ₁	N ₂	N ₃	N ₄	N ₅	N ₆	N ₇	N ₈	N ₉	10	11	N _{tot}
2	42.8	55.4	25.4	13.2	18.6	25.8	34.8	62.3	23.9	13.8	156.2	509.3
1	44.3	56.3	25.2	9.7	21.2	28.3	35.5	63.5	23.6	13.3	112.8	476.0
sum	87.1	111.7	50.6	22.9	39.8	54.1	70.3	125.8	47.5	27.1	269.0	985.3

Table 6.15: Normal forces acting on each wall at each floor level, dimensions in kN

The last column presents the sum of the normal forces at each floor level. And hence the concentrated storey masses are given by:

$$m_2 = \frac{509.3}{10} = 51 \text{ t} \text{ and } m_1 = 48 \text{ t} .$$

Step 4) Capacity curves of the walls

The calculation of the capacity curve of a wall follows the procedure described in Section 4.2. It is demonstrated using again wall 1 as an example.

First, the height of zero moment h_0 which depends on the ratio of the flexural stiffness of the spandrel to the flexural stiffness of the pier (cf. Section 3.5.3) has to be determined. The depth of the spandrel is equal to 1.46 m, its length $l_o = 2.78$ m, the length of the pier of wall 1 $l_w = 1.48$ m and the height of the first storey $h_{st} = 2.92$ m. Hence the ratio of the stiffnesses:

$$\frac{EI_{sp}}{EI_p} \cdot \frac{h_{st}}{l_o} = \frac{E \cdot \frac{t \cdot 1.46^3}{12}}{E \cdot \frac{t \cdot 1.48^3}{12}} \cdot \frac{2.92}{2.78} = 1.0.$$

Taking into account early cracking of the spandrels by reducing the stiffness of the spandrels to 50%, the ratio of the stiffnesses $(EI_{sp}/EI_p)(h_{st}/l_o) = 0.5$. Using the relations shown in Figure 3.6 a) the ratio of $h_0/h_p \approx 0.75$ and hence

$$h_0 = 0.75 \cdot h_p = 0.75 \cdot 1.5 = 1.125 \text{ m}.$$

Next, the conditions (4.13) - (4.15) have to be solved for the shear force V using Equations (4.9) - (4.12) and (4.16) - (4.19). Since the system of equations is statically indeterminate the eccentricities of the vertical and the inclined stress strut at the bottom of the pier are taken to be equal as explained in Section 4.2.1:

$$e_{2v} = e_{2n} = e_2 = \frac{M_2}{N}. \quad (6.7)$$

Hence, from conditions (4.13) and (4.15) the maximum admissible shear force that does not violate neither the stress nor the sliding criterion is:

$$V_m = \frac{f_{my} \cdot l_w \cdot t \cdot N \cdot \tan \phi}{N + N \cdot (\tan \phi)^2 + 2 \cdot f_{my} \cdot t \cdot h_0 \cdot \tan \phi}. \quad (6.8)$$

Condition (4.14) is checked in a further step but is usually not critical.

For wall 1 Equation (6.8) gives:

$$V_m = \frac{1.5 \cdot 10^3 \cdot 1.48 \cdot 0.39 \cdot 87.1 \cdot 0.8}{87.1 + 87.1 \cdot 0.8^2 + 2 \cdot 1.5 \cdot 10^3 \cdot 0.39 \cdot 0.75 \cdot 1.5 \cdot 0.8} = 50.5 \text{ kN}.$$

From Equations (4.18) and (4.19) the moments M_1 and M_2 at the top and at the bottom of the pier can be calculated:

$$M_1 = V \cdot (h_0 - h_p) = 50.5 \cdot (1.125 - 1.5) = -18.9 \text{ kNm}$$

$$M_2 = V \cdot h_0 = 50.5 \cdot 1.125 = 56.8 \text{ kNm}.$$

Hence the length of the vertical and the inclined stress strut using Equations (4.16) and (6.7):

$$l_{2v} = l_{2n} = l_2 = l_w - 2e_2 = l_w - 2 \cdot \frac{M_2}{N} = 1.48 - 2 \cdot \frac{56.8}{87.1} = 0.18 \text{ m} .$$

For slender piers the angle of inclination of the inclined stress field α may be limited by the geometry:

$$\tan \alpha_{\max} \leq \frac{l_w - l_2}{h_p} = \frac{1.48 - 0.18}{1.5} = 0.87 .$$

In the case of wall 1 the geometry is not critical and hence $\tan \alpha_{\max} = \tan \phi = 0.8$ as supposed in Equation (6.8).

The normal force that passes through the inclined stress field N_v can then be calculated using Equation (4.12) and solving for N_v :

$$N_v = \frac{V}{\tan \alpha_{\max}} = \frac{50.5}{0.8} = 63.2 \text{ kN} .$$

Using Equation (4.9) the normal force that passes through the vertical stress strut N_n can be determined:

$$N_n = N - N_v = 87.1 - 63.2 = 23.9 \text{ kN} .$$

Hence, the stresses in the vertical strut can be checked (condition (4.14)):

$$f_{\text{vertical}} = \frac{N_n}{l_2 \cdot t} = \frac{23.9}{0.18 \cdot 0.39 \cdot 10^3} = 0.34 \text{ MPa} \leq 3.5 \text{ MPa} = f_{\text{mx}} - f_{\text{my}} .$$

The stresses in the vertical strut are not critical. Finally, the sliding criterion (4.15) should be checked in the uppermost storey of the building, as this could be critical especially for squat walls. The normal force acting at the upper storey of wall 1 is $N_{\text{OG}} = 42.8 \text{ kN}$. Assuming a triangular distribution of the horizontal forces, the shear force acting at the upper storey of wall 1 is:

$$V_{\text{OG}} = \frac{2}{3} \cdot V_m = \frac{2}{3} \cdot 50.5 = 33.7 \text{ kN} .$$

Hence, the inclination of the stress strut in the upper storey can be determined from Equation (4.12):

$$\tan \alpha = \frac{V_{\text{OG}}}{N_{\text{OG}}} = \frac{33.7}{42.8} = 0.78 .$$

In the case of wall 1 the sliding criterion in the upper storey is not critical. However, the angle of internal friction ϕ is very nearly attained and it might be worth considering the effect of cohesion, especially in this case where the normal force in the upper storey is rather low. This seems appropriate as long as the wall element in the upper storey is un-

Application to buildings in Basel

cracked. Taking into account cohesion, the shear force acting at the upper storey need to satisfy following relationship:

$$V_{OG} \leq l_w \cdot t \cdot c + N_{OG} \cdot \tan \phi. \quad (6.9)$$

Assuming a value of the cohesion $c = 0.02 \cdot f_{my} = 0.03$ MPa, the maximum shear force that can be transmitted through the upper storey is:

$$V = 1.5 \cdot 0.39 \cdot 0.03 \cdot 10^3 + 42.8 \cdot 0.8 = 17.6 + 34.2 = 51.7 \text{ kN} > V_{OG}.$$

Hence, sliding in the upper storey is not critical.

Having found the shear capacity of the wall, the yield and ultimate displacement at the top of the wall have to be determined. Using Equation (4.25) the yield displacement at the top of the wall Δ_y is calculated:

$$\begin{aligned} \Delta_y &= V_m \cdot H_{tot} \cdot \left(\frac{h_p \cdot (3h_0 - h_p)}{6 \cdot EI_{eff}} + \frac{\kappa}{GA_{eff}} \right) \\ &= 50.5 \cdot 10^3 \cdot 5.84 \cdot \left(\frac{1.5 \cdot (3 \cdot 1.125 - 1.5)}{6 \cdot 0.5 \cdot 3000 \cdot 10^6 \cdot \frac{0.39 \cdot 1.48^3}{12}} + \frac{\frac{6}{5}}{0.5 \cdot 1000 \cdot 10^6 \cdot 0.39 \cdot 1.48} \right) \\ &= 0.00210 \text{ m} = 2.1 \text{ mm} \end{aligned}$$

The ductility of the pier is determined as a function of the normal stress σ_n acting on the pier:

$$\sigma_n = \frac{N}{t \cdot l_w} = \frac{87.1}{0.39 \cdot 1.48 \cdot 10^3} = 0.15 \text{ MPa}.$$

The maximum admissible drift of the pier is then (Equation (4.29)):

$$\delta_u = 0.8 - 0.25 \cdot \sigma_n = 0.8 - 0.25 \cdot 0.15 = 0.76 \text{ \%}.$$

The aspect ratio of the pier being close to one, $h_p/l_w = 1.5/1.48 = 1.01$, no geometry factor is applied to the maximum admissible drift and hence the ductility of the pier is determined to

$$\mu_{WE} = \max\left(\frac{\delta_u}{\delta_y}, 12\right) = \max\left(\frac{0.76}{0.036}, 12\right) = 12.$$

From this, the displacement ductility of the wall μ_w can be determined using Equation (4.34):

$$\mu_w = 1 + \frac{h_p}{H_{tot}} \cdot (\mu_{WE} - 1) = 1 + \frac{1.5}{5.84} \cdot (12 - 1) = 3.83.$$

And hence the ultimate displacement at the top of the wall (Equation (4.26)):

$$\Delta_u = \mu_w \cdot \Delta_y = 3.83 \cdot 2.1 = 8.0 \text{ mm}.$$

Thus, the monotonic capacity of wall 1 is determined. In the same way the monotonic capacities of all the other walls are determined. Table 6.16 summarizes the results.

wall	1	2	3	4	5	6	7	8	9	10
h_0/h_p	0.75	0.70	0.55	0.60	1.66	1.66	0.60	0.75	0.55	0.60
V_m [kN]	50.5	66.5	30.5	10.3	3.4	6.4	35.7	74.8	14.6	5.7
M_1 [kNm]	-18.9	-29.9	-9.6	-2.9	6.6	12.5	-21.4	-28.0	-9.9	-3.4
M_2 [kNm]	56.8	69.8	11.7	4.3	16.5	31.5	32.1	84.1	12.1	5.1
d_y [mm]	0.5	0.5	0.3	0.2	5.5	3.9	0.6	0.6	0.7	0.8
δ_y [%]	0.036	0.036	0.048	0.034	0.186	0.132	0.040	0.037	0.041	0.056
Δ_y [mm]	2.1	2.1	2.8	2.0	10.9	7.7	2.3	2.2	3.0	3.3
μ_{WE}	12	12	12	12	4.6	6.5	12	12	12	12
μ_w	3.83	3.83	2.32	2.32	2.81	3.78	3.83	3.83	3.83	3.83
Δ_u [mm]	8.0	8.1	6.5	4.6	30.5	29.1	8.9	8.2	11.4	12.5
k_{eff} [kN/mm]	24.0	31.4	10.9	5.2	0.3	0.8	15.3	34.7	4.9	1.8

Table 6.16: Capacities of the walls

As explained in Section 4.2.5 the monotonic capacity of the wall is multiplied by a force and a displacement reduction factor, RF_F and RF_D , in order to take into account the cyclic nature of the loading. With respect to the comparison with test results (4.4) both factors are set to 1. The bottom row of Table 6.16 presents the effective stiffnesses of the linear elastic part of the bilinear capacity curves of the walls (cf. Figure 3.9).

Step 5) Capacity curve of the building

The capacity curve of the building can be easily obtained by superposition of the capacity curves of the walls, following Equation (3.3). The result is shown in Figure 6.16.

Step 6) Identification of damage grades

The damage grades according to the EMS 98 [EMS 98] are identified on the capacity curve of the building as explained in Section 4.2.7.

Damage Grade 1

For each wall the shear force at the onset of cracking is determined using Equation (4.37). For wall 1 this yields:

$$V_{cr} = \frac{N \cdot I_w}{6 \cdot h_0} = \frac{87.1 \cdot 1.48}{6 \cdot 1.125} = 19.1 \text{ kN}$$

The corresponding displacement at the top of wall 1 Δ_{cr} is determined, using as before Equation (4.25) substituting V_{cr} for V_m :

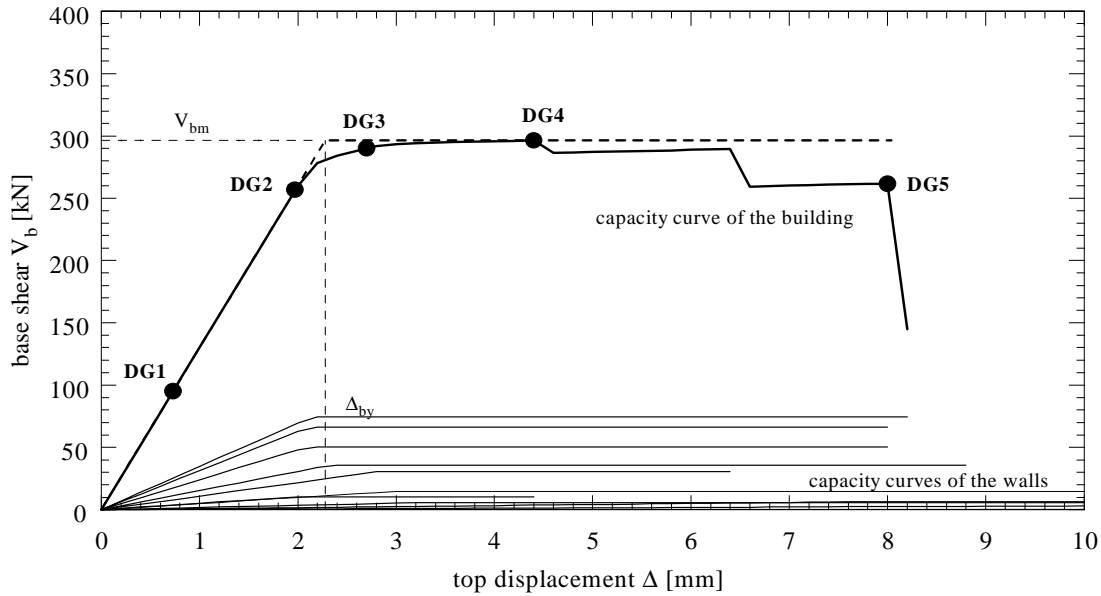


Figure 6.16: Capacity curve of the example building

$$\begin{aligned} \Delta_y &= V_{cr} \cdot H_{tot} \cdot \left(\frac{h_p \cdot (3h_0 - h_p)}{6 \cdot EI_{eff}} + \frac{\kappa}{GA_{eff}} \right) \\ &= 19.1 \cdot 10^3 \cdot 5.84 \cdot \left(\frac{1.5 \cdot (3 \cdot 1.125 - 1.5)}{6 \cdot 0.5 \cdot 3000 \cdot 10^6 \cdot \frac{0.39 \cdot 1.48^3}{12}} + \frac{\frac{6}{5}}{0.5 \cdot 1000 \cdot 10^6 \cdot 0.39 \cdot 1.48} \right) \\ &= 0.0079 \text{ m} = 0.8 \text{ mm} \end{aligned}$$

Table 6.17 summarizes the results for all the walls.

wall	1	2	3	4	5	6	7	8	9	10
V_{cr} [kN]	19.1	29.8	12.9	3.8	1.2	2.3	13.7	34.1	5.7	2.1
Δ_{cr} [mm]	0.8	1.0	1.2	0.7	3.9	2.8	0.9	1.0	1.2	1.2

Table 6.17: Cracking of the walls

The wall that cracks first, i.e. at the smallest displacement, determines damage grade 1. In this case it is wall 4 that cracks first at a displacement of 0.7 mm. The corresponding base shear of the building can be read off the capacity curve (Figure 6.16):

$$V_{bcr} = V_b(\Delta_{cr}) = 95.0 \text{ kN}.$$

And hence the couple $(\Delta_{cr}, V_{bcr}) = (0.7 \text{ mm}, 95.0 \text{ kN})$ determines the point on the capacity curve of the building at which the building enters damage grade 1 (cf. Figure 6.16).

Damage Grade 2

This damage grade is identified by the first wall entering the plastic state, i.e. the minimum Δ_y from Table 6.16. For the example building it is wall 4 that yields first at the smallest displacement:

$$\Delta_{y4} = 2.0 \text{ mm}.$$

The corresponding base shear of the building is read off the capacity curve (Figure 6.16):

$$V_b(\Delta = 2.0 \text{ mm}) = 256.7 \text{ kN}.$$

And hence the couple (2.0 mm , 256.7 kN) determines the point on the capacity curve of the building at which the building enters damage grade 2 (cf. Figure 6.16).

Damage Grade 3

This damage grade is identified as the point at which the stiffness of the capacity curve tends to zero. That is the case when the last wall enters the plastic state. However, as mentioned in Section 4.2.7, it often happens that the first wall fails before the last wall has yielded. This is also the case for the example building. The last wall to enter the plastic state is wall 5 with a yield displacement $\Delta_{y5} = 10.9 \text{ mm}$. However, wall 4 already fails at $\Delta_{u4} = 4.6 \text{ mm}$. Looking at the shape of the capacity curve the stiffness is already very close to zero just beyond the yield point of the building Δ_{by} . The building is therefore considered to enter damage grade 3 at a displacement of $\Delta \sim 2.7 \text{ mm}$. The corresponding base shear of the building is read off the capacity curve (Figure 6.16):

$$V_b(\Delta = 2.7 \text{ mm}) = 290.0 \text{ kN}.$$

And hence the couple (2.7 mm, 290.0 kN) determines the point on the capacity curve of the building at which the building enters damage grade 3 (cf. Figure 6.16).

This shows clearly that it is not possible to apply the evaluation method in a rigid way but engineering judgement is required to apply the evaluation method in a sensible way.

Damage Grade 4

This damage grade is identified by the first wall that fails leading to a decrease in the base shear of the building i.e. the minimum Δ_u from Table 6.16. In the case of the example building the first wall to fail is wall 4 at a displacement of $\Delta_{u4} = 4.6 \text{ mm}$, and hence the couple (4.6 mm , 296.7 kN) determines the point on the capacity curve of the building at which the building enters damage grade 4 (cf. Figure 6.16).

Damage Grade 5

The building is not considered to have collapsed at the point of failure of wall 4, the base shear of the building being still more than 2/3 of its maximum value. Only the failure of the third wall, wall 1, at a displacement $\Delta_{u1} = 8.0 \text{ mm}$ closely followed by the failure of wall 2 reduces the base shear of the building to such an extent that it is assumed to have collapsed. The base shear of the building at the point of failure of wall 1 is (Figure 6.16):

Application to buildings in Basel

$$V_b(\Delta = 8.0 \text{ mm}) = 261.7 \text{ kN}.$$

And hence the couple (8.0 mm , 261.7 kN) determines the point on the capacity curve of the building at which the building enters damage grade 5 (cf. Figure 6.16).

Step 7) Bilinear approximation of the capacity curve of the building

The simplest bilinear approximation is shown in Figure 6.16 by a dashed line. The stiffness of the linear elastic part is determined by the sum of the effective stiffnesses of the walls:

$$k = \sum_j k_{\text{eff}j} = 130 \text{ kN/mm}.$$

Assuming the shear capacity of the bilinear approximation to be equal to the shear capacity of the “real” capacity curve of the building, $V_{\text{bm}} = 296.4 \text{ kN}$, the yield displacement of the building is given by:

$$\Delta_{\text{by}} = \frac{V_{\text{bm}}}{k} = \frac{296.4}{130} = 2.3 \text{ mm}.$$

Step 8) Equivalent SDOF system

The building can be considered as a MDOF system with two concentrated masses m_1 and m_2 as calculated in step 2. Table 6.18 shows the important parameters of the MDOF system: the height of the floor levels h_i , the concentrated masses at each floor level m_i and the normalized first mode displacement at the floor levels ϕ_i . The last three columns give quantities needed for the modal analysis (cf. Section 3.6). The shape of the first mode is assumed to be linear with a unit displacement at the top.

floor level i	h_i [m]	m_i [kg]	ϕ_i	$m_i\phi_i$	$m_i\phi_i^2$	$h_i m_i \phi_i$
2	5.84	50933	1.0	50933	50933	297448
1	2.92	47599	0.5	23799	11900	69495
sum	-	-	-	74732	62833	366943

Table 6.18: MDOF parameters

The equivalent stiffness k_E of the SDOF system is set equal to the stiffness of the real building (Equations (3.9)):

$$k_E = k = 130 \text{ kN/mm}.$$

Hence, the equivalent mass is given by Equation (3.10):

$$m_E = \sum_i m_i \phi_i = 74732 \text{ kg}.$$

The frequency of the SDOF system can then be calculated:

$$f = \frac{1}{2\pi} \cdot \sqrt{\frac{k_E}{m_E}} = \frac{1}{2\pi} \cdot \sqrt{\frac{130 \cdot 10^6}{74732}} = 6.6 \text{ Hz}$$

This is also the fundamental frequency of the building in the x-direction. Note that due to the fact that the fire protection wall is shared between two buildings their frequencies are coupled. The calculation of an independent frequency for one building is therefore strictly speaking not allowed. The extent of the coupling depends on the floor-wall connection. In the case of a perfect connection, the attached buildings will move together and act in fact as one system with one common frequency. In the case, however, where the timber beams of the floor run parallel to the fire protection walls, the floor is hardly connected to the fire protection walls and hence the coupling is rather weak.

In the case of the example building, the building is one of several terrace houses all with the same layout, the frequencies being thus the same.

The equivalent height of the SDOF system is calculated using Equation (3.11)

$$h_E = \frac{\sum h_i m_i \phi_i}{\sum m_i \phi_i} = \frac{366943}{74732} = 4.91 \text{ m}$$

and the modal participation factor using Equation (3.13):

$$\Gamma = \frac{\sum m_i \phi_i}{\sum m_i \phi_i^2} = \frac{74732}{62833} = 1.19.$$

Step 9) Vulnerability

For any given elastic response spectrum the required displacement at the top of the building and hence the corresponding damage grade shall be determined. This is demonstrated by means of the elastic acceleration response spectrum for 5% damping for medium stiff soils proposed in the Swiss standard [SIA160 89] for zone 3a with a maximum ground acceleration $a_g = 1.3 \text{ m/s}^2$ (Figure 6.17).

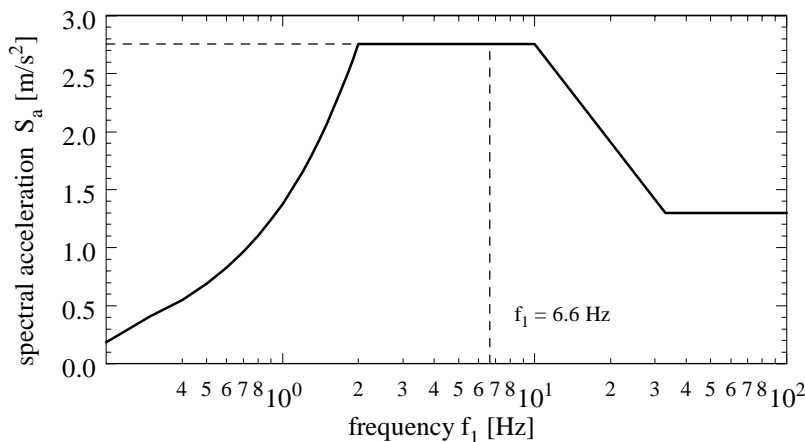


Figure 6.17: Elastic acceleration response spectrum (5% damping) for medium stiff soils proposed in the Swiss standard [SIA160 89] for zone 3a

Application to buildings in Basel

From the spectrum, the spectral acceleration at the fundamental frequency of the building $f_1 = 6.6$ Hz is (Figure 6.17):

$$S_a(f_1) = 2.76 \text{ m/s}^2.$$

As the method is based on displacements, the spectral acceleration has to be transformed into a spectral displacement using Equation (3.7):

$$S_d(f_1) = \frac{S_a(f_1)}{\omega_1^2} = \frac{S_a(f_1)}{(2\pi \cdot f_1)^2} = \frac{2.76}{(2\pi \cdot 6.6)^2} = 0.0016 \text{ m} = 1.6 \text{ mm}.$$

The required elastic displacement at the top of the building:

$$\Delta_{be} = \Gamma \cdot S_d(f_1) = 1.19 \cdot 1.6 = 1.9 \text{ mm}.$$

And hence the required elastic base shear of the building:

$$V_{be} = k \cdot \Delta_{be} = 130 \cdot 1.9 = 245.1 \text{ kN}.$$

As $V_{be} < V_{bm} = 296.4$ kN, the shear capacity of the building, the building is still in the elastic part of the capacity curve and hence the required displacement at the top of the building is:

$$\Delta_b = \Delta_{be} = 1.9 \text{ mm}.$$

For this top displacement the building will have experienced damage grade 1 (cf. Figure 6.16).

If the spectral displacement is now increased to $S_d(f_1) = 3.2$ mm (this corresponds to twice the maximum ground acceleration of zone 3a) the required elastic displacement at the top of the building is:

$$\Delta_{be} = \Gamma \cdot S_d(f_1) = 1.19 \cdot 3.2 = 3.8 \text{ mm}.$$

Hence, the required elastic base shear of the building:

$$V_{be} = k \cdot \Delta_{be} = 130 \cdot 3.7 = 489.1 \text{ kN}.$$

Comparing this to the shear capacity of the building $V_{bm} = 296.4$ kN it can be seen that the behaviour of the building is beyond the yield point and hence the strength reduction factor R is greater than 1 (Equation (3.17)):

$$R = \frac{V_{be}}{V_{bm}} = \frac{489.1}{296.4} = 1.65.$$

Thus the required ductility can be calculated using Equation (3.20):

$$\mu_D = \frac{1}{2} \cdot (R^2 + 1) = \frac{1}{2} \cdot (1.65^2 + 1) = 1.86.$$

The displacement demand is then:

$$\Delta_D = \mu \cdot \Delta_{by} = 1.86 \cdot 2.28 = 4.2 \text{ mm}.$$

For this top displacement the building will have experienced damage grade 3 (cf. Figure 6.16).

In this way the top displacement demand of the building and hence the corresponding damage grade can be determined for any spectral displacement. The presentation of the damage grades as a function of the spectral displacement leads to the vulnerability function of the building as shown in Figure 6.18.

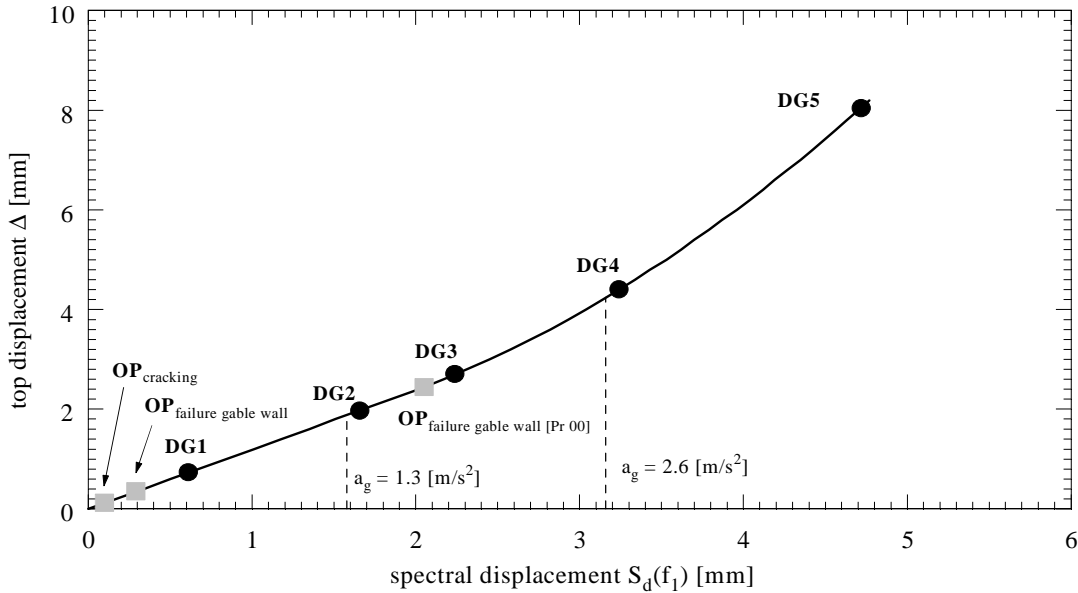


Figure 6.18: Vulnerability function of the example building

Step 10) Out-of-plane cracking

Considering the x-direction, the only wall orthogonal to that direction and hence excited in its out-of-plane mode is wall 11. Assuming that a global out-of-plane mechanism is prevented, the out-of-plane behaviour will be most critical in the uppermost storey (cf. Section 4.3.2). Wall 11 extends into the roof where it forms a gable wall with a base length $l_w = 10.0 \text{ m}$. The height of the roof storey is $h_{\text{roof}} = 5.0 \text{ m}$. The total normal force acting on wall 11 at the roof storey is due to self weight only: $N = 100 \text{ kN}$.

Hence, the moment at which cracking occurs can be calculated using Equation (4.48):

$$M_{\text{qcr}} = \frac{N \cdot t}{6} = \frac{100 \cdot 0.25}{6} = 4.2 \text{ kNm}.$$

It is assumed that no additional out-of-plane moment due to the roof load is acting on the gable wall.

The gable wall behaves as a cantilever. Assuming an effective height of the gable wall $h_{\text{eff}} = 3.33 \text{ m}$ the corresponding out-of-plane loading of the gable wall at the roof storey, is calculated using Equation (4.47) and solving for q :

Application to buildings in Basel

$$q_{cr} = \frac{2 \cdot M_{qcr}}{h_{eff}^2} = \frac{2 \cdot 4.2}{3.33^2} = 0.75 \text{ kN/m} .$$

The effective length of the gable wall can be deduced to:

$$l_{eff} = \frac{0.5 \cdot l_w \cdot h_{roof}}{h_{eff}} = \frac{0.5 \cdot 10.0 \cdot 5}{3.33} = 7.50 \text{ m} ,$$

and hence the mass per unit height of the wall plane at the roof storey can be calculated:

$$m = \frac{\gamma_m}{g} \cdot l_{eff} \cdot t = \frac{16 \cdot 1000}{10} \cdot 7.50 \cdot 0.25 = 3000 \text{ kg/m} .$$

The acceleration that causes cracking is obtained using Equation (4.44):

$$a_{cr} = \frac{q_{cr}}{m} = \frac{0.75 \cdot 1000}{3000} = 0.25 \text{ m/s}^2 .$$

This is the acceleration at the height of the centre of gravity of the gable wall i.e. at a height of $h_{3m} = 7.51 \text{ m}$. Hence the corresponding spectral acceleration using Equation (4.42) is:

$$S_a(f_1)_{OPcr} = \frac{h_E}{h_{3m}} \cdot a_{cr} = \frac{4.91}{7.51} \cdot 0.25 = 0.17 \text{ m/s}^2 .$$

In order to compare out-of-plane cracking with in-plane cracking the spectral acceleration has to be converted into spectral displacement. Using again Equation (3.7) the spectral displacement at which out-of-plane cracking occurs:

$$S_d(f_1)_{OPcr} = \frac{S_a(f_1)_{OPcr}}{(2\pi \cdot f_1)^2} = \frac{0.17}{(2\pi \cdot 6.6)^2} = 0.0001 \text{ m} = 0.1 \text{ mm} .$$

Comparing this result with the vulnerability function obtained for in-plane behaviour, it can be seen that

$$S_d(f_1)_{OPcr} = 0.1 \text{ mm} < 0.7 \text{ mm} = S_d(f_1)_{DG1} .$$

This means that out-of-plane cracking is critical, the vulnerability curve has to be corrected by displacing the identifier for damage grade 1 down to $S_d(f_1)_{OPcr} = 0.1 \text{ mm}$.

Step 11) Out-of-plane failure

Again the gable wall at the roof storey is considered. The out-of-plane moment at failure M_{qu} depends on the applied normal force and can be determined using Equations (4.53) and (4.54):

$$n = \frac{N}{l_{eff} \cdot t \cdot f_{mx}} = \frac{100}{7.50 \cdot 0.25 \cdot 5.1 \cdot 1000} = 0.0105$$

$$m = \frac{1}{2} \cdot n \cdot (1 - n) = \frac{1}{2} \cdot 0.0105 \cdot (1 - 0.0105) = 0.0052$$

$$M_{qu} = m \cdot l_{eff} \cdot t^2 \cdot f_{mx} = 0.0052 \cdot 7.50 \cdot 0.25^2 \cdot 5.1 \cdot 1000 = 12.4 \text{ kNm}.$$

The corresponding out-of-plane loading for a cantilever wall is calculated using Equation (4.47) and solving for q :

$$q_u = \frac{2 \cdot M_{qu}}{h_{eff}^2} = \frac{2 \cdot 12.4}{3.33^2} = 2.23 \text{ kN/m}.$$

The floor acceleration that causes failure is obtained from Equation (4.44):

$$a_u = \frac{q_u}{m} = \frac{2.23 \cdot 1000}{3000} = 0.74 \text{ m/s}^2.$$

The corresponding spectral acceleration is:

$$S_a(f_1)_{OPu} = \frac{h_E}{h_{3m}} \cdot a_u = \frac{4.91}{7.51} \cdot 0.74 = 0.49 \text{ m/s}^2,$$

from which the spectral displacement can be obtained using again Equation (3.7):

$$S_d(f_1)_{OPu} = \frac{S_a(f_1)_{OPu}}{(2\pi \cdot f_1)^2} = \frac{0.49}{(2\pi \cdot 6.64)^2} = 0.0003 \text{ m} = 0.3 \text{ mm}.$$

Out-of-plane failure of the gable wall indicates damage grade 3. Comparing this result with the vulnerability function (Figure 6.18) obtained for in-plane behaviour, it can be seen that

$$S_d(f_1)_{OPu} = 0.3 \text{ mm} < 2.6 \text{ mm} = S_d(f_1)_{DG3}.$$

Hence the vulnerability curve has to be corrected by displacing the identifier for damage grade 3 down to $S_d(f_1) = 0.3 \text{ mm}$.

Thus, in this case the out-of-plane behaviour of the building is always critical. However, it is reminded that even though the moment that causes out-of-plane failure M_{qu} is calculated considering ultimate conditions, the corresponding spectral acceleration at failure $S_a(f_1)_{OPu}$ is still assumed to be an elastic value. This gives very conservative results as the non-linear deflection capacity of the wall is neglected. Taking into account the inelastic capacity following the method proposed by Priestley [Pr 00] the spectral displacement that causes out-of-plane failure of the gable wall would increase to $S_d(f_1)_{OPu} = 2.0 \text{ mm}$.

The points of out-of-plane cracking and out-of-plane failure of the gable wall are shown as grey boxes in Figure 6.18, indicating the corrected vulnerability function.

Application to buildings in Basel

7 Earthquake scenarios

The evaluation method, developed in Chapters 3 to 5, was applied to the buildings in a small target area in Basel comprising four building blocks chosen to be representative of the building stock of the residential areas in Basel (cf. Chapter 6). The buildings range between two and seven storeys, some of them have a small shop, restaurant or workshop at the ground floor. As a presupposition of the evaluation of the buildings a detailed inventory was established using plans and elevations of the buildings which exist in the archives of the city. These data were supplemented by a street survey to obtain additional information on the state of preservation such as the presence of cracks or on possible alterations. An example database record of the building inventory is given in the Appendix A4.

In Section 7.1 the results of the evaluation of the buildings in the small target area are presented and in Section 7.2 possible classifications of the buildings with regard to earthquake scenarios are considered. A comparison of the results of the evaluated buildings in the small target area with other vulnerability investigations is discussed in Section 7.3 and, finally, some conclusive remarks are given in Section 7.4.

7.1 Results

A total number of 87 buildings constituting the four building blocks were evaluated. 59 out of the 87 buildings are of unreinforced masonry, all of them with timber floors (URM). 26 out of the 87 buildings are mixed systems of vertical reinforced concrete elements combined with unreinforced masonry elements having reinforced concrete floors (URM + RC). The remaining two buildings are rather special, one containing steel columns at the ground floor, the other building being made of Durisol[®] masonry (other). Figure 7.1 shows the distribution of the buildings in the target area by construction period and by number of storeys.

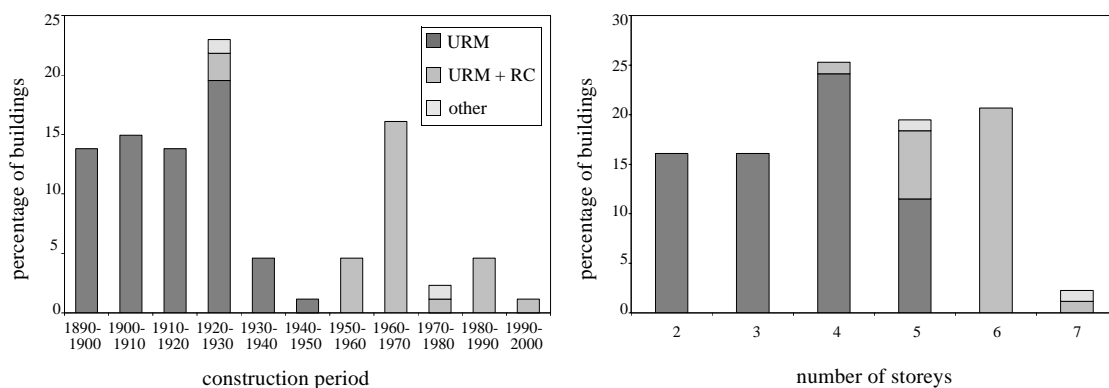


Figure 7.1: Distribution of the buildings in the target area by construction period (left) and by number of storeys (right)

Almost all buildings dating from the first half of the 20th century are of unreinforced masonry with timber floors except for three five-storey buildings constructed between 1920 and 1930 which contain reinforced concrete or steel columns at the ground floor which replace masonry wall elements at the upper floors in order to create a larger space for shops, restaurants or workshops. Towards the middle of the century there was a decline in the building activity, possibly due to the second world war. This needs to be confirmed over a larger area, though. In the 1960's there was again a considerable building activity; hardly any buildings in the small target area, however, date from recent years. Except for a single building made of Durisol[®] masonry, all buildings from the second half of the 20th century are mixed systems of vertical reinforced concrete elements combined with unreinforced masonry elements having reinforced concrete floors. Their number of storeys ranges between five and seven (except for a single four storey building) whereas the number of storeys of the unreinforced masonry buildings ranges between two and five. Hence, knowing the construction period and the number of storeys of a building it is possible to deduce the type of structure with a rather good reliability. This is demonstrated in Figure 7.2 showing the distribution of the unreinforced masonry buildings and of the buildings with a mixed system of vertical reinforced concrete elements combined with unreinforced masonry elements by construction period and number of storeys.

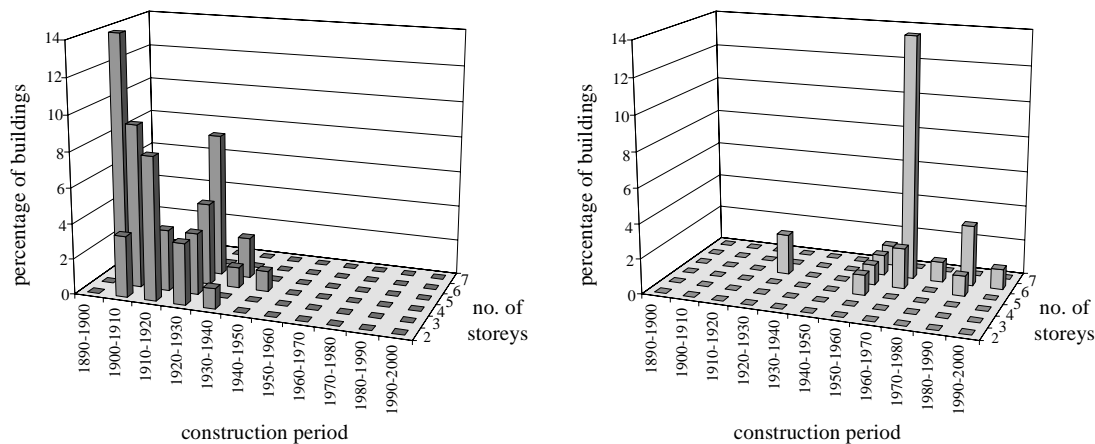


Figure 7.2: Distribution of the unreinforced masonry buildings (left) and of the buildings with a mixed system of vertical reinforced concrete elements combined with unreinforced masonry elements (right) by construction period and number of storeys

The identification of the type of structure by means of construction period and number of storeys becomes important with regard to earthquake scenarios for larger areas or for a whole city where it is not possible to prepare a detailed inventory with plans and elevations and to carry out the corresponding evaluation for each individual building. It is also desirable to use existing data bases such as can be found for the city of Basel containing the height of the building and/or the number of storeys and the year of construction linked to address and the corresponding coordinates.

As explained in detail in Chapters 3 to 5, for each building in the target area a vulnerability function in terms of damage grade - spectral displacement was established. For unreinforced masonry, both the in-plane behaviour and the out-of-plane behaviour were

considered. For unreinforced masonry buildings with timber floors, out-of-plane cracking is usually critical. For unreinforced masonry wall panels which are part of a mixed structure of vertical reinforced concrete elements combined with unreinforced masonry elements having reinforced concrete floors, out-of-plane cracking is hardly ever critical. Concerning out-of-plane failure taking into account the inelastic displacement capacity as proposed by Priestley [Pr 00] it is usually not critical, except for gable walls, assuming that an overall out-of-plane mechanism of a whole wall plane is prevented.

The seismic behaviour of the buildings in the small target area is summarized using as seismic input the design spectrum for medium stiff soil proposed by the Swiss Standard SIA 160 [SIA160 89] for zone 3a with a maximum ground acceleration $a_g = 1.3 \text{ m/s}^2$. The distribution of damage is given in Figure 7.3.

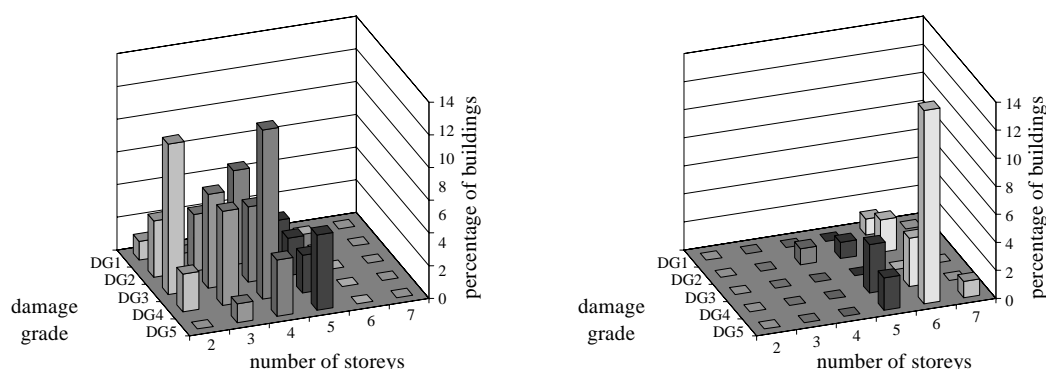


Figure 7.3: Distribution of damage for the unreinforced masonry buildings (left) and for the buildings with a mixed system of vertical reinforced concrete elements combined with unreinforced masonry elements (right) given the design spectrum for medium stiff soil for zone 3a [SIA160 89]

It is striking that the buildings with a mixed system of vertical reinforced concrete elements combined with unreinforced masonry elements have a higher seismic vulnerability than pure unreinforced masonry buildings. 80% of these buildings experience damage grade 4 (heavy damage) or 5 (destruction) according to the European Macroseismic Scale [EMS 98]. This needs further explanations. Most of these buildings have six storeys and date from the 1960's. Two different types of building structure can be found. The first one (type 1) is characterised by very open façade wall planes i.e. the façade wall planes are reduced to very few walls, if not columns, in order to increase the window area. This is especially true for the ground floors, where the load bearing elements are reduced to a few short wall elements or columns in order to create more space for shops, restaurants and workshops (soft storey). The resistance to horizontal forces in the plane of the façades is left to some inner walls creating staircases and lift shafts but which, however, in the upper storeys are often of unreinforced masonry. The resulting structures are hence extremely vulnerable to horizontal earthquake forces. The second type of building structure (type 2) is characterised by a rather strong base floor of reinforced concrete constituting the entrance level, also containing the air-raid shelter; the upper storeys are of unreinforced masonry. Hence, these buildings behave like five-storey unreinforced masonry buildings which are also fairly vulnerable.

Strictly speaking, these buildings do not have a reinforced concrete wall structure, as discussed in Chapter 5, which implies reinforced concrete walls extending over the whole height of the building. On the contrary, the elevations of these buildings are usually characterised by a high irregularity with unreinforced masonry elements replacing reinforced concrete elements in the upper storeys determining the vulnerability of the building. Only one building in the target area contains reinforced concrete walls extending over the whole building height (type 3). This building behaves much better than the above mentioned buildings reducing the damage down to damage grade 1 for the given seismic input.

Considering the unreinforced masonry buildings nearly 45% of the buildings experience damage grade 4 and 5. A correlation between damage and number of storeys is weakly perceptible.

7.2 Classification

For earthquake scenarios for larger areas or for a whole town, it is hardly possible any more to evaluate each individual building using the method presented in Chapters 3 to 5. It is therefore desirable to classify the buildings by means of a few characteristic parameters using the results of the evaluation of the buildings in the small target area. It is obvious that the structural type plays the most important role. Other important parameters are the number of storeys and the construction period which can be easily derived from existing data bases. Further important parameters such as the number of walls and their lengths, normal forces etc. are more difficult to obtain needing a detailed inventory. They are therefore not taken into account in the proposed classification. This, however, is only a necessary simplification with regard to the earthquake scenario project; their neglect does not imply that their influence on the vulnerability of a building is negligible. It follows that even though the buildings are grouped together in classes, it is not possible to deduce from the vulnerability function of a building class the vulnerability function of an individual building which can be very different.

The structural system being considered the key factor in the seismic performance of a building, three building classes are defined:

- class 1: low rise (1-3 storeys) unreinforced masonry buildings with timber floors (low-rise URM),
- class 2: medium rise (4-6 storeys) unreinforced masonry buildings with timber floors (med-rise URM),
- class 3: medium rise buildings with a mixed systems of vertical reinforced concrete elements combined with unreinforced masonry elements having reinforced concrete floors (med-rise URM+RC).

This building classification is close to typical building classifications used elsewhere [ATC 13][FEMA 178]. It also results in an equal distribution of the buildings in the small target area among the building classes (31% in class 1, 36% in class 2 and 33% in class 3).

The results of Section 7.1 allow the determination of the building class by means of the number of storeys and the construction year. In Table 7.1 the median values m_x , the standard deviations s_x and the coefficients of variation v_x of the fundamental frequencies f_1 and the spectral displacements at the onset of each damage grade $S_d(f_1)_{DG_i}$, $i = 1 \dots 5$, are summarized for each building class.

	class 1			class 2			class 3		
	low-rise URM			med-rise URM			med-rise URM+RC		
	m_x	s_x	v_x	m_x	s_x	v_x	m_x	s_x	v_x
f_1 [Hz]	4.8	1.1	0.24	3.8	0.8	0.21	2.7	0.8	0.30
$S_d(f_1)_{DG1}$ [mm]	0.9	0.4	0.46	1.6	0.5	0.30	1.5	0.5	0.34
$S_d(f_1)_{DG2}$ [mm]	1.9	0.7	0.37	2.5	0.9	0.38	3.3	1.2	0.37
$S_d(f_1)_{DG3}$ [mm]	2.8	1.0	0.35	3.9	1.2	0.30	6.5	2.0	0.31
$S_d(f_1)_{DG4}$ [mm]	4.3	1.7	0.38	4.9	1.6	0.33	7.0	2.4	0.34
$S_d(f_1)_{DG5}$ [mm]	5.7	1.9	0.33	6.7	2.4	0.35	10.3	3.8	0.37

Table 7.1: Median values of the fundamental frequencies f_1 and the spectral displacements at the onset of each damage grade $S_d(f_1)_{DG_i}$ for each building class

v_x ranges between 21% and 46%, indicating a rather large dispersion of the vulnerability functions of the buildings in one building class. The mean vulnerability functions of the three building classes, however, are clearly distinct (Figure 7.4). DG0 indicates undamaged.

A more refined classification, subdividing classes 1, 2 and 3 to take into account the exact number of storeys n or the construction period, does not seem practical as the sets of values for each building class become very small. Also, the resulting vulnerability functions are not clearly distinguishable any more (Figure 7.4). Figure 7.3 has shown that the correlation between number of storeys and vulnerability is rather weak. Likewise the

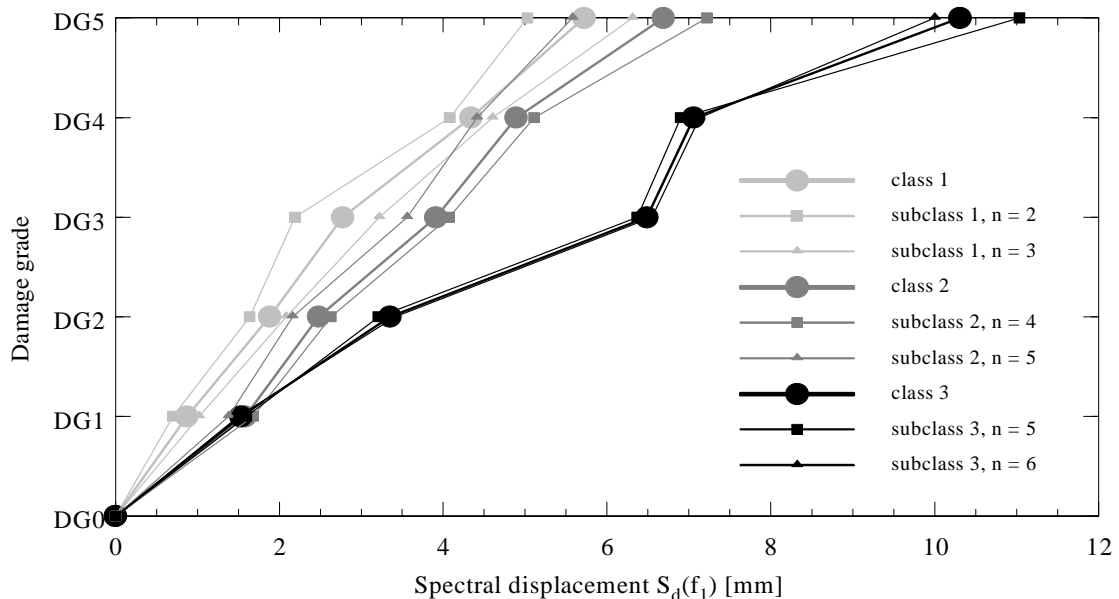


Figure 7.4: Mean vulnerability functions of the different building classes

correlation between construction period and vulnerability is not very strong for the period considered. Although the type of construction of unreinforced masonry buildings with timber floors has changed over the first half of the 20th century, for example from rather high ceilings and very thick walls at the lower floors to lower ceilings and walls with a uniform thickness over the whole building height, the change has taken place over a period of 20 to 30 years and a clear rupture, such as around 1950 when reinforced concrete became customary, is not perceptible.

A distinction between the different types of buildings of class 3 (open façade wall planes (type 1), strong base floor of reinforced concrete (type 2) and continuous reinforced concrete walls over building height (type 3)) seems advisable, however, they are not easily distinguishable without plans and elevations. Furthermore, the results of the evaluation of the buildings in the small target area do not show clearly distinct vulnerability functions for type (1) and type (2).

Considering the dispersion of the vulnerability functions in each building class it suggests itself to express the vulnerability function of a building class using a probabilistic distribution instead of a single deterministic vulnerability curve. Each set of values of a building class (fundamental frequencies f_1 and the spectral displacements at the onset of each damage grade $S_d(f_1)_{DGi}$, $i = 1 \dots 5$) can be represented by a normal distribution which is defined by the mean μ_x and the standard deviation σ_x . The cumulative distribution for each damage grade is called in the literature a fragility curve [KNKH 97] [HLH 97]. The mean and the standard deviation are estimated using the median value and the standard deviation of the sample: $\mu_x = m_x$ and $\sigma_x = s_x$.

Building class fragility curves are functions that describe the probability of a building belonging to a certain building class of reaching or exceeding a particular damage grade given a deterministic estimate of the spectral response, here the spectral displacement:

$$P(D \geq DGi | S_d(f_1)) = \Phi \left(\frac{S_d(f_1)_{DGi} - \mu_{S_{di}}}{\sigma_{S_{di}}} \right) \quad (7.1)$$

$\mu_{S_{di}}$ is the mean value of the spectral displacement at which the threshold of damage grade i , DGi , is reached, $\sigma_{S_{di}}$ is the standard deviation of the spectral displacement of damage grade i and Φ is the standard normal cumulative distribution function.

The fragility curves of a building class thus take into account the variability associated with the vulnerability function of a building class. Figure 7.5 shows the fragility curves and the probability density functions of the fundamental frequencies of the three building classes.

Note that due to the fact that the standard deviations of the spectral displacements at the onset of each damage grade are rather large, especially for $DG5$, the fragility curves of the higher damage grades only tend to zero for very small spectral displacements. This suggests that even at very small spectral displacements there will be always a small probability of complete collapse which is not very reasonable. This deficiency could be overcome by a bigger sample which might diminish the standard deviation or by a better fitted distribution. This, however, goes beyond the scope of this work.

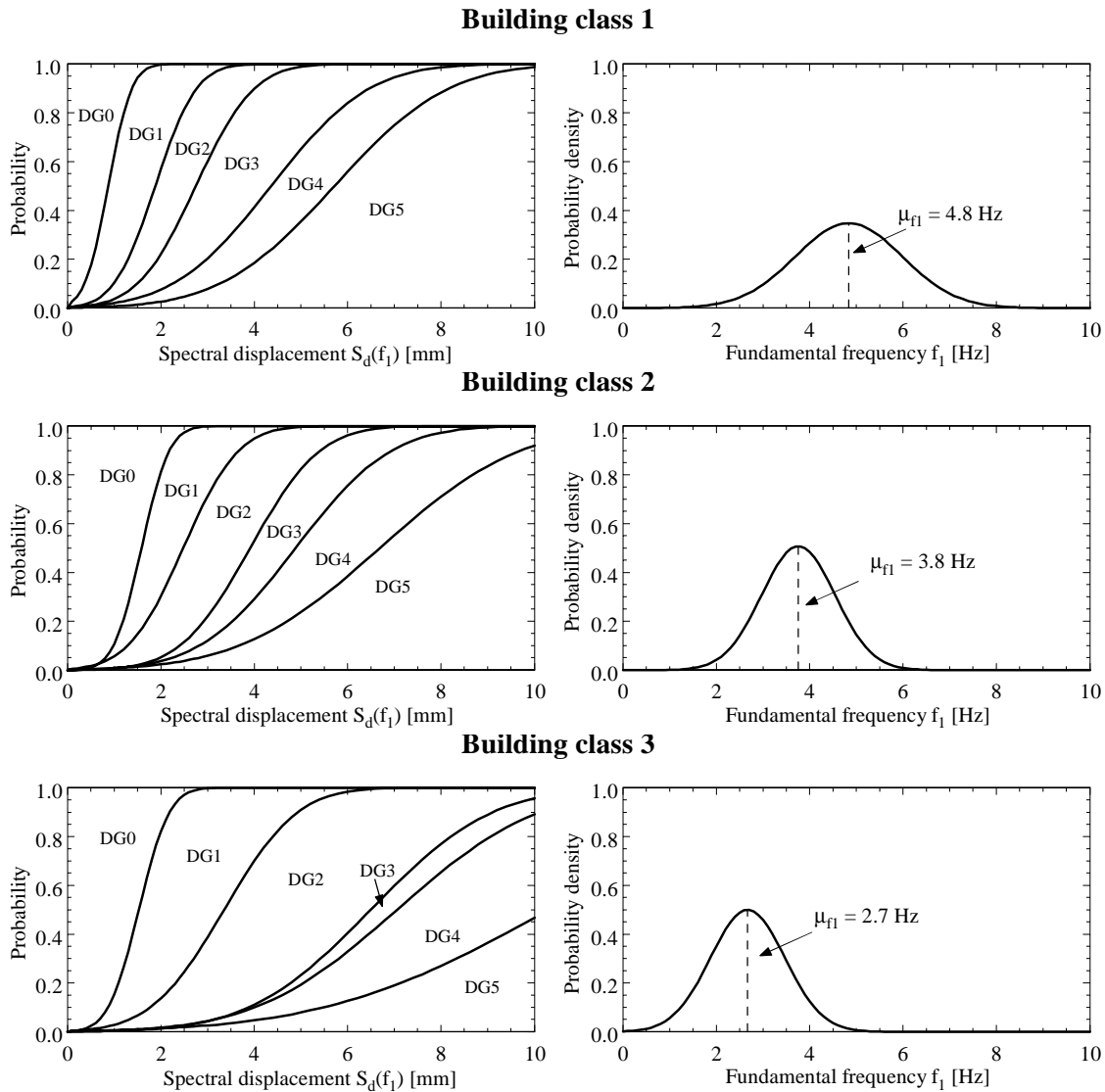


Figure 7.5: Fragility curves (left) and probability density functions of the fundamental frequencies (right) of the three building classes

7.3 Comparison with other vulnerability investigations

After the evaluation of the buildings in the small target area and the classification into three building classes for which representative vulnerability functions were established it suggests itself to compare the vulnerability of the investigated building stock in Basel with other vulnerability investigations. This is, however, not easily accomplished as most vulnerability functions are given in terms of intensity. The relationships between spectral values, ground movement and intensity are rather vague and not equally valid for all locations, making a direct comparison impossible as is demonstrated in the following.

Two comparisons are attempted: One with the vulnerability classes defined in the European Macroseismic Scale 1998 [EMS 98] and a second one with the fragility curves for low rise brick masonry buildings obtained after the compilation of damage distribution

for 103 surveys of brick masonry buildings at individual locations in a number of earthquakes from a range of different countries [CS 92].

The European Macroseismic Scale defines six vulnerability classes, vulnerability classes A to F, with vulnerability class A being the most vulnerable class. Depending on the type of structure (steel, wood, rubble stone masonry, simple stone masonry, reinforced concrete walls without earthquake-resistant design etc.) the buildings are assigned to the vulnerability classes. From the type of structure of the buildings in the small target area, the expected vulnerability classes of the different building classes are: vulnerability class B for building class 1 (low-rise URM), between vulnerability classes A and B for building class 2 (med-rise URM) and vulnerability class A for building class 3 (med-rise URM+RC).

In order to compare the vulnerability of the three building classes with the vulnerability classes of the European Macroseismic Scale the spectral displacements $S_d(f_1)$ have to be converted into intensities. No reliable relationship exists and the most obvious way seems the relationship assumed in the Swiss Standard SIA 160 [SIA160 89]. The conversion follows in two steps: From spectral displacements $S_d(f_1)$ into maximum ground accelerations a_g (peak ground accelerations or effective ground accelerations) and then from maximum ground accelerations a_g into intensities I_{EMS} . For the first step the shape of the acceleration response spectrum is assumed corresponding to the design spectrum for medium stiff soil with the two corner frequencies of the plateau at 2 and 10 Hz and an amplification factor of 2.12. For the second step the assumed correlation of maximum ground acceleration a_g and intensity I_{MSK} is shown in Table 7.2. The intensities of the European Macroseismic Scale correspond to the intensities of the MSK Scale $I_{EMS} = I_{MSK}$.

Zone	Intensity I_{MSK}	a_g [g]
1	VI - VII	0.06
2	VII+	0.10
3a	VIII-	0.13
3b	VIII+	0.16

Table 7.2: Correlation between intensity I_{MSK} and maximum ground acceleration a_g according to SIA 160 [D044 89]

Based on these relationships the distribution of damage corresponding to $a_g = 1.5 \text{ m/s}^2$ (supposed to be equivalent to an intensity $I_{EMS} = \text{VIII}$) is shown on the left hand side of Figure 7.6.

The European Macroseismic Scale defines intensity VIII: Many buildings (15-55%) of vulnerability class A suffer damage grade 4, a few (< 15%) of damage grade 5; many buildings (15-55%) of vulnerability class B suffer damage grade 3, a few (< 15%) of damage grade 4. Comparing this definition with the distribution of damage for the three building classes it seems that the buildings of building class 1 behave similar to vulnerability class A, whereas the other two classes are even more vulnerable.

The second comparison with the fragility curves for low rise brick masonry buildings obtained from statistical evaluations of observed damage (Figure 7.7) gives similar results.

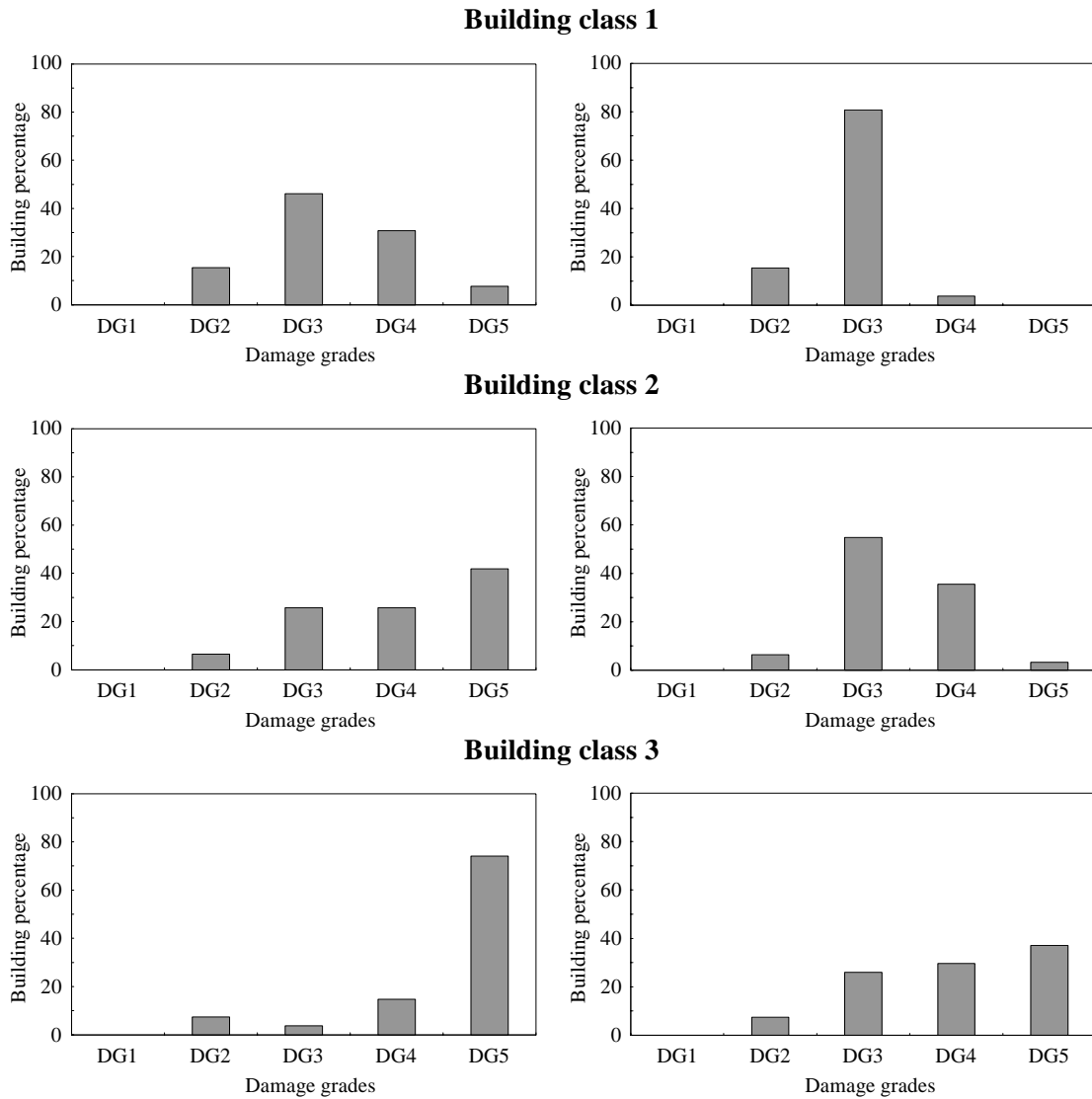


Figure 7.6: Distribution of damage corresponding to $a_g = 1.5 \text{ m/s}^2$ ($I_{EMS} = VIII$) (left) and taking into account an increased plastic deformation capacity (right)

The low rise masonry buildings in the small target area in Basel seem to be more vulnerable than the average.

The apparent discrepancy between the vulnerability of the building stock in Basel and general observed vulnerabilities may have several reasons which will be discussed in the following.

1) Conservative assumption of the capacity of the buildings

The estimate of the capacity of the buildings using the evaluation method may be conservative due to following reasons:

- Use of lower bound theorem of plasticity
The use of the lower bound theorem of plasticity results in a shear capacity which will be always less or equal to the true shear capacity of a masonry wall element. As a consequence the corresponding elastic displacements may be underestimated.

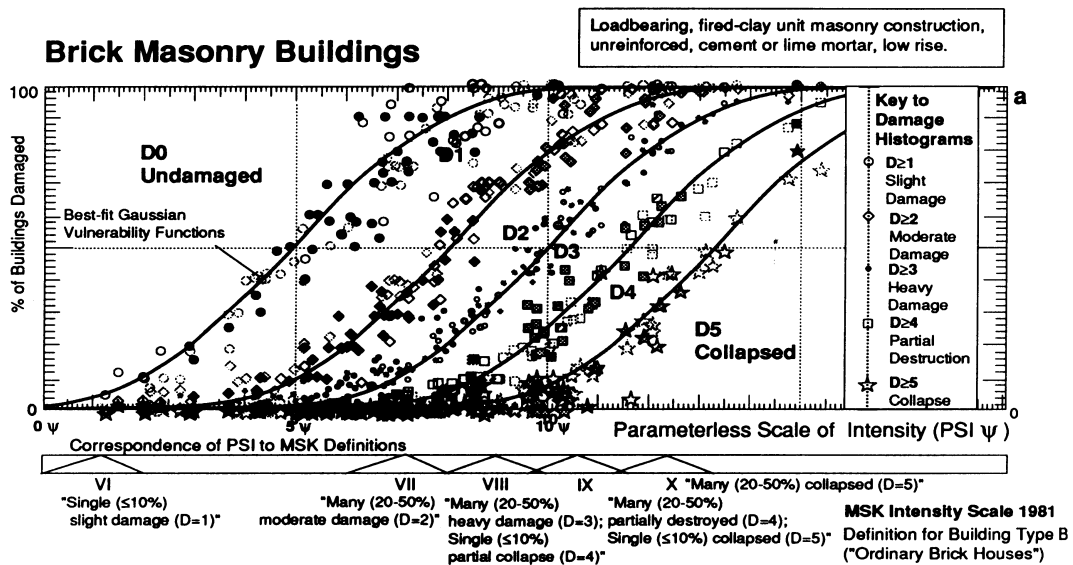


Figure 7.7: Fragility curves for low-rise brick masonry buildings after [CS 92], Figure 8.8 a

It is, however, the opinion of the author, that the influence is negligible (cf. Section 4.4: Comparison with test results).

- **Conservative assumptions**
Some conservative assumptions on the failure conditions for unreinforced masonry were made such as the neglect of the tensile strength of masonry and of the cohesion in the mortar beds. Again, the influence should be very small. Concerning the simplifications of the model of the buildings (e.g. capacity of the spandrels only taken into account implicitly) the influence is considered to be rather small in the elastic range, however, it could be more important in the plastic range requiring a more refined model.
- **Underestimation of the plastic deformation capacity of unreinforced masonry**
The estimation of the plastic deformation capacity of unreinforced masonry is based on a single test series on masonry elements subjected to normal and shear forces available in Switzerland (cf. Section 4.2.4). Comparisons with capacity curves of unreinforced masonry model buildings tested (Section 4.4) have shown that the plastic deformation capacity is always underestimated by the evaluation method. This affects damage grade 4 and 5. Here, further research on the plastic deformation capacity of masonry and a more refined modelling taking into account the behaviour of the spandrels and their influence on the plastic mechanism could improve the results.
The influence of an underestimation of the plastic deformation capacity is investigated by increasing the plastic deformation capacity of the buildings arbitrarily by 50% (Figure 7.6 right). As expected this will reduce the vulnerability of the buildings, however, this needs to be verified.

2) Seismic input

In order to enable a comparison spectral displacements had to be converted into intensities. This was done in two steps, each step accompanied with large uncertainties.

- Spectral displacement - maximum ground acceleration relationship

The conversion from spectral displacements into maximum ground accelerations via spectral accelerations was done assuming the shape of the design response spectrum. The most simple way to construct design response spectra is to use a mean spectrum of different spectra suitable for a certain region. Although individual spectra may have peak spectral accelerations more than four times the maximum ground acceleration, the frequency range is very narrow and the remaining spectral accelerations are rather small. Taking the mean of the spectra, a plateau develops with an amplification around $2.0 \div 2.5$ which is consistent with most design response spectra. This is demonstrated in Figure 7.8 using different acceleration response spectra from all over Europe normalised to a unit maximum ground acceleration. Also shown is the design response spectrum for stiff soil according to the Swiss Standard with corner frequencies of the plateau value of 3 and 10 Hz. Here, the design spectrum for stiff soil was used for a comparison as most real spectra were measured on stiff soil sites.

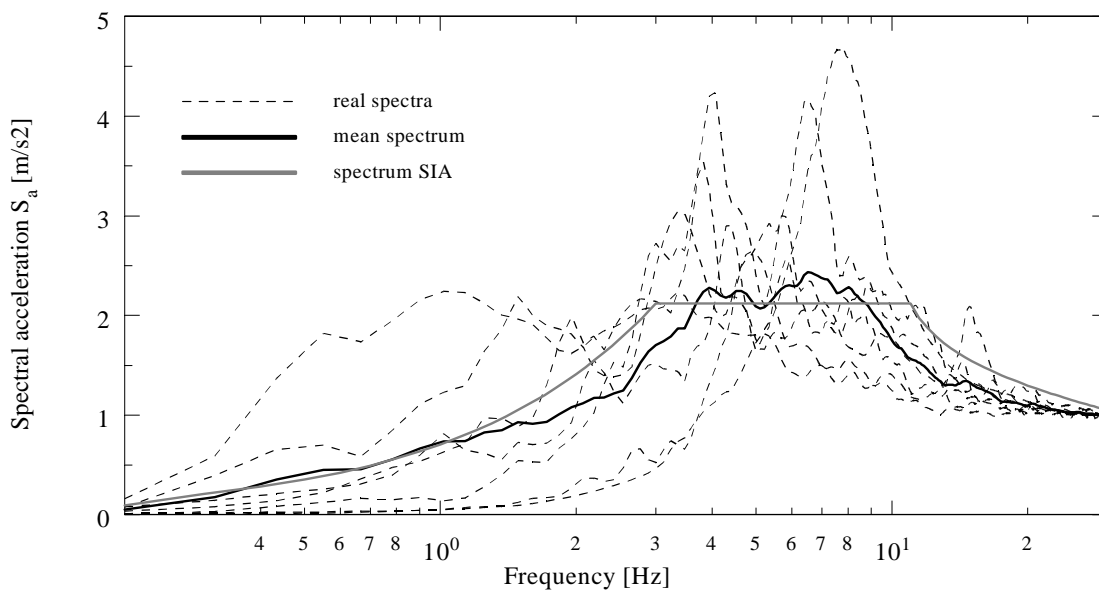


Figure 7.8: Normalised acceleration response spectra, normalised mean spectrum and normalised design response spectrum according to SIA

A full discussion of the problematic nature of design response spectra is beyond the scope of this work, but it is obvious that even though the design spectrum represents a mean spectrum, an individual spectrum can be very different and, depending on its frequency content, can lead to very different results.

Other methods [DSOP 97] assume an infinite stiffness of the structural model for masonry buildings i.e. an amplification factor equal to one. This, however, is con-

sidered unrealistic by the author, as shaking table tests on masonry buildings have shown that unreinforced masonry is not infinite stiff and amplification factors of two and more are possible [BP 96].

- Intensity- maximum ground acceleration relationship
 Numerous empirical relationships between maximum ground acceleration and intensity exist, however, the uncertainties are considerable and the variations between different relationships are enormous. Figure 7.9 shows various relationships. The three intensity scales MM, MSK and EMS are comparable for the intensity range considered. The spread is enormous and hence, the use of one relationship or another can lead to very different results.

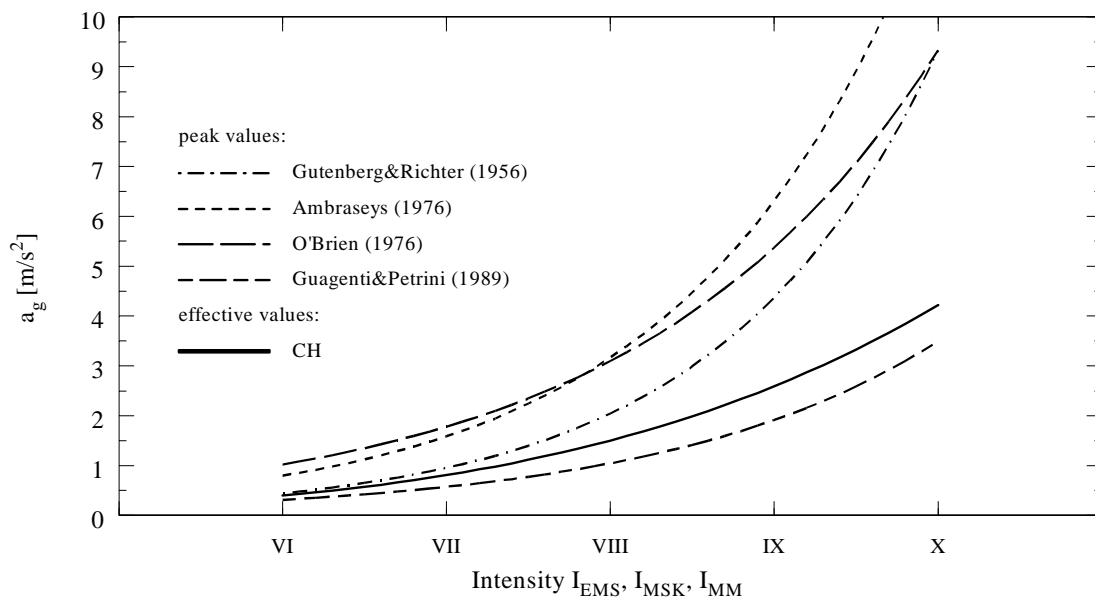


Figure 7.9: Empirical relationships between maximum ground acceleration (peak ground acceleration and effective ground acceleration) and intensity I_{EMS}, I_{MSK}, I_{MM}

It follows that the uncertainties in the seismic input expressed in terms of intensity exceeds considerably the uncertainties in the capacity of the buildings. The resulting damage distribution using $S_d - I_{EMS}$ relationships should be therefore considered with care.

Figure 7.10 shows horizontal displacement spectra for stiff soils predicted for Europe by Ambraseys et al. [ASB 96] for magnitudes M_S ranging between 6.2 and 6.8 and epicentral distances of 10 and 20 km. Those spectra can be considered as mean spectra for a whole area, such as the city of Basel, the amplification effects of the local underground are not taken into account yet.

The black curve indicates the displacement spectrum corresponding to the design spectrum for medium stiff soil proposed by the Swiss Standard scaled to a maximum ground acceleration of $a_g = 1.5 \text{ m/s}^2$. The comparison shows that for frequencies $f > 2 \text{ Hz}$ it corresponds more or less to a displacement spectrum for magnitude $M_S = 6.5$ and an epicentral distance of 20 km. This, however, could as well correspond to an intensity $I_{EMS} = IX$ [GMR 98].

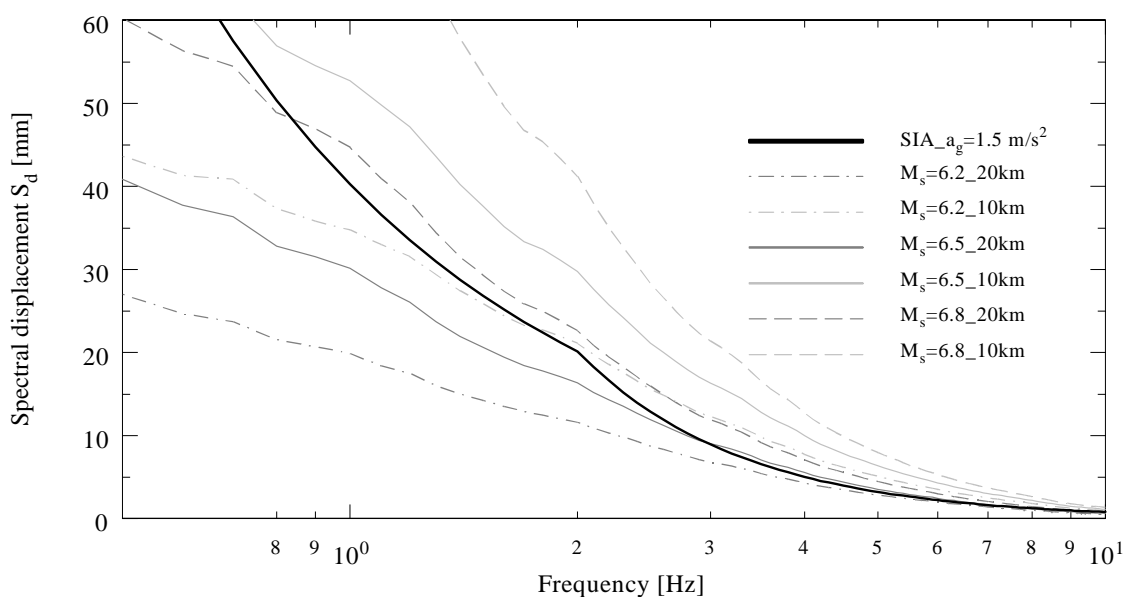


Figure 7.10: Displacement spectra for Europe [ASB 96]

In this light the distribution of damage for the buildings in the small target area corresponding to the design spectrum for medium stiff soil and a maximum ground acceleration of $a_g = 1.5 \text{ m/s}^2$ (Figure 7.6 left) seems more reasonable with respect to other vulnerability investigations. For a definite statement on the damage distribution the final results of research line 2 and 3, regional hazard [Bay 02] and microzonation [Ki 02], have to be waited for.

Finally, the distribution of damage for the buildings in the small target area was calculated using as seismic input the displacement spectrum of the Fribourg earthquake / Switzerland from 14 February 1999 (Figure 7.11 left). The magnitude M_L was 4.3 and the peak horizontal ground acceleration measured at a station 13 km from the epicentre was 0.4 m/s^2 . The macroseismic intensity in the epicentral area reached $I_o = V$ [DBB 00]. According to the EMS 98 this corresponds to a few buildings of vulnerability class A and B suffering damage grade 1. This is well reflected by the calculated distribution of damage for the buildings in the small target area (Figure 7.11 right): 17% of all buildings suffer damage grade 1.

7.4 Conclusions

87 buildings were evaluated in a small target area in Basel and the results presented in terms of building characteristics (construction type, number of storeys and construction period) and resulting damage grades given the design spectrum for medium stiff soil for zone 3a [SIA160 89]. The results reveal that due to unsuitable building layout (soft storeys, no lateral force resisting elements in one direction) buildings dating from the 1960's with a mixed system of vertical reinforced concrete elements combined with unreinforced masonry elements having reinforced concrete floors are extremely vulnerable to seismic lateral forces, even more than pure unreinforced masonry buildings.

Earthquake scenarios

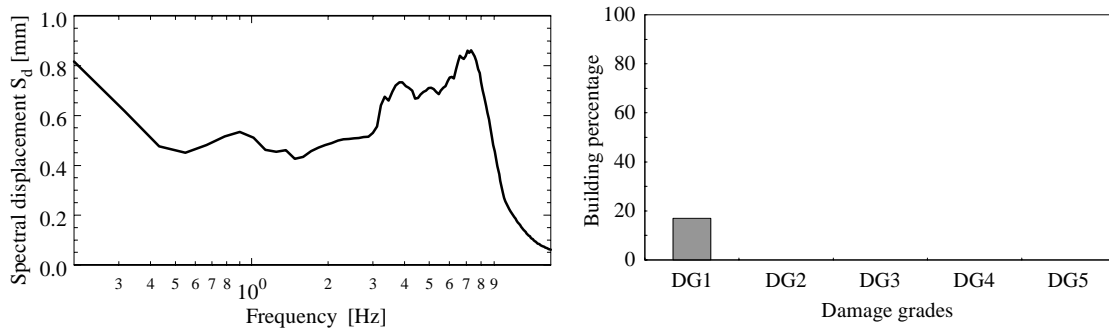


Figure 7.11: Displacement spectrum for the Fribourg earthquake 1999 (left) and corresponding distribution of damage for the buildings in the small target area (right)

Based on the results of the evaluation of the buildings in the small target area three clearly distinct building classes are defined which can be identified solely by their construction period and the number of storeys. The vulnerability function of a building class is given in terms of fragility curves which take into account the variability associated with the vulnerability function of a building class.

Comparison with other vulnerability functions in terms of intensity are not feasible as the $S_d - I$ relationship is full of uncertainties. For a realistic estimation of damage distribution in the small target area in Basel an appropriate ground motion has to be considered.

8 Summary and conclusions

8.1 Summary

Within the scope of the project “Earthquake Scenarios for Switzerland” the evaluation of the vulnerability of existing buildings is required. Due to the lack of major earthquakes in Switzerland in the last century no observed damage patterns of existing buildings are available. A simple evaluation method based on engineering models of the building structure is therefore proposed that allows the evaluation of a larger number of buildings.

Chapter 2 gives an overview of existing earthquake scenario projects and the respective vulnerability functions or matrices used. Their determination range from very simplified and rather global loss estimation methods based on observed damage patterns in earthquake-struck areas and expert opinions, via simple analytical models and score assignments, to rather detailed analysis procedures.

Based on the knowledge of existing vulnerability functions and matrices, an evaluation method adequate for the needs and conditions of the earthquake scenario project for the city of Basel is developed in a general way in Chapter 3. The difference between the design of new buildings and the evaluation of existing buildings is stressed in order to facilitate the choice of the right parameters, especially concerning a satisfactory structural model of the building. It follows the definition of the vulnerability function and the basic concept that the expected damage of a building can be obtained by a comparison of the capacity of the building and the seismic demand on the building. Simple approaches to calculating the capacity of the building and the seismic demand on the building are then proposed.

The evaluation method introduced in a general way in Chapter 3 is discussed in more detail with respect to unreinforced masonry buildings in Chapter 4. A distinguishment is made between the in-plane behaviour and the out-of-plane behaviour. Considering first the in-plane behaviour, the shear behaviour of unreinforced masonry is briefly reviewed and the failure criteria developed by Ganz [Ga 85] are introduced. These are then used to derive the shear capacity of an unreinforced masonry wall. With the help of test results on unreinforced masonry wall elements tested at the ETH Zürich [GT 84] the plastic deformation capacity is deduced. The capacity curve of the wall is then approximated bilinearly with a linear elastic part up to the point where the shear capacity of the wall is reached followed by a perfectly plastic part with zero stiffness. The capacity curve of the building is obtained by superposition of the capacity curves of all the walls. An important point is the consideration of the frame action due to the coupling of the walls by floors and spandrels as this has a crucial influence on the capacity curve of a building. Next, the damage grades according to the European Macroseismic Scale [EMS 98] are identified on the capacity curve of the building. The vulnerability function of the building is obtained by relating the damage to the seismic input. For out-of-plane behaviour, the occurrences of cracking and failure are considered, leading to possible corrections of the

Summary and conclusions

vulnerability function of the building. Finally, the evaluation method for unreinforced masonry buildings is validated by application to two unreinforced masonry model buildings that have been tested, one under cyclic-static action at the university of Pavia [MKC 95], the other one dynamically on the shaking table at the testing centre ISMES [BP 96]. The comparisons are rather satisfactory in terms of overall behaviour, however, it is not possible to describe the correct crack pattern.

In Chapter 5, the evaluation method is discussed in more detail with respect to reinforced concrete buildings. Since the seismic behaviour of reinforced concrete structures is much more thoroughly investigated and therefore better known, it is possible to use existing models. The aim is to fit these into the evaluation method proposed in Chapter 3 allowing an equivalent treatment of all buildings. Three types of reinforced concrete buildings are distinguished, the simplest one is a cantilever wall structure, whereas the other two include frame action. Depending on the type of reinforced concrete building, three different approaches are outlined. Analogous to masonry buildings the capacity curve of the building is obtained by superposition of the capacity curves of the walls. The damage grades according to the European Macroseismic Scale [EMS 98] are then identified on the capacity curve of the building. Relating the damage to the seismic input, the vulnerability function of the building is eventually obtained. In the absence of test results on reinforced concrete wall structures the evaluation method for reinforced concrete buildings is validated by a comparison with another approach proposed by Dazio [Da 00] based on [BD 97]. Again, the comparison is satisfactory in terms of overall behaviour.

Chapter 6 treats the local construction conditions in Basel and the consequences on the evaluation method. The implication of the presence of flexible timber floors with respect to an idealised rigid diaphragm is briefly discussed. A review of the development of the material properties throughout the last century, both for unreinforced masonry and reinforced concrete, is given resulting in a short guideline for the derivation of the material properties of existing buildings as a function of the construction year avoiding time consuming and expensive in situ testing. The chapter finishes with an example of the evaluation of an unreinforced masonry building which is typical for the city of Basel.

In Chapter 7, a summary of the results of the evaluation of the buildings in a small target area in Basel is given. Three building classes are defined in order to allow earthquake scenarios for larger areas. The dispersion of the vulnerability functions of the buildings in one class is rather large, illustrating the difficulty in classifying the buildings using solely parameters such as construction year and number of storeys for which data bases would be easily available. Finally the results are compared with other existing vulnerability investigations which are given in terms of intensity. The discrepancies illustrate the fact that general assumptions on the seismic input are not good enough for the estimation of the seismic risk but that the realistic seismic input is needed.

8.2 Conclusions

A simple evaluation method was developed within the scope of the earthquake scenario project for Switzerland which allows the assessment of the seismic vulnerability of existing buildings. The method is based on a nonlinear static approach acknowledging the

importance of the nonlinear deformation capacity of the buildings subjected to seismic action. The main advantages of the method are summarized briefly:

- The method is simple allowing the evaluation of a larger number of buildings without neglecting important features such as the nonlinear deformation capacity of the buildings and the coupling of the walls by floors and spandrels.
- It is based on mostly well known engineering models and hence, it can be applied by practising engineers without large prerequisites.
- Since reinforced concrete buildings and unreinforced masonry buildings are considered in the same way it is possible to evaluate buildings with a mixed structure of reinforced concrete elements and unreinforced masonry elements.
- In a further step, it is also possible to consider certain upgrading strategies by an appropriate change in the capacity curves of the walls, thus changing the capacity curve of the building.

The comparison with test results of masonry model buildings show that the proposed method suitably forecasts the capacity of a building, especially when considering the scatter of the test results. However, in order to prevent conservatism the force reduction factor and the displacement reduction factor which were introduced to take into account the effect of the cyclic nature of the seismic input are both set equal to 1. Still, the plastic deformation capacity of a building is always underestimated by up to 50%. This conservatism is beneficial for the design of new buildings, however, it is less desirable for the evaluation of existing buildings.

In the case of reinforced concrete buildings no test data were available and hence, the method was compared with a recently proposed and thoroughly checked deformation orientated method. Again, the comparison is rather satisfactory, provided that the right failure mechanism is chosen. The results of the evaluation method can be therefore regarded with some confidence.

The proposed method is rather more detailed than other analytical approaches developed for the evaluation of a whole building population (cf. Section 2.4). This is due to a lack of experience with earthquake damages in Switzerland requiring a more precise analysis which allows a better understanding of the behaviour of the buildings under seismic action.

The time required for the evaluation of a building ranges between two and six hours. It is thus not feasible to evaluate each individual building in a large target area, even though a relatively large number of buildings can be evaluated. Hence, unlike the other analytical approaches proposed by Calvi [Ca 99] and D'Ayala [DSOP 97] where each building is evaluated, a classification of the buildings is necessary in order to allow the extrapolation of the results for the use in earthquake scenario projects.

With regard to the evaluation of an individual building using detailed analysis procedures (cf. section 2.6), certain simplifications were necessary in order to reduce the time expenditure. Those simplifications concern especially the assumption of a linear displacement shape, rigid diaphragms and ideal floor-wall connections, and the neglect of torsion, interaction of adjacent buildings and pounding. Also, the capacity of the span-

Summary and conclusions

drels is only taken into account implicitly. The evaluation method is therefore rather suitable for regular buildings. For very irregular buildings and for the purpose of the assessment of an individual building in order to decide on upgrading strategies, these simplifications have to be checked, but the same approach can be used. Also, for the evaluation of an individual building, the exact material properties as obtained from in-situ tests are required.

The results of the evaluation of the buildings in the small target area in Basel revealed that, assuming the design response spectrum for medium stiff soils proposed by the Swiss standard [SIA160 89] for zone 3a, 45% of the unreinforced masonry buildings behave inadequately, i.e. they would experience damage grade 4 (very heavy damage) and 5 (destruction) according to the European Macroseismic Scale [EMS 98]. Buildings with a mixed structure of reinforced concrete elements combined with unreinforced masonry elements behave even worse due to bad configurations in plan and elevation (soft storeys etc.). This suggests that the seismic risk for the city of Basel is considerable. A statement on the actual seismic risk, however, is not yet possible without the knowledge of the local seismic hazard i.e. the local response spectrum as obtained from the regional hazard [Bay 02] taking into account the local soil conditions by a microzonation for the city of Basel [Ki 02]; general assumptions on the seismic hazard may be misleading.

Finally, regarding risk mitigation, it is not valid to interpolate conclusions from the behaviour of a class of buildings to the behaviour of individual buildings. It was shown in Chapter 7 that the discrepancies can be enormous.

8.3 Outlook

This work on the seismic evaluation of existing buildings has risen many questions both on the fundamental basis required for the evaluation of buildings and the use of the evaluation method for risk assessment. The results of the evaluation of the buildings in a small target area in Basel also lead to the question of upgrading of existing buildings.

Fundamental research

Concerning the fundamental basis, this work has revealed major gaps in the understanding of the behaviour of unreinforced masonry. Most studies on masonry focus on retrofit strategies. While the effects of reinforcement or other post-strengthening methods such as the bonding of fibre-composite materials are investigated, the behaviour of the material itself is rarely subject of research. One major gap identified is the description of the nonlinear behaviour of unreinforced masonry. In fact, for a long time the material was believed to behave completely brittle. Test results have proven this to be wrong. An adequate description of the plastic deformation capacity, however, is not available. The test results of Ganz [GT 84] allow a quantification of the influence of the acting normal force on the ultimate drift which was used to estimate the plastic deformation capacity in this work. Other parameters could not be considered, or only in a very simplistic way, as the necessary data is not available. It therefore seems recommendable to investigate the plastic deformation capacity of unreinforced masonry by a suitable test program on unrein-

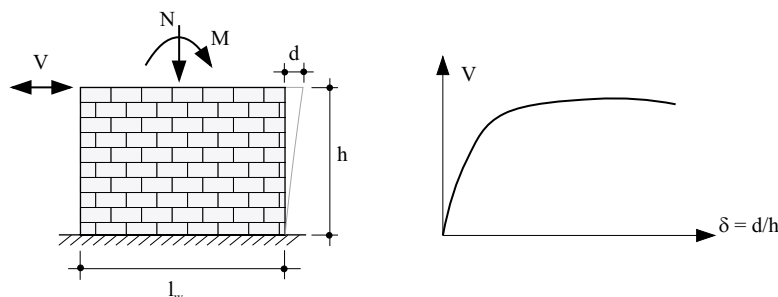


Figure 8.1: Test on unreinforced masonry wall elements (piers)

forced masonry wall elements where the important parameters such as the acting normal stress σ_n , the aspect ratio h/l_w , the material properties and the boundary conditions are systematically varied (Figure 8.1).

The nonlinear behaviour of a building, however, depends not only on the plastic deformation capacity of a wall element but also on the failure mechanism. In this work, a pier sidesway mechanism was always assumed for unreinforced masonry buildings. The failure mechanism, however, depends also on the capacity of the spandrels which was not considered explicitly in this work. For a better understanding of the capacity of unreinforced masonry spandrels their behaviour could be investigated by a series of tests on unreinforced masonry beam elements of varying geometry and material properties (Figure 8.2).

The results of the two test series could then be used for a refined model of unreinforced masonry buildings using a macroelement approach such as proposed by Brencich, Gambarotta and Lagomarsino [BGL 98] or by Magenes [Mag 00] where the piers and the spandrels are modelled by macroelements joined by rigid elements (Figure 8.3).

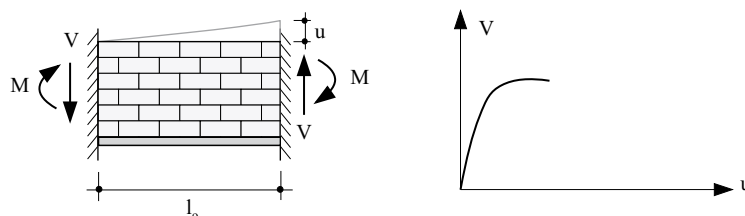


Figure 8.2: Tests on unreinforced masonry beam elements (spandrels)

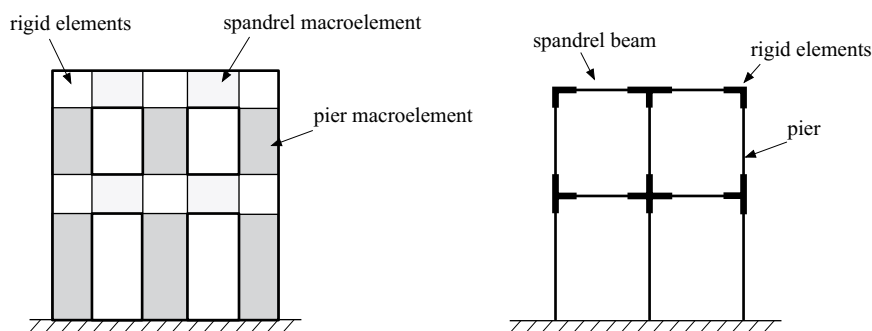


Figure 8.3: Refined model of unreinforced masonry buildings using a macroelement approach such as proposed by Brencich, Gambarotta and Lagomarsino (left) and by Magenes (right)

Summary and conclusions

Risk assessment

Concerning the use of the evaluation method for risk assessment, a larger number of buildings should be evaluated allowing a better statistical interpretation. The fragility curves obtained for each building class assuming the data to be normally distributed display a very low onset of the higher damage grades, especially DG5, due to a very large standard deviation of the data sets. A bigger sample could diminish the standard deviation.

Using the defined building classes the results of the small target area can then be extrapolated to other residential areas in Basel. Since it is possible to identify the building classes by the number of storeys and the construction year, available data bases on the building stock can be used avoiding time consuming inventory.

So far, only residential buildings were considered. In order to assess the seismic risk for the whole city of Basel, other building types such as office buildings, lifelines, industrial facilities and the old town centre have to be considered as well. Here, the results of other studies on industrial facilities [Si 98] and on lifelines [BH 92] can be taken into account.

The use of a qualitative description of the damage allows, in a further step, the evaluation of the financial loss and casualties. In order to estimate the financial loss, a damage factor range and a central damage factor CDF have to be assigned to each damage grade where the damage factor DF is defined as:

$$DF = \frac{\text{expected repair cost in CHF}}{\text{value in CHF}} \quad (8.1)$$

The repair cost already includes the fact that repairing or replacing an element in an existing building might be more expensive than the original one. Once the repair cost exceeds the value of the building, the damage factor equals 100%. This is the case for DG4 where the building is not completely destroyed but repair is neither feasible nor economically reasonable any more. The data on the actual value of the building and its content can be obtained from the building insurance company of the canton.

In order to estimate the casualties, a probability of casualties has to be assigned to each damage grade from the physical condition of the building. From the mean of the daytime and nighttime occupancy which is related to the social function of the building and its size (number of apartments, number of offices), the number of casualties can be roughly approximated.

Finally, a global validation of the evaluation method could be performed by its application to earthquake-struck areas and comparing observed damage patterns to predicted damage patterns.

Upgrading Strategies

The results of the evaluation of the buildings in a small target area in Basel suggest that the seismic risk for the city of Basel is considerable. The question on appropriate upgrading strategies therefore arises.

The majority of the buildings in the small target area are of unreinforced masonry with timber floors. For these building the first step in every upgrading strategy should be a check of the integrity of the building structure i.e. a positive floor-wall connection in order to prevent the walls separating from the floors leading to a global collapse of the building.

If the possibility of a global collapse is eliminated by an appropriate floor-wall anchorage the in-plane capacity can be considered. Possible upgrading strategies for unreinforced masonry walls are:

- Increase of normal force by external post-tensioning. This strategy is very effective in cases of low normal forces where sliding is critical.
- The application of a steel reinforcement net fixed onto the masonry and bonded by cement grout. This is a traditional upgrading strategy applied in earthquake prone areas in Europe.
- The application of fibre-composite materials; these can be a woven fabric such as polyester fabric which is very time effective and can be applied in less than an hour or laminates such as carbon fibre laminates. So far this type of upgrading strategy has been used primarily for reinforced concrete structures. Only recently the interest in the use of fibre-composite materials for upgrading of unreinforced masonry has arisen. Cyclic static tests on masonry wall elements upgraded by the bonding of fibre-composite materials at the Swiss Federal Laboratories for Materials Testing and Research have shown an increase of 30 to 50% in the shear capacity and of 290 to 380% in the deformation capacity of the wall elements [Sc 94]. At present, the behaviour of upgraded masonry wall elements using composite fibres is investigated under dynamic action at the Swiss Federal Institute of Technology [ELB 01].

The effect of upgrading of masonry walls can be assessed by an appropriate change in the capacity curves of the walls resulting in a change in the capacity curve of the building.

For buildings with very bad configuration in plan such as the majority of the buildings in the small target area dating from the 1960's with insufficient elements in one direction to resist the equivalent horizontal forces, major intervention have to be applied such as additional reinforced concrete walls to carry the horizontal forces.

Summary and conclusions

Appendix

A1 Classification of damage according to EMS 98

A1.1 Classification of damage to masonry buildings

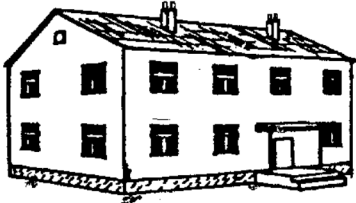




	<p>Grade 1: Negligible to slight damage (no structural damage, slight non-structural damage) Hair-line cracks in very few walls. Fall of small pieces of plaster only. Fall of loose stones from upper parts of buildings in very few cases.</p>
	<p>Grade 2: Moderate damage (slight structural damage, moderate non-structural damage) Cracks in many walls. Fall of fairly large pieces of plaster. Partial collapse of chimneys.</p>
	<p>Grade 3: Substantial to heavy damage (moderate structural damage, heavy non-structural damage) Large and extensive cracks in most walls. Roof tiles detach. Chimneys fracture at the roof line; failure of individual non-structural elements (partitions, gable walls).</p>
	<p>Grade 4: Very heavy damage (heavy structural damage, very heavy non-structural damage) Serious failure of walls; partial structural failure of roofs and floors.</p>
	<p>Grade 5: Destruction (very heavy structural damage) Total or near total collapse.</p>

Figure A1.1: Classification of damage to masonry buildings [EMS 98]

A1.2 Classification of damage to reinforced concrete buildings

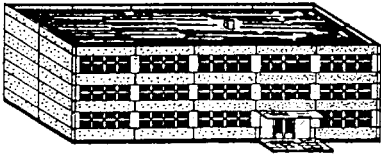
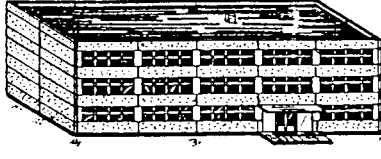
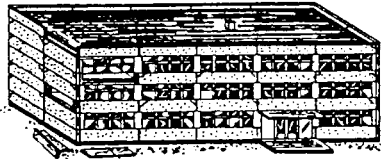


	<p>Grade 1: Negligible to slight damage (no structural damage, slight non-structural damage) Fine cracks in plaster over frame members or in walls at the base. Fine cracks in partitions and infills.</p>
	<p>Grade 2: Moderate damage (slight structural damage, moderate non-structural damage) Cracks in columns and beams of frames and in structural walls. Cracks in partition and infill walls; fall of brittle cladding and plaster. Falling mortar from the joints of wall panels.</p>
	<p>Grade 3: Substantial to heavy damage (moderate structural damage, heavy non-structural damage) Cracks in columns and beam column joints of frames at the base and at joints of coupled walls. Spalling of concrete cover, buckling of reinforced rods. Large cracks in partition and infill walls, failure of individual infill panels.</p>
	<p>Grade 4: Very heavy damage (heavy structural damage, very heavy non-structural damage) Large cracks in structural elements with compression failure of concrete and fracture of rebars; bond failure of beam reinforced bars; tilting of columns. Collapse of a few columns or of a single upper floor.</p>
	<p>Grade 5: Destruction (very heavy structural damage) Collapse of ground floor or parts (e. g. wings) of buildings.</p>

Figure A1.2: Classification of damage to reinforced concrete buildings [EMS 98]

A2 Example RC building - Detailed calculations

Analogous to the example masonry building of Section 6.4 the detailed calculations of the example reinforced concrete building of Section 5.7 are given below. The plan of the example building and the wall section of walls 1, 2 and 3 are given again in Figure A2.1.

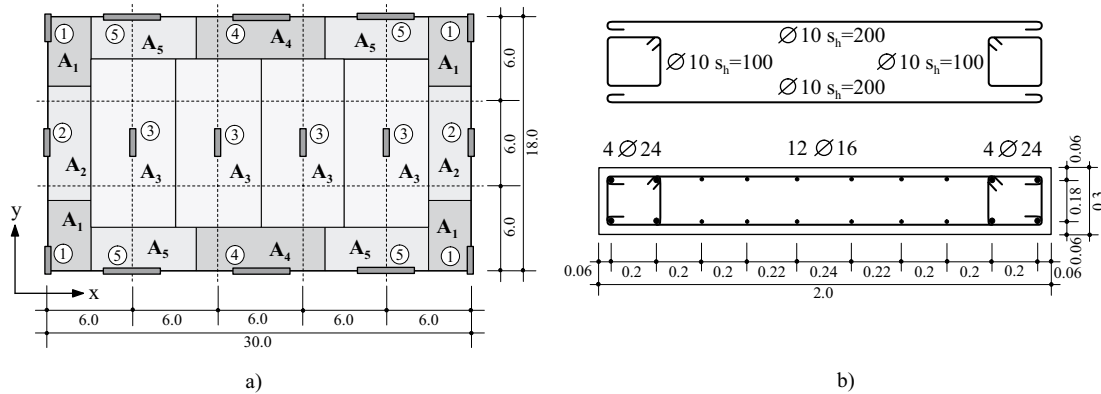


Figure A2.1: a) Plan of the example reinforced concrete building and b) wall section of walls 1, 2 and 3

The evaluation is done in 9 steps as outlined in Section 5.8.

Step 1) Input Data

Overall Geometry

Total floor area	$A_{\text{tot}} = l_x \cdot l_y = 30.0 \cdot 18.0 = 540.0 \text{ m}^2$
Number of storeys	$n = 6$
Total building height	$H_{\text{tot}} = 20.4 \text{ m}$
Storey height	$h_{\text{st}} = 3.4 \text{ m}$
Floor slab thickness	$d_f = 0.24 \text{ m}$
Depth of underbeams	$d_u = 0.4 \text{ m}$

Materials

The properties of the materials used are summarized in Table 5.2 following the example building in [Da 00]. In addition following properties are calculated:

Tensile strength of concrete	$f_{\text{ct}} = 0.75 \cdot \sqrt{f_c} = 0.75 \cdot \sqrt{45} = 5 \text{ MPa}$
Ultimate tensile strain of concrete	$\epsilon_{\text{ct}} = f_{\text{ct}}/E_c = 5/37500 = 0.00013$
Yield strain of steel	$\epsilon_y = f_y/E_s = 500/210000 = 0.00238$

Vertical loads

The surface load per storey excluding the self weight of the walls is assumed to be $q_{\text{fl}} = 12.5 \text{ kN/m}^2$.

Step 2) Identification of structural walls

The direction considered is the y-direction. In this direction 10 structural walls can be identified, 4 x wall 1, 2 x wall 2 and 4 x wall 3. All walls have the same length $l_w = 2.0$ m, the thickness $t = 0.3$ m and the height of the pier, i.e. the height of the adjacent opening, $h_p = h_{st} = 3.4$ m.

Step 3) Calculation of normal forces

In this step the normal forces acting on the walls have to be calculated. In the case of this example building, no gravity load columns exist and hence the vertical loads are carried entirely by the walls. The tributary areas A_1 to A_5 are shown in Figure A2.1 a).

For wall 1 this gives:

$$\text{Tributary area } A_1 \qquad A_1 = 3.0 \cdot 5 = 15.0 \text{ m}^2$$

$$\text{Floor load carried by wall 1} \qquad Q_1 = 15.0 \cdot 12.5 = 188 \text{ kN}$$

In this way the floor load carried by each wall can be calculated. The results are summarized in Table A2.1. The total floor load adds up to 6750 kN.

wall	1	2	3	4	5	sum
tributary area A [m ²]	15	24	72	27	23	540
floor load Q [kN]	188	300	900	338	281	6750

Table A2.1: Floor loads acting on each wall

For this example building it is assumed that the roof load is equal to the floor load. Including the self weight of the walls, dividing the mass of the walls at mid height between two floor levels, the following matrix can be established, presenting the normal forces acting on each wall at each floor level (Table A2.2).

level\wall	N ₁	N ₂	N ₃	N ₄	N ₅	N _{tot}
6	211	324	924	385	329	7271
5	235	347	947	432	376	7793
4	235	347	947	432	376	7793
3	235	347	947	432	376	7793
2	235	347	947	432	376	7793
1	235	347	947	432	376	7793
sum	1386	2061	5661	2546	2209	46235

Table A2.2: Normal forces acting on each wall at each floor level, dimensions in kN

The last column presents the sum of the normal forces at each floor level. And hence the concentrated storey masses are given by:

$$m_6 = \frac{7271}{10} = 727 \text{ t} \text{ and } m_1 = m_2 = m_3 = m_4 = m_5 = 779 \text{ t}$$

Step 4) Capacity curves of the walls

The calculation of the capacity curve of a wall follows the method described in Section 5.4.3. It is demonstrated using wall 1 as an example.

First, the moment curvature relationship of the wall section at the base of the wall has to be determined. This is done with reference to Figure 5.1. From Figure A2.1 b):

depth of extreme compressive reinforcement $d' = 0.06$ m

depth of extreme tensile reinforcement $d = 1.94$ m .

At the point of first yield of the tensile reinforcement equilibrium of the stress resultants gives:

Depth of the neutral axis $x_y = 0.51$ m ,

Moment at first yield $M_y = 3034$ kN .

From Equation (5.1) the first yield curvature is obtained:

$$\phi'_y = \frac{\varepsilon_y}{(d - x_y)} = \frac{0.00238}{(1.94 - 0.51)} = 0.0017 \text{ 1/m.}$$

It should be checked that the compressive strains are less than 0.0015:

$$\varepsilon_c = \frac{x_y}{d - x_y} \cdot \varepsilon_y = \frac{0.51}{1.94 - 0.51} \cdot 0.00238 = 0.00085 \text{ . O.K.}$$

Ultimate conditions are defined by the extreme compressive fibre reaching the ultimate compressive strain of concrete ε_{cu} . Taking into account the confining effect due to the transverse reinforcement using the model developed by Mander et al. [MPP 88]: $\varepsilon_{cu} = 0.0096$.

Equilibrium of the stress resultants at ultimate gives:

Depth of the neutral axis $x_u = 0.34$ m ,

Moment at ultimate $M_u = 4786$ kN .

From Equation (5.3) the ultimate curvature is obtained:

$$\phi_u = \frac{\varepsilon_{cu}}{x_u} = \frac{0.0096}{0.34} = 0.0285 \text{ 1/m.}$$

Checking the strain in the extreme tensile reinforcement:

$$\varepsilon_s = \frac{d - x_u}{x_u} \cdot \varepsilon_{cu} = \frac{1.94 - 0.34}{0.34} \cdot 0.0096 = 0.0457 \text{ O.K.}$$

From Equation (5.5) the yield curvature of the bilinear approximation is:

$$\phi_y = \phi'_y \cdot \frac{M_u}{M_y} = 0.0017 \cdot \frac{4786}{3034} = 0.0026 \text{ .}$$

Hence, the rotational ductility can be determined from Equation (5.6):

Appendix

$$\mu_{\phi} = \frac{\phi_u}{\phi_y} = \frac{0.0285}{0.0026} = 10.87.$$

The effective section stiffness of the cracked section can be determined using Equation (5.36):

$$EI_{\text{eff}} = \frac{M_y}{\phi'_y} = \frac{3034}{0.0017} = 1824 \cdot 10^3 \text{ kNm}^2.$$

This corresponds to a stiffness reduction to 24% of the uncracked stiffness:

$$\frac{EI_{\text{eff}}}{EI_p} = \frac{1824 \cdot 10^3}{37500 \cdot 10^3 \cdot \frac{0.3 \cdot 2^3}{12}} = 0.24 = 24\%.$$

Next, the height of zero moment h_0 which depends on the ratio of the flexural stiffness of the spandrel to the flexural stiffness of the pier (see Section 3.5.3) has to be determined. In the case of the example building the spandrels consist of the floor with underbeams. For the estimation of the stiffness of the floors with underbeams, the effective width of the floor slab is estimated following the rules suggested by Bachmann and Dazio [BD 97]:

$$\text{slab on both side:} \quad b_{\text{eff}} = t + 2 \cdot d_f, \quad (\text{A.1})$$

$$\text{slab on one side:} \quad b_{\text{eff}} = t + d_f. \quad (\text{A.2})$$

In the case of wall 1 this gives:

$$b_{\text{eff}} = t + d_f = 0.3 + 0.24 = 0.54 \text{ m}.$$

Hence, the second moment of area of the floor section with underbeams can be calculated to 0.0262 m^4 .

Finally the ratio of the stiffnesses, taking into account a cracked stiffness of the floor section with underbeam of 20% of its uncracked stiffness and a cracked stiffness of the wall section of 24% of its uncracked stiffness:

$$\frac{EI_{\text{sp}}}{EI_p} \cdot \frac{h_{\text{st}}}{l_o} = \frac{0.2 \cdot 30 \cdot 0.0262}{0.24 \cdot 37.5 \cdot \frac{0.3 \cdot 2^3}{12}} \cdot \frac{3.4}{8} = 0.04.$$

Using the relation shown in Figure 3.6 the ratio of $h_0/h_p \approx 1.8$ and hence

$$h_0 = 1.8 \cdot h_p = 1.8 \cdot 3.4 = 6.1 \text{ m}.$$

Knowing the height of zero moment h_0 and the ultimate moment capacity of the wall section M_u the shear capacity of the wall can be determined using Equation (5.34):

$$V_m = \frac{M_u}{h_0} = \frac{4786}{6.1} = 782 \text{ kN}.$$

At this point it should be verified that the shear strength of the wall is not critical. The contribution of the concrete to the shear strength is estimated using Equation (5.48), the factor k is taken to be 0.1 as the ultimate curvature ductility $\mu_\phi = 10.87 > 4$:

$$V_c = t \cdot z \cdot k \cdot \sqrt{f'_c} = 0.3 \cdot 0.8 \cdot 2.0 \cdot 0.1 \cdot \sqrt{45} \cdot 10^3 = 322 \text{ kN}.$$

The contribution of the transverse reinforcement based on a 30° truss mechanism is calculated using Equation (5.49):

$$V_s = A_{sh} \cdot f_{yh} \cdot \frac{z'}{s_h} \cdot \cot 30^\circ = \frac{\pi \cdot 0.01^2}{4} \cdot 500 \cdot 10^3 \cdot \frac{1.91}{0.2} \cdot \cot 30^\circ = 651 \text{ kN}.$$

Finally, the enhancement of the shear strength due to the axial load (Equation (5.50)):

$$V_N = N \cdot \tan \alpha = 1386 \cdot \frac{2.0 - 1386 / (0.3 \cdot 45 \cdot 10^3)}{2 \cdot 6.1} = 216 \text{ kN}.$$

Hence, the total shear strength of wall 1 (Equation (5.47)):

$$V_{\text{shear}} = V_c + V_s + V_N = 322 + 651 + 216 = 1189 \text{ kN}.$$

This should be less than the upper limit of the shear strength determined by concrete crushing (Equation (5.46)):

$$V_{\text{shear}} < 0.9 \cdot t \cdot z \cdot \sqrt{f'_c} = 0.9 \cdot 0.3 \cdot 0.8 \cdot 2.0 \cdot \sqrt{45} \cdot 10^3 = 2898 \text{ kN O.K.}$$

$V_{\text{shear}} > V_m$, consequently the shear strength is not critical for wall 1.

Using Equation (5.35) the yield displacement at the top of the wall Δ_y can be calculated:

$$\Delta_y = V_m \cdot H_{\text{tot}} \cdot \left(\frac{h_p \cdot (3h_0 - h_p)}{6 \cdot EI_{\text{eff}}} \right) = 782 \cdot 20.4 \cdot \left(\frac{3.4 \cdot (3 \cdot 6.1 - 3.4)}{6 \cdot 1824 \cdot 10^3} \right) = 0.074 \text{ m} = 74 \text{ mm}.$$

Assuming a pier sidesway mechanism the ultimate displacement of the wall can be calculated using Equation (5.39):

$$\Delta_u = \Delta_y + \left(h_{st} - \frac{l_p}{2} \right) \cdot (\phi_u - \phi_y) \cdot l_p = 0.074 + \left(3.4 - \frac{1.12}{2} \right) \cdot (0.0285 - 0.0026) \cdot 1.12 = 0.157 = 157 \text{ mm}$$

The length of the plastic hinge l_p was calculated using Equation (5.42):

$$l_p = \frac{h_0}{2} \cdot \left(1 - \frac{M_y}{M_u} \right) = \frac{6.1}{2} \cdot \left(1 - \frac{3034}{4786} \right) = 1.12 \text{ m}.$$

Assuming a spandrel sidesway mechanism the ultimate displacement of the wall can be calculated using Equation (5.37):

$$\Delta_u = \Delta_y + \left(n \cdot h_{st} - \frac{l_p}{2} \right) \cdot (\phi_u - \phi_y) \cdot l_p = 0.074 + \left(20.4 - \frac{1.12}{2} \right) \cdot (0.0285 - 0.0026) \cdot 1.12 = 650 \text{ mm}.$$

The difference in the ultimate displacement for a pier sidesway mechanism and a spandrel sidesway mechanism is enormous, demonstrating the importance of the right choice of the mechanism.

Appendix

Thus, the capacity of wall 1 is determined. The force and displacement reduction factors RF_F and RF_D to take into account of the cyclic nature of the loading are both set equal to unity in this example.

In the same way the bilinear capacity curves of all the other walls are determined. Table A2.3 summarizes the results.

wall	1	2	3
h_0/h_p	1.8	1.7	1.7
M_y [kNm]	3034	3521	5955
ϕ_y [1/m]	0.0026	0.0026	0.0025
M_u [kNm]	4786	5279	7318
ϕ_u [1/m]	0.0285	0.0306	0.0179
μ_ϕ	10.87	11.83	7.29
l_p	1.12	1.029	0.54
EI_{eff} [MNm^2]	1824	2043	2980
V_m [kN]	782	863	1266
Δ_y [mm]	74	73	68
$\Delta_{u, PSM}$ [mm]	157	155	94
$\mu_{\Delta, PSM}$	2.11	2.13	1.38
$\Delta_{u, SSM}$ [mm]	650	640	236
$\mu_{\Delta, SSM}$	8.77	8.77	3.44
k_{eff} [kN/m]	10545	11015	18494

Table A2.3: Capacity of the walls

The bottom row of Table A2.3 presents the effective stiffnesses of the linear elastic part of the bilinear capacity curves of the walls (cf. Figure 3.9).

Step 5) Capacity curve of the building

The capacity curve of the building can be easily obtained by superposition of the capacity curves of the walls, following Equation (3.3). The result is shown in Figure A2.2.

Step 6) Identification of damage grades

The damage grades according to the EMS 98 [EMS 98] are identified on the capacity curve of the building as explained in Section 5.5.

Damage Grade 1

For each wall the shear force at the onset of cracking is determined. At the onset of cracking equilibrium of the stress resultants gives for wall 1:

$$\text{Depth of the neutral axis } x_{cr} = 1.20 \text{ m}$$

$$\text{Moment at first yield } M_{cr} = 905 \text{ kN}.$$

From Equation (5.53) the curvature on the bilinear approximation of the moment curvature relationship at the onset of cracking is obtained:

$$\phi_{cr} = \frac{M_{cr}}{M_u} \cdot \phi_y = \frac{905}{4786} \cdot 0.0026 = 0.00049.$$

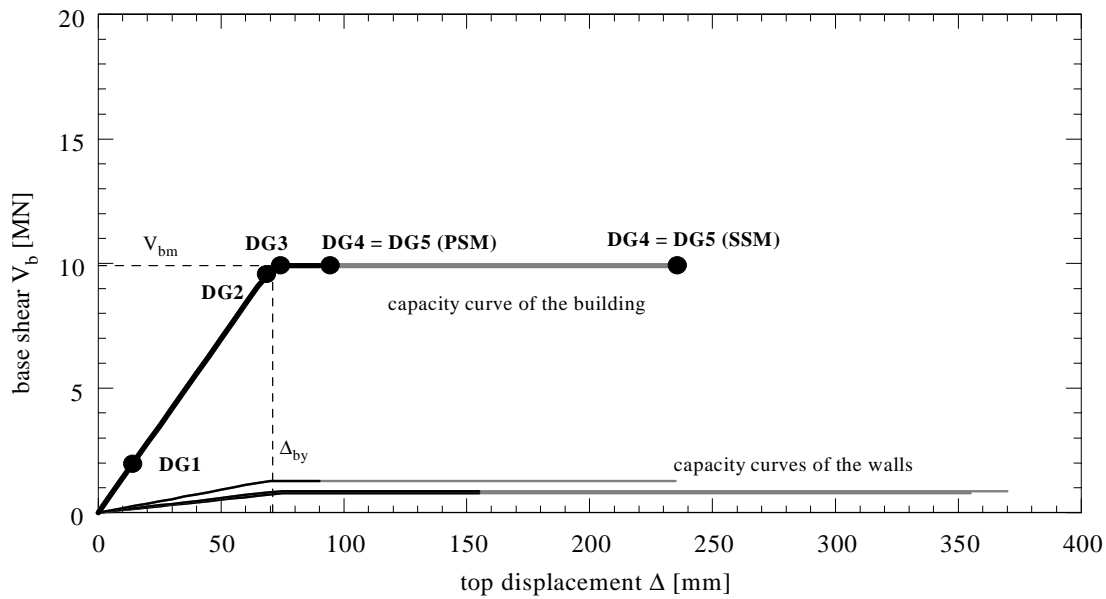


Figure A2.2: Capacity curve of the example reinforced concrete building

The shear force at the onset of cracking is determined using Equation (5.34):

$$V_{cr} = \frac{M_{cr}}{h_0} = \frac{905}{6.1} = 148 \text{ kN}.$$

The corresponding displacement at the top of wall 1 is determined, using Equation (5.35):

$$\Delta_{cr} = V_{cr} \cdot H_{tot} \cdot \left(\frac{h_p \cdot (3h_0 - h_p)}{6 \cdot EI_{eff}} \right) = 148 \cdot 20.4 \cdot \left(\frac{3.4 \cdot (3 \cdot 6.1 - 3.4)}{6 \cdot 1824 \cdot 10^3} \right) = 0.014 \text{ m} = 14 \text{ mm}$$

Table A2.4 summarizes the results for all the walls.

wall	1	2	3
V_{cr} [kN]	148	199	465
Δ_{cr} [mm]	14	17	25

Table A2.4: Cracking of the walls

The wall that cracks first, i.e. at the smallest displacement, determines damage grade 1. In this case it is wall 1 that cracks first at a displacement of 14 mm. The corresponding base shear of the building is given by (Figure A2.2):

$$V_{bcr} = V_b(\Delta_{cr} = 14 \text{ mm}) = 1960 \text{ kN}.$$

And hence the couple $(\Delta_{cr}, V_{bcr}) = (14 \text{ mm}, 1960 \text{ kN})$ determines the point on the capacity curve of the building at which the building enters damage grade 1 (cf. Figure A2.2).

Appendix

Damage Grade 2

This damage grade is identified by the wall that yields first, i.e. the minimum Δ_y from Table A2.3. For the example building it is again wall 3 that yields first at the smallest displacement:

$$\Delta_{y3} = 68 \text{ mm}.$$

The corresponding base shear of the building is given by (Figure A2.2):

$$V_b(\Delta = 68 \text{ mm}) = 9570 \text{ kN}.$$

And hence the couple (68 mm , 9570 kN) determines the point on the capacity curve of the building at which the building enters damage grade 2 (cf. Figure A2.2).

Damage Grade 3

This damage grade is identified as the point, at which the stiffness of the capacity curve tends to zero. That is the case when the last wall yields. In the case of the example building the last wall to yield is wall 1 at a displacement $\Delta_{y1} = 74 \text{ mm}$. The corresponding base shear of the building is given by (Figure A2.2):

$$V_b(\Delta = 74 \text{ mm}) = 9918 \text{ kN}.$$

And hence the couple (74 mm, 9918 kN) determines the point on the capacity curve of the building at which the building enters damage grade 3 (cf. Figure A2.2).

Damage Grade 4

This damage grade is identified by the first wall that reaches its ultimate displacement leading to a decrease in the base shear of the building, i.e. the minimum Δ_u from Table A2.3. In the case of the example building the first wall that reaches its ultimate displacement is wall 3 at a displacement of $\Delta_{u3} = 94 \text{ mm}$ for a pier sidesway mechanism and $\Delta_{u3} = 236 \text{ mm}$ for a spandrel sidesway mechanism. And hence the point on the capacity curve of the building at which the building enters damage grade 4 is either determined by the couple (94 mm, 9593 kN) assuming a pier sidesway mechanism or by the couple (236 mm, 9593 kN) assuming a spandrel sidesway mechanism (cf. Figure A2.2).

Damage Grade 5

Beyond the ultimate displacement of wall 3 the base shear of the building reduces to less than 2/3 of its maximum value. Hence the ultimate condition of the first wall signifies the collapse of the building, i.e. DG5 = DG4 (cf. Figure A2.2).

Step 7) Bilinear approximation of the capacity curve of the building

The simplest bilinear approximation of the capacity curve of the building is determined by a shear capacity equal to the shear capacity of the “real” capacity curve of the building, $V_{bm} = 9918 \text{ kN}$, and a stiffness of the linear elastic part equal to the sum of the effective stiffnesses of the walls:

$$k = \sum_j k_{\text{eff}j} = 139785 \text{ kN/m}.$$

The yield displacement of the building is given by:

$$\Delta_{\text{by}} = \frac{V_{\text{bm}}}{k} = \frac{9918}{139785} \cdot 10^3 = 71 \text{ mm}.$$

Step 8) Equivalent SDOF system

The building can be considered as a MDOF system with six concentrated masses m_1 to m_6 as calculated in step 2. Table A2.5 shows the important parameters of the MDOF system, the height of the floor levels h_i , the concentrated masses at each floor level m_i and the normalized first mode displacement at the floor levels ϕ_i . The last three columns give quantities needed for the modal analysis (cf. Section 3.6).

floor level i	h_i [m]	m_i [t]	ϕ_i	$m_i\phi_i$	$m_i\phi_i^2$	$h_i m_i \phi_i$
6	20.4	727	1.00	727	727	14834
5	17.0	779	0.77	602	466	10241
4	13.6	779	0.55	429	236	5836
3	10.2	779	0.34	268	92	2732
2	6.8	779	0.17	131	22	894
1	3.4	779	0.05	36	2	123
sum	-	-	-	2194	1545	34661

Table A2.5: MDOF parameters

The equivalent stiffness k_E of the SDOF system is set equal to the stiffness of the real building (Equation (3.9)):

$$k_E = k = 139785 \text{ kN/m}.$$

Hence, the equivalent mass is given by Equation (3.10):

$$m_E = \sum_i m_i \phi_i = 2194 \text{ t}.$$

The frequency of the SDOF system can then be calculated:

$$f_1 = \frac{1}{2\pi} \cdot \sqrt{\frac{k_E}{m_E}} = \frac{1}{2\pi} \cdot \sqrt{\frac{139785}{2194}} = 1.27 \text{ Hz}.$$

This is also the fundamental frequency of the building in the y-direction. The equivalent height of the SDOF system is calculated using Equation (3.11):

$$h_E = \frac{\sum h_i m_i \phi_i}{\sum m_i \phi_i} = \frac{34661}{2194} = 15.8 \text{ m}$$

and the modal participation factor using Equation (3.13):

$$\Gamma = \frac{\sum m_i \phi_i}{\sum m_i \phi_i^2} = \frac{2194}{1545} = 1.42 .$$

Step 9) Vulnerability

For any given elastic response spectrum the required displacement at the top of the building and hence the corresponding damage grade shall be determined. This is demonstrated by means of the elastic acceleration response spectrum for 5% damping for medium stiff soils proposed in the Swiss standard [SIA160 89] for zone 3a (Figure A2.3).

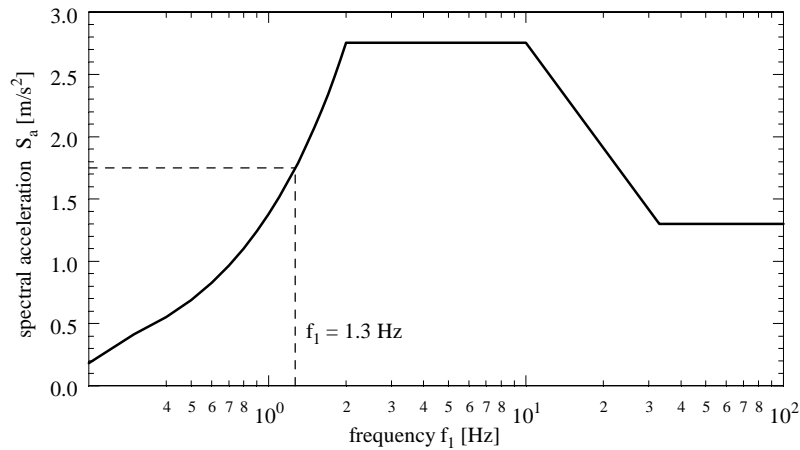


Figure A2.3: Elastic acceleration response spectrum (5% damping) for medium stiff soils proposed in the Swiss standard [SIA160 89] for zone 3a

From the spectrum the spectral acceleration at the fundamental frequency of the building $f_1 = 1.3$ Hz is (Figure A2.3):

$$S_a(f_1) = 1.75 \text{ m/s}^2 .$$

As the method is based on displacements, the spectral acceleration has to be transformed into a spectral displacement using Equation (3.7):

$$S_d(f_1) = \frac{S_a(f_1)}{\omega^2} = \frac{S_a(f_1)}{(2\pi \cdot f_1)^2} = \frac{1.75}{(2\pi \cdot 1.3)^2} = 0.027 \text{ m} = 27 \text{ mm} .$$

The required elastic displacement at the top of the building:

$$\Delta_{be} = \Gamma \cdot S_d(f_1) = 1.42 \cdot 27 = 39 \text{ mm} .$$

And hence the required elastic base shear of the building:

$$V_{be} = k \cdot \Delta_{be} = 139785 \cdot 39 / 10^3 = 5455 \text{ kN} .$$

As $V_{be} < V_{bm} = 9918$ kN, the shear capacity of the building, the building is still in the elastic part of the capacity curve and hence the required displacement at the top of the building is:

$$\Delta_b = \Delta_{be} = 39 \text{ mm} .$$

For this top displacement, the building will have experienced damage grade 1 (cf. Figure A2.2).

If the spectral displacement is now increased to $S_d = 55 \text{ mm}$ (this corresponds to twice the peak ground acceleration of zone 3a) the required elastic displacement at the top of the building is:

$$\Delta_{be} = \Gamma \cdot S_d(f_1) = 1.42 \cdot 55 = 78 \text{ mm} .$$

Hence, the required elastic base shear of the building:

$$V_{be} = k \cdot \Delta_{be} = 139785 \cdot 78 / 10^3 = 10911 \text{ kN} .$$

Comparing this to the shear capacity of the building $V_{bm} = 9918 \text{ kN}$ it can be seen that the behaviour of the building is beyond the yield point and hence the strength reduction factor R is greater than 1 (Equation (3.17)):

$$R = \frac{V_{be}}{V_{bm}} = \frac{10911}{9918} = 1.10 .$$

Thus the required ductility can be calculated using Equation (3.19) for $f_1 < 1.4 \text{ Hz}$:

$$\mu_D = R = 1.10 = 1.10 .$$

The displacement demand is then:

$$\Delta_D = \mu_D \cdot \Delta_{by} = 1.10 \cdot 78 = 86 \text{ mm} .$$

For this top displacement the building will have experienced damage grade 3 (cf. Figure A2.2).

In this way the required top displacement of the building and hence the corresponding damage grade can be determined for any spectral displacement. The presentation of the damage grades as a function of the spectral displacement leads to the vulnerability function of the building as shown in Figure A2.4.

Appendix

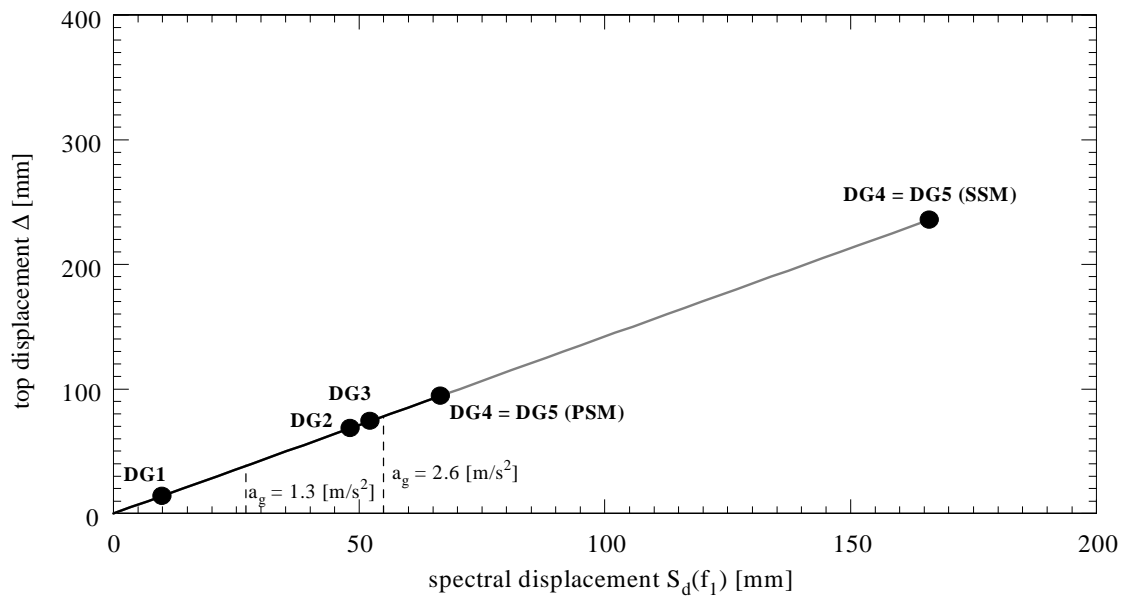


Figure A2.4: Vulnerability function of the example reinforced concrete building

A3 Example building with a mixed structure

In this section an example of a building with a mixed structure of vertical reinforced concrete elements combined with unreinforced masonry elements having reinforced concrete floors which is typical for the buildings of building class 3 is given (cf. Section 7.2). The detailed calculations are similar to those of the example masonry building in Section 6.4 and of the example reinforced concrete building in Section A2 and are therefore omitted here. It is a 6-storey building with a strong base floor of reinforced concrete constituting the entrance level and 5 upper storeys. Figure A3.1 shows a plan view of an upper storey. The walls shaded in dark grey are existing walls i.e. they belong to already existing buildings at the time of construction of the example building considered. The example building was constructed between the existing walls which were provided with some support slots for the new reinforced concrete floors. The direction considered is the x-direction (cf. Section 6.2). In this direction only 4 masonry walls (wall type 1, 2 x wall type 2 and wall type 3) and 4 reinforced concrete columns (2 x column type 4 and 2 x column type 5) act to resist the seismic action. The contribution of the fire-protection walls (existing and new extensions) in this direction is very small and therefore neglected in the following.

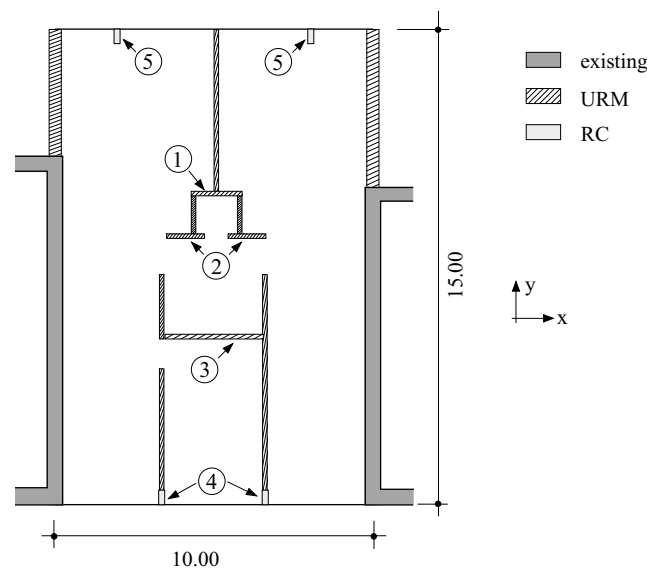


Figure A3.1: Plan view of the 6-storey example building with a mixed structure of vertical reinforced concrete elements combined with unreinforced masonry elements having reinforced concrete floors

As the base floor is rather strong, the first floor determines the capacity of the building. The capacity curve in x-direction is shown in Figure A3.2. The capacity of the building is determined by the capacity of the masonry walls which are very stiff in comparison with the reinforced concrete columns. At the point of failure of the masonry walls the reinforced concrete columns have not even reached their shear capacity.

The vulnerability function in x-direction of the building is shown in Figure A3.3. The fundamental frequency of the building in this direction being 1.4 Hz, assuming the shape of the design spectrum proposed by the Swiss Standard for medium stiff soil [SIA160 89], damage grade 5 is reached for a maximum ground acceleration

Appendix

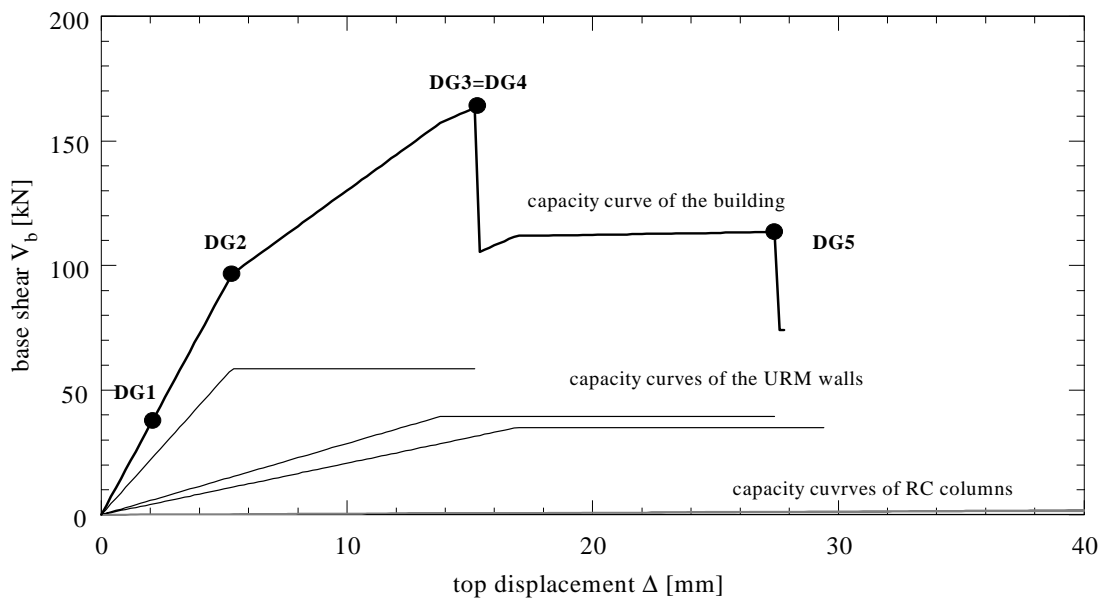


Figure A3.2: Capacity curve in x-direction of the example building with a mixed structure of vertical reinforced concrete elements combined with unreinforced masonry elements having reinforced concrete floors

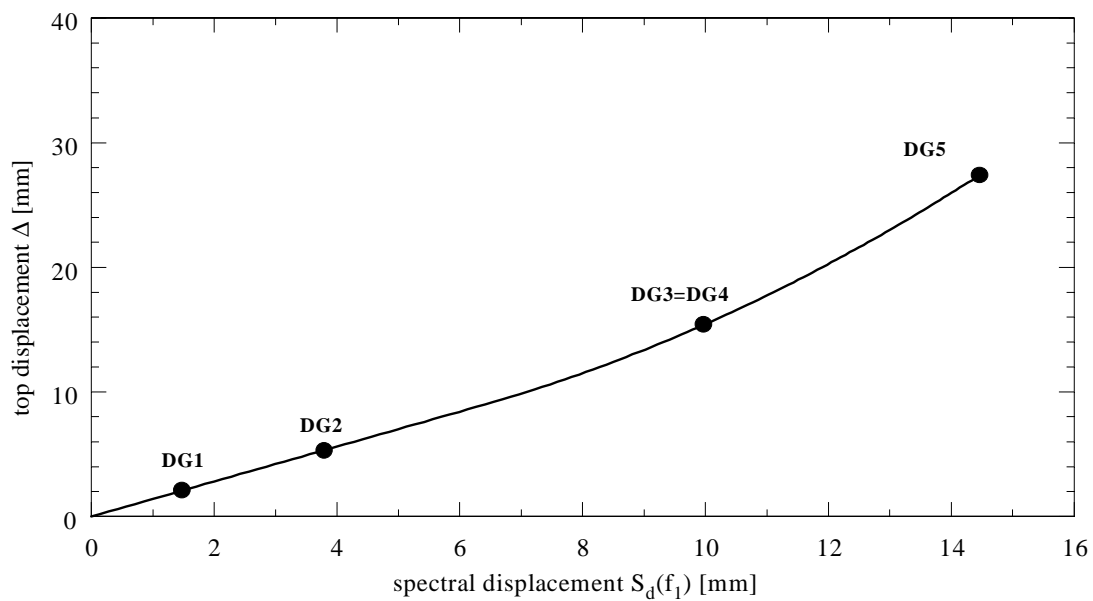
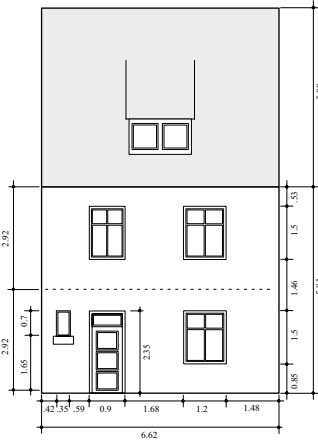
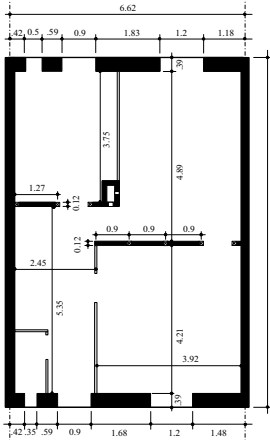


Figure A3.3: Vulnerability function in x-direction of the example building with a mixed structure of vertical reinforced concrete elements combined with unreinforced masonry elements having reinforced concrete floors

$a_g = 0.7 \text{ m/s}^2$. This is just over half the maximum ground acceleration proposed for Zone 3a. This high vulnerability of the building in x-direction, however, is not surprising considering the layout in plan of the building.

A4 Example database record

ID Number: 116	Owner: xxx	
Address: xxx	Tel.: xxx	
Longitude:	Latitude:	
Construction year: 1922	Standard: -	
Structural type: unreinforced brick masonry		
Non-structural elements: unreinforced brick masonry		
Number of storeys (+ basements): 2 (+1)		
Building height: 5.84 m (height of gutter)	Storey height: 2.92 m	
Elevation¹	Plan¹	
		
Length: 6.62 m	Width: 10.00 m	Area: 66.20 m ²
Floors: timber floors with beams running parallel to the fire protection walls		
Foundation: basement in unreinforced masonry with isolated footings		
Roof¹: gable roof with tiles at 45° and timber roof structure	Material properties	
	-	
Irregularities: -	Details¹	
Preservation: good, no cracks visible	-	
History: -		
Social function: residential, one family home	Content: furniture, kitchen and bath facilities	
Value of building:	Value of content:	
Daytime occupancy:	Nighttime occupancy:	
Adjacent buildings: fire protection wall shared between two adjacent buildings, no joint		
Other: -		

¹ more detailed information or sketches or photos can be included in the inventory

The information concerning the exact coordinates of the building for the incorporation into the GIS and its value and occupancy for the estimation of loss and casualties is not obtained yet and the corresponding fields were left blank.

Appendix

Symbols

Roman upper case

A	area amplification factor
A_{gt}	percentage total elongation at maximum force
A_{sh}	area of transverse reinforcement
A_{tot}	total floor area
C_i	coefficients to take into account issues like stiffness degradation, force reduction due to anticipated inelastic behaviour etc.
D	damage displacement of the single SDOF system
E	modulus of elasticity
E_c	modulus of elasticity of concrete
E_D	energy dissipated by damping
E_m	modulus of elasticity of masonry
E_s	modulus of elasticity of steel
E_{s0}	maximum strain energy
EI	section stiffness
EI_{eff}	effective section stiffness
EI_p	section stiffness of the pier
EI_{sp}	section stiffness of the spandrel
F	force in general
F_E	force acting on the equivalent SDOF system
F_i	horizontal storey force
G	shear modulus
G_c	shear modulus of concrete
G_m	shear modulus of masonry
GA_{eff}	effective shear stiffness
H_{tot}	total building height
I	second moment of area macroseismic intensity
I_{EMS}, I_{MSK}, I_{MM}	intensity according to the EMS, the MSK scale, the MM scale
I_o	epicentral intensity
K_1, K_2	coefficient to calculate the yield curvature of a wall
M	bending moment centre of mass
M_1, M_2	bending moment at top, bottom of wall element
$M(x)$	bending moment at x due to the real forces
M_{cr}	bending moment at cracking
M_L	local magnitude
M_q	out-of-plane moment
M_{qcr}	out-of-plane moment at cracking
M_{qu}	out-of-plane moment at failure
M_u	bending moment at yield
M_s	surface wave magnitude
M_y	bending moment at ultimate

Symbols

N	normal force
N_n, N_v	normal force transmitted through vertical stress strut, inclined stress strut
P	cumulative probability
Q	quantity in the MDOF system Floor load
Q_E	quantity in the SDOF system
R	centre of rigidity strength reduction factor
RF_F, RF_D	force, deformation reduction factor
S_a	spectral acceleration
S_d	spectral displacement
T	duration period
T_0	transition period as a function of ductility
T_1	fundamental period
T_c	characteristic period of ground motion
V	shear force
V_b	base shear of the building
V_{be}	equivalent elastic base shear of the building
V_{bm}	shear capacity of the building
V_{bcr}	base shear at cracking
V_c	shear carried by the concrete
V_{cr}	shear force at the onset of cracking of a wall
V_m	shear capacity of the wall
V'_m	increased shear force at the base of the wall due to the influence of higher modes
V_N	shear strength enhancement resulting from axial compression
V_s	shear carried by transverse reinforcement
V_{shear}	shear strength of concrete wall
$V(x)$	shear force at x due to the real forces

Roman lower case

a	acceleration extension of compression zone distance between node of assemblage and point of contraflexure (Figure 5.6)
a', a''	defined in Figure 5.6
a_g	maximum ground acceleration (peak or effective)
a_i	floor acceleration
a_{cr}	acceleration that causes out-of-plane cracking
a_e	equivalent elastic acceleration
a_u	acceleration that causes out-of-plane failure
a_{top}	top floor acceleration
b_{eff}	effective width
c	cohesion in the mortar beds
c_n	constant to take into account nonlinearity
d	horizontal deformation of the pier depth of extreme tensile reinforcement
d'	depth of extreme compressive reinforcement
d_{cr}	deformation of the pier at the onset of cracking
d_f	floor thickness
dm	additional out-of-plane moment
d_u	ultimate deformation of the pier depth of underbeam

d_y	yield deformation of the pier
e_{1n}, e_{2n}	eccentricity of the resultant of the vertical stress strut at top and bottom of wall element
e_{1v}, e_{2v}	eccentricity of the resultant of the inclined stress strut at top and bottom of wall element
f	frequency
f_1	fundamental frequency
f_b	compressive strength of brick units
f_c	cube compressive strength of concrete
f'_c	cylinder compressive strength of concrete
f_{ct}	tensile strength of concrete
$f_{inclined}$	stress in the inclined stress strut
f_m	cube compressive strength of mortar
f_{mx}, f_{my}	compression strength of masonry orthogonal to the mortar bed, parallel to the mortar bed
f_u	ultimate strength of reinforcement
$f_{vertical}$	stress in the vertical stress strut
f_y	yield strength of reinforcement
f_{yh}	yield strength of transverse reinforcement
g	acceleration due to gravity
g_w	self weight of the walls
g_{fl}	self weight of the floors
h	height of a wall element
h_0	height of zero moment
h_E	equivalent height
h_{eff}	effective height
h_i	height of the i -th story from the base
h_{im}	height of the mid height of the i -th story from the base
h_p	height of the pier
h_R	height of resultant force
h_{st}	story height
k	stiffness of the building factor to calculate shear carried by concrete taking into account ductility
k_0	uncracked stiffness
k_E	equivalent stiffness
k_{eff}	effective stiffness of the wall
k_{equ}	secant stiffness
k_s	shear stiffness of an assemblage
$k_{s,tot}$	shear stiffness of one storey
l	length
l_0	length of spandrel
l_2	length of stress strut
l_{2n}, l_{2v}	length of vertical, inclined stress strut
l_{eff}	effective length
l_p	length of plastic hinge
l'_p	height of region over which reinforcement has yielded
l_w	wall length
l_x	length of the building in x -direction
l_y	length of the building in y -direction
m	mass per unit height
m	dimensionless bending moment
m	mass

Symbols

m_E	equivalent mass
m_i	concentrated storey mass
$m(x)$	bending moment at x due to a virtual unit force
m_x	median value of a sample x
n	dimensionless normal force number of storeys
q	vertically distributed force
q_{cr}	vertically distributed force that causes out-of-plane cracking
q_d	surcharge floor
q_{fl}	total floor load
q_u	vertically distributed force that causes out-of-plane failure
q_N	live load
q_{roof}	roof load
q_w	surcharge wall
s_h	spacing of transverse reinforcement
s_i	horizontally distributed storey load
s_x	standard deviation of a sample x
t	thickness of wall, wall element, pier
u_{cr}, u_u	out-of-plane displacement at cracking, at ultimate
u_e	equivalent elastic out-of-plane displacement
$v(x)$	shear force at x due to a virtual unit force
v_x	coefficient of variation of a sample
x	coordinate direction orthogonal to the mortar bed of masonry
x_{cr}	depth of neutral axes at cracking
x_u	depth of neutral axes at ultimate
x_y	depth of neutral axes at yield
y	coordinate direction parallel to the mortar bed of masonry
z	effective depth of wall section
z'	distance between centres of peripheral transverse reinforcement

Greek upper case

Γ	modal participation factor
Δ	horizontal top displacement
Δ_{be}	equivalent elastic top displacement of the building
Δ_{bu}	ultimate top displacement of the building
Δ_{by}	yield top displacement of the building
Δ_{cr}	top displacement at the onset of cracking
Δ_D	displacement demand
Δ_e	equivalent elastic displacement
Δ_u	ultimate top displacement of the wall
Δ_y	yield top displacement of the wall
Φ	standard normal cumulative distribution function

Greek lower case

α	angle of inclination, defined in Figure 4.3 coefficient, defined in Figure 3.9
α_1, α_2	assemblage factors (Figure 5.6)
β	coefficient to calculate the displacement ductility of a wall
β_{equ}	equivalent viscous damping

β_v	viscous damping
γ_m	specific weight of masonry
δ	drift
δ_{cr}	drift at the onset of cracking
δ_y	yield drift
δ_u	ultimate drift
ϵ_c	concrete compressive strain at the extreme compressive fibre
ϵ_{ct}	concrete tensile strain at the extreme tensile fibre at the onset of cracking
ϵ_{cu}	ultimate compressive strain of concrete
ϵ_s	strain in the extreme tensile reinforcement
ϵ_y	yield strain of reinforcement
ϕ	angle of internal friction curvature
ϕ_{cr}	equivalent curvature at cracking on the bilinear moment-curvature relationship
ϕ'_{cr}	curvature at cracking
ϕ_i	first mode displacement at the i-th story
ϕ_n	first mode displacement at the n-th story
ϕ_p	plastic curvature
ϕ_u	ultimate curvature
ϕ'_y	first yield curvature
ϕ_y	yield curvature
η	correction factor for elastic response spectra with damping > 5%
κ	form factor
μ	ductility
μ_D	ductility demand
μ_ϕ	rotational ductility of a wall section
μ_Δ	displacement ductility of the building
μ_W	displacement ductility of the wall
μ_{WE}	displacement ductility of the wall element
μ_x	mean of a distribution x
θ_p	plastic rotation
ρ_c	density of concrete
σ_1, σ_2	principal stresses
σ_n	normal stress
σ_x, σ_y	stresses in x- and y-direction
σ_x	standard deviation of a distribution x
τ_{xy}	shear stress
ζ	coefficient defined in Equation (5.29)
χ	coefficient to calculate yield displacement of a cantilever wall
ω	circular frequency
ω_d, ω_m	dimensionless parameters to take into account the effect of frame action
ω_n	dynamic magnification factor

Special notations

\emptyset	diameter of reinforcement
O_{cm}, O_{lm}	using cement mortar, using lime mortar
O_{DGi}	at damage grade i
O_j, O_i	enumerating of
O_{max}, O_{min}	maximum value of, minimum value of
$O_{monoton}, O_{cyclic}$	under monotonic loading, under cyclic loading
O_{net}	net value of

Symbols

O_o, O_u	upper, lower
O_{OG}	at upper storey
O_{OPcr}, O_{OPu}	at out-of-plane cracking, at out-of-plane failure
O_{sys}	whole structural system of walls and frame action considered
O_{tot}	sum of
O_w	cantilever walls considered only

Abbreviations

ADRS	acceleration-displacement response spectrum
ASCE	American Society of Civil Engineers
ATC	Applied Technology Council
BH	high grade brick / concrete
BN	normal brick / concrete
BS	special brick / concrete
BSH	basic structural hazard score
CDF	central damage factor
DF	damage factor
DG	damage grade
DPM	damage probability matrix
EMPA	Institute for the Testing of Buildings Material
EMS	European Macroseismic Scale
ETH	Swiss Federal Institute of Technology
FEMA	Federal Emergency Management Agency
GIS	geographical information system
GNDT	Gruppo Nazionale per la Difesa dai Terrimoti
IBK	Institute of Structural Engineering
IP	in-plane
K	cold worked reinforcing steel
KR	cold worked reinforcing coiled rods
LS	limit state
MB	brick masonry
MBL	light brick masonry
MDOF	multi degree of freedom
MDF	mean damage factor
MSK	Medvedev-Sponheuer-Karnik
MM	modified Mercalli
NEHRP	National Earthquake Hazard Reduction Program
NH	naturally hard reinforcing steel
NIBS	National Institute of Building Science
OP	out-of-plane
PSM	pier sway mechanism
RC	reinforced concrete
SDOF	single degree of freedom
SED	Swiss Seismological Service
SIA	Swiss Society of Engineers and Architects
SSM	spandrel sway mechanism
T	heat treated reinforcing steel bars
URM	unreinforced masonry
WR	hot rolled reinforcing coiled rods
TR	heat treated reinforcing coiled rods

Glossary

Aspect ratio

Ratio of height to length of a wall element.

Base shear

Shear reaction at the base of a building; corresponds to the sum of the lateral story forces.

Capacity

General term to express the ability of a structure or a structural element to cope with given constraints (forces and displacements).

Capacity curve

Plot of the total shear force V acting on a structure or structural element as a function of the lateral deflection Δ at the top of the structure or the structural element. This is often referred to as a pushover curve.

Coupled walls

A system of walls linked by spandrels which are deep enough to produce a coupling effect. The analysis of such a system can be carried out using a frame model.

Damage

Result of the performance of a building under earthquake loading. Can be expressed qualitatively in terms of damage grades (none, slight, moderate, substantial, heavy, destruction) or quantitatively either as a percentage of structural damage or in terms of financial loss (repair cost as a percentage of the initial construction cost).

Diaphragm

Horizontal structural element used to distribute inertial lateral forces to the vertical elements of the lateral force resisting system.

Displacement capacity

Ultimate displacement of a structure or a structural element under the forces considered.

Ductility

Ability of a structure or a structural element to undergo large deformations beyond its yield point and maintain its strength without significant degradation.

Effective stiffness

Slope of the straight line drawn from the origin of the capacity curve of a structure or a structural element to the yield point of the bilinear representation of the capacity curve. The effective stiffness will be always less than the initial elastic stiffness of the structure.

Elastic response spectrum

The 5% damped response spectrum representing the maximum response of the structure in terms of spectral acceleration S_a or spectral displacement S_d as a function of the fundamental frequency of the structure f_1 .

Evaluation method

A method to evaluate the vulnerability of a building.

Fragility curves

Functions that describe the probability of a building belonging to a certain building class of reaching or exceeding a particular damage grade given a deterministic estimate of the spectral response.

Fundamental mode

Lowest eigenfrequency of a structure and the corresponding displacement vector in the direction considered.

In-plane behaviour

Refers to a wall element: The behaviour (horizontal forces and displacements) of the wall element is considered in the plane of the wall.

Intensity

Measurement of the perceived local effects of an earthquake on the environment. Until recently the most widely used scale in Europe was the MSK-Scale (Medvedev-Sponheuer-Karnik), replaced by the EMS (European Macroseismic Scale).

Interacting cantilever walls

A system of walls linked at each floor level by an infinitely rigid diaphragm which has no flexural stiffness. Therefore the walls are assumed to displace equally at each

floor level, however, no coupling effect is produced and the analysis of such a system can be carried out using a cantilever model for each wall.

Out-of-plane behaviour

Refers to a wall element: The behaviour of the wall element is considered in the plane orthogonal to the plane of the wall element.

Pier

A wall element of length l_w and a height h_p equal to the height of the adjacent opening which can be a door or a window.

Seismic demand

Constraints on the building due to the earthquake ground motion. This can be determined using intensity, peak ground acceleration or a response spectrum.

Self weight

That part of the dead loads resulting from the weight of the structure.

Shear capacity

Maximum shear force a structure or a structural element can sustain.

Spandrel

That part of a building lying between two openings (windows or doors) one upon the other, thus joining two walls in one plane.

Strength reduction factor

Ratio of equivalent elastic shear force to the shear capacity of a building.

Structural element

Element of a structure contributing to the capacity of the structure. In the case of a wall structure this can be a wall, a pier or a spandrel.

Structural system

Sum of all structural elements.

Surcharge

That part of the dead loads not resulting from the weight of the structure but from all other permanently attached materials such as non structural elements and furniture. They are usually applied at the floor levels.

Vulnerability

Expected damage due to earthquake ground motion.

Vulnerability function

Relationship which defines expected damage or losses for a building or a class of buildings as a function of the ground motion input.

Wall

Vertical element of a building of length l_w and a height equal to the total height of the building, H_{tot} .

Wall element

Any element of a wall of length l_w and a general height h .

Wall panel

Part of a wall plane of any length l and a height equal to the storey height h_{st} .

Wall plane

All the walls in one plane.

Yield point

Point on the bilinear representation of the capacity curve where the ultimate capacity is reached and the initial linear elastic force-deformation relationship ends and the effective stiffness becomes zero.

Bibliography

- [Ab 92] Abrams D.P.: "Strength and behaviour of unreinforced masonry elements". Proceedings of the Tenth World Conference on Earthquake Engineering, Madrid, Spain, 1992.
- [Ab 97] Abrams D.P.: "Response of unreinforced masonry buildings". Journal of Earthquake Engineering, Vol. 1, No. 1, 1997.
- [Ab 00a] Abrams D.P.: "Nonlinear seismic behaviour of masonry elements and building systems". Lecture notes for the seminar on the seismic assessment of monuments, Pavia, 2000.
- [Ab 00b] Abrams D.P.: "Performance-based rehabilitation of unreinforced masonry buildings". Lecture notes for the seminar on the seismic assessment of monuments, Pavia, 2000.
- [AK 91] Ahnert R., Krause K.H.: "Typische Baukonstruktionen von 1860 bis 1960". Verlag für Bauwesen, Berlin, 1991.
- [AMM 94] Anthoine A., Magonette G., Magenes G.: "Shear-compression testing and analysis of brick masonry walls". Proceedings of the Tenth European Conference on Earthquake Engineering, Vienna, Austria, 1994.
- [ASB 96] Ambraseys N.N., Simpson K.A., Bommer J.J.: "Prediction of horizontal response spectra in Europe ". Earthquake Engineering and Structural Dynamics, Vol. 25, pp. 371-400, 1996.
- [ATC 13] Applied Technology Council "Earthquake damage evaluation data for California". ATC-13, Redwood City, California, 1985.
- [ATC 14] Applied Technology Council "Evaluating the seismic resistance of existing buildings". ATC-14, Redwood City, California, 1987.
- [ATC 40] Applied Technology Council "Seismic evaluation and retrofit of concrete buildings". ATC-40, Redwood City, California, 1996.
- [Ba 94] Bachmann H.: "Hochbau für Ingenieure - Eine Einführung". vdf Hochschulverlag an der ETH Zürich, 2. Auflage 1997.
- [Ba 95] Bachmann H.: "Erdbebensicherung von Bauwerken". Birkhäuser Verlag, Basel, 1995.
- [Ba 00] Bachmann H.: "Duktiler Bewehrungsstahl - unentbehrlich für Stahlbetontragwerke". Institut für Baustatik und Konstruktion, ETH Zürich, Sonderdruck Nr. 0025, Birkhäuser Verlag Basel, 2000.

Bibliography

- [Bay 02] Bay F.: "Ground Motion Scaling in Switzerland: An Implication to Probabilistic Seismic Hazard Assessment". Swiss Seismological Service, ETH Zürich, Dissertation, in preparation.
- [BBP 88] Benedetti D., Benzoni G., Parisi M.A.: "Seismic vulnerability and risk evaluation for old urban nuclei". *Earthquake Engineering and Structural Dynamics*, Vol. 16, pp. 183-201, 1988.
- [BCE 01] Borzi B., Calvi G.M., Elnashai A.S., Faccioli E., Bommer J.J.: "Inelastic spectra for displacement-based seismic design". *Soil Dynamics and Earthquake Engineering*, Vol. 21, pp. 47-61, 2001.
- [BD 97] Bachmann H., Dazio A.: "A Deformation-Based Seismic Design Procedure for Structural Wall Buildings". *Proceedings of the International Workshop on Seismic Design Methodologies for the Next Generation of Codes*, Bled/Slovenia, 24-27 June 1997, A.A. Balkema, Rotterdam, 1997.
- [BDG 01] Becker A., Davenport C., Giardini D.: "Palaeoseismicity studies on end-Pleistocene and Holocene lake deposits around Basel". Submitted to *Geophysical Journal International*, 2001.
- [BGL 98] Brencich A., Gambarotta L., Lagomarsino S.: "A macroelement approach to the three-dimensional seismic analysis of masonry buildings". *Proceedings of the Eleventh European Conference on Earthquake Engineering*, Paris, France, 1998.
- [BH 92] Basler&Hofmann: "Einschätzung der Erdbebensicherheit wichtiger Gebäude". *Leitfaden im Rahmen einer Risikoanalyse für den Kanton Basel-Stadt*, Zürich, 1992.
- [BK 33] "Baukunde für die Praxis". herausgegeben von der Staatlichen Beratungsstelle für das Baugewerbe beim Württembergischen Landesgewerbeamt, Stuttgart, 1933.
- [BKNS 97] Bürge M., Kölz E., Neujahr M., Schneider J.: "Handlungsprioritäten für die Erdbebensicherung bestehender Bauten der öffentlichen Hand". In "Erdbebensicherung bestehender Bauwerke und aktuelle Fragen der Baudynamik", SGEB/SIA Dokumentation D 0145, Schweizerischer Ingenieur- und Architekten-Verein, Zürich, 1997.
- [BP 96] Benedetti D., Pezzoli P.: "Shaking table tests on masonry buildings - Results and comments". ISMES, Seriate Bergamo Italy, 1996.
- [Br 94a] Bruneau M.: "Seismic evaluation of unreinforced masonry buildings - a state-of-the-art report". *Canadian Journal of Civil Engineering*, Vol. 21, pp. 512-539, 1994.
- [Br 94b] Bruneau M.: "State-of-the-art report on seismic performance of unreinforced masonry buildings". *Journal of Structural Engineering*, Vol. 120, No. 1, 1994.

- [BW 98] Bachmann H., Wenk T.: “Ungenügende Duktilität beim Bewehrungsstahl”. Institut für Baustatik und Konstruktion, ETH Zürich, Sonderdruck Nr. 0019, Birkhäuser Verlag Basel, 1998.
- [Ca 99] Calvi G.M.: “A displacement-based approach for vulnerability evaluation of classes of buildings”. *Journal of Earthquake Engineering*, Vol. 3, No. 3, 1999.
- [Cap 00] Capron M.: “Evaluation de la tenue au séisme des bâtiments du réseau vital valaisan”. In “Erdbebenvorsorge in der Schweiz - Massnahmen bei neuen und bestehenden Bauwerken”, SGEB/SIA Dokumentation D 0162, Schweizerischer Ingenieur- und Architekten-Verein, Zürich, 2000.
- [CG 99] Chopra A.K, Goel R.K: “Capacity-demand-diagram methods based on inelastic desing spectrum”. *Earthquake Spectra*, Vol. 15, No. 4, 1999.
- [Ch 95] Chopra A.K.: “Dynamics of Structures - Theory and Applications to Earthquake Engineering”. Prentice-Hall, Upper Saddle River, New Jersey 1995.
- [CKM 96] Calvi G. M., Kingsley G. R., Magenes G.: “Testing of masonry structures for seismic assessment”. *Earthquake Spectra*, Vol. 12, No. 1, 1996.
- [CS 92] Coburn A., Spence R.: “Earthquake Protection”. John Wiley & Sons, Chichester, 1992.
- [CY 97] Cardona O.D., Yamín L.E.: “Seismic Microzonation and Estimation of Earthquake Loss Scenarios: Integrated Risk Mitgation Project of Bogotá, Colombia”. *Earthquake Spectra*, Vol. 13, No. 4, 1997.
- [D044 89] Bachmann H., Ammann W., Derron M.H., Lüchinger P., Mayer-Rosa D., Sägesser R., Somaini D., Studer J., Wütherich W.: “Die Erdbebenbestimmungen der Norm SIA 160”. SGEB/SIA Dokumentation D 044, Schweizerischer Ingenieur- und Architekten-Verein, Zürich, 1989.
- [D0171 02] Bachmann H., Dazio A., Bruchez P., Mittaz X., Peruzzi R., Tissières P.: “Erdbebengerechter Entwurf und Kapazitätsbemessung eines Gebäudes mit Stahlbetontragwänden”. SGEB/SIA Dokumentation D 0171, Schweizerischer Ingenieur- und Architekten-Verein, Zürich, in preparation.
- [Da 00] Dazio A.: “Entwurf und Bemessung von Tragwandgebäuden unter Erdbebeneinwirkung”. Institut für Baustatik und Konstruktion, ETH Zürich, Bericht Nr. 254, Birkhäuser Verlag Basel, 2000.
- [DBB 00] Deichmann N., Baer M., Braunmiller J., Ballarin Dolfín D., Bay F., Delouis B., Fäh D., Giardini D., Kastrop U., Kind F., Kradolfer U., Künzle W., Röthlisberger S., Schler T., Salichon J., Sellami S., Spühler E., Wiemer S.: “Earthquakes in Switzerland and surrounding regions during 1999. *Eclogae Geol. Helv.*, Vol. 93, pp. 395-406, 2000.

Bibliography

- [DWB 99] Dazio A., Wenk T., Bachmann H.: “Versuche an Stahlbetontragwänden unter zyklisch-statischer Einwirkung”. Institut für Baustatik und Konstruktion, ETH Zürich, Bericht Nr. 239, Birkhäuser Verlag Basel, 1999.
- [DSOP 97] D’Ayala D., Spence R., Oliveira C., Pomonis A.: “Earthquake loss estimation for Europe’s historic town centres”. *Earthquake Spectra*, Vol. 13, No. 4, 1997.
- [EC 8] Eurocode 8: “Design provisions for earthquake resistance of structures”. ENV 1998-1-3, CEN Comité Européen de Normalisation, Brüssel, 1995.
- [ELB 01] Elgwady M.A., Lestuzzi P., Badoux M.: “Seismic upgrading of URM walls using composite fibres laminates”. *Proceedings of the Twentieth European Regional Earthquake Engineering Seminar*, Sion, Switzerland, 2001.
- [EMS 98] European Macroseismic Scale 1998, Centre Européen de Géodynamique et de Séismologie, Luxembourg, 1998.
- [Fa 98] Fajfar P.: “Capacity spectrum method based on inelastic demand spectra”. IKPIR Report EE - 3/98, Institute of Structural Engineering, Earthquake Engineering and construction IT, University of Ljubljana, 1998.
- [FEMA 154] “Rapid Visual Screening of Buildings for Potential Seismic Hazards: A Handbook”. FEMA 154, Washington, 1988.
- [FEMA 155] “Rapid Visual Screening of Buildings for Potential Seismic Hazards: Supporting Documentation”. FEMA 155, Washington, 1988.
- [FEMA 178] NEHRP “Guidelines for the Seismic Rehabilitation of Buildings”. FEMA 178, Washington, 1992.
- [FEMA 273] NEHRP “Handbook for the Seismic Evaluation of Existing Buildings”. FEMA 273, Washington, 1997.
- [FEMA 310] NEHRP “Handbook for the Seismic Evaluation of Existing Buildings - a Prestandard”. FEMA 310, Washington, 1998.
- [FG 96] Fajfar P., Gašperšič P.: “The N2 method for the seismic damage analysis of RC buildings”. *Earthquake Engineering and Structural Dynamics*, Vol. 25, pp. 31-46, 1996.
- [FKLG 01] Fäh D., Kind F., Lang K., Giardini D.: “Earthquake scenarios for the city of Basel”. *Soil Dynamics and Earthquake Engineering*, Vol. 21, pp. 405-413, 2001.
- [FPCB 99] Faccioli E., Pessina V., Calvi G.M., Borzi B.: “A study on damage scenarios for residential buildings in Catania city”. *Journal of Seismology*, Vol. 3, No. 3, 1999.
- [Ga 85] Ganz H. R.: “Mauerwerksscheiben unter Normalkraft und Schub”. Institut für Baustatik und Konstruktion, ETH Zürich, Bericht Nr. 148, Birkhäuser Verlag Basel, 1985.

- [GMR 98] Grünthal G., Mayer-Rosa D.: "Einheitliche Erdbebengefährdungskarte für Deutschland, Österreich und die Schweiz (D-A-CH)". Schweizerischer Pool für Erdbebendeckung, Bern, 1998.
- [Gr 24a] Graf O.: "Aus Versuchen über die Druckelastizität von Mauerwerk". Die Bautechnik, Heft 14, pp. 151-152, 1924.
- [Gr 24b] Graf O.: "Versuche über die Druckelastizität und Druckfestigkeit von Mauerwerk, namentlich zur Ermittlung des Einflusses verschiedener Mörtel auf die Druckelastizität von Beton- und Backsteinmauerwerk". Beton und Eisen, Heft 5, pp. 52-58, 1924.
- [Gr 26] Graf O.: "Versuche mit großen Mauerpfeilern. Druckelastizität und Druckfestigkeit von Mauerwerk bei Verwendung von verschiedenen Mauersteinen und verschiedenen Mörteln". Die Bautechnik, Heft 16, pp. 229-232, Heft 17, pp. 254-256, 1926.
- [GT 84] Ganz H. R., Thürlimann B.: "Versuche an Mauerwerksscheiben unter Normalkraft und Querkraft". Institut für Baustatik und Konstruktion, ETH Zürich, Versuchsbericht Nr. 7502-4, Birkhäuser Verlag Basel, 1984.
- [HAZUS 99] National Institute of Building Science (NIBS): "Earthquake Loss Estimation Methodology, HAZUS[®]99 Technical Manual". Report prepared for the Federal Emergency Management Agency, Washington D.C., 1999.
- [HLH 97] Hwang H.H.M., Lin H., Huo J.-R.: "Seismic performance evaluation of fire stations in Shelby county, Tennessee". Earthquake Spectra, Vol. 13, No. 4, 1997.
- [IT 05] "Des Ingenieurs Taschenbuch". Akademischer Verein Hütte, Verlag von Wilhelm Ernst & Sohn, Berlin, 1905.
- [KB 01] Kölz E., Bürge M.: "Priorities in Earthquake Upgrading of Existing Structures". Structural Engineering International, Vol. 11, No. 3, 2001.
- [Ke 90] Keintzel E.: "Seismic design shear forces in RC cantilever shear wall structures". European Earthquake Engineering, Vol. 4, No. 3, 1990.
- [Ki 02] Kind F.: "Development of microzonation methods: Application to Basel, Switzerland". Swiss Seismological Service, ETH Zürich, Dissertation, in preparation.
- [KK 97] King S.A., Kiremidjian A.S., Basöz N., Law K., Vucetic M., Doroudian M., Oloson R.A., Eidinger J.M., Goettel K.A., Horner G.: "Methodologies for Evaluating the Socio-Economic Consequences of Large Earthquakes". Earthquake Spectra, Vol. 13, No. 4, 1997.
- [KNKH 97] Kircher C.A., Nassar A.A., Kustu O., Homes W.T.: "Development of building damage functions for earthquake loss estimation". Earthquake Spectra, Vol. 13, No. 4, 1997.

Bibliography

- [KPM 95] Kowalsky M.J., Priestley M.J.N., Macrae G.A.: "Displacement-based design of RC bridge columns in seismic regions". *Earthquake Engineering and Structural Dynamics*, Vol 24, pp. 1623-1643, 1995.
- [Li 00] Lindemuth A.: "Verletzbarkeit von Mauerwerksbauten". Diploma thesis, ETH Zürich, 2000.
- [LB 00] Lang K., Bachmann H.: "Erdbebenverletzbarkeit bestehender Gebäude aus unbewehrtem Mauerwerk". In "Erdbebenvorsorge in der Schweiz - Massnahmen bei neuen und bestehenden Bauwerken", SGE/SIA Dokumentation D 0162, Schweizerischer Ingenieur- und Architekten-Verein, Zürich, 2000.
- [LWB 99] Lestuzzi P., Wenk T., Bachmann H.: "Dynamische Versuche an Stahlbetontragwänden auf dem ETH-Erdbebensimulator". Institut für Baustatik und Konstruktion, ETH Zürich, Bericht Nr. 240, Birkhäuser Verlag Basel, 1999.
- [Ma 94] Maissen A.: "Tragsicherheit und Gebrauchstauglichkeit von Mauerwerk. Statische Versuche zur Ermittlung der Druck- und Biegezugfestigkeit". Bericht Nr. 228 Mauerwerk heute, Eidgenössische Materialprüfungs- und Forschungsanstalt Dübendorf, 1994.
- [Ma 00] Macchi G.: "Non destructive techniques for the safeguard of the leaning tower of Pisa". Lecture notes for the seminar on the seismic assessment of monuments, Pavia, 2000.
- [Mag 00] Magenes G.: "A method for pushover analysis in seismic assessment of masonry buildings". *Proceedings of the Twelfth World Conference on Earthquake Engineering*, Auckland, New Zealand, 2000.
- [MB 94] Miranda E., Bertero V.V.: "Evaluation of strength reduction factors for earthquake resistant design". *Earthquake Spectra*, Vol. 10, No. 2, 1994.
- [MC 97] Magenes G., Calvi G. M.: "In-plane seismic response of brick masonry walls". *Earthquake Engineering and Structural Dynamics*, Vol. 26, pp. 1091-1112, 1997.
- [MCR 97] McCormack T.C., Rad F.N.: "An Earthquake Loss Estimation Methodology for Buildings based on ATC-13 and ATC-21". *Earthquake Spectra*, Vol. 13, No. 4, 1997.
- [MKC 95] Magenes G., Kingsley G. R., Calvi G. M.: "Static testing of a full-scale, two-story masonry building: test procedure and measured experimental response". Università degli Studi di Pavia, 1995.
- [Mo 93] Moser K.: "Erdbebentauglichkeit von Stahlbetonhochbauten". Institut für Baustatik und Konstruktion, ETH Zürich, Bericht Nr. 201, Birkhäuser Verlag Basel, 1993.

- [MPP 88] Mander J.B., Priestley M.J.N., Park R.: "Theoretical stress-strain model for confined concrete". ASCE Journal of Structural Engineering, Vol. 114, No. 8, 1988.
- [Pa 96] Page A.W.: "Unreinforced masonry structures - an Australian overview". Bulletin of the New Zealand Society for Earthquake Engineering, Vol. 29, No. 4, 1996.
- [Pa 97] Park R.: "A Static Force-Based Procedure for the Seismic Assessment of Existing Reinforced Concrete Moment Resisting Frames". Bulletin of the New Zealand Society for Earthquake Engineering, Vol. 30, No. 3, 1997.
- [PC 91] Priestley M.J.N., Calvi G.M.: "Towards a capacity-design assessment procedure for reinforced concrete frames". Earthquake Spectra, Vol. 7, No. 3, 1991.
- [PCM 00] Pujades L.G., Canas J.A., Mena U., Espinoza F., Alfaro A., Caselles J.: "Seismic risk evaluation in Barcelona, Spain". Proceedings of the Twelfth World Conference on Earthquake Engineering, Auckland, New Zealand, 2000.
- [Pe 00] Peter K.: "Erdbeben-Überprüfung bestehender Stahlbeton-Gebäude". Ecole Polytechnique Fédérale de Lausanne, Thèse No. 2285, 2000.
- [PK 98] Priestley M.J.N., Kowalsky M.J.: "Aspect of drift and ductility capacity of rectangular cantilever structural walls". Bulletin of the New Zealand National Society for Earthquake Engineering, Vol. 31, No. 2, 1998.
- [PP 92] Paulay T., Priestley M.J.N.: "Seismic design of reinforced concrete and masonry buildings". John Wiley & Sons, New York, 1992.
- [Pr 95] Priestley M.J.N.: "Displacement-Based Seismic Assessment of Existing Reinforced Concrete Buildings". Pacific Conference on Earthquake Engineering, Australia, 20-22 November 1995.
- [Pr 00] Priestley M.J.N.: "Seismic assessment of face-loaded walls and cantilever monuments". Lecture notes for the seminar on the seismic assessment of monuments, Pavia, 2000.
- [PS 89] Porro B., Schraft A.: "Investigation of Insured Earthquake Damage". Natural Hazard, Vol 2, pp. 173-184, 1989.
- [PSC 96] Priestley M.J.N., Seible F., Calvi G.M.: "Seismic Design and Retrofit of Bridges". John Wiley & Sons, New York, 1996.
- [PVX 94] Priestley M.J.N., Verma R., Xiao Y.: "Seismic Shear Strength of Reinforced Concrete Columns". ASCE Journal of Structural Engineering, Vol. 120, No. 8, 1994.

Bibliography

- [RC 00] Restrepo J.I., Cowan H.A.: “ The Eje Cafetero Earthquake, Colombia of January 25 1999”. Bulletin of the New Zealand Society for Earthquake Engineering, Vol. 33, No. 1, 2000.
- [Re 92] Recordon B.: “Baukonstruktions-Lehre 1. Theil”. Vorlesungsskript, Polytechnischer Ingenieur Verein, Zürich, 1892.
- [Ro 42] Ros M.: “Festigkeit und Verformung von auf Biegung beanspruchten Eisenbeton-Balken”. Eidgenössische Materialprüfungs- und Versuchsanstalt für Industrie, Bauwesen und Gewerbe, Bericht Nr. 141, Zürich 1942.
- [Ro 50] Ros M.: “Die materialtechnischen Grundlagen und Probleme des Eisenbetons im Hinblick auf die zukünftige Gestaltung der Stahlbeton-Bauweise”. Eidgenössische Materialprüfungs- und Versuchsanstalt für Industrie, Bauwesen und Gewerbe, Bericht Nr. 162, Zürich 1950.
- [SBB 24] “Besondere Bestimmungen für die Ausführung des Mauerwerkes der Tiefbauarbeiten”. Schweizerische Bundesbahn, Bern, 1924.
- [SBBM 00] Sarà G., Barbetti G., Boni A., Marilli F., Nudo R., Viti S.: “Umbria-Marches earthquake of 26 September 1997: Damage scenarios and vulnerability sources in the not-aseismic masonry buildings”. Proceedings of the Twelfth World Conference on Earthquake Engineering, Auckland, New Zealand, 2000.
- [Sc 93] Schwegler, G.: “Verstärken von Mauerwerk mit Hochleistungsfaserverbundwerkstoffen”. Bericht Nr. 135 794-1, Eidgenössische Materialprüfungs- und Forschungsanstalt Dübendorf, 1993.
- [SD 99] Spence R., D’Ayala D.: “Damage Assessment and Analysis of the 1997 Umbria-Marche Earthquakes”. Structural Engineering International, Vol. 9, No. 3, 1999.
- [Si 98] Simon C.: “Erdbebensicherheit in der Basler Industrie”. Lecture at the building insurance company BS, Basel, 23.11.1998
- [SIA 03] “Provisorische Normen für Projektierung, Ausführung und Kontrolle von Bauten in armiertem Beton”. Schweizerischer Ingenieur- und Architekten- Verein. Zürich, 1903.
- [SIA112 35] SIA 112 (Norm): “Normen für die Berechnung, die Ausführung und den Unterhalt der Bauten aus Stahl, Beton und Eisenbeton”. Schweizerischer Ingenieur- und Architekten- Verein. Zürich, 1935.
- [SIA113 43] Sia 113 (Norm): “ Provisorische Normen für die Berechnung und Ausführung von Mauerwerk aus natürlichen und künstlichen Bausteinen”. Schweizerischer Ingenieur- und Architekten- Verein. Zürich, 1943.
- [SIA113 65] Sia 113 (Norm): “ Normen für die Berechnung und Ausführung von Mauerwerk aus künstlichen und natürlichen Bausteinen”. Schweizerischer Ingenieur- und Architekten- Verein. Zürich, 1965.

- [SIA160 89] SIA 160 (Norm): "Einwirkung auf Tragwerke". Schweizerischer Ingenieur- und Architekten- Verein. Zürich, 1989.
- [SIA162 56] SIA 162 (Norm): "Normen für die Berechnung und Ausführung der Beton- und Eisenbetonbauten". Schweizerischer Ingenieur- und Architekten- Verein. Zürich, 1956.
- [SIA162 68] SIA 162 (Norm): "Normen für die Berechnung, Konstruktion und Ausführung von Bauwerken aus Beton, Stahlbeton und Spannbeton". Schweizerischer Ingenieur- und Architekten- Verein. Zürich, 1968.
- [SIA162 93] SIA 162 (Norm): "Betonbauten". Schweizerischer Ingenieur- und Architekten- Verein. Zürich, 1993.
- [SIA177 80] SIA 177 (Norm): "Mauerwerk". Schweizerischer Ingenieur- und Architekten-Verein, Zürich, 1980.
- [SIA177/2 92] SIA 177/2 (Norm): "Bemessung von Mauerwerkswänden". Schweizerischer Ingenieur- und Architekten- Verein, Zürich, 1992.
- [SIA177 95] SIA V 177 (Empfehlung in verlängerter Vernehmlassung): "Mauerwerk". Schweizerischer Ingenieur- und Architekten-Verein, Zürich, 1995.
- [SKW 90] Schickert G., Krause M., Wiggenhauser H.: "Zerstörungsfreie Prüfverfahren für Ingenieurbauwerke". Kompendium der Bundesanstalt für Materialforschung und -prüfung (BAM), Berlin, 1990.
- [Sm 96] Smit P.: "Datenerfassung und Bestimmung der Abminderung der Bodenbewegung bei Erdbeben in der Schweiz". Schweizerischer Erdbebendienst, ETH Zürich, Dissertation, 1996.
- [SMR 78] Sägesser R., Mayer-Rosa D.: "Erdbebengefährdung in der Schweiz". Schweizerische Bauzeitung, Heft 7, 1978.
- [SS 76] Shibata A., Sozen M. A.: "Substitute-structure method for seismic design in R/C". Journal of the structural Division ASCE, Vol. 102, pp. 1-18, 1976.
- [St 04] Stade F.: "Die Holzkonstruktionen". Schäfer Verlag, Leipzig, 1904.
- [SZ 83] Studer J., Ziegler A.: "Grundlagen zur Berechnung von Bemessungserdbeben". Mitteilungen des Institutes für Grundbau und Bodenmechanik, ETH Zürich, Nr. 258, 1983.
- [TBI 28] "Taschenbuch für Bauingenieure". Verlag Julius Springer, Berlin, 1928.
- [TBI 49] "Taschenbuch für Bauingenieure". Springer Verlag, Berlin, 1949.
- [VFF 94] Vidic T., Fajfar P., Fischinger M.: "Consistent inelastic design spectra: Strength and displacement". Earthquake Engineering and Structural Dynamics, Vol. 23, pp. 507-521, 1994.
- [VN 60] Veletsos A.S., Newmark N.M.: "Effect of inelastic behaviour on the response of simple systems to earthquake motions". Proceedings of the Sec-

Bibliography

- ond World Conference on Earthquake Engineering, Vol. 2, pp. 895-912, Tokyo, Japan, 1960.
- [VNC 65] Veletsos A.S., Newmark N.M., Chelapati C.V.: "Deformation spectra for elastic and elastoplastic systems subjected to ground shock and earthquake motions". Proceedings of the Third World Conference on Earthquake Engineering, Vol. 2, pp. 663-680, Wellington, New Zealand, 1965.
- [Vr 92] Vratsanou V.: "Das nichtlineare Verhalten unbewehrter Mauerwerksscheiben unter Erdbebenbeanspruchung - Hilfsmittel zur Bestimmung der q-Faktoren". Schriftenreihe des Instituts für Massivbau und Baustofftechnologie, Heft 16, Karlsruhe, 1992.
- [We 87] Wechsler E.: "Das Erdbeben von Basel 1356". Publication Series of the Swiss Seismological Service No. 102, Zürich, 1987.
- [WRH 74] Whitman R.V., Reed J.W., Hong S.-T.: "Earthquake damage probability matrices". Proceedings of the fifth World Conference on Earthquake Engineering, pp. 2531, Rome, 1974.
- [Wu 78] Wurstisen C.: "Basler Chronik". Reprint of the editions of Basel 1580, Editions Slatkine, Genève, 1978.
- [ZSS 99] Zimmerli B., Schwartz J., Schwegler G.: "Mauerwerk - Bemessung und Konstruktion". Birkhäuser Verlag, Basel, Boston, Berlin, 1999.
- [ZV 00] Zwicky D., Vogel T.: "Bruchversuche an ausgebauten Brückenträgern aus Spannbeton". Institut für Baustatik und Konstruktion, ETH Zürich, Bericht Nr. 258, Birkhäuser Verlag Basel, 2000.